UNCLASSIFIED

AD NUMBER

AD479131

NEW LIMITATION CHANGE

TO

Approved for public release, distribution unlimited

FROM

Distribution authorized to U.S. Gov't. agencies and their contractors; Critical Technology; DEC 1965. Other requests shall be referred to Air Force Materials Lab., Attn: Metals and Ceramics Div. [MAM], Wright-Patterson AFB, OH 45433.

AUTHORITY

AFML ltr dtd 24 Oct 1974

THIS PAGE IS UNCLASSIFIED

ML-TDR-64-173
PART III

479131

HIGH TEMPERATURE PROTECTIVE COATINGS FOR GRAPHITE

J. M. CRISCIONE
H. F. VOLK
J. W. NUSS
R. A. MERCURI
S. SARIAN
F. W. MESZAROS

UNION CARBIDE CORPORATION
PARMA, OHIO

TECHNICAL DOCUMENTARY REPORT ML-TDR-64-173, PART III

DECEMBER 1965

This document is subject to special export controls and each transmittal to foreign nationals may be made only with prior approval of the Metals and Ceramics Division (MAM), Air Force Materials Laboratory, Wright-Patterson AFB, Ohio.

AIR FORCE MATERIALS LABORATORY
RESEARCH AND TECHNOLOGY DIVISION
AIR FORCE SYSTEMS COMMAND
WRIGHT-PATTERSON AIR FORCE BASE, OHIO

NOTICES

When Government drawings, specifications, or other data are used for any purpose other than in connection with a definitely related Government procurement operation, the United States Government thereby incurs no responsibility nor any obligation whatsoever; and the fact that the Government may have formulated, furnished, or in any way supplied the said drawings, specifications, or other data, is not to be regarded by implication or otherwise as in any manner licensing the holder or any other person or corporation, or conveying any rights or permission to manufacture, use or sell any patented invention that may in any way be related thereto.

Copies of this report should not be returned to the Research and Technology Division unless return is required by security considerations, contractual obligations, or notice on a specific document.

300 - February 1966 - 773-30-581

HIGH TEMPERATURE PROTECTIVE COATINGS FOR GRAPHITE

J. M. CRISCIONE
H. F. VOLK
J. W. NUSS
R. A. MERCURI
S. SARIAN
F. W. MESZAROS

UNION CARBIDE CORPORATION
PARMA, OHIO

This document is subject to special export controls and each transmittal to foreign nationals may be made only with prior approval of the Metals and Ceramics Division (MAM), Air Force Materials Laboratory, Wright-Patterson AFB, Ohio.

FOREWORD

This Summary Technical Report was prepared by Union Carbide Corporation, Carbon Products Division, Technical Center, Parma, Ohio 44130, under USAF Contract No. AF 33(657)-11253. This contract was initiated under Project No. 7350, "Refractory Inorganic Non-Metallic Materials,", Task No. 735002, "Refractory Inorganic Non-Metallic Materials: Graphite." The title of the project is "High Temperature Protective Coatings for Graphite". This work is being administered under the direction of the Air Force Materials Laboratory, Research and Technology Division, with Mr. J. D. Latva and Captain W. C. Simmons as project engineers.

This report covers the work from 1 July 1964 to 31 May 1965.

The authors would like to express their thanks to Mr. C. E. Lowell for his interpretation of X-ray diffraction data and the work on the high temperature investigation of the Ir-C system by X-ray diffraction techniques, to Mr. J. D. Ruggiero for the metallographic analyses, and to Drs. E. P. Schram and A. W. Smith for their contributions to the technical effort. Acknowledgment is made for guidance and helpful suggestions from J. C. Bowman and E. Epremian.

This technical report has been reviewed and is approved.

W. G. RAMKE
Chief, Ceramics and Graphite Branch
Air Force Materials Laboratory
Research and Technology Division

ABSTRACT

The second year progress is reported in several areas of research on high temperature oxidation protective coatings for graphite.

Work presented includes: the oxidation kinetics of iridium and rhodium; the permeability of $ZrSiO_4$, ZrO_2, ThO_2, Al_2O_3, and BeO to oxygen; an investigation of the iridium-carbon system by means of high temperature X-ray diffraction techniques and the deposition of iridium on graphite; the volatility of HfO_2, ZrO_2, ThO_2, $ThZrO_4$, $SrZrO_3$, $BaZrO_3$, $ZrSiO_4$, and $HfSiO_4$ in the presence of water vapor; the chemical kinetics of the carbothermic reduction of ZrO_2, ThO_2, HfO_2, $ThZrO_4$, and $HfSiO_4$; the chemical kinetics of the reaction of ZrO_2, HfO_2, and ThO_2 with ZrC, HfC, and ThC_2 respectively; the chemical reactions of HfO_2, ZrO_2, and ThO_2 with HfB_2 and ZrB_2; initial work on carbon diffusion through diborides and carbides; and the mechanical compatibility of components of multilayer oxidation protective coatings for graphite.

The experimental results are discussed as to their practical implication to oxidation-protective coatings.

TABLE OF CONTENTS

I.	INTRODUCTION	1
II.	SUMMARY	2
	1.0 Research Results	2
	2.0 Practical Implications	9
III.	PROGRAM MANAGEMENT	16
IV.	OXIDATION OF IRIDIUM AT HIGH TEMPERATURES .	17
V.	PERMEABILITY OF COATING MATERIALS	36
VI.	MECHANICAL COMPATIBILITY OF IRIDIUM WITH GRAPHITE	75
VII.	MECHANICAL COMPATABILITY OF MULTILAYER COATINGS WITH GRAPHITE	87
VIII.	CHEMICAL REACTIONS OF OXIDES WITH DIBORIDES .	93
IX.	CARBOTHERMIC REDUCTION OF OXIDES	104
X.	CHEMICAL REACTIONS OF OXIDES WITH CARBIDES .	129
XI.	TRANSPORT OF OXIDES IN WATER VAPOR (SINGLE OXIDES)	148
XII.	TRANSPORT OF OXIDES IN WATER VAPOR (MIXED OXIDES)	152
XIII.	CARBON DIFFUSION THROUGH THE MONOCARBIDES AND DIBORIDES OF Hf AND Zr	160
XIV.	ARC PLASMA TEST—METALLOGRAPHIC ANALYSIS OF JTA TEST SPECIMENS	163
	APPENDIX A	175
	APPENDIX B	195

ILLUSTRATIONS

FIGURE		PAGE
1.	Permeability Constant, $P\ell$, Versus Temperature of Materials Studied	11
2.	2000°C TGA Furnace	18
3.	Iridium Metal As-Received, (150 X Magnification)	20
4.	Iridium Metal Annealed for One Hour at 1950°C, (150 X Magnification)	20
5.	Electromagnetic Flux Concentrator	21
6.	Flux Concentrator Attached to Vacuum System	22
7.	Schematic Diagram of Entire Apparatus	23
8.	High-Temperature Induction Furnace Reaction Chamber	24
9.	Gas Flow Control Panel	24
10.	Stagnation Point Recession Versus Time	27
11.	Stagnation Point Recession Rate Versus Gas Flow Velocity	28
12.	Recession Rate Versus Oxygen-Partial Pressure at 1900°C	29
13.	Recession Rate Versus Reciprocal Absolute Temperature	30
14.	Photomacrograph of Iridium Oxidized at 1150°C	34
15.	Photomicrographs of Cross Sections of Yttria-Stabilized Zirconia Sample (150 X Magnification)	40
16.	Photomicrographs of Cross Sections of Yttria-Stabilized Zirconia Sample (300 X Magnification)	41
17.	Photomicrographs of Cross Sections of ZIRCOA 1027 Sample (500 X Magnification)	43
18.	Photomicrographs of Cross Sections of MORGANITE Alumina Sample (500 X Magnification)	45
19.	Photomicrographs of Cross Sections of LUCALOX Sample (150 X Magnification)	47
20.	Photomicrographs of Cross Sections of Zirconium Silicate Sample	49
21.	Temperature Dependence of Permeability Constant, $P\ell$, of Thoria to 50 torr of Oxygen	51
22.	Flow Versus Pressure of N_2 in Inner Chamber for BeO Sample No. 2	52
23.	Pressure Dependence of Permeability, P, of $Zr_{0.91}Y_{0.09}O_{1.96}$ to Oxygen at 1426°C	53

ILLUSTRATIONS (Cont'd)

FIGURE		PAGE
24.	Pressure Dependence of Permeability, P, of $Zr_{0.91}$ $Y_{0.09}$ $O_{1.96}$ to Oxygen at 1520°C	53
25.	Temperature Dependence of Permeability Constant, Pℓ, of $Zr_{0.91}$ $Y_{0.09}$ $O_{1.96}$ to 50 torr of Oxygen	55
26.	Temperature Dependence of Permeability Constant, Pℓ, of ZIRCOA 1027 to 50 torr of Oxygen	56
27.	Temperature Dependence of Permeability Constant, Pℓ, of MORGANITE Alumina and LUCALOX Alumina to 50 torr of Oxygen	57
28.	Pressure Dependence of Permeability, P, of LUCALOX Alumina to Oxygen at 1745°C	58
29.	Zirconium Silicate Tube Heated to 1750°C	60
30.	Permeability of $ZrSiO_4$ to Oxygen	61
31.	Pressure Dependence of Permeability, P, of Zirconium Silicate to Oxygen at 1588°C	62
32.	Photomicrographs of Cross Sections of Calcia-Stabilized Zirconia Sample (300 X Magnification)	63
33.	Photomicrographs of Cross Sections of Calcia-Stabilized Hafnia Sample (300 X Magnification)	64
34.	Photomicrographs of Cross Sections of Thoria Sample (300 X Magnification)	65
35.	Electron Image (Calcia-Stabilized Zirconia, Cold End 700 X Magnification)	66
36.	Zr Distribution (Calcia-Stabilized Zirconia, Cold End 700 X Magnification)	66
37.	Ca Distribution (Calcia-Stabilized Zirconia, Cold End 700 X Magnification)	66
38.	Si Distribution (Calcia-Stabilized ZrO_2, Cold End 700 X Magnification)	67
39.	Fe Distribution (Calcia-Stabilized ZrO_2, Cold End 700 X Magnification)	67
40.	Al Distribution (Calcia-Stabilized ZrO_2, Cold End 700 X Magnification)	67
41.	Electron Image (Calcia-Stabilized ZrO_2, Hot End 700 X Magnification)	68
42.	Ca Distribution (Calcia-Stabilized ZrO_2, Hot End 700 X Magnification)	68

ILLUSTRATIONS (Cont'd)

FIGURE		PAGE
43.	Zr Distribution (Calcia-Stabilized ZrO_2, Hot End 700 X Magnification)	68
44.	Hf Distribution (Calcia-Stabilized ZrO_2, Hot End 700 X Magnification)	68
45.	Electron Image (Calcia-Stabilized HfO_2, Cold End 700 X Magnification)	69
46.	Si Distribution (Calcia-Stabilized HfO_2, Cold End 700 X Magnification)	69
47.	Ca Distribution (Calcia-Stabilized HfO_2, Cold End 700 X Magnification)	69
48.	Zr Distribution (Calcia-Stabilized HfO_2, Cold End 700 X Magnification)	69
49.	Ti Distribution (Calcia-Stabilized HfO_2, Cold End 700 X Magnification)	70
50.	Hf Distribution (Calcia-Stabilized HfO_2, Cold End 700 X Magnification)	70
51.	Al Distribution (Calcia-Stabilized HfO_2, Cold End 700 X Magnification)	70
52.	Fe Distribution (Calcia-Stabilized HfO_2, Cold End 700 X Magnification)	70
53.	Electron Image (Calcia-Stabilized HfO_2, Hot End 700 X Magnification)	71
54.	Si Distribution (Calcia-Stabilized HfO_2, Hot End 700 X Magnification)	71
55.	Ca Distribution (Calcia-Stabilized HfO_2, Hot End 700 X Magnification)	71
56.	Al Distribution (Calcia-Stabilized HfO_2, Hot End 700 X Magnification)	72
57.	Zr Distribution (Calcia-Stabilized HfO_2, Hot End 700 X Magnification)	72
58.	Hf Distribution (Calcia-Stabilized HfO_2, Hot End 700 X Magnification)	72
59.	Vapor-Plated Iridium Coating	76
60.	Iridium Graphite Interface	77
61.	Electroplated (A), Vapor-Plated (B), and Sintered (C) Iridium Coating	77
62.	Graphite "D", (250 X Magnification)	78

ILLUSTRATIONS (Cont'd)

FIGURE		PAGE
63.	Modified Apparatus for Iridium Vapor Plating	80
64.	Vapor-Plated Iridium Coating	81
65.	4 Mil Iridium Plate, (500 X Magnification) Electroeteched in 0.2 N HCl for Three Hours	82
66.	Iridium Metal As-Received, (150 X Magnification)	84
67.	Iridium Sheet Annealed at 1475°C, (150 X Magnification)	84
68.	Iridium Sheet Annealed at 1650°C, (150 X Magnification)	85
69.	Iridium Sheet Annealed at 1830°C, (150 X Magnification)	85
70.	Iridium Sheet Annealed at 1950°C, (150 X Magnification)	86
71.	Photomicrographs of a Pellet of Yttria-Stabilized Hafnia and Similar Samples which have been heated to 2200°C in HfB_2 and ZrB_2	
	71 a. Hafnia As-Received, (500 X Magnification)	
	71 b. Hafnia Heated to 2200°C in HfB_2, (500 X Magnification)	
	71 c. Hafnia Heated to 2200°C in ZrB_2, (500 X Magnification)	98
72.	Pellet of Thoria and Similar Pellets which have been Heated to 2200°C in HfB_2 and ZrB_2	
	72 a. Thoria As-Received, (500 X Magnification)	
	72 b. Thoria Heated to 2200°C in HfB_2, (500 X Magnification)	
	72 c. Thoria Heated to 2200°C, in ZrB_2, (500 X Magnification)	99
73.	Pellet of Yttria-Stabilized Zirconia and Similar Pellets which have been Heated to 2200°C in HfB_2 and ZrB_2	
	73 a. Zirconia As-Received, (500 X Magnification)	
	73 b. Zirconia Heated to 2500°C in HfB_2, (500 X Magnification)	
	73 c. Zirconia Heated to 2500°C in ZrB_2, (500 X Magnification)	100
74.	Stabilized Hafnia Heated in Contact with a ZrB_2 Plate, (500 X Magnification)	102
75.	Stabilized Hafnia Heated in Contact with a HfB_2 Plate, (500 X Magnification)	103
76.	Reaction Furnace Assembly	106
77.	Glass Vacuum System	107

ILLUSTRATIONS (Cont'd)

FIGURE		PAGE
78.	Sintering Apparatus for Mixed Oxide Pellets	108
79.	Photomicrograph of $HfSiO_4$ Pellet, (400 X Magnification)	109
80.	Photomicrograph of $ThZrO_4$ Pellet, (400 X Magnification)	109
81.	Variation of Rate Constant with Temperature for ZrO_2-C	112
82.	Arrhenius Plot for ZrO_2-C	113
83.	Photomicrograph of ZrC Layer on ZT Graphite Crucible, (500 X Magnification)	114
84.	Variation of Rate Constant with Temperature for HfO_2-C Reaction System	116
85.	Arrhenius Plot for HfO_2-C System	117
86.	Variation of Rate Constant with Temperature for ThO_2-C System	118
87.	Arrhenius Plot for ThO_2-C System	119
88.	Variation of Rate Constant with Temperature for $ThZrO_4$-C System	121
89.	Arrhenius Plot for $ThZrO_4$	122
90.	Photomicrograph of ThC_2-ZrC Layer on ATJ Graphite Crucible, (400 X Magnification)	123
91.	Variation of Rate Constant with Temperature for $HfSiO_4$-C Reaction System	124
92.	Arrhenius Plot for $HfSiO_4$-C System	125
93.	Bottom of ATJ Graphite Crucible after Reaction Between $HfSiO_4$ and Graphite, (25 X Magnification)	126
94.	Carbon Monoxide Evolution with Time for the Carbothermic Reduction of ZrO_2 with ZT Grade Graphite	127
95.	Arrhenius Plot for the Carbothermic Reduction of ZrO_2 with Grade ZT Graphite	127
96.	Die Assembly	130
97.	Hot-Pressed Furnace	130
98.	Carbon Monoxide Evolution Versus Time for ThO_2-HfC Reaction	132
99.	Arrhenius Plot for ThO_2-HfC Reaction	133
100.	Value of n Versus Temperature for ThO_2-ZrC Reaction	134
101.	Zirconium Carbide Crucible after Reaction with Thoria at 2070°C, Showing Zirconium Metal at the Grain Boundaries, Etched with 20 Per Cent Ferric Chloride in Methanol--(500 X Magnification)	135

ILLUSTRATIONS (Cont'd)

FIGURE		PAGE
102.	Carbon Monoxide Evolution Versus Time for HfO_2-ZrC Reaction	137
103.	Arrhenius Plot for HfO_2-ZrC Reaction	138
104.	Carbon Monoxide Evolution Versus Time for ZrO_2-ZrC Reaction	139
105.	Arrhenius Plot for ZrO_2-ZrC Reaction	140
106.	Carbon Monoxide Evolution Versus Time for ZrO_2-HfC Reaction	143
107.	Arrhenius Plot for ZrO_2-HfC Reaction	144
108.	Carbon Monoxide Evolution Versus Time for HfO_2-HfC Reaction	145
109.	Arrhenius Plot for HfO_2-HfC Reaction	146
110.	Barium Zirconate Starting Material, (67 X Magnification)	157
111.	Barium Zirconate After 108 Hours in Water Vapor at 1900°C, (67 X Magnification)	157
112.	JTA Atmospheric Test Specimen Showing an Outer Edge of Coating with Intermixed Agglomerates of Zircon and Zirconium Oxide	164
113.	JTA Atmospheric Specimen Showing the Intermediate Zone having Aggregate Particles of Zircon and Zirconium Oxide Dispersed in an Amorphous Glass Phase	165
114.	JTA Atmospheric Specimen Showing Outer Zone of Side Opposite Flame Point. The Large Light Grey Particles are Zircon Containing some White Zirconium Oxide	166
115.	JTA Vacuum Specimen Showing Agglomerated Fine Crystals of Zirconium Oxide Dispersed in Amorphous Glass Phase. Flame Side	168
116.	JTA Vacuum Specimen Showing Graphite Interface with a Continuous Covering of Amorphous Glass Phase. Flame Side	169
	Appendix A	
1.	Pyrex Glass Tube	
	1 a. Apparatus for Studying the Oxidation Rate of Iridium Wire	
	1 b. A View of the Iridium Wire Through the Construction and Glass Window	177
2.	The Effect of Oxygen Flow Rate on the Oxidation Rate of Iridium Foil	182

ILLUSTRATIONS (Cont'd)

FIGURE		PAGE
3.	The Effect of Gas Flow Rate on the Oxidation Rate of Iridium Wire	183
4.	The Effect of Oxygen Partial Pressure on the Oxidation Rate of Iridium	185
5.	The Influence of Oxygen Partial Pressure on the Oxidation Rate of Iridium Wire	186
6.	Arrhenius Plot for the Oxidation of Iridium	187
7.	Arrhenius Plot for the Oxidation of Iridium Wire	189

TABLES

TABLE		PAGE
1	Reaction Rate of Refractory Oxides on Graphite at 2000°C	13
2	Recession Rate Versus Oxygen Partial Pressure and Specimen Temperature	28
3	Manufacturer's Typical Chemical Analysis of the Beryllia Samples	38
4	Manufacturer's Typical Chemical Analysis of the Yttria-Stabilized Zirconia Samples	38
5	Spectrographic Analysis of Yttria-Stabilized Zirconia Sample	39
6	Spectrographic Analysis of Morganite Alumina Sample	44
7	Spectrographic Analysis of Lucalox Sample	46
8	Manufacturer's Typical Chemical Analysis of the Zirconium Silicate Samples	46
9	Spectrographic Analysis of Zirconium Silicate Sample	48
10	Oxygen Permeation Through Thoria as Function of Pressure	50
11	Oxygen Permeation Through Yttria-Stabilized Zirconia as Function of Pressure	54
12	Electron Microprobe Analysis of Oxide Tubes	73
13	Density of Various Oxide Tubes	74
14	Tensile Strength of Iridium	82
15	CTE of HfB_2 and ZrB_2 Calculated from Lattice Parameter Determinations	88
16	CTE of Refractory Oxides	89
17	Stabilized Zirconia Compositions	89
18	Analysis of Oxide Powders	90
19	Chemical Analysis of the Diborides	90
20	Chemical Analyses of the Diborides	93
21	Analyses of the Oxide Powders	94
22	Analyses of the Oxide Pellets	94
23	Treatment of the Oxides with Borides	95
24	Conditions and Results of Oxide and Boride Heats	97
25	Variation of Reaction Rate Constant with Temperature for the ZrO_2-C System	111
26	Variation of Reaction Rate Constant with Temperature for the HfO_2-C System	115

TABLES (Cont'd)

TABLE		PAGE
27	Variation of Reaction Rate Constant with Temperature for the ThO_2-C System	118
28	Variation of Reaction Rate Constant with Temperature for $ThZrO_4$-C System	120
29	Variation of Reaction Rate Constant with Temperature for $HfSiO_4$-C System	123
30	Variation of Rate Constant, K, with Temperature for ZrO_2 + ATJ and ZrO_2 + ZT Graphite	128
31	Rate Constant for Carbon Monoxide Evolution from ThO_2-HfC System	132
32	Variation of Reaction Order with Temperature	134
33	Rate Constant for Carbon Monoxide Evolution from HfO_2-ZrC System	136
34	Rate Constant for Carbon Monoxide Evolution from ZrO_2-ZrC System	136
35	Rate Constant for Carbon Monoxide Evolution from ZrO_2-HfC System	142
36	Rate Constant for Carbon Monoxide Evolution from HfO_2-HfC System	142
37	Weight Change Data on Oxide Samples Treated with Water Vapor	150
38	Manufacturer's Analyses of the Mixed Oxides	152
39	Transpiration Rate of Alkaline-Earth Zirconates in a Low Velocity Argon Stream Containing 0.66 Atmosphere of Water Vapor	154
40	Transport of $BaZrO_3$ in Water Vapor at 1880°C in Various Partial-Pressures of Water	155
41	Transport of $BaZrO_3$ in Various Flow Rates of Water Vapor in a Partial-Pressure of 280 Torr and a Temperature of 1870°C	155
42	Transport of Barium Zirconate by Water Vapor	156
43	Melting Point of Equimolar Mixtures of the Mixed Oxides and Alumina	159
	Appendix A	
1	Emissivity of Iridium in Air from Thermocouple Studies	179
2	Emissivity of Ir in Argon from Blackbody Studies	179
3	Emissivity of Ir in He-O_2 Mixture from Blackbody Studies	180

TABLES (Cont'd)

TABLE		PAGE
4	The Effect of Oxygen Flow Rate on the Oxidation of Iridium	182
5	The Effect of Gas Flow Rate on the Oxidation Rate of Iridium Wire	183
6	The Effect of Oxygen Partial Pressure at 1181°C	184
7	The Influence of Oxygen Partial Pressure on the Oxidation Rate of Iridium Wire at 1717°C	185
8	Linear Rate Constants for the Oxidation of Iridium at Various Temperatures at 1 Atm. Oxygen Pressure	187
9	Linear Rate Constants for the Oxidation of Iridium Wire in Cold-Walled Reaction Vessel	188
10	Linear Rate Constants for the Oxidation of Iridium Wire in Cold-Walled Reaction Vessel	188
	Appendix B	
1	The Effect of Gas Flow Rate on the Oxidation Rate of Rhodium Wire	196
2	Oxidation Rates of Rhodium Wire at Various Temperatures	196
3	Recession Rates of Rhodium Wire Under Various Oxygen-Partial Pressures	198

I. INTRODUCTION

The demonstrated structural properties of graphite at temperatures in excess of 2000°C have created a need for oxidation protection at these temperatures. The empirical approach has not successfully met this need, and the lack of high temperature thermochemical data does not permit a valid theoretical solution to the problem. Specific data requirements include vaporization, evaporation rates, and chemical interactions for potential coating systems above 2000°C. Specific information is also required on the mechanisms controlling rates of reaction, such as diffusion of carbon or oxygen through the system components.

The technical background, the basis for selecting classes of materials for this investigation, the program outline, and the objectives have been reported previously,[1,2] along with the progress of the first year's research effort.

This report deals with oxidation kinetics of iridium and rhodium; the permeability of beryllia, zirconia, thoria, and zirconium silicate to oxygen; the mechanical compatibility of iridium with graphite; the mechanical compatibility of multilayer coatings with graphite; chemical stability of oxides with diborides; carbothermic reductions of oxides; chemical reactions of oxides with carbides; and carbon diffusion in carbides and diborides.

II. SUMMARY

1.0 Research Results

Research has been conducted on the oxidation kinetics of iridium in high velocity and slow moving gas streams at temperatures up to 1900°C, and the oxidation of rhodium in the temperature range 1340° to 1840°C. Other kinetic studies carried out are those for the carbothermic reduction of single and mixed refractory oxides, and the reaction of single oxides with carbides. Further investigations concerning oxidation protective coatings for graphite include: a study of the permeability of $ZrSiO_4$, ZrO_2 ThO_2, and Al_2O_3 to oxygen; the chemical stability of HfO_2, ZrO_2, and ThO_2 with respect to HfB_2 and ZrB_2; the transport of single and compound oxides by water vapor; the mechanical compatibility of iridium with graphite; and initial work on carbon diffusion and mechanical compatibility studies on components for multilayer oxidation protective coatings.

1.1 Oxidation of Iridium

The oxidation of iridium was carried out in high velocity gas streams (up to 25,000 feet per minute) at various oxygen-partial pressures. The experimental approach described for the oxidation of iridium could be used to determine the oxidation resistance of other space-age materials since the method permits distinguishing between mass-transport controlled and surface-reaction controlled rates. In this investigation, the surface-controlled reaction rates were determined for the oxygen-iridium system at temperatures up to 1900°C and oxygen pressures to 710 torr. An arrhenius plot of the data shows that in the temperature range of 1500° to 1900°C, and an oxygen pressure of 142 torr, the logarithm of the recession rate is a linear function of the reciprocal absolute temperature. The data are expressed by the equation

$$R' = 39.9\, e^{-23 \times 10^3/RT},$$

where R' is the iridium recession rate in mils per minute at 142 torr oxygen pressure; R is the gas constant, and T is the absolute temperature. In the temperature interval 1500° to 1450°C, an anomaly was observed in that the recession rate decreased with increasing temperature. Below 1450°C, the recession rate decreased with decreasing temperature.

The equation

$$R'' = 2.78 \times 10^{-4} p^{1.34}$$

represents the rate of recession of iridium as a function of oxygen pressure at 1900°C. In this equation, R'' is the recession rate in mils per minute and p is the oxygen-partial pressure in torr.

Factors that influence the rate controlling mechanism for a given gas-solid reaction are temperature, pressure, gas velocity, and specimen configuration. Iridium sheet specimens that were oxidized at temperatures below 1900°C in slow moving oxygen and air showed nonuniform oxidation. Above 1900°C, the sheet specimens oxidized uniformly (i.e., no edge effects were observed). The data obtained indicated that for the sheet specimens the reaction rates obtained were kinetically limited by mass transport through a gaseous boundary layer. Iridium, at 1730°C, did not experience a weight change when exposed to nitrogen.

A portion of the iridium-oxidation work was subcontracted to Rice University (Appendix A). In this work the oxidation of iridium was investigated by oxidizing an iridium wire in oxygen-helium mixtures with oxygen-partial pressures of 15 torr and 152 torr to temperatures of 2200°C. At an oxygen pressure of 15 torr and a flow rate of 2.3 liters/min (14.7 feet per minute linear velocity), the iridium-recession rate increased from 0.07 mil per hour at 1487°C to 1.11 mils per hour at 2217°C. At 152 torr oxygen pressure and a gas-flow rate of 103 feet per minute, the recession rate increased from 0.74 mil per hour at 1198°C to 13.88 mils per hour at 2217°C.

The emissivity of iridium determined in air was found to decrease from 0.58 at 1040°C to 0.50 at 1600°C. In pure argon, the emissivity was essentially constant at 0.3 to temperatures of 1760°C; and in a helium-oxygen mixture, the emissivity decreased from 0.56 at 960°C to 0.43 at 1850°C.

A modified system is being used, with a Bendix time-of-flight mass spectrometer, to detect volatile iridium-oxide species at temperatures up to 2000°C. Preliminary results indicate the presence of Ir_2O_3 as the gaseous species at the temperature range 1150° to 1200°C.

1.2 Oxidation of Rhodium

This portion of the program was also subcontracted to Rice University (Appendix B). In this work, the oxidation of rhodium was investigated by measuring recession rates at temperatures between 1330° and 1830°C using the wire technique previously utilized for studies of iridium oxidation. Determination of the emissivity (λ = 6500Å) of rhodium in air shows a slight change from 0.26 at 1200°C to 0.30 at 1966°C, the melting point. The recession rate of rhodium in a 20 per cent O_2-80 per cent He mixture is found to be independent of flow rate up to 12 liters/minute (78 ft/min linear velocity) at 1827°C. The recession rate constant increases from 3.4×10^{-2} mils/hour at 1337°C to 6.0×10^{-1} mils/hour at 1827°C in an oxygen-partial pressure of 142 torr. An activation energy of 40 kcal/mole was found for the oxidation reaction.

1.3 Permeability Studies

A further investigation of the permeability of thoria to oxygen was carried out. At 1535°C with the oxygen pressure on one side of a thoria tube being maintained at 25 torr and the oxygen pressure on the other side being varied from 0.01 torr to 0.22 torr, the permeability of thoria was found to be independent of pressure. The permeability of alumina-doped

thoria was investigated in the temperature range 1150° to 1630°C. Doping of thoria with alumina was found to have very little effect on the permeability of oxygen.

The permeability of beryllia to oxygen was investigated in the temperature range 1235° to 1860°C at a pressure of 50 torr. Within the detection limits of the apparatus used (3×10^{-10} gm/cm sec), beryllia was impervious to oxygen up to 1790°C. At 1860°C, the beryllia became pervious even to argon and nitrogen.

The permeabilility of yttria-stabilized zirconia was investigated in the temperature range 1315° to 1960°C. Data at 50 torr oxygen pressure are summarized by the expression,

$$P\ell = 2.1\, e^{-65,900/RT} \text{ (gm/cm sec)},$$

where P is the permeability and ℓ the membrane thickness. The permeability exhibited a one-fourth power dependence on the oxygen pressure in the range 5 to 100 torr. As with thoria, the permeability of zirconia to oxygen was found to be independent of pressure with variations of 0.02 torr to 0.07 torr on the low pressure side of the zirconia tube. The permeability of ZIRCOA Grade 1027 zirconia to oxygen was determined at 25 torr oxygen pressure in the temperature range 1300° to 1525°C. The data are expressed by

$$P\ell = 4.9\, e^{-70,900/RT} \text{ (gm/cm sec)}.$$

The permeability of Morganite alumina and Lucalox polycrystalline alumina to 50 torr oxygen pressure was investigated in the temperature range 1745° to 1870°C. The permeability constant, $P\ell$, is expressed by

$$P\ell = 3.1 \times 10^4\, e^{-134,000/RT} \text{ (gm/cm sec)}$$

where P is the permeability and ℓ is the thickness. Lucalox polycrystalline alumina and Morganite alumina exhibit essentially identical permeabilities even though the former is 100 per cent dense and the latter 95 per cent dense.

A study of the permeability of zirconium silicate to 50 torr oxygen pressure was carried out at temperatures up to 1640°C. In these experiments, a carbon-heating element was found to reduce the mixed oxide; therefore, it was necessary to use an oxide-coated iridium susceptor to heat the test specimen. The permeability constant is expressed by

$$P\ell = 16.0\, e^{-87,500/RT} \text{ (gm/cm sec)}$$

in the temperature range 1430° to 1665°C. No oxygen permeation was detected below 1430°C. The softening of zirconium silicate at temperatures in excess of 1700°C prohibited studying the oxygen permeability at higher temperatures.

An electron microprobe analysis of the thoria, calcia-stabilized zirconia, and calcia-stabilized hafnia tubes used for oxygen permeability studies is presented to further characterize these materials.

1.4 Mechanical Compatibility of Iridium with Graphite

A combination of methods of depositing iridium on graphite has been used to demonstrate the feasibility of using the advantages of various deposition processes to form a pore-free adherent coating on graphite. A slurry-dip process was used to obtain excellent bonding to the substrate. The pores in this coating were closed by a thin layer (0.4 mil) of vapor-deposited iridium, a process which at present is slow and costly if considered in terms of thick (5 mil) layers. Closing of the pores in the subcoating allowed further deposition by electroplating without penetration of the fused salt electroplating bath into the substrate.

Union Carbide's PT-0114 graphite was coated with 2.6 mils of iridium by the slurry-dip process. This specimen exhibited excellent thermal shock resistance in the temperature range 400° to 2000°C. An oxidation test at 2050° ± 50°C in air resulted in less than 0.3 mil recession for one hour. Subsequent metallographic examination showed the slurry-dip coating on PT-grade graphite to be significantly less porous than the deposits previously made on normal graphite. This phenomenon is attributed to the fact that PT graphite is more porous than dense graphite and, therefore, would allow escape of gases through the bulk material instead of through the coating during the sintering process.

Problems were encountered in coating another sample of Union Carbide Grade PT-0114 graphite with iridium by the slurry-dipping technique. In this case, a 2 mil coating cracked and peeled due to stresses created by the very severe mismatch in the thermal expansion of PT-0114 and iridium.

Several attempts to form a smooth uniform coating were unsuccessful when fusing iridium foil on a flat graphite surface by heating the sandwiched materials above the melting point of iridium. In all of these experiments, the iridium layer was discontinuous, showing either large bubble-like pores or pinholes.

The tensile strength of electrodeposited and of annealed foil iridium was measured. The tensile strength of the electrodeposited material was 2.46×10^4 lbs/in^2 in the direction perpendicular to its characteristic columnar growth. The foil (which was 10 mils thick) had a tensile strength of 2.67×10^4 lbs/in^2.

High temperature X-ray methods of analyses were used to investigate both the carbon-rich and the carbon-poor end of the iridium-carbon binary system at room temperature, and in the interval 800° to 2200°C. No iridium carbide was detected in this system.

Iridium metal annealed at 1475°, 1650°, 1830°, and 1950°C demonstrated crystallite growth with increasing temperature.

1.5 Mechanical Compatibility of Multilayer Coatings with Graphite

In connection with the mechanical compatibility of the constituents of multilayer coating systems, information is reviewed on the thermal expansion behavior of ThO_2, ZrO_2, HfO_2, ZrB_2, and HfB_2. Existing information on the thermal expansion of the oxides is considered adequate; however, bulk thermal expansion measurements are needed for the diborides.

The alkaline-earth and rare-earth borides are being considered as additives to the diborides of hafnium and zirconium. These additives will serve to stabilize the ZrO_2 and HfO_2 which form upon oxidation of ZrB_2 and HfB_2, respectively.

Prior to determining the thermal expansion of ZrB_2 and HfB_2 doped with CaB_6 and LaB_6, the chemical compatibility of these hexaborides with ZrO_2, HfO_2, ZrB_2, HfB_2, and graphite was investigated. CaB_6 and LaB_6 are stable with respect to ZrB_2 and HfB_2 in the temperature range studied (1970° to 2190°C). The hexaborides were found to react with ZrO_2 and HfO_2 at 1800°C. Zirconium and hafnium diborides were identified as reaction products, the hexaboride in turn is oxidized; CaB_6 and LaB_6 react with graphite at 2000°C. One of the reaction products is identified as B_4C.

1.6 Chemical Stability of Oxides with Diborides

The chemical stability of ThO_2, ZrO_2, and HfO_2 with respect to ZrB_2 and HfB_2 has been investigated to temperatures of 2200°C. The systems ThO_2-ZrB_2, ThO_2-HfB_2, ZrO_2-ZrB_2, and HfO_2-HfB_2 exhibit excellent chemical compatibility when heated in vacuo for three hours. The systems ZrO_2-HfB_2 and HfO_2-ZrB_2 react according to the scheme

$$HfO_2 + ZrB_2 \underset{<2100°C}{\overset{>2100°C}{\rightleftharpoons}} ZrO_2 + HfB_2$$

1.7 Carbothermic Reduction of Oxides

The carbothermic reduction of yttria-stabilized zirconia pellets was investigated in the temperature range 1885° to 2125°C. The kinetics are described by the parabolic rate expression,

$$\frac{d[CO]}{dt} = 4.28 \times 10^5 e^{-127,000/2RT} t^{-1/2} \text{ mmoles CO cm}^{-2} \text{ (contact area) min}^{-1}.$$

The carbothermic reduction of yttria-stabilized hafnia in the compacted state (i.e., dense oxide pellets) was investigated in the temperature range 1785° to 2110°C. The reaction kinetics follow the parabolic expression,

$$\frac{d[CO]}{dt} = 1.26 \times 10^5 \, e^{-120,000/2RT_t} \, t^{-1/2}$$

where the units are mmoles CO cm^{-2} (solid contact area) min^{-1}.

An investigation of the carbothermic reduction of thoria (dense pellet) was carried out in the temperature range 1770° to 2200°C. The kinetics follow a linear rate law for the first 60 per cent of reaction and are expressed by

$$\frac{d[CO]}{dt} = 1.05 \times 10^{11} \, e^{-126,000/RT} \text{ mmoles CO } cm^{-2} \text{ (contact area) } min^{-1}.$$

Possible reaction mechanisms for the carbothermic reduction of hafnia and thoria involving oxygen ion migration are being considered. The reduction of thoria may involve gas-phase reactions and/or rapid diffusion of carbon through a thorium dicarbide layer.

A study of the kinetics of the carbothermic reduction of the oxides, thorium zirconate ($ThZrO_4$), and hafnium silicate ($HfSiO_4$) has been carried out. The reaction of thorium zirconate ($ThZrO_4$), with ATJ graphite was investigated in the temperature range 1515° to 2050°C. The kinetics are described by the parabolic rate expression

$$\frac{d[CO]}{dt} = 3.38 \times 10^5 \, e^{-118,000/2RT} \, t^{-1/2} \text{ mmoles CO } cm^{-2} \text{(contact area) } min^{-1}.$$

The chemical kinetics for the carbothermic reduction of hafnium silicate were investigated at five temperatures in the range 1505° to 1675°C. An activation energy of 70 kcal/mole was found for the reaction which follows the parabolic rate expression

$$\frac{d[CO]}{dt} = 2.82 \times 10^7 \, e^{-132,000/2RT_t} \, t^{-1/2} \text{ mmoles CO } cm^{-2} \text{ (contact area) } min^{-1}.$$

The carbothermic reduction of zirconia pellets in contact with Union Carbide ZT graphite was investigated in the temperature range 1840° to 2070°C. The reaction follows a parabolic function and is expressed by the equation

$$\frac{d[CO]}{dt} = 3.45 \times 10^4 \, e^{-52,300/2RT_t} \, t^{-1/2} \text{ mmoles CO } cm^{-2} \text{ (contact area) } min^{-1}.$$

1.8 Chemical Reaction of Carbides with Oxides

The reaction of thoria with hafnium carbide was investigated in the range 1695°C to 2070°C. The reaction obeyed a linear rate law over the entire temperature range. The rate expression is:

$$\frac{d[CO]}{dt} = 6.52 \times 10^5 \exp^{-71,500/RT} \text{ mmoles CO cm}^{-2} \text{ min}^{-1}$$

The reaction of thoria with zirconium carbide was investigated in the range 1730° to 2070°C. The reaction is described by

$$ThO_2 + 2ZrC \rightarrow 2CO + (Th, 2Zr)$$

A parabolic rate law describes the reaction at the lower end of the temperature range; there is a continuous increase to a linear rate law at 2070°C. Formation of a molten solution of Th and Zr in the reaction mixture at high temperatures is presented as an explanation for the transition from a parabolic to linear rate law.

An investigation of the reaction of hafnia with zirconium carbide was carried out in the range 1535-2050°C. The kinetics obey a parabolic rate law and are expressed by

$$\frac{d[CO]}{dt} = 1.14 \times 10^4 \exp^{-90,900/2RT} t^{-1/2} \text{ mmoles CO cm}^{-2} \text{ min}^{-1}$$

The kinetics of the reaction of zirconia with zirconium carbide studied in the range 1660-2055°C, also follow a parabolic rate expression and are summarized by

$$\frac{d[CO]}{dt} = 8.95 \times 10^4 \exp^{-109,600/2RT} t^{-1/2} \text{ mmoles CO cm}^{-2} \text{ min}^{-1}$$

The parabolic rate expression,

$$\frac{d[CO]}{dt} = 2.47 \times 10^5 \exp^{-117,500/2RT} t^{-1/2} \text{ mmoles CO cm}^{-2} \text{ min}^{-1}$$

was found for the reaction of zirconia with hafnium carbide in the temperature range 1630°-1995°C.

The reaction of hafnia with hafnium carbide in the range 1575°-2175°C also follows a parabolic rate law and the reaction rate is expressed by

$$\frac{d[CO]}{dt} = 1.38 \times 10^4 \exp^{-98,200/2RT} t^{-1/2} \text{ mmoles CO cm}^{-2} \text{ min}^{-1}$$

1.9 Transport of Oxides in Water Vapor (Single Oxides)

High temperature thermogravimetric experiments have been conducted to investigate the behavior of yttria-stabilized zirconia, yttria-stabilized hafnia, and thoria in the presence of water vapor. Experiments at 1800° and 1900°C in argon saturated with water vapor at 88°C show that zirconia,

hafnia, and thoria are not transported by water vapor.

1.10 Transport of Oxides in Water Vapor (Mixed Oxides)

The water-vapor transport of the mixed oxides, $CaZrO_3$, $BaZrO_3$, $SrZrO_3$, $ThZrO_4$ and $HfSiO_4$ was investigated in the temperature range 1600° to 1900°C. The alkaline earth zirconate-water vapor interaction shows an appreciable transport of the alkaline earth constituent while the ZrO_2 portion remains as a residue on the surface of the mixed oxide. Thorium zirconate and hafnium silicate are not transported by interaction with water vapor.

1.11 Carbon Diffusion in Carbides and Diborides

The intended procedure for determining the diffusion of carbon through the carbides and diborides of hafnium and zirconium is presented, and the present status of equipment assembly is described.

1.12 Arc Plasma Test ——Metallographic Analysis of JTA Test Specimens

A metallographic investigation of the oxidized surface of Union Carbide's grade JTA refractory composite (ZrB_2, Si, and C) has revealed a surface consisting primarily of a porous cellular structure of large particles of a zircon-zirconium oxide mixture, a glass phase, and a small quantity of globular metallic occlusions.

2.0 Practical Implications

The Practical Implications Section is presented mainly to stimulate the application of program findings. The interpretations and implications may, in some cases, be somewhat tenuous; however, this information may motivate others to seek a solution for coatings problems in general.

2.1 Iridium as an Oxidation Protective Coating

The investigation of the iridium oxidation kinetics determined at high gas velocities established the rate for the reactions occurring at the gas-solid interface. By carrying out experiments under conditions which minimize the role of gaseous diffusion to and from the surface through the boundary layer, maximum reaction rates are obtained. Therefore, these surface-controlled reaction rates allow one to predict the life of an iridium coating under the most severe operating conditions.

The equation

$$R'' = 2.78 \times 10^{-4} p^{1.34} \text{(mils/minute)}$$

allows one to predict the highest probable recession rate of an iridium coating subjected to high velocity gas streams of various oxygen partial pressures at 1900°C. For example, in high velocity air at 75 torr pressure (oxygen partial pressure of 15 torr), the rate of recession of iridium at 1900°C would be $2.78 \times 10^{-4} \times 15^{1.34}$, or 0.006 mil/minute.

2.2 Rhodium as an Oxidation Protective Coating for Graphite

The use of rhodium as a protective coating for graphite will be effective at temperatures up to its melting point (~1950°C), provided a barrier is used to avoid the formation of the lower melting rhodium-carbon eutectic (~1700°C). With a recession rate of 0.6 mil/hour at 1827°C in air at atmospheric pressure (P_{O_2} = 142 torr), a 5-mil rhodium coating would last $8\frac{1}{2}$ hours. At 1337°C and a recession rate of 0.034 mil/hour, a 5-mil rhodium coating would last 145 hours.

Earlier in our work it was found that ZrB_2, HfB_2, ZrC, ThC_2, and HfC reacted with rhodium at low temperatures (~1200°C), excluding their further consideration as inert intermediate layer materials in multilayer coating systems with rhodium. Perhaps a more suitable intermediate layer separating rhodium from graphite would be osmium. Although this metal is one of the least oxidation resistant of the platinum group elements, the minimum melting point for the osmium-carbon system is 2732°C, far above the Rh-C eutectic.

2.3 Permeability Studies

Our previous Summary Report [2] pointed out that permeability data provided a basis for assessing the merit of various coating materials. It was suggested then that coatings, which will only permit corrosion rates of one mil/hour or less, should provide good oxygen barriers for short-time protection. Coatings with a ($P\ell$) factor of $< 1 \times 10^{-9}$ g cm^{-1} sec^{-1} should perform adequately as barriers to oxygen. Those with a ($P\ell$) factor $> 1 \times 10^{-7}$ g cm^{-1} sec^{-1} would very likely lead to loss of adherence of the coating, and those exhibiting permeability factors between 10^{-9} and 10^{-8} g cm^{-1} sec^{-1} should be viewed with caution.

So far in this program, oxygen permeabilities have been measured for HfO_2 and ZrO_2 stabilized with CaO, ZrO_2 stabilized with Y_2O_3, ThO_2, and BeO. For comparison purposes, Figure 1 shows the temperature dependence of the permeability constant for all these oxides. The solid lines represent actual measurements, and the dotted lines are extrapolations to 2200°C. The permeability of beryllia was below our detection limit; therefore, only a single point is shown representing an upper permeability limit at 1788°C.

At 2200°C the permeability of ZrO_2, HfO_2, and ThO_2 is such that, for extended use periods, oxidation protective coatings of these latter materials would require an intermediate layer of a more oxidation-resistant material to further protect the graphite.

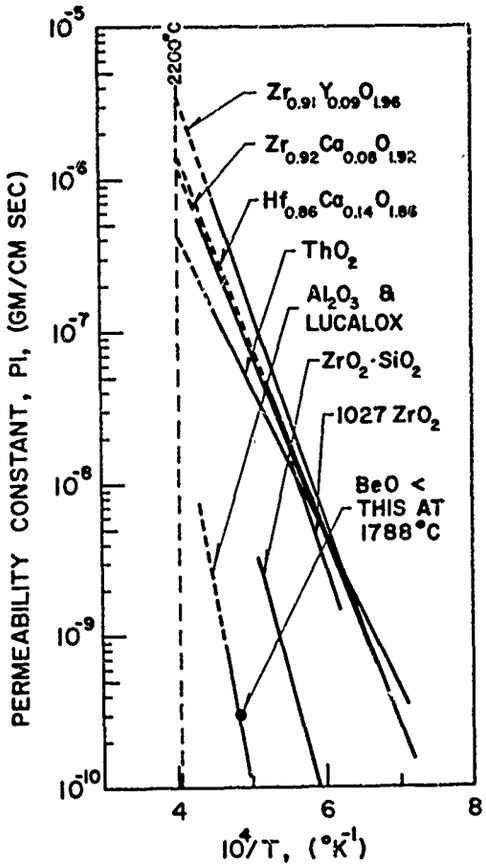

Figure 1. Permeability Constant, Pℓ, Versus Temperature of Materials Studied

The permeability of zirconium silicate up to 1700°C is quite low, and should perform as an adequate oxygen barrier up to this temperature. Although the softening of the zirconium silicate at 1750°C does not necessarily preclude its use as a protective coating at higher temperatures, the low temperature dissociation (1700°C) at reduced pressures indicates that the zirconium silicate may have the limitation usually observed with silicon-based coatings, namely the loss of silicon content via vaporization. Beryllia appears to be an outstanding oxygen-barrier material, at least from the diffusion point of view. Unfortunately, other properties, such as volatility with water vapor and a destructive second order transition at approximately 2050°C,[3] appear to preclude the use of beryllia for many applications. The oxygen permeability of the other single oxides, ThO_2, HfO_2, and ZrO_2, is low enough to warrant their continued consideration as oxygen barriers, provided they can be protected from reacting with carbon by an intermediate layer.

Alumina has the lowest permeability to oxygen and should thus provide an excellent barrier to this element. Alumina will, however, be limited

to a use temperature corresponding to its melting point (2045°C).

2.4 Mechanical Compatibility Data

Mechanical compatibility studies on iridium were concerned mostly with methods of depositing a dense, well-adherent coating. A combination of slurry-dip, vapor deposition, and electroplating techniques was used. The slurry-dip and sintered coating provide a base coat to afford good adherence to the substrate. The deposition of iridium by vapor decomposition is a slow and costly process; however, a very thin coating (less than 0.5 mil) will make the substrate impervious to the fused salt, permitting a thick coating of iridium to be electroplated on graphite. Although electroplating provides a rapid and efficient means of coating-varied geometrical shapes, it has one disadvantage; the fused-salt electrolyte readily penetrates into the graphite and causes rupture of the coating upon being heated.

Although PT-grade graphites have a low CTE (1.1×10^{-6} in/in/°C at room temperature with grain and 1.9×10^{-6} in/in/°C against grain) they also have a low modulus of elasticity which probably accounts for the observation that iridium-coated PT-0114 graphite exhibits excellent thermal shock resistance. These results with iridium-coated PT graphites suggest their use as high temperature, high strength structural materials in corrosive atmospheres.

The tensile strength tests of the electrodeposited-iridium and foil-iridium demonstrate that iridium with the columnar structure characteristic of electrodeposited material is as strong as the polycrystalline sheet iridium.

In general, the CTE's of oxygen barriers, intermediate layers, and graphite follow the order, oxides > diborides > substrate, where the oxides are ThO_2, HfO_2, and ZrO_2; the diborides are HfB_2 and ZrB_2; and the substrate is graphite. Since the differences in thermal expansion coefficients are fairly large, i.e., of the order of 2×10^{-6}/°C at each interface, severe mechanical compatibility problems must be anticipated. Thermal gradients present during friction heating will make the mismatch in thermal expansion even worse, although thermal gradients during the cooling cycle will ameliorate the problem.

The thermal expansion coefficients for the diborides were derived from lattice parameter measurements and thus pertain to single crystals. Polycrystalline materials of less than theoretical density might have considerably lower CTE's due to possible internal expansion into void space. Bulk thermal expansion measurements are needed, therefore, to better assess the mechanical compatibility of the diborides with the oxides and graphite.

2.5 Chemical Reaction Data

Data for the kinetics of reactions between the oxides and graphite provide other means of evaluating these materials as single layer coatings.

The reactions of the oxides (HfO_2, ThO_2, and ZrO_2) with graphite using the reactants in bulk form provide a means of investigating the chemical kinetics and interfacial behavior under conditions more nearly approximating those of a coated substrate. The rate of corrosion resulting from the reaction of an oxide coating with graphite is shown in Table 1. Data obtained from reactions involving powdered reactants, and the method of computing the corrosion rate of the coating have been previously reported[2].

TABLE 1

REACTION RATE OF REFRACTORY OXIDES ON GRAPHITE AT 2000°C

Oxide	Reaction Rate-Powders (sec/mil)	Reaction Rate-Pellets (sec/mil)
HfO_2 (yttria-stabilized)	0.72	60
HfO_2	0.96	-
ThO_2	0.72	95
ZrO_2	1.02	105

The reaction rate between the dense reactants is at least two orders of magnitude lower than the reaction rate involving the powdered reactants. On the basis of chemical reactions, 10-mil thick coatings of hafnia, thoria, and zirconia could be used in direct contact with graphite for a short time (10 to 15 min.) at 2000°C. The order of preference would be $ZrO_2 > ThO_2 > HfO_2$. However, considering the permeability of oxygen through these materials and chemical reactivity with graphite, thoria would be a better candidate for a short-time-use coating directly on graphite.

In addition, thorium compounds and zirconium compounds are suggested as good candidates for oxidation resistant graphite-based refractory composites since the ultimate protection of the composite will be through the formation of an oxide layer in contact with graphite.

The reaction rate for the carbothermic reduction of $ThZrO_4$ is even more rapid than for that of the individual constituent oxides. For example, at 2050°C, the rate constant for the reaction of $ThZrO_4$ with graphite is 1.90 mmole CO cm^2 contact area/minute as compared with rate constants of 1.02 and 0.11 for ZrO_2 and ThO_2, respectively. Hence, $ThZrO_4$ shows little promise as a single-layer protective coating directly on graphite. Also, the rate of carbon monoxide evolution for the carbothermic reduction of hafnium silicate is higher than that of any of the single refractory oxides; therefore, $HfSiO_4$ would be even less desirable than these materials as a protective coating in direct contact with graphite at high temperatures.

Since the carbothermic reduction of the oxides is so rapid, they can only be used as oxygen barriers for graphite if an intermediate layer is used to separate the substrate from the oxide coatings. Because the systems, ThO_2-ZrB_2, ThO_2-HfB_2, ZrO_2-ZrB_2, and HfO_2-HfB_2, do not grossly interact at 2200°C, these materials are very promising components for multilayer coatings on graphite. The oxides exhibit a low permeability to oxygen, and the borides are very stable with respect to carbon, even at 2200°C. The rate of diffusion of carbon through the diborides and the mechanical compatibility of these multilayer systems has yet to be determined.

The addition of alkaline-earth or rare-earth elements to the hafnium- and zirconium-diboride intermediate layers would provide a possible means of stabilizing the hafnia or zirconia, which would eventually form upon oxidation of the intermediate layer.

The information gain thus far on the chemical stability of the potential additives CaB_6 and LaB_6 with respect to graphite, HfO_2, ZrO_2, HfB_2, and ZrB_2, indicates that the hexaboride-diboride composite (e.g., ZrB_2-CaB_6) may adhere to graphite since a chemical bond will be formed by the formation of B_4C. The hexaborides, however, will be readily oxidized if used as intermediate layers in contact with an oxide.

The chemical reactions of ZrO_2, HfO_2, and ThO_2 with ZrC and HfC are even more rapid than the reactions of the oxides with carbon. This fact presents a strong argument for the exclusion of carbides as intermediate barrier materials based on the kinetic effect. However, a consideration of the thermodynamic effect shows that the carbides should function adequately as intermediate layers provided the diffusion of carbon through the carbides is low enough to negate its direct reaction with the oxide. For example, if one considers the $\Delta F°$ values at 2200°K for ZrO_2, ZrC, and CO obtained from the JANAF tables, one obtains $\Delta F° = -27.4$ kcal/mole for the reaction summarized by

$$ZrO_2 + 3C \rightarrow ZrC + 2CO .$$

Since $\Delta F° = -RT \ln Kp = P^2_{CO}$, one calculates a carbon monoxide equilibrium pressure of 22 atmospheres for the carbothermic reduction of zirconia at 2200°K; however, using the same reasoning, $\Delta F° = +96.5$ kcal/mole for the reaction expressed by

$$2ZrC + ZrO_2 \rightarrow 3Zr + 2CO .$$

In this case $Kp = P^2_{CO} = 2 \times 10^{-10}$ atms. The carbon monoxide equilibrium pressure would be 1×10^{-2} mm Hg at 2200°K. These calculations and experimental evidence reported in Section X support the conclusion that a dense zirconia coating would be chemically compatible with a zirconium carbide intermediate layer, since reaction would cease when the

CO pressure is only .01 torr.

The rate of oxidation of the carbon substrate would then be controlled by (1) the rate of carbon diffusion through the intermediate carbide layer to the carbide-oxide interface, (2) the diffusion of oxygen through the outer oxide layer to the carbide-oxide interface, or (3) the diffusion of oxygen through the carbide layer to the carbon-carbide interface.

2.6 Transport of Oxides in Water Vapor

The influence of water vapor on the volatility of a coating material has been determined because of its pertinence to possible application areas. Recent information indicates it may be desirable to aspirate water from leading edges of re-entry vehicles to act as a coolant and to dispel the ion sheath which interferes with communications.

Since it was demonstrated that neither ZrO_2, HfO_2, nor ThO_2 is transported by water vapor even at 1900°C, these materials should not present a problem if used as oxidation protective coatings in moist air.

However, existing information on the water vapor transport of BeO shows that the volatility and, hence, the loss of this material, is enhanced in the presence of water vapor. The formula

$$\log n_{BeO} = 1.62 - 8.8 \times 10^3/T°K + \log n_{H_2O}$$

derived by Stuart and Price[4] presents a means of calculating the recession of a BeO surface which is in equilibrium with a known amount of water vapor. This information also could be used to obtain an upper limit for the recession of a BeO coating on a space vehicle leading edge which is subjected to water cooling.

For example, for one mole of water at 2000°K one calculates from the Stuart and Price equation a loss of 1.66 mmoles of BeO. Thus, from the relationship

$$V_{BeO} = \frac{n M_{BeO}}{\rho BeO}$$

one obtains the volume of evaporation and thence the thickness per cm^2.

The alkaline-earth zirconates are attacked slowly by water vapor at high temperatures by preferential transpiration of the alkaline-earth oxide constituents. Since it is not a congruent corrosion, a meaningful erosion rate cannot be calculated. Since the single oxides, HfO_2, ZrO_2, and ThO_2, appear stable in water vapor, they should be employed in situations where a high concentration of water vapor is to be used on coatings for extended periods of time.

III. PROGRAM MANAGEMENT

Official award of Contract No. AF 33(657)-11253 was made on 1 June 1963 to the National Carbon Company (renamed the Carbon Products Division of Union Carbide Corporation on 1 September 1963). Union Carbide, as Prime Contractor of this program, is to provide a detailed description of the major parameters controlling the oxidation behavior of selected protective coating systems for graphite at temperatures as high as 2200°C. The research is being carried out as a group effort with Dr. J. M. Criscione as Principal Investigator.

The research on all tasks except those outlined in ML-TDR-64-173, Part II, is being performed by personnel at the Union Carbide Corporation, Carbon Products Division, Parma Technical Center.

Research on the oxidation of rhodium, a portion of the research on the oxidation of iridium, and the vaporization of compound oxides were subcontracted to Dr. J. L. Margrave at Rice University, Houston, Texas, beginning 1 January 1964.

Mr. J. D. Latva and Captain W. C. Simmons are serving as Project Engineers for the Air Force Materials Laboratory, Research and Technology Division.

IV. OXIDATION OF IRIDIUM AT HIGH TEMPERATURES

TASK A1-1

Introduction

The rate at which gases react with solid material is often studied experimentally by exposing the solid to a slowly moving gas in a controlled atmosphere reaction chamber. The weight change experienced by the solid may be automatically recorded as a function of time. By determining the geometrical surface area of the solid, one then arrives at a reaction rate having the unit weight change per unit area per unit time. If the reaction product is a dense adherent solid, diffusion through the product limits the reaction rate, and the reaction may be expected to follow a parabolic expression. For heterogeneous systems in which the reaction products are gases, the rate of the chemical reaction may be surface-reaction controlled or mass-transport controlled. At elevated temperatures the reaction product in the iridium-oxygen system is a gas. A surface-reaction controlled rate, in the system of present interest, is defined by the chemical reaction between oxygen and the iridium surface. In mass-transport controlled reactions, the rate of interaction is limited by the diffusion of reactants or products through a gaseous film. This gaseous film, or boundary layer, separates the main gas stream from the solid iridium surface.

Factors which influence the rate-controlling mechanism for a given gas-solid reaction are temperature, pressure, gas velocity, and specimen configuration. The purpose of this investigation is to determine the effect of these factors on the high temperature oxidation of iridium.

Experimental - TGA Furnace

Material

The iridium metal (0.010-inch thick sheet) was supplied by the Baker Platinum Division of Engelhard Industries and was stated to be 99.8 per cent iridium. A spectrographic analysis showed minor (<0.1 per cent) amounts of Fe, Rh, Si, Al, and Pd and trace amounts of Mg, Mn, and Cu.

Apparatus

The apparatus used in conducting this investigation is shown in Figure 2.

The iridium sample support wire (1) is suspended from an automatic recording balance and supports the sample (2) in the center of the impervious alumina furnace liner tube (3). The alumina thermowell (4) and gas inlet (5) tubes are sealed into the bottom of the furnace liner tube with alumina cement (6). Around the liner is a graphite susceptor (7); the entire assembly

is insulated with graphite felt (8) and contained in a quartz envelope (9). The thermowell, gas inlet, and a furnace flush inlet (10) go through the bottom of the quartz envelope and are sealed to it with Sauereisen cement (11); tops of both the furnace liner and quartz envelope are closed with alumina plates (12). The assembly is heated with an induction furnace (13) powered by a 6 KW spark gap converter.

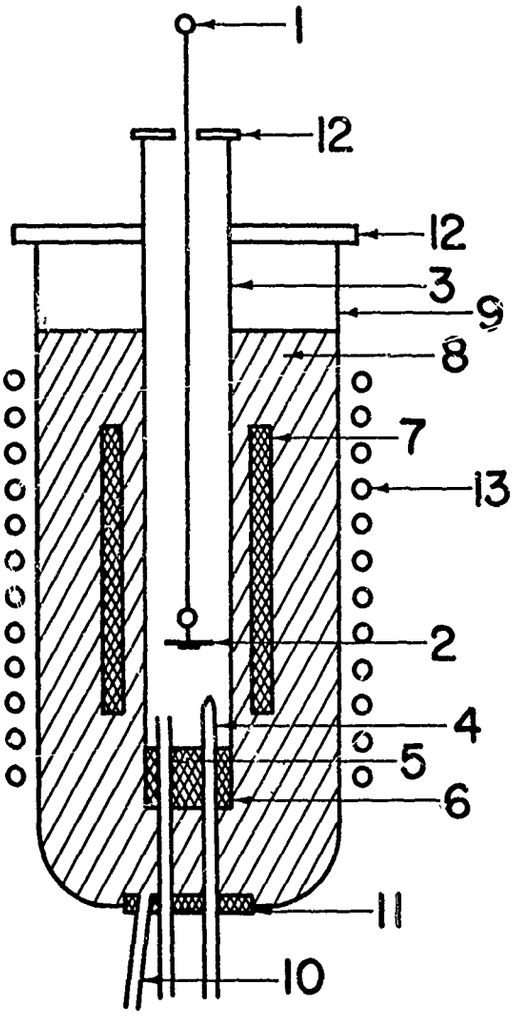

1. Iridium support wire
2. Iridium sample
3. McDanel impervious alumina tube
4. McDanel impervious alumina thermowell
5. McDanel impervious alumina gas inlet tube
6. Morganite 961 alumina cement
7. Graphite susceptor (grade ATJ)
8. Graphite felt (grade WDF) insulation
9. Amersil opaque quartz envelope
10. Quartz furnace flush tube
11. Sauereisen No. 1 cement
12. Sintered alumina plates
13. Ajax Northrup 309 Induction furnace powered with a 6 KW Type "C" converter

Figure 2. 2000°C TGA Furnace

This system is capable of heating a sample to < 2050°C in an oxidizing or neutral environment while continuously recording its weight.

Procedure

In a typical experiment, a 0.500-inch diameter x 0.010-inch disk of iridium, which had been annealed for one hour at about 2000°C, was suspended from the recording balance into the center of the hot zone of the furnace. The disk is held perpendicular to the gas stream. The furnace is brought to a predetermined temperature and held at temperature for thirty minutes in an argon atmosphere. Oxygen is then introduced into the system at a flow rate generally twice that required to obtain a maximum oxidation rate at a given temperature, and the flow is continued to approximately 10 per cent weight loss. The maximum oxidation rate is established by increasing the gas flow at a given temperature until further increase has no effect on the rate of weight loss of the sample. Since the recorded weight loss represented the combined loss of both the sample and the iridium wire support, it is assumed that both lost weight at a constant rate (since the total rate is constant). A suitable correction factor is applied to the data to negate the influence of the weight loss of the wire. Then, based on the rate of weight loss of the sheet, a value is calculated in terms of weight loss in milligrams per cm^2 of surface per hour.

Experiments were accomplished with annealed iridium in the presence of nitrogen, air, and oxygen at temperatures between 1730° and 2010°C. Nitrogen did not affect iridium in a one-hour exposure at 1730°C; however, a volatile oxide was formed with air and O_2.

The iridium samples were held at about 2000°C for one hour in argon prior to the oxidation test. This procedure was used in an attempt to insure that the crystallite size was well developed in each sample and would have a minimal influence on the oxidation rate. Figures 3 and 4 show an iridium sheet as-received and after annealing for one hour at 1950°C. The photographs were taken at 150 X magnification of the samples which had been polished and then a.c. electroetched in dilute HCl to bring out the structure. Figure 3 shows the small, coarse, elongated grains of the as-received iridium sample indicative of the distortion generally exhibited by rolled, unannealed sheet stock. Figure 4 shows the large equiaxed grains of the annealed sample, a condition which denotes complete recrystallization.

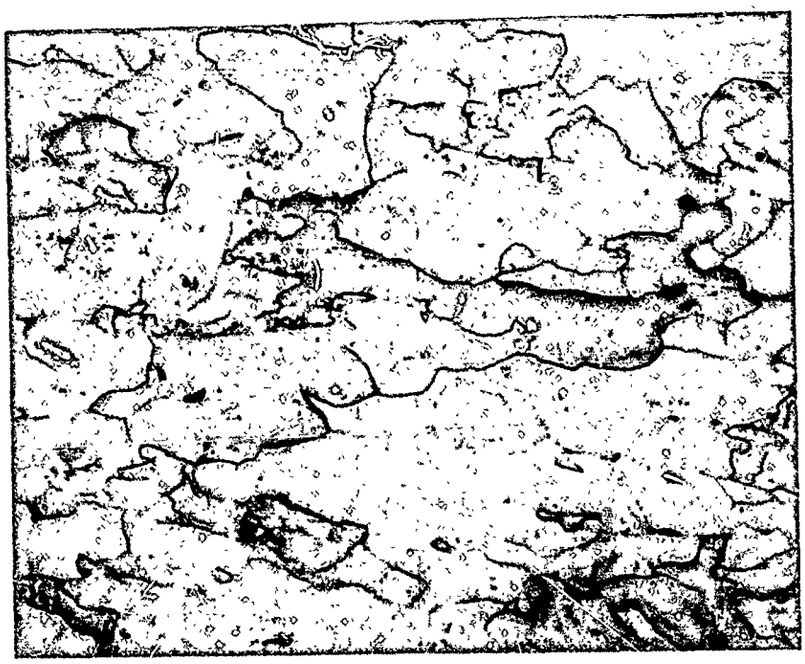

Figure 3. Iridium Metal As-Received, (150 X Magnification)

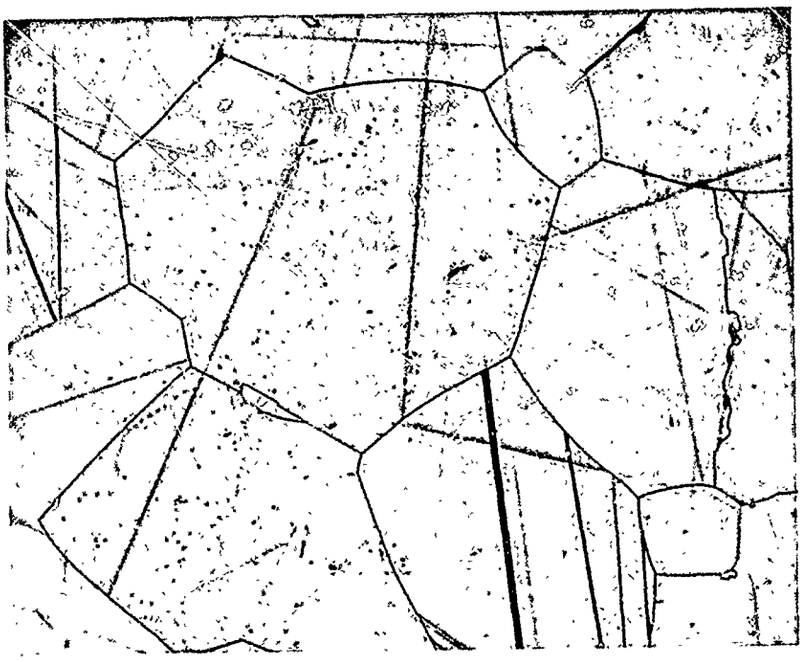

Figure 4. Iridium Metal Annealed for One Hour at 1950° C, (150 X Magnification)

Experimental - High Velocity Gas Apparatus

Materials

The iridium specimen oxidized in this program was a cast rod, initially measuring approximately $1\frac{3}{4}$ inches in height and $\frac{1}{2}$ inch in diameter, obtained from Engelhard Industries, Inc. The top of the specimen was machined to a hemispherical shape, and a hole approximately $\frac{1}{4}$ inch deep by $\frac{1}{4}$ inch in diameter was drilled into the bottom. The gases used were commercially available argon (high purity dry argon, 99.995 per cent minimum purity), and oxygen (USP 99.5 per cent minimum purity with a tolerance of ± 0.1 per cent). The major impurity was nitrogen with trace impurities of argon, neon, krypton, helium, hydrogen, and carbon dioxide.

Apparatus

The iridium specimen was heated using an electromagnetic flux concentrator (shown schematically in Figure 5 and attached to the vacuum system in Figure 6). The electromagnetic flux concentrator efficiently performed the task of linking the field of an induction coil to the iridium sample.

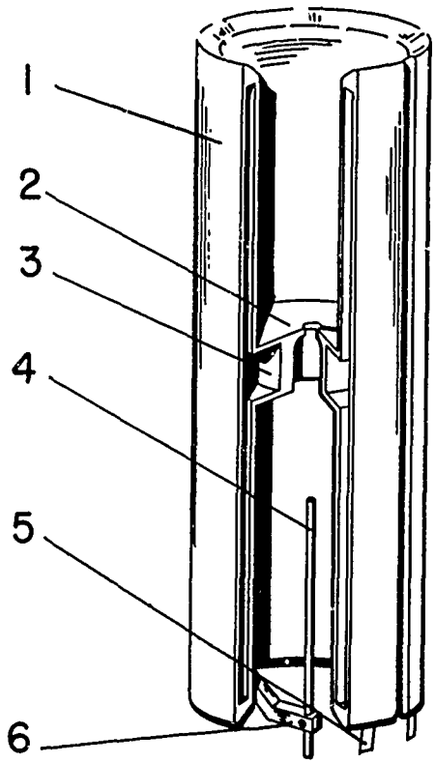

1. Concentrator "Barrel"
2. Concentrator "Donut"
3. Water Channel
4. Tungsten Rod
5. Water Leads and Concentrator Support
6. Specimen Support Plate

Figure 5. Electromagnetic Flux Concentrator

Figure 6. Flux Concentrator Attached to Vacuum System

A Pyrex glass mantle, shown in Figures 7 and 8, electrically insulated the induction coil from the concentrator and acted as a controlled atmosphere reaction chamber. The flow system, shown schematically in Figure 7, contained three Brooks Rotameters, shown in Figure 9, with overlapping flow capacities. Gases flowing at known velocities were introduced into the reaction chamber through a quartz tube extending from above the top of the Pyrex glass mantle to the concentrator. The gas issuing from the $1/4$-inch opening in the bottom of the quartz tube was directed normal to the specimen surface. Unreacted gases were exhausted from the bottom of the reaction chamber by means of auxiliary pumps. The auxiliary pumps served the dual purpose of keeping the reaction chamber pressure at the desired level while maintaining unidirectional gas flow to minimize recirculation of reaction products in the reaction vessel.

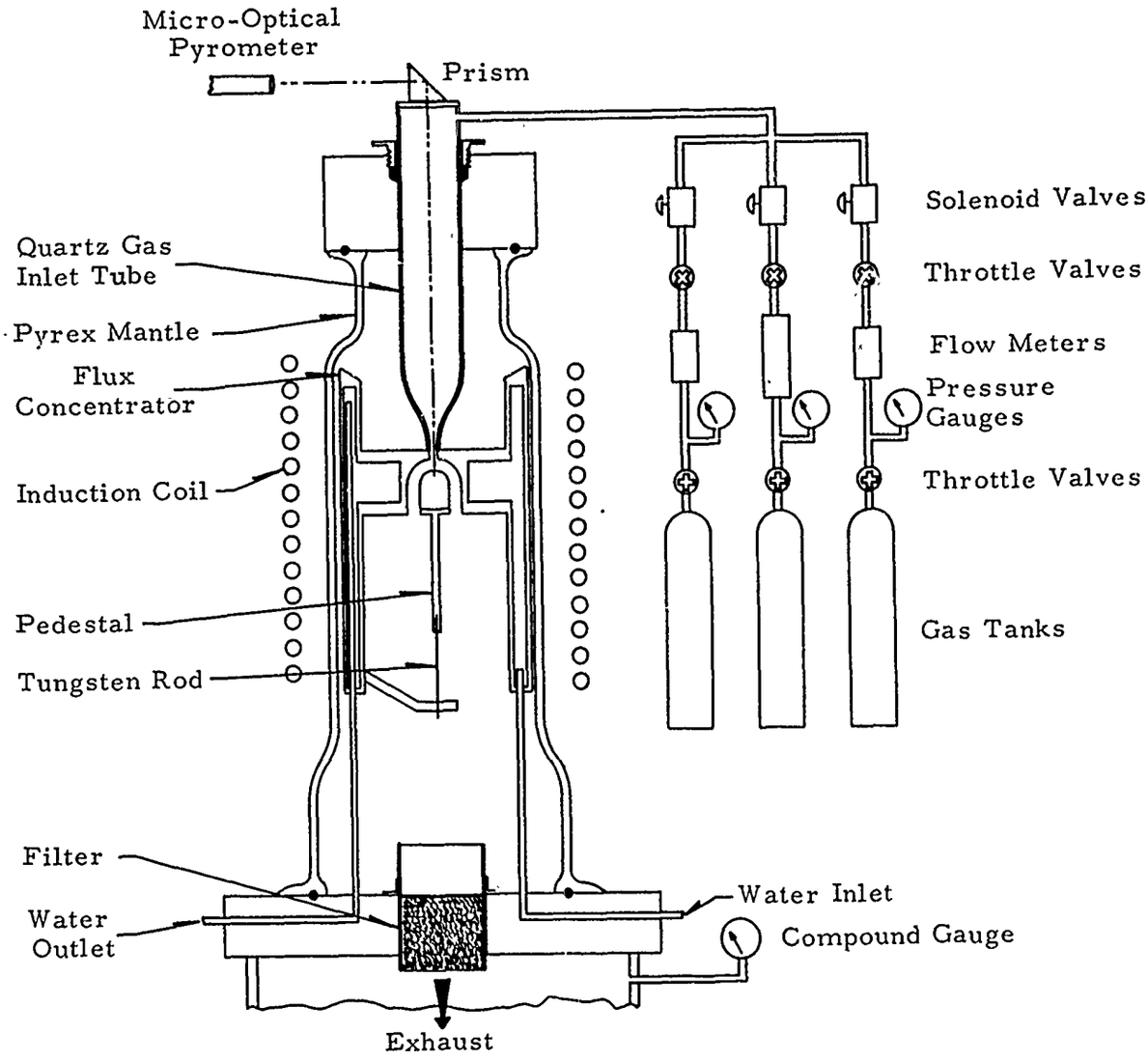

Figure 7. Schematic Diagram of Entire Apparatus

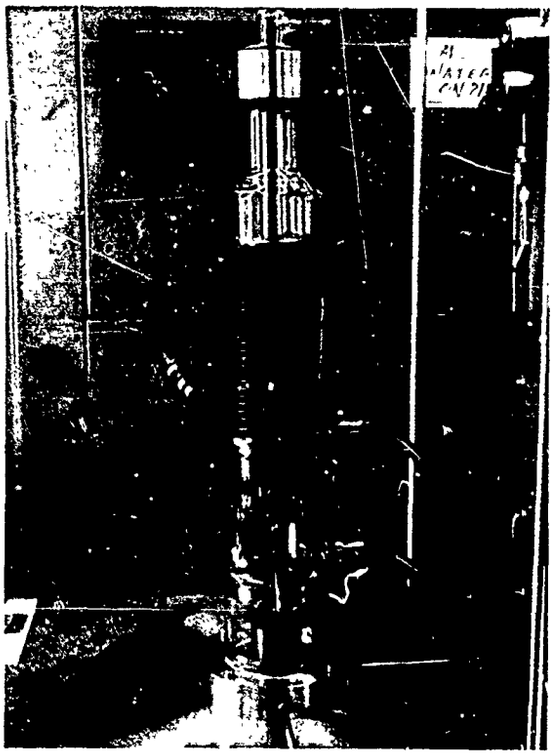

Figure 8. High-Temperature Induction Furnace Reaction Chamber

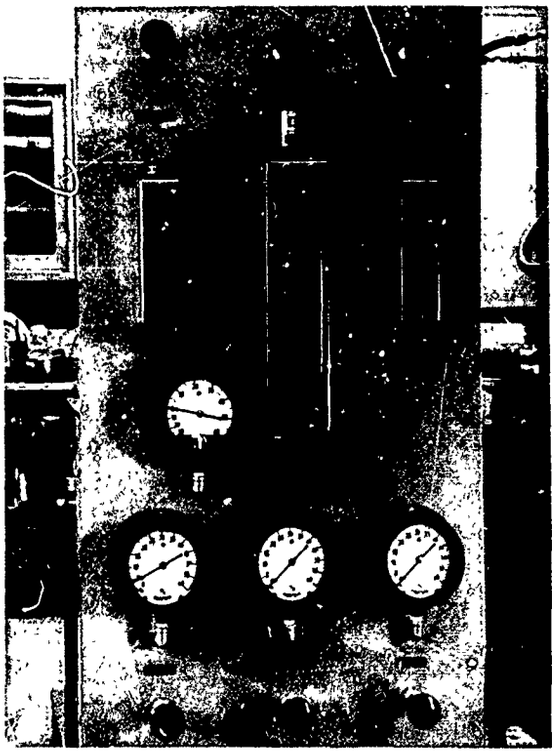

Figure 9. Gas Flow Control Panel

Temperature readings were taken through a prism and window located at the top of the quartz flow tube. A disappearing filament Pyro-Micro-Optical Pyrometer was used to read specimen surface temperatures at the stagnation point. The pyrometer (Serial No. M-5232) was calibrated to temperatures up to 3770°K by means of a National Bureau of Standards calibrated tungsten ribbon lamp and a standard arc with sectored disks as radiation sources. Corrections were made for glass absorption.

The power source used to energize the flux concentrator was a 25 KW output Thermionic Electronic Induction Generator that operates at a frequency of about 400 kilocycles. The output of the generator was controlled by means of a saturable core reactor.

The change in height of the specimen due to oxidation at the stagnation point was determined by means of a Starrett dial gauge comparator. At the outset of the previous study on graphite corrosion, an effort was made to use a traveling microscope; but it was found that the uncertainty in a single measurement was sometimes larger than the recession due to oxidation, and this measurement technique was abandoned in favor of the dial gauge comparator. With the latter instrument, sample height could be measured consistently, both before and after oxidation, to a maximum uncertainty of ± 0.05 mil.

Procedure

The height of the machined specimen was measured before placing it on a recrystallized alumina pedestal. The specimen and pedestal were then positioned in the electromagnetic flux concentrator by means of a tungsten support rod $1/16$ inch in diameter. The glass mantle, induction coil, and flow tube were then positioned (as shown in Figure 8) and the reaction chamber evacuated by means of a mechanical pump and an oil diffusion pump. If no leaks were present, the induction coil surrounding the concentrator was energized and the specimen heated. An initial temperature slightly above the reaction temperature was needed because of the cooling effect of the flowing gases. When the desired temperature was obtained, the reaction chamber was isolated from the high-vacuum equipment and the selected gas velocity and reaction chamber pressure established. When the predetermined reaction time for the experiment was reached, power to the induction coil was cut off and electrically controlled solenoids interrupted the gas flow. The auxiliary pumps were operated continuously to maintain a constant reaction chamber pressure during oxidation and to evacuate the system promptly after the reaction period. This practice minimized further reaction while cooling the specimen to room temperature. The height of the oxidized sample was then measured.

Since surface temperatures at the stagnation point were measured, an emissivity correction was necessary. On the basis of work done by Kuriakose and Margrave at Rice University (see Appendix A) under a subcontract to this investigation, a spectral emissivity of 0.30 was used for the polished iridium surface. This highly polished surface corresponds to that observed by Kuriakose et al., for their emissivity determinations in argon. After an initial conditioning run, the iridium surface appeared

highly polished, and the surface retained this appearance through all subsequent runs.

Results and Discussion

Iridium-Oxygen Reaction, TGA Furnace

The reaction of iridium disks with oxygen at 760 torr was investigated at temperatures between 1740° and 1990°C. Efforts were made to determine gas velocity effects by flowing the oxygen at 9.8 and 17 feet per minute. At temperatures to 1900°C, oxidation occurred preferentially on the edges of the iridium disks; thus, the weight loss data could not be used to determine reaction rates. For example, at 1900°C, the recession at the edges of the disk was three mils per hour (off the radius), whereas the recession of the flat surface of the disk could not be measured with a micrometer that was accurate to 0.2 mil.

At temperatures between 1955° and 1990°C the iridium disks oxidized uniformly (i.e., no edge effects were observed). The accuracy of the data obtained in this temperature interval negated obtaining a velocity dependence for the reaction rates. An average rate of 56 ± 5 mg/cm^2/hr was obtained, which is equivalent to a recession rate of about one mil per hour.

Iridium-Air Reaction, TGA Furnace

The reaction between iridium disks, at temperatures between 1730° and 2010°C, and air (P_{O_2} = 152 torr) flowing at 27 feet per minute were investigated. Again, at temperatures below 1900°C the oxidation was nonuniform and the weight loss data could not be used to calculate reaction rates. Uniform oxidation at 1950° and 2010°C resulted in calculated reaction rates of 39 and 55 mg/cm^2/hr, respectively. These rates are probably accurate to about 5 mg/cm^2/hr.

A comparison of the work of this investigation, in which the gas velocities were between 9.8 and 27 feet per minute, with that of Krier and Jaffee[6] (gas velocity of 2 feet per minute), Kuriakose, Kent and Margrave (velocities between 2 and 103 feet per minute), and Rexer (velocities between 5,000 and 25,000 feet per minute), indicates that all of the rates obtained were mass transport limited. Even at the edges of the nonuniformly oxidized specimens, where the effective thickness of the gaseous boundary layer would be expected to be less than that on a flat surface for a given velocity, the reactions were kinetically limited by mass transport.

Iridium-Oxygen Reactions at High Gas Velocities

In a previous investigation[5] on the interactions of a specific grade of graphite with various gaseous species, it was demonstrated that surface-reaction controlled rates could be obtained at high temperatures by impinging a high velocity gas normal to the solid specimen surface. This technique was used to study the iridium-oxygen reaction kinetics.

Recession rates were obtained by determining the stagnation point recession as a function of time and then calculating the recession rate after steady-state conditions had been obtained. Figures 10 and 11 typify the data obtained. Figure 10 shows the surface recession-time dependence at different constant gas velocities for reactions in which the oxygen pressure was 710 torr and the specimen surface temperature was 1900°C. The calculated recession rates (obtained from the data shown in Figure 10) are shown as a function of gas flow velocity in Figure 11. Graphs similar to those shown in Figures 10 and 11 were constructed for all of the data obtained at a specimen surface temperature of 1900°C. For the reactions

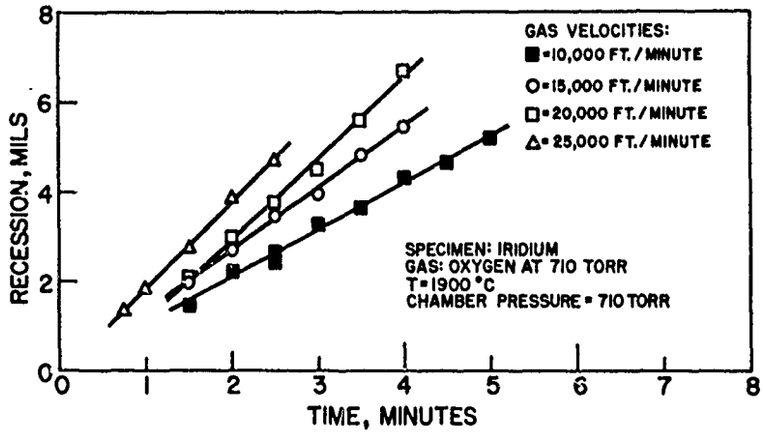

Figure 10. Stagnation Point Recession versus Time

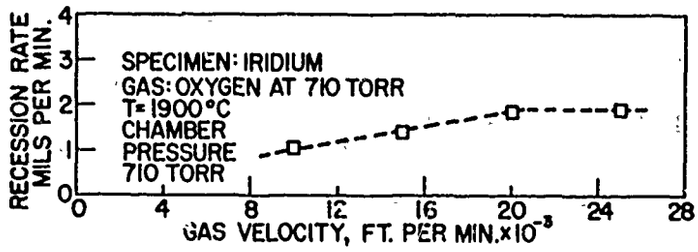

Figure 11. Stagnation Point Recession Rate versus Gas Flow Velocity

occurring at temperatures below 1900°C, reaction rates were determined using a gas flow velocity above the minimum needed at 1900°C to yield a recession rate that did not change with increased gas velocity. The data obtained are given in Table 2.

TABLE 2

RECESSION RATE VERSUS OXYGEN PARTIAL PRESSURE AND SPECIMEN TEMPERATURE

Specimen Temperature, °C	Oxygen Pressure torr*	Recession Rate, mils/minute
1900	14.2	0.01
1900	710	1.93
1900	142	0.175
1730	142	0.107
1615	142	0.080
1500	142	0.052
1450	142	0.066
1400	142	0.057
1330	142	0.040
1270	142	0.031
1150	142	0.016
1500	710	0.29
1270	710	0.79

* Reaction chamber pressure is 710 torr.

The recession rates obtained at 1900°C are shown as a function of the oxygen pressure (on a log, log plot) in Figure 12. The logarithm of the recession rates is shown as a function of reciprocal absolute temperature in Figure 13 together with data obtained by other investigators. The recession rates used to show the rate, temperature, and pressure dependence were rates that did not change with changing gas velocity.

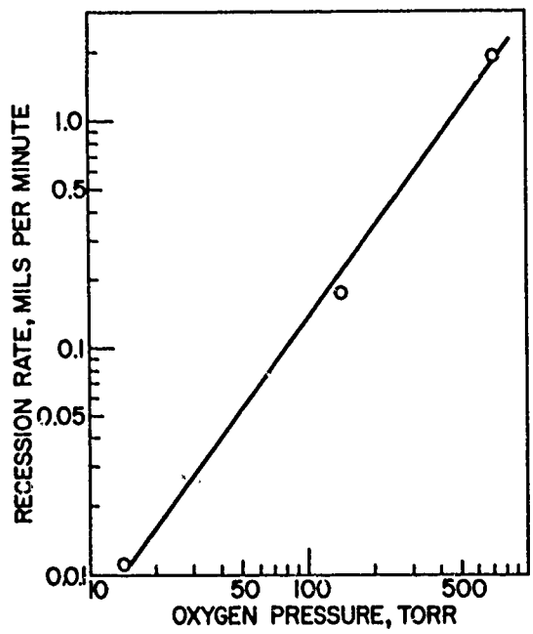

Figure 12. Recession Rate versus Oxygen-Partial Pressure at 1900°C

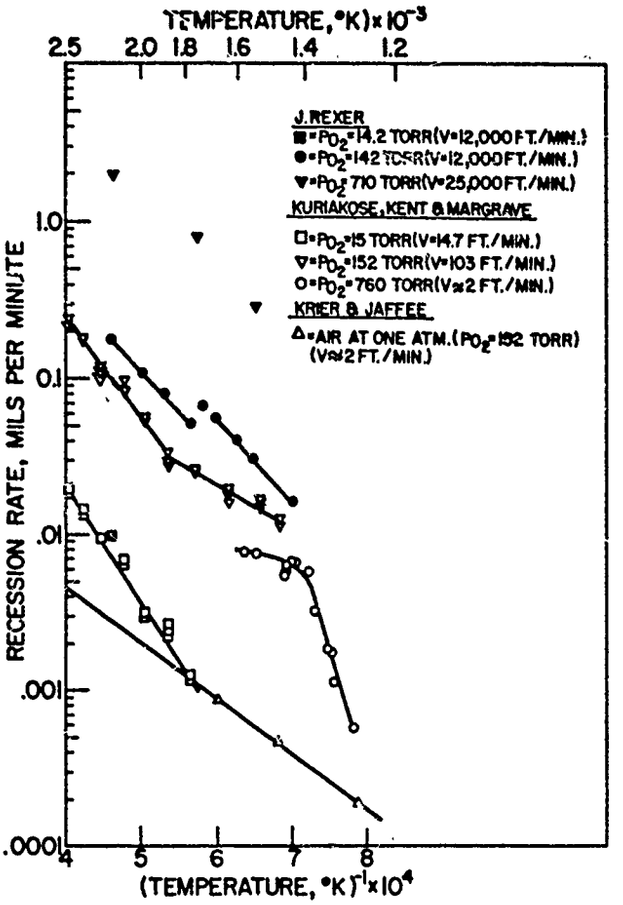

Figure 13. Recession Rate versus Reciprocal Absolute Temperature

Discussion of Results

The linearity of the recession-versus-time curves, shown in Figure 10, supports the accuracy of the experimental data obtained, since a recession rate was calculated from the data of a number of experiments and not by a single experimental determination. The slopes of the curves of Figure 10 represent the steady-state recession rates of the stagnation points at 1900°C, 710 torr oxygen pressure, and at different gas injection velocities. The rates were determined by the method of least squares.

A reaction rate that does not change with increasing gas velocity is indicative of a rate kinetically limited by the surface reaction. The data of Figure 11 show that, under stagnation point flow conditions, reaction rates became kinetically limited by the surface reactions at moderate gas velocities for the highest specimen surface temperature and the highest oxygen pressure studied. Since reaction rates kinetically limited by the surface reaction are expected to decrease with pressure and temperature, the minimum gas flow velocity needed to yield the surface-controlled reaction rates should also decrease. A reaction rate that does not change with increasing gas velocity also indicates that the rate is independent of the temperature of the gas directed against the hot surface. Thus, a system in which a cold gas is directed against the hot surface instead of one in which a hot gas is directed against the hot surface appears to be practical for obtaining surface reaction rates.

The recession rate pressure dependence for reactions occurring at 1900°C is shown in Figure 12. The data show an increase in the reaction rate with pressure and fit the equation

$$R'' = 2.78 \times 10^{-4} p^{1.34}.$$

The data of Figure 13 are a compilation of the work of this investigation, that of Kuriakose, Kent, and Margrave, and the work of Krier and Jaffee.[6] For the reactions occurring at 142 torr oxygen pressure, the reaction rate temperature dependence shows the anomalous feature of a decrease in reaction rate with increasing temperature over a limited temperature range. In the temperature interval between 1500° and 1900°C, the data can be expressed by the equation

$$R' = 39.9 e^{-23 \times 10^3/RT}.$$

A line joining the data in the temperature interval between 1270° and 1400°C appears to have approximately the same slope as given by the above equation.

Although the rate data obtained by other investigators (shown in Figure 13) were obtained under different experimental conditions, certain observations can be made. At low oxygen partial pressures, iridium oxidizes at a very slow rate. At a reaction temperature of 1900°C and oxygen pressures of 14 or 15 torr, the oxidation rate obtained by Kuriakose, Kent, and Margrave is very close to that obtained in this investigation. As the oxygen partial pressure increases, the surface-controlled reaction rate increases and the importance of determining reaction rates as a function of gas flow velocity becomes more apparent. For the reactions occurring at oxygen pressures of 142 to 152 torr, the reaction rates obtained by Kuriakose et al. are lower than those obtained in this investigation; Kuriakose et al. did not observe the anomalous decrease in rate with

increasing temperature over a small temperature interval. The data of Kuriakose et al. were obtained using a gas flow velocity of 103 feet per minute, and the data of this investigation were obtained using a gas flow velocity of 12,000 feet per minute. Krier and Jaffee[6] determined reaction rates for iridium with air (P_{O_2} = 152 torr) flowing at about 2 feet per minute. They obtained rates at least an order of magnitude lower than those obtained by Kuriakose et al. using oxygen at the same pressure. It is interesting that the rates obtained by Kuriakose et al. when the oxygen pressure was 760 torr (and gas velocity approximately 2 feet per minute) are lower than those obtained when their oxygen pressure was 152 torr (gas velocity was 103 feet per minute). The data obtained by Kuriakose et al. at an oxygen pressure of one atmosphere seems to indicate that at temperatures between 1000° and 1150°C, their determined rates were surface-reaction controlled; and at 1150°C the rates became mass-transport limited. Above 1150°C, their rates do not show a large temperature dependence. This behavior would be expected for reaction rates limited by mass-transport through a boundary layer. The reaction rates of this investigation, obtained at an oxygen pressure of 710 torr, cannot be predicted by extrapolating the data obtained by Kuriakose et al. with oxygen at 760 torr to the higher temperatures.

The reaction rate temperature dependence for reactions occurring between iridium and oxygen at a pressure of 142 torr and between graphite and various gases[5] shows the anomalous feature of a decrease in reaction rate with increasing temperature over a limited temperature range. For reactions occurring between graphite and various gases, a mechanism was proposed for theoretically calculating reaction rates for heterogeneous gas-solid reactions in general. The boundary conditions imposed on the derived rate expression were such that if the rate was kinetically limited by mass transport, the rate expression reduced to

$$R = \frac{D}{t} p_{i,o},$$

where R = the reaction rate,

D = the diffusivity of the reactant gas, species i, from the main stream (assumed homogeneous and of constant composition) through the boundary layer to the gas-solid interface,

t = the effective boundary layer thickness,

and $p_{i,o}$ = pressure of the reactant gas, species i, in the main stream.

As the boundary layer thickness approaches zero, the reacting rate may be given by

$$R = \frac{k_r k_{ad} p_{i,o} (1-\sigma_p)}{k_e + k_r}$$

where k_r = the specific reaction rate constant,

k_{ad} = the rate of adsorption of species i,

σ_p = the fraction of the surface covered by products or other substances preventing adsorption of species i,

and k_e = the rate of evaporation of species i.

The parameters k_{ad}, k_r, k_e, and σ_p are temperature dependent and may be of the form A exp. $(-\Delta E/RT)$ where A is a constant and the other symbols have their usual designation. Graphite has a layered structure and is known to be anisotropic in many of its properties. For graphite, the anomalous feature of a decrease in reaction rate with increasing temperature over a limited temperature range is explained by the theory that two types of active surface sites are present. These active sites may be edge and layer atoms each having a different temperature dependence.

During the oxidation experiments with iridium, it was observed that the iridium surface morphology changed with changes in oxidation temperature. At oxidation temperatures between 1500° and 1900°C, the oxidized iridium surface was like a highly polished mirror. Individual grains and grain boundaries were not discernible, indicating that the oxidation rate was independent of grain orientation or surface structural imperfections. At oxidation temperatures below 1450°C, individual grains were observed. The individual crystallites became more pronounced with decrease in oxidation temperature, and, as can be seen in Figure 14 (a macrophotograph of iridium oxidized at 1150°C for fifty minutes) beautiful facets formed. The surface roughness of the individual grains became more pronounced with decreasing oxidation temperature. The oxidized specimen shown in Figure 14 shows some preferred grain boundary attack and a strong indication of preferred grain orientation oxidation rates. The change in specimen surface appearance with oxidation temperature and the anomaly in the rate temperature dependence may be due to the increase in the solid atom mobility with temperature. No information is available at the present time on the surface self-diffusion of iridium. However, studies with other solids[7] indicate that the surface self-diffusion is an exponential of temperature and may be strongly influenced by the chemisorption of various gas species.

Figure 14. Photomacrograph of Iridium Oxidized at 1150°C

If the theory that the anomaly in the Arrhenius plot occurs because of a transition from a mechanism in which the surface atom mobility is too slow to anneal out the surface defects caused by product formation and desorption to one in which high solid atom mobility yields uniform oxidation, there should be a pressure and temperature dependence for this transition. An increase in the oxygen pressure results in an increase in the oxidation rate; therefore, the transition temperature should increase with pressure. The parameters of the rate equation proposed for reactions kinetically limited by surface reactions could not be evaluated within the duration of the program. Similarly, sufficient experiments to prove or disprove the proposed mechanism for the anomaly in the Arrhenius plot could not be performed.

Conclusions and Recommendations

On the basis of experiments performed in the various ZTA graphite-gas systems and the iridium-oxygen system, a procedure and capability have been established for obtaining useful and meaningful results on reaction rates

for heterogeneous gas-solid reactions. Specifically, this work has shown that reaction rates kinetically limited by surface reactions can be achieved and measured for the iridium-oxygen system at temperatures up to 1900°C under conditions of stagnation point flow. At an oxygen pressure of 142 torr, the iridium-oxygen system showed the anomalous effect of a decrease in the reaction rate with increasing temperature over a limited temperature range.

An occurrence of this nature makes futile any estimate of high temperature behavior through extrapolation of low temperature data. A mechanism was proposed for theoretically calculating reaction rates for heterogeneous gas-solid reactions in general. This permits an explanation of the anomaly in the Arrhenius plot in terms of surface self-diffusion.

The experimental approach described in this report should be used to determine the oxidation resistance of other space-age materials since the method permits distinguishing between mass-transport controlled and surface-reaction controlled rates. Experiments should also continue on the iridium-oxygen system to determine if the theoretical model proposed is a feasible model applicable to other systems as well.

V. PERMEABILITY OF COATING MATERIALS

TASK A2-2 AND A3-3

Introduction

The ability of a given material to serve as an oxidation protective coating on graphite depends, among other factors, on the rate at which oxygen can diffuse through the coating. This rate of permeation can be limited either by reaction at the surface of by diffusion through the barrier[8]. However, if the barrier is thick enough, diffusion will, in any case, become the rate-determining process. Reactions at the surfaces will be in equilibrium and will, therefore, establish the concentration gradient of the diffusing species.

The steady state of mass transport through a membrane (coating) is given by Fick's first law

$$P = -D \frac{dc}{dx}$$

where P = the permeability
D = the diffusivity
and $\frac{dc}{dx}$ = the concentration gradient.

Most oxygen diffusion measurements on oxides reported in the literature are concerned with the determination of the diffusivity, D. However, since the concentration gradient, dc/dx, is generally unknown and since D is not necessarily independent of dc/dx, one cannot calculate permeabilities from the measurements of the diffusivity alone. For this reason, direct permeability determinations are preferable for the purpose of evaluating the possible usefulness of oxides as coating materials. Such measurements were carried out and are reported and discussed for the following oxides: two grades of zirconia (zirconia-stabilized with 8 per cent yttria and zirconia grade ZIRCOA 1027), beryllia, thoria, two grades of alumina (LUCALOX and MORGANITE), and zirconium silicate.

Experimental

The oxide samples were in the form of impervious tubes closed at one end. Their imperviousness was frequently checked, and all reported results are on tubes which showed no detectable permeability for either argon or nitrogen at any of the temperatures of the investigation.

The tubes were heated using either a graphite or an iridium susceptor. When a graphite susceptor was used, the procedure was identical to that described previously[2], i.e., oxygen was contained inside the tube and, after diffusing through the tube walls, reacted with the carbon susceptor to form carbon monoxide. The carbon monoxide flow was monitored with a

mass spectrometer and its associated vacuum equipment and provided a measure of the rate of permeation of oxygen through the oxide. The presence of the graphite susceptor on the detection side of the sample resulted in a carbon monoxide background pressure which, in the case of oxides of very low permeability, limited the sensitivity of the measurements and also made it impossible to determine the permeability of the sample as a function of the oxygen pressure on the low pressure side.

The use of an iridium susceptor avoided these problems. Preliminary experiments showed that even at very low oxygen pressure there was some reaction between iridium and oxygen, and it was, therefore, not possible to use the susceptor on the detection side of the system. The procedure was, therefore, reversed, i.e., oxygen was on the outside of the tube in contact with the susceptor, which was protected from excessive oxidation by a thin (approximately one mil) coating of sintered-on hafnia. The inside of the tube was continuously evacuated, and oxygen permeating through the tube walls was again monitored with a mass spectrometer. This experimental procedure increased our sensitivity by a factor of about one hundred.

To obtain a low pressure side pressure dependence, the oxygen pressure on the low pressure side of the sample was varied by means of a leak valve which restricted the flow of oxygen to the main detection system and pumps. The oxygen pressure on the high pressure side was kept at 25 torr.

The use of a graphite susceptor was adequate for most measurements, and, unless noted otherwise, all results quoted in this report were obtained in that way. The iridium susceptor was required only in the case of oxides of very low permeability and for measurements of the pressure dependence on the low pressure side of the system.

The vacuum system used to detect the flow of oxygen through the sample and the method of temperature measurement have already been reported in the previous Summary Report[2].

Materials Characterization

1. Beryllia

Two 9-inch long x $^3/_8$ inch O.D. x $^9/_{32}$ inch I.D., impervious beryllia tubes were used. They had a density of 2.70 gm/cm^3 and a maximum porosity of 10 per cent, as stated by the manufacturer, National Beryllia Corporation. The manufacturer's typical chemical analysis of the samples is given in Table 3. The samples had a minimum BeO content of 99.3 per cent by weight.

TABLE 3

MANUFACTURER'S TYPICAL CHEMICAL ANALYSIS OF THE BERYLLIA SAMPLES

Element	Parts Per Million
Total Al, Mg, and Si	Less than 6000
Total Ca, Sr, and Ba	Less than 500
Total Fe, Ni, Co, and Cu	Less than 300
Total Na, Li, and K	Less than 200
Total C	Less than 20

No analyses were performed at these Laboratories on the beryllia samples due to the inherent danger of handling beryllium without the proper facilities.

2. Yttria-Stabilized Zirconia

Two 9-inch long x $^3/_8$ inch O. D. x $^9/_{32}$ inch I. D., 8 weight per cent yttria-stabilized zirconia tubes were used. The tubes had a density of 5.45 gm/cm^3 and a porosity of 5 per cent, as stated by the manufacturer, Zirconium Corporation of America. Our measurements of the buoyancy of the sample immersed in water yielded a density of 5.83 gm/cm^3. This density cannot be translated into a porosity value, since the theoretical (single crystal)density of this material is a function of the yttria content and is not known. The manufacturer's typical chemical analysis of the samples is given in Table 4 and the spectrographic analysis performed at this Laboratory in Table 5.

TABLE 4

MANUFACTURER'S TYPICAL CHEMICAL ANALYSIS OF THE YTTRIA-STABILIZED ZIRCONIA SAMPLES

Compound	Per Cent
ZrO_2	91.5
Y_2O_3	8.0
CaO	max. 0.02
MgO	max. 0.01
SiO_2	max. 0.30
Al_2O_3	max. 0.10
Fe_2O_3	max. 0.015
HfO_2	max. 0.010
TiO_2	max. 0.005

TABLE 5.

SPECTROGRAPHIC ANALYSIS OF YTTRIA-STABILIZED ZIRCONIA SAMPLE

Element	Per Cent
Zr	greater than 0.1
Y	greater than 0.1
Mg	0.01 to 0.1
Si	greater than 0.1
Al	0.01 to 0.1
Fe	0.01 to 0.1
Ti	0.01 to 0.1
Ni	0.01 to 0.1
Mn	0.01 to 0.1
Cr	0.01 to 0.1
Cu	less than 0.01

The photomicrographs of the yttria-stabilized zirconia hot and cold zones are shown in Figure 15 at a magnification of 150 X and in Figure 16 at a magnification of 300 X. The hot zone photomicrographs were taken after the sample had been subjected to a temperature of 2050°C. There appears to be a secondary phase present in the cold zone which has almost disappeared in the hot zone. This homogenization had no effect on the permeability, since the permeability at the lower temperatures, determined before and after the high temperature runs, remained unchanged.

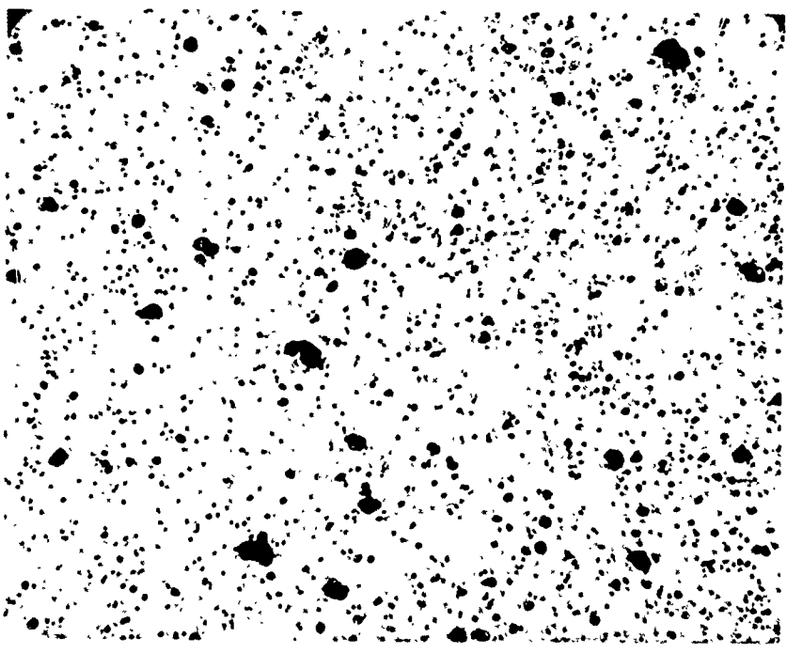

Cold Zone

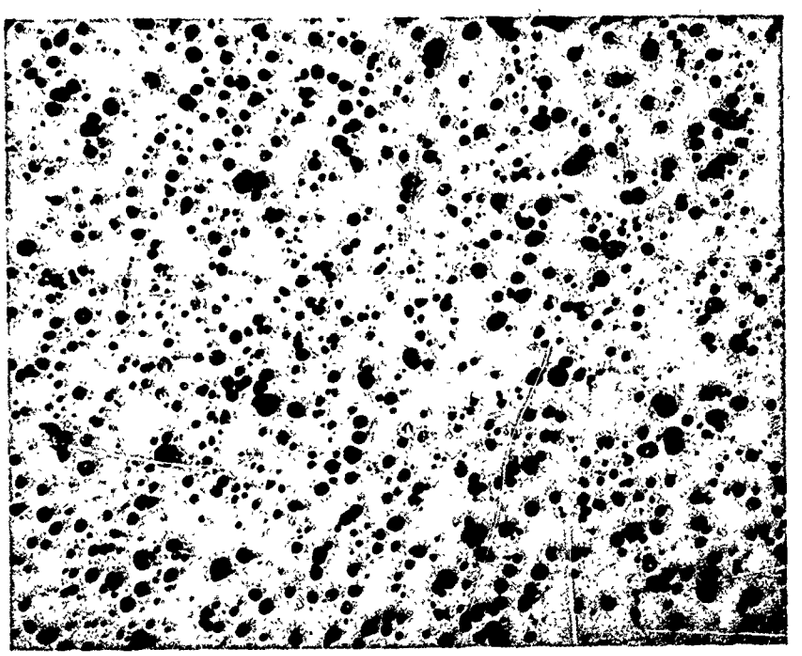

Hot Zone
(after heating
to 2050°C)

Figure 15. Photomicrographs of Cross Sections of Yttria-Stabilized Zirconia Sample (150 X Magnification)

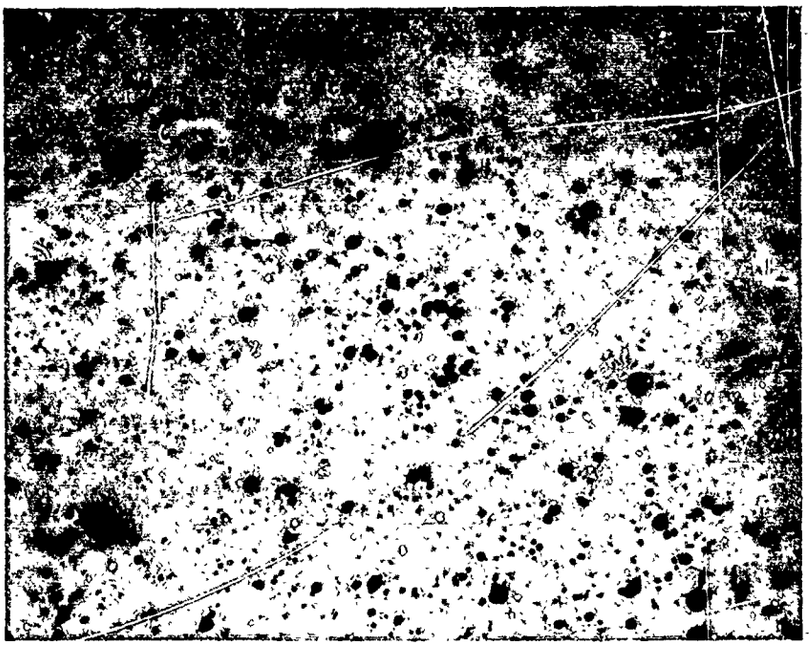

Cold Zone

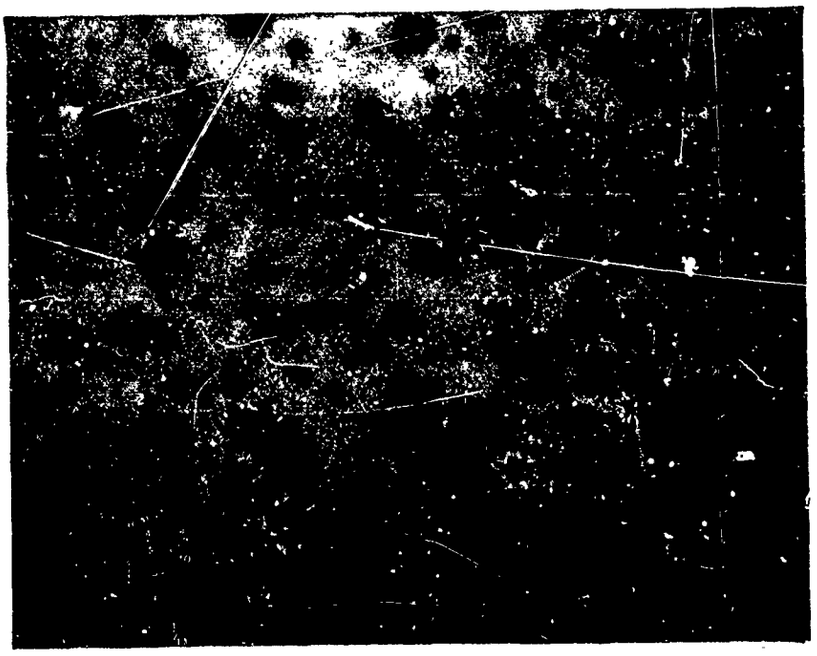

Hot Zone
(after heating
to 2050°C)

Figure 16. Photomicrographs of Cross Sections of Yttria-Stabilized Zirconia Sample (300 X Magnification)

3. Zirconia Grade ZIRCOA 1027

Two 9-inch long x $^3/_8$-inch O.D. x $^9/_{32}$-inch I.D. tubes were used. The manufacturer's reported density was 5.6 gm/cm^3 and our measured density was 5.3 gm/cm^3. The exact composition of this material is held proprietary by the manufacturer, Zirconium Corporation of America, and hence, no analysis was supplied. This material was of interest because it has a reported coefficient of thermal expansion of only 5 x 10^{-6}/°C, as compared with 10×10^{-6}/°C for either yttria- or calcia-stabilized zirconia.

Photomicrographs of ZIRCOA 1027 hot and cold zones are shown in Figure 17 at a magnification of 500 X. The hot zone photomicrographs were taken after the sample had been subjected to a temperature of 1700°C. Two representative areas of the hot zone are shown since one section of the hot zone had many cracks which caused the sample to become pervious, while other parts of the hot zone apparently remained intact.

The photomicrographs show extensive grain growth on heating. Also, the voids have become larger in the hot zone. The cold zone shows a secondary phase which has almost disappeared in the hot zone.

4. MORGANITE Alumina

Several 9-inch long x $^5/_{16}$-inch O.D. x $^3/_{16}$-inch I.D., impervious recrystallized alumina tubes, Grade Triangle RR, manufactured by Morganite Incorporated, were used. The manufacturer reported a purity of 99.7 per cent and a density of 3.78 gm/cm^3. Density measurements made by determining the buoyancy of the sample in water yielded a density of 3.80 gm/cm^3. Comparing this density with that of single crystal alumina gives a porosity of approximately 5 per cent. The microporosity, however is less than 5 per cent since, on grinding samples, large voids (up to 2 mm diameter) were repeatedly detected. It should also be stated that of fifteen tubes received, only four were impervious to argon and nitrogen.

Results of the spectrographic analysis performed on a MORGANITE alumina sample at this Laboratory are given in Table 6.

Cold Zone

Hot Zone
(after heating
to 1700°C)

Hot Zone
(after heating
to 1700°C)

Figure 17. Photomicrographs of Cross Sections of ZIRCOA 1027 Sample (500 X Magnification)

TABLE 6

SPECTROGRAPHIC ANALYSIS OF MORGANITE ALUMINA SAMPLE

Element	Per Cent
Al	greater than 0.1
Fe	0.01 to 0.1
Si	0.01 to 0.1
Mg	less than 0.01
Mn	less than 0.01
Cr	less than 0.01
Ni	less than 0.01
Cu	less than 0.01
Ag	less than 0.01

Figure 18 shows the photomicrographs of the hot zone and cold zone MORGANITE alumina cross sections with a 500 X magnification. The pores have become larger and more uniform in the hot zone, but the pore volume appears to be about the same. The white spots present in the photomicrographs are pores which show through the polished alumina since the material is translucent.

5. LUCALOX Alumina

LUCALOX is General Electric's trade name for a polycrystalline, essentially pore-free, 99.9 per cent alumina material. Two tubes, 9-inch long x $^{3}/_{8}$-inch O.D. x $^{5}/_{16}$-inch I.D., were used. The manufacturer's reported density was 3.98 gm/cm^3, and the value measured at this Laboratory was 4.00 gm/cm^3. These densities are very close to that of single crystal alumina and hence the tubes have essentially zero porosity.

Results of a spectrographic analysis are given in Table 7.

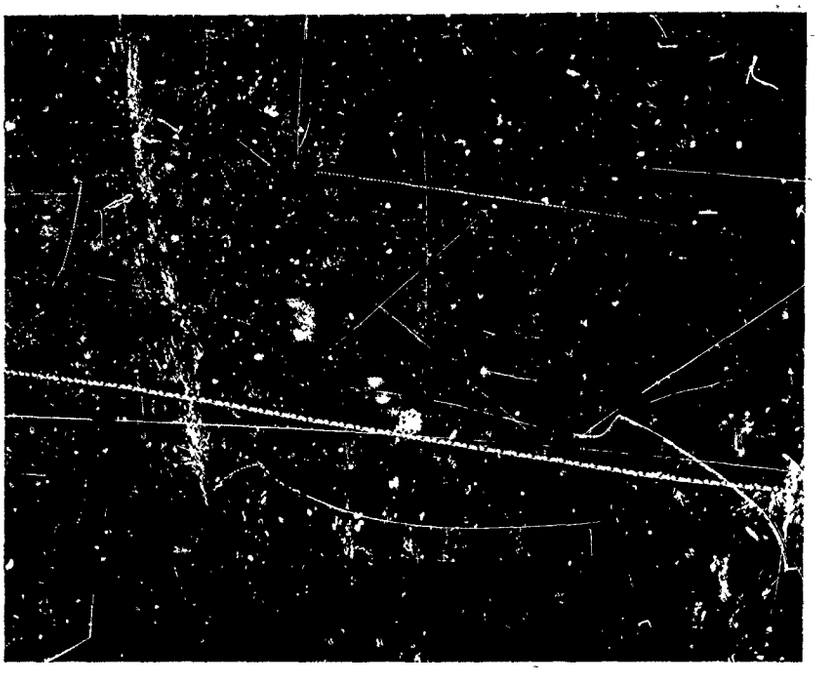

Cold Zone

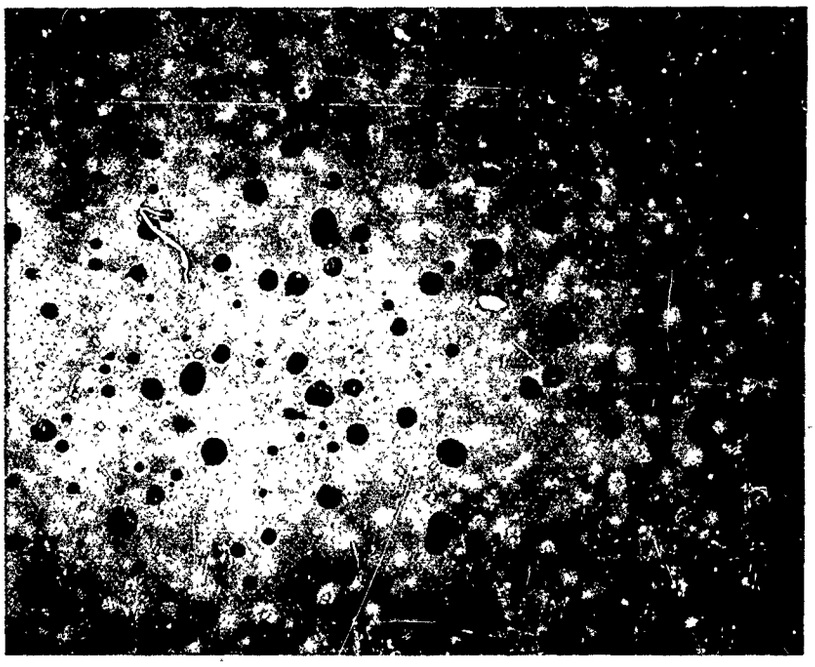

Hot Zone
(after heating
to 1870°C)

Figure 18. Photomicrographs of Cross Sections of MORGANITE Alumina Sample (500 X Magnification)

TABLE 7

SPECTROGRAPHIC ANALYSIS OF LUCALOX SAMPLE

Element	Per Cent
Al	greater than 0.1
Mg	0.01 to 0.1
Si	0.01 to 0.1
Fe	less than 0.01
Cr	less than 0.01
Sn	less than 0.01
Ni	less than 0.01
Cu	less than 0.01
Mn	less than 0.01
Pb	less than 0.01
Ag	less than 0.01

Photomicrographs of the hot and cold zone cross sections (Figure 19, 150 X magnification) show some grain growth on heating and further substantiate the very low porosity of this type of alumina.

6. Zirconium Silicate

Three 9-inch long x approximately $^{25}/_{64}$-inch O.D. x $^{17}/_{64}$-inch I.D. zirconium silicate tubes manufactured by the Zirconium Corporation of America were used. The manufacturer's reported density was 4.32/gm/cm^3. and the density as measured at this Laboratory was 4.03 gm/cm^3. Table 8 shows the manufacturer's chemical analysis of the samples and Table 9 gives our spectrographic analysis.

TABLE 8

MANUFACTURER'S TYPICAL CHEMICAL ANALYSIS OF THE ZIRCONIUM SILICATE SAMPLES

Compound	Per Cent
$ZrSiO_4$	96
Solid Solution of MULLITE	max. 3.8 %
K_2O, Na_2O, CaO, MgO, and Fe_2O_3	max. 0.2 %

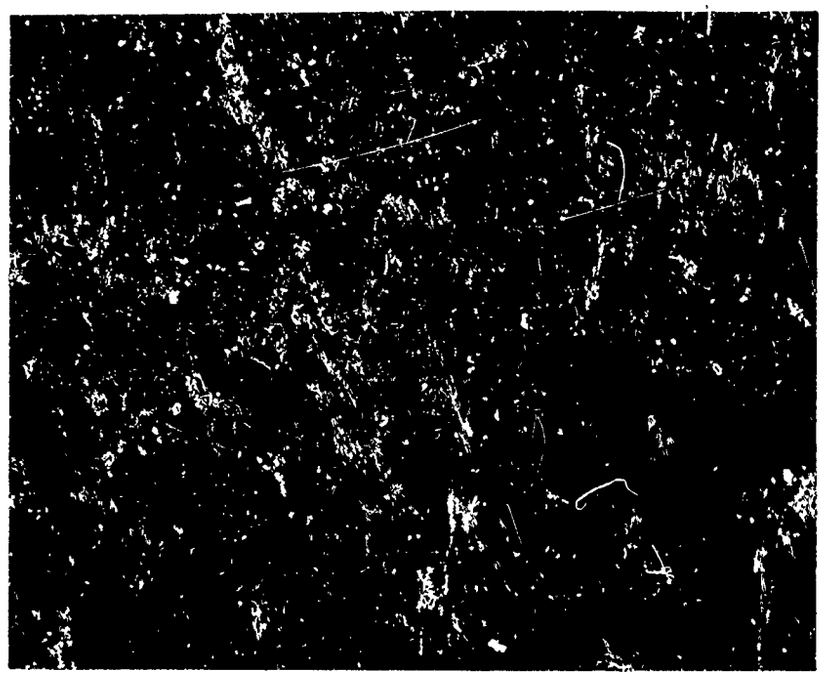

Cold Zone

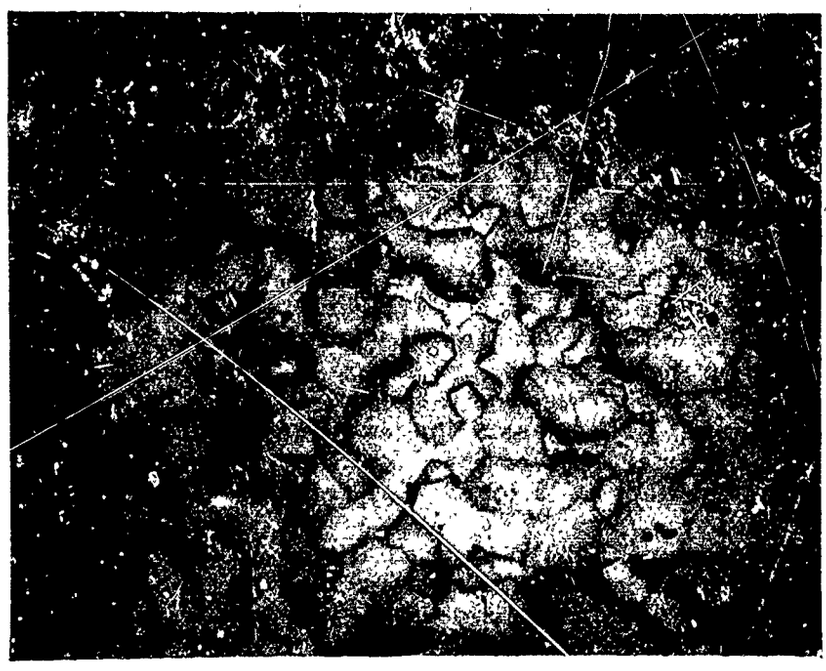

Hot Zone
(after heating
to 1850°C)

Figure 19. Photomicrographs of Cross Sections of LUCALOX Sample (150 X Magnification)

TABLE 9

SPECTROGRAPHIC ANALYSIS OF ZIRCONIUM SILICATE SAMPLE

Element	Per Cent
Zr	greater than 0.1
Si	greater than 0.1
Y	0.01 to 0.1
Al	0.01 to 0.1
Ti	0.01 to 0.1
Hf	0.01 to 0.1
Fe	0.01 to 0.1
Mg	0.01 to 0.1
Mn	0.01 to 0.1
Pb	0.01 to 0.1
Cu	less than 0.01
Ni	less than 0.01
Cr	less than 0.01

Figure 20 shows the photomicrographs of the zirconium silicate hot zone and cold zone cross sections. The magnification of the cold zone is 150 X and the hot zone 25 X. A lower magnification was used for the hot zone to better depict the extreme porosity.

Results and Discussion

1. Permeability of Thoria to Oxygen

Some studies on the permeability of thoria to oxygen have already been reported in the previous Summary Report[2]. There it was stated that the permeability varied approximately with the one-fourth to one-fifth power of the oxygen pressure on the high pressure side. In the present work the permeability dependence on the oxygen pressure on the low pressure side of the sample was determined. The measurements were carried out using the iridium susceptor, at a temperature of 1535°C. The oxygen pressure on the high pressure side was kept at 25 torr. The results are given in Table 10.

The data in Table 10 show that the permeability is nearly independent of the oxygen pressure on the low pressure side. Comparison between the present data and those obtained previously[2] with a graphite susceptor further proves this point. In the previous runs, the downstream oxygen partial pressure was many orders of magnitude lower than in the present investigation (since all the oxygen diffusing through the tube immediately reacted with the susceptor to form carbon monoxide) yet the measured

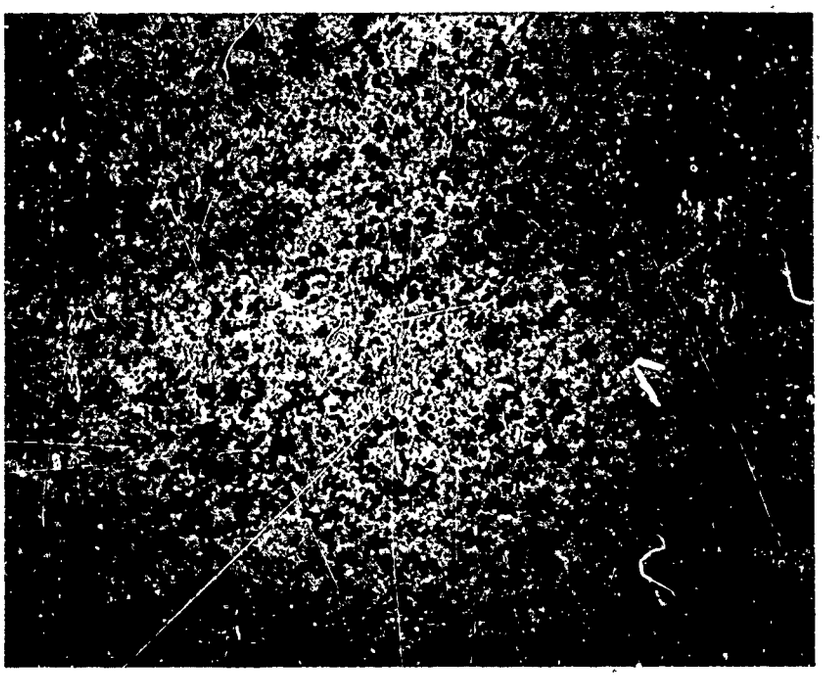

Cold Zone
150 X Mag.

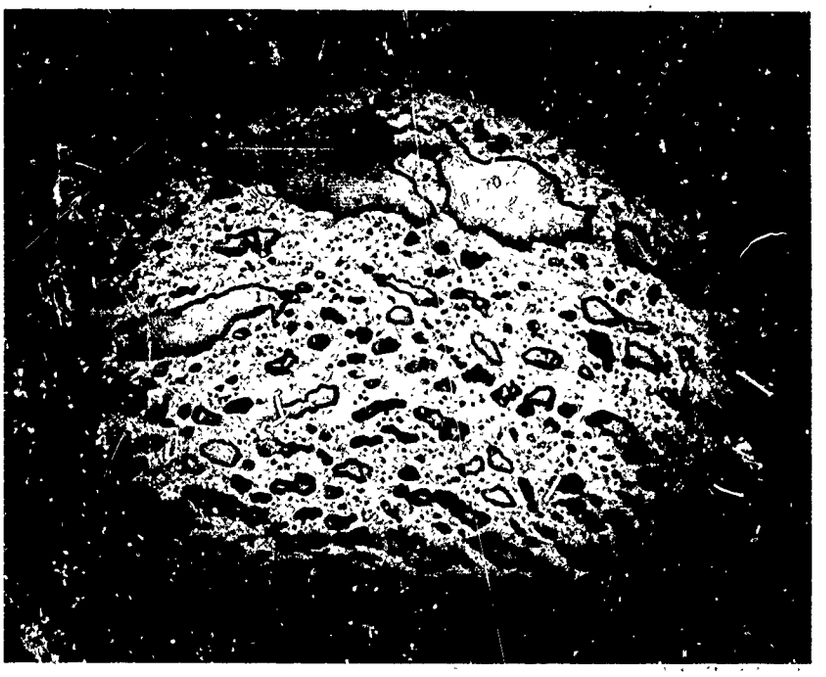

Hot Zone
25 X Mag.
(after heating
to 1745°C)

Figure 20. Photomicrographs of Cross Sections of Zirconium Silicate Sample

TABLE 10

OXYGEN PERMEATION THROUGH THORIA AS FUNCTION OF PRESSURE

Oxygen pressure on high-pressure side constant at 25 torr

Pressure (torr)	O_2 Flow Rate (gm/sec)
1.2×10^{-2}	5.94×10^{-7}
5.1×10^{-2}	5.90×10^{-7}
2.2×10^{-1}	5.55×10^{-7}

permeability was only twice as high. The comparison is somewhat uncertain, however, since the permeabilities are based on two different tubes. Thus, although the permeability varies with the one-fourth to one-fifth power of the oxygen pressure on the high pressure side, there is no corresponding pressure dependence on the low pressure (downstream) side; at most, the pressure dependence is so small that it does not significantly influence the usefulness of the oxides as coating materials.

2. Permeability of Alumina-Coated Thoria to Oxygen

Previous measurements[2] on thoria gave slightly smaller oxygen permeabilities when LUCALOX washers were used instead of tantalum washers to separate the thoria tube from the graphite susceptor. The effect, although very small, appeared real and could conceivably have been due to doping of the thoria with alumina via solid state diffusion. A further investigation seemed warranted. For this purpose, a thoria tube (obtained from the Zirconium Corporation of America) was coated with a thin, discontinuous layer of alumina by immersing in a Al_2O_3 slurry and subsequent firing for four hours to 1700°C in pure oxygen at atmospheric pressure. Due to the larger contact area between ThO_2 and Al_2O_3 and the long firing time, any effect of alumina diffusion on the permeability should have been enhanced. The results of permeability measurements on this tube are shown in Figure 21.

The points represent permeability data obtained on the alumina-coated thoria sample using 50 torr of oxygen inside the sample. The dotted and dashed lines show the permeability data obtained on the two previously studied uncoated thoria samples. Although the two uncoated thoria samples were from the same shipment, they exhibited slightly different permeabilities, showing the variation that can be expected between two samples of supposedly identical structure and composition. The alumina-coated thoria sample is from the same manufacturer but from a different lot from the two uncoated thoria samples. Although the alumina-coated sample has a slightly lower permeability and a somewhat higher activation energy for oxygen permeation, the differences are too small to be considered significant.

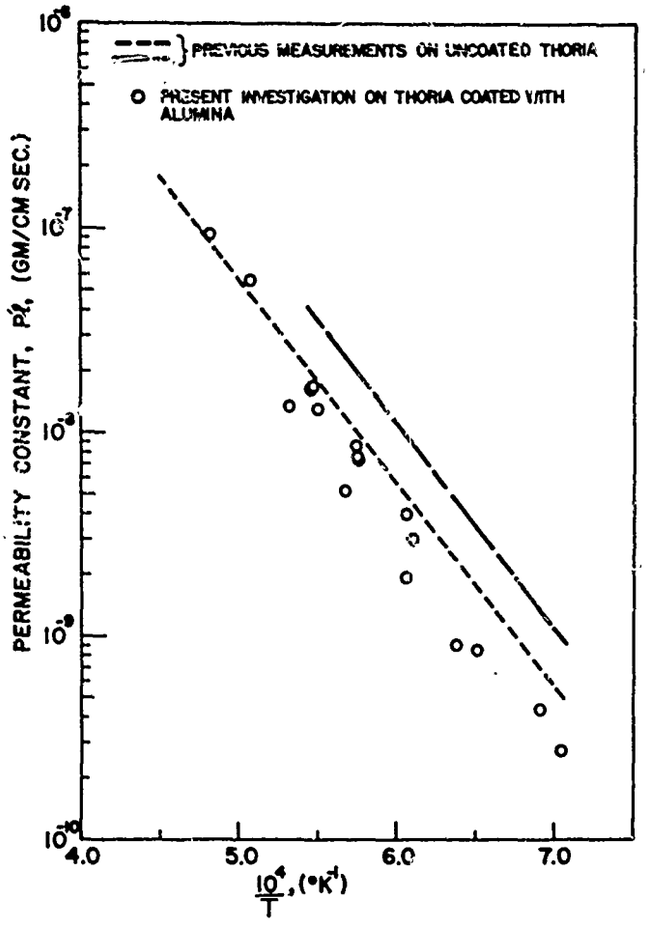

Figure 21. Temperature Dependence of Permeability Constant, $P\ell$, of Thoria to 50 torr of Oxygen

3. Permeability of Beryllia to Oxygen

Permeability measurements were made on two separate samples. The first sample exhibited no observable permeability to 50 torr of oxygen from 1235° to 1535°C; however, when a run was attempted at 1600°C, the sample became pervious as indicated by argon and nitrogen permeation and could not be used for any further studies. The second sample exhibited no observable permeability to 50 torr of oxygen from 1545° to 1790°C but became pervious at 1860°C. Sintered beryllia seems to have the characteristic of becoming pervious at elevated temperatures.

After the second sample became pervious, an attempt was made to obtain the permeability to oxygen by separately measuring the diffusion of oxygen and nitrogen through the sample. By subtracting the nitrogen diffusion (which consists of pore diffusion) from the oxygen diffusion (which consists of pore diffusion and other diffusion mechanisms) it was hoped that some idea of the permeability of beryllia to oxygen could be obtained. However, this method failed, since the pore structure kept changing with each successive run. Since the flow of nitrogen at a constant pressure difference across the sample is proportional to the conductance of the pores, the data in Figure 22 show how the pore structure changed with each run. (Note particularly the difference between the two runs at 1110°C.) It is impossible to get meaningful data when this type of behavior is observed. An attempt was made to sinter the sample to a nonporous state by holding it at a temperature of 1900°C for six hours with high vacuum on both sides. This effort proved unsuccessful.

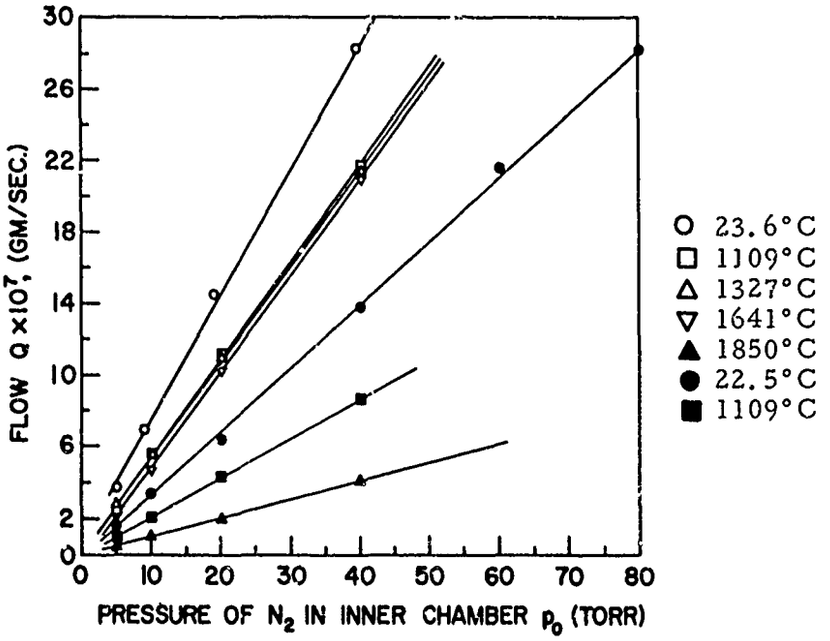

Figure 22. Flow Versus Pressure of N_2 in Inner Chamber for BeO Sample No. 2

Since there was no observable permeability of beryllia to oxygen in the temperature range of 1235° to 1790°C, an upper limit for the permeability constant can be calculated. The permeability constant, $P\ell$, of beryllia to oxygen at 50 torr is less than 3×10^{-10} gm/cm sec in the temperature range of 1235° to 1790°C.

4. Permeability of Yttria-Stabilized Zirconia to Oxygen

Oxygen permeability measurements were carried out on two yttria-stabilized zirconia samples over the temperature range of 1315° to 1960°C. As shown in Figures 23 and 24, the permeability was pressure dependent, changing with approximately the one-fourth power of the oxygen pressure on the high pressure side at both 1426° and 1520°C.

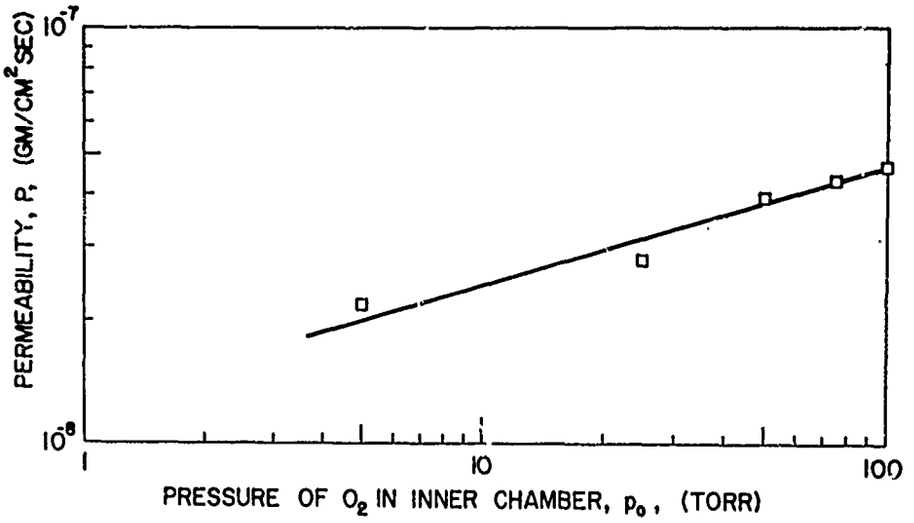

Figure 23. Pressure Dependence of Permeability, P, of $Zr_{0.91}Y_{0.09}O_{1.96}$ to Oxygen at 1426°C

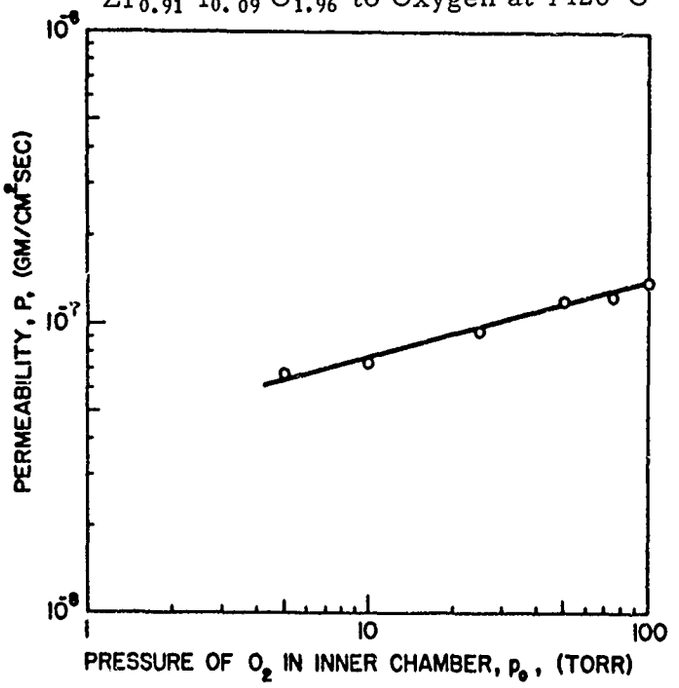

Figure 24. Pressure Dependence of Permeability, P, of $Zr_{0.91}Y_{0.09}O_{1.96}$ to Oxygen at 1520°C.

The permeability as a function of the oxygen pressure on the low pressure side was also determined, using the iridium susceptor. Table 11 gives the results obtained at 1535°C and shows that the permeability is nearly independent of the oxygen pressure on the low pressure side.

TABLE 11

OXYGEN PERMEATION THROUGH YTTRIA-STABILIZED ZIRCONIA AS FUNCTION OF PRESSURE

Oxygen pressure on high pressure side constant at 25 torr

Pressure (torr)	O_2 Flow Rate (gm/sec)
2.0×10^{-2}	10.3×10^{-7}
3.2×10^{-2}	10.4×10^{-7}
5.1×10^{-2}	9.8×10^{-7}
6.4×10^{-2}	9.6×10^{-7}
7.3×10^{-2}	9.6×10^{-7}

Previous determinations on the same sample using a graphite susceptor[2] further substantiate this conclusion. In the previous runs, the downstream oxygen partial pressure was orders of magnitude lower than in the present investigation, since all the oxygen diffusing through the tube immediately reacted to form carbon monoxide, yet the permeability was only 30 per cent higher.

The temperature dependence of the permeability constant is given in Figure 25. The data were obtained directly by measuring the permeability with 50 torr of oxygen in the inner chamber of the tube or were determined by correcting the known oxygen pressure to 50 torr, using the pressure dependence shown in Figures 23 and 24. The permeability constant for yttria-stabilized zirconia in the temperature range of 1315° to 1960°C can be expressed by

$$P\ell = 2.1\, e^{-65,900/RT} \text{ (gm/cm sec)}$$

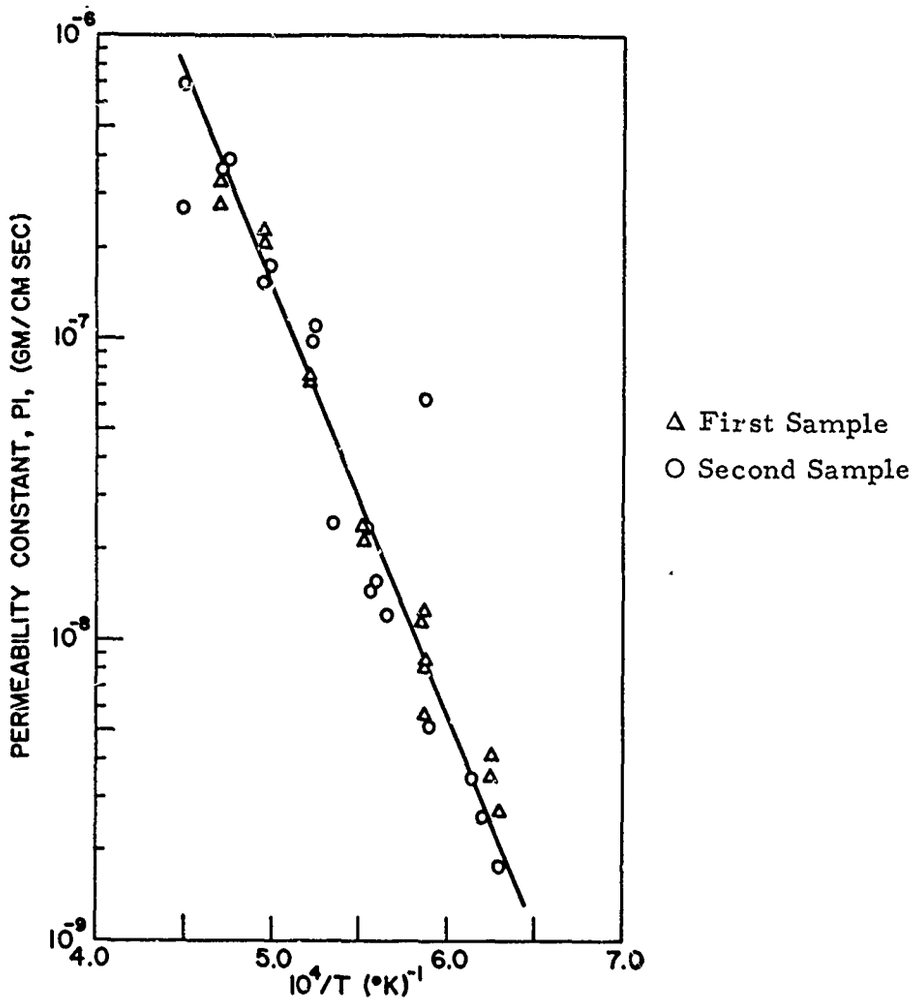

Figure 25. Temperature Dependence of Permeability Constant, $P\ell$, of $Zr_{0.91}\ Y_{0.09}\ O_{1.96}$ to 50 torr of Oxygen

5. Permeability of Zirconia Grade ZIRCOA 1027 to Oxygen

Permeability measurements were carried out on two samples of zirconia ZIRCOA 1027. The first sample became pervious during an initial run at 1700°C, and the second sample became pervious at 1525°C. During heating, large quantities of silicon monoxide distilled off the samples and after heating, the tubes were extremely brittle. These characteristics nearly eliminate this material for use as a coating to protect graphite, although it would have been attractive on the basis of its low thermal expansion and, hence, better thermal shock resistance and better mechanical compatibility with graphite.

The temperature dependence of the permeability constant for ZIRCOA 1027 at 50 torr oxygen pressure is shown in Figure 26 and given by

$$P\ell = 4.9\, e^{-70,900/RT} \text{ (gm/cm sec)}$$

in the range 1300° to 1525°C.

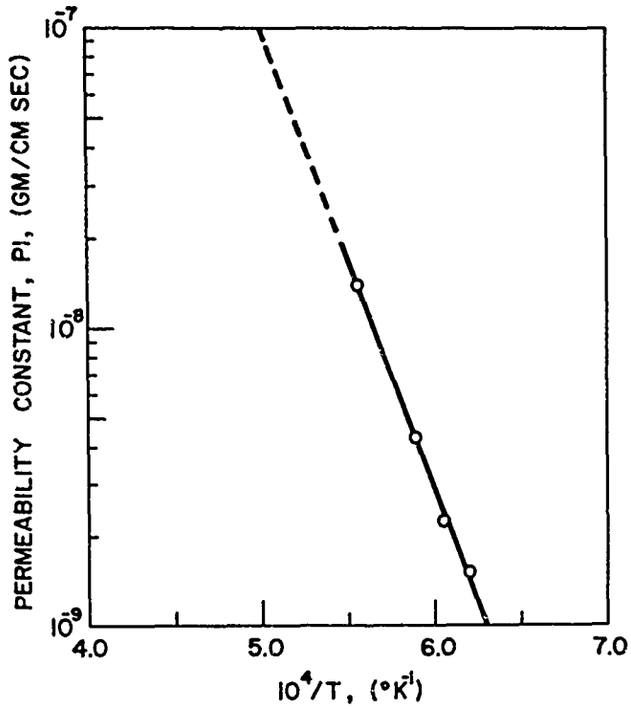

Figure 26. Temperature Dependence of Permeability Constant, $P\ell$, of ZIRCOA 1027 to 50 torr of Oxygen

6. Permeability of Alumina to Oxygen

a. Polycrystalline Alumina, MORGANITE Grade RR

Preliminary permeability measurements on MORGANITE alumina, using the graphite susceptor, showed that the permeability to oxygen was extremely low. Moreover, there was some reaction between Al_2O_3 and CO, leading to formation of aluminumoxicarbide, Al_4O_4C, which condensed on the cooler portions of the tube and was identified by X-ray structural analysis. The existence of Al_4O_4C is a relatively new discovery, first described by Foster and co-workers[9]. All results reported here on alumina were obtained using the iridium susceptor. Very long outgassing times were used, until the background pressure was reduced to 10^{-6} torr.

The permeability of MORGANITE alumina to 50 torr oxygen in the temperature range 1745° to 1870°C is shown in Figure 27 and can be expressed by

$$P\ell = 3.1 \times 10^4 \, e^{-134,000/RT} \ (gm/cm\ sec)$$

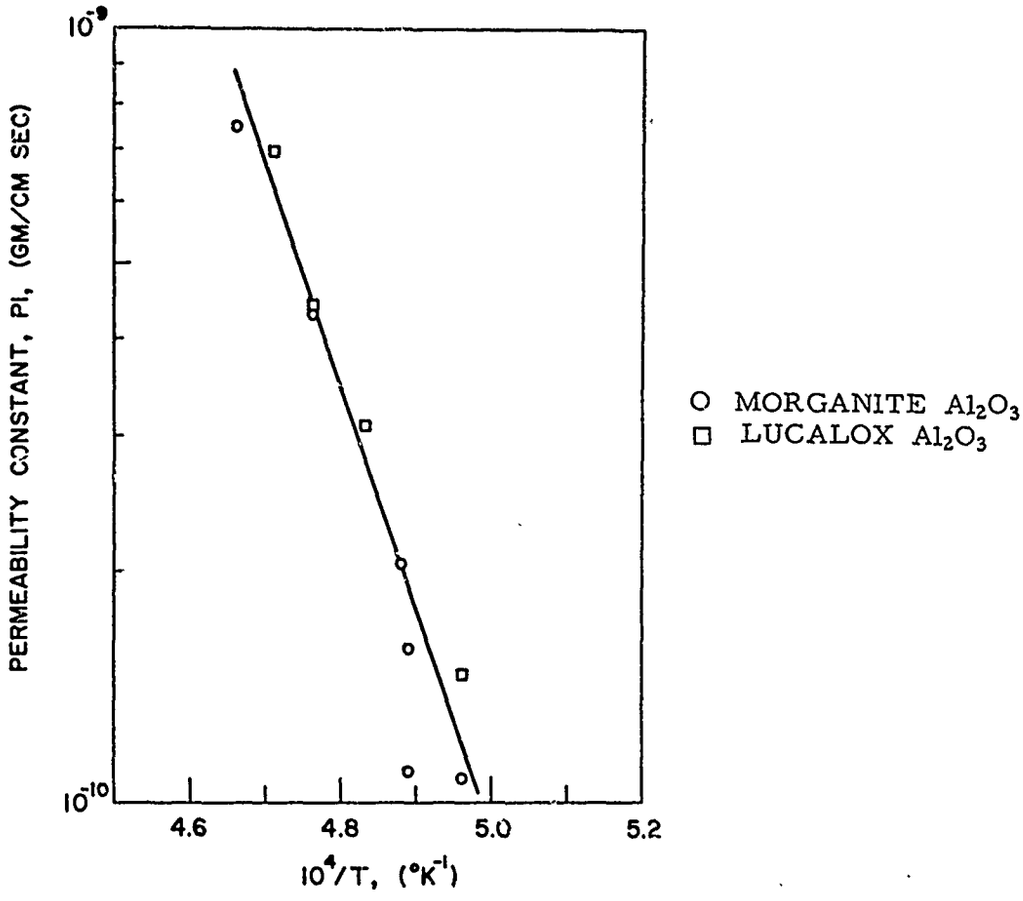

Figure 27. Temperature Dependence of Permeability Constant, $P\ell$, of MORGANITE Alumina and LUCALOX Alumina to 50 torr of Oxygen

At temperatures below 1745°C, the amount of oxygen coming through the sample was too small for accurate measurement. At temperatures above 1870°C the results became erratic, with oxygen frequently coming through in great bursts. Also, several tubes became pervious on heating to 1900°C.

b. LUCALOX Polycrystalline Alumina

The permeability of LUCALOX alumina tubes to oxygen was investigated in the temperature range 1745° to 1850°C using the iridium susceptor. At 50 torr oxygen pressure, the permeability constant is given by the same expression as for MORGANITE alumina. The graphical results of the temperature dependence of the permeability constant are given in Figure 27 together with the results for MORGANITE alumina. Below 1745°C the amount of O_2 coming through the sample was again too small for accurate measurements. Above 1850°C the sample changed, the permeability became erratic, and meaningful measurements could not be obtained.

New (as received) LUCALOX tubes exhibited a permeability proportional to the one-fourth power of the oxygen pressure (see Figure 28). However, in later runs on the same samples, the pressure dependence was much smaller. Furthermore, fresh (as received) tubes outgassed very little on heating in vacuo; and consequently, a very low background pressure could be obtained. Once a tube had been exposed to oxygen at high temperatures, however, it degassed considerably and mass spectrometric analysis showed that the gas was almost pure oxygen. The rate of degassing decreased only very slowly with time and was considerable even after ten hours in vacuo at 1750°C. The quantity of oxygen removed from a tube during ten hours at 1750°C corresponded to approximately one-tenth of one per cent of the total oxygen content of the hot section of the LUCALOX Al_2O_3 tube. MORGANITE alumina did not show this peculiar degassing behavior, for which no explanation is, as yet, available.

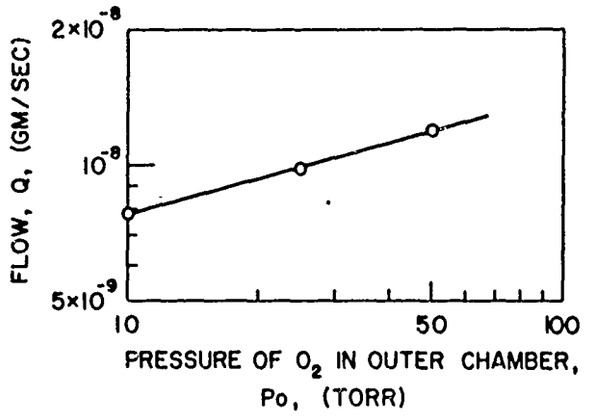

Figure 28. Pressure Dependence of Permeability, P, of LUCALOX Alumina to Oxygen at 1745°C.

The difference in permeabilities between the MORGANITE alumina and the LUCALOX are so small as to be essentially within our limits of error. Since LUCALOX is 100 per cent dense alumina, while MORGANITE has a porosity of 5 per cent, this indicates that a small degree of porosity does not affect the permeability.

It is interesting to compare our data on alumina with those of Oishi and Kingery [10] who measured oxygen self-diffusion in single crystal and polycrystalline alumina. Kingery found activation energies of 152 kcal/mole for single crystal and of 110 kcal/mole for polycrystalline samples. Our value of 134 kcal/mole is between these values. Furthermore, since the permeability is related to the diffusivity by Fick's law

$$P = -D \frac{dc}{dx},$$

one may calculate the concentration of the diffusing species (oxygen vacancies or, less likely, oxygen interstitials). For this, we assume that the diffusivity, D, is independent of concentration, in which case

$$P\ell = D\,(C_1 - C_2),$$

where C_1 and C_2 are the concentrations of the diffusing species at the two boundaries. At 1750°C, $P\ell \approx 10^{-10}$ g cm^{-1} sec^{-1} and Kingery's $D \approx 10^{-12}$ cm^2 sec^{-1} (for polycrystalline alumina). Thus, one calculates $(C_1 - C_2) \approx 10^2$ gm cm^{-3}, an obviously impossible result. The disagreement can be explained only by assuming that the diffusion mechanism in the presence of a concentration gradient (our case) differs substantially from the process of oxygen self-diffusion as measured in Kingery's work. This points out the danger inherent in any attempt to convert self-diffusion coefficients into permeabilities, which are required for predictions of coating performance.

7. Permeability of Zirconium Silicate to Oxygen

Oxygen permeability studies were made on three tubes using the graphite susceptor. The first tube softened and blew out on heating to 1750°C (with 50 torr of oxygen inside and vacuum outside), as shown in Figure 29. This softening is apparently caused by dissociation into the component single oxides, which has been reported to occur at 1730°C [11]. As a precaution, the second tube was heated no higher than 1600°C; it remained impervious to argon and nitrogen up to this temperature. However, the oxygen "permeability" as measured by the quantity of CO reaching the detection system was found to be independent of the oxygen pressure inside the tube, remaining constant even when the tube was evacuated. Since under these conditions the only possible oxygen source was the zirconium silicate itself, it is obvious that the material was being reduced on heating to 1300°C or higher in vacuo. This reduction of one or both constituents of the mixed oxide apparently takes place by the following chain reaction:

$$MeO_2 + CO \rightarrow MeO + CO_2$$

$$CO_2 + C \text{ (graphite susceptor)} \rightarrow 2\,CO.$$

Figure 29. Zirconium Silicate Tube Heated to 1750°C

To prevent this reaction, a third tube was studied using the iridium susceptor and meaningful results could then be obtained. Between 1430° and 1665°C the permeability constant of zirconium silicate to oxygen at 50 torr pressure is shown in Figure 30 and given by the expression:

$$P\ell = 16.0\, e^{-87,500/RT} \text{ (gm/cm sec)}.$$

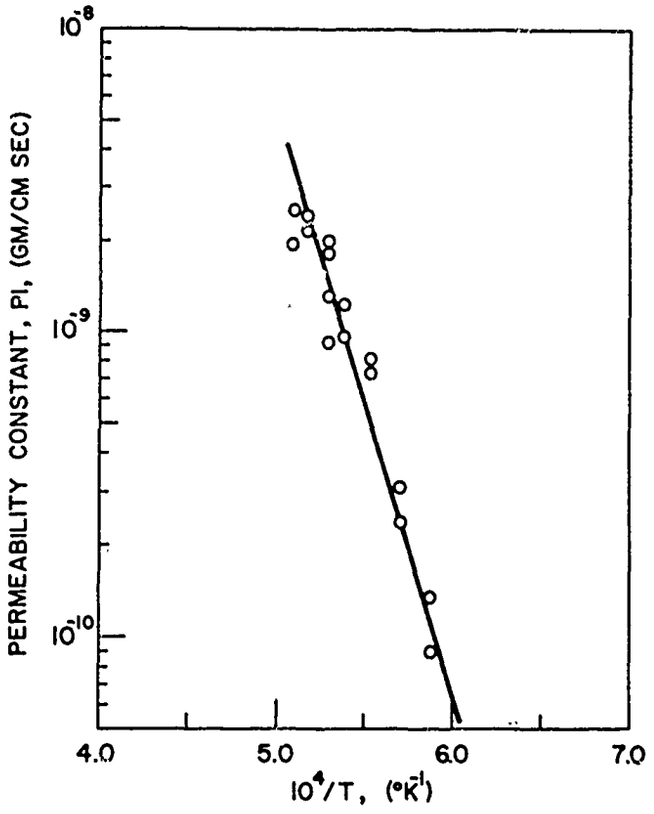

Figure 30. Permeability of $ZrSiO_4$ to Oxygen

The data in Figure 30 were either obtained using an oxygen pressure of 50 torr or were corrected to 50 torr using the experimentally measured one-third power pressure dependence. An attempt was made to obtain permeability data at 1745°C, but the sample again softened and became pervious. Below 1430°C the amount of oxygen diffusing through the sample was so small that it approached the limit of detection.

The permeability of zirconium silicate at 1588°C changed with the one-third power of the oxygen pressure as shown in Figure 31.

Up to 1700°C the permeability of zirconium silicate to oxygen is substantially lower than that of zirconia, and comparable to that of alumina or beryllia. However, at approximately 1700°C zirconium silicate decomposes into the component oxides.

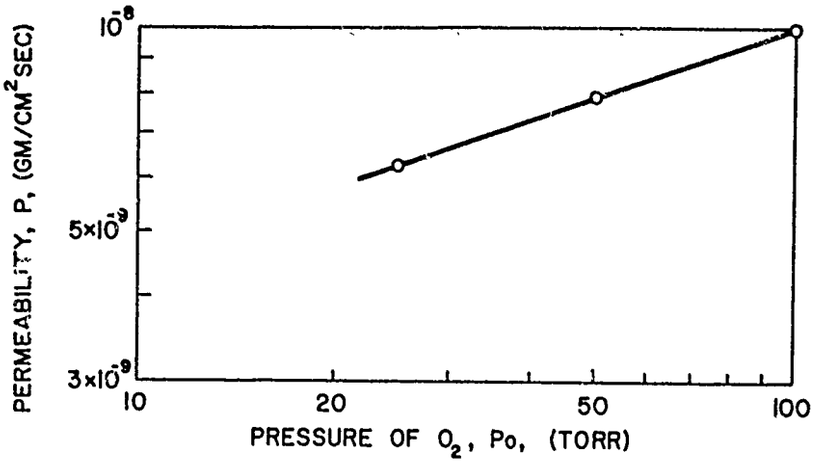

Figure 31. Pressure Dependence of Permeability, P, of Zirconium Silicate to Oxygen at 1588°C

Characterization of Previously Studied Materials

1. Photomicrographs of Previously Studied Materials

In the previous Summary Report, photomicrographs of the structure of some of the sintered oxides used in the oxygen permeation studies were at a magnification of 150 X. New photomicrographs (Figures 32, 33, and 34) of the same materials at 300 X magnification have now been made and better depict the structural changes which occurred on heating. For calcia-stabilized zirconia and calcia-stabilized hafnia, these changes have been discussed in the previous Summary Report[2]; the larger magnification pictures only confirm the observations. The 150 X photomicrographs of thoria, however, showed few details due to the extremely small particle size of the sintered material. The larger magnification photos show that definite changes occurred in thoria also when it was heated to 1930°C. A small amount of a secondary phase can be seen in the as-received material; the secondary phase is no longer discernible after heating. In addition, sintering has progressed further, since point contacts between grains have virtually disappeared in the 1930°C material. The pore structure has changed slightly: most of the smaller pores appear to have combined with the larger ones.

2. Electron Microprobe Analysis of Previously Studied Materials

An electron microprobe analysis was performed at the Union Carbide Corporation, Metals Division, on the hot and cold zones of the previously studied thoria, calcia-stabilized zirconia, and calcia-stabilized hafnia tubes. The typical electron and X-ray scanning images are shown in Figures 35 through 58. The pulse counts for each of the areas on the electron images are summarized in Table 12.

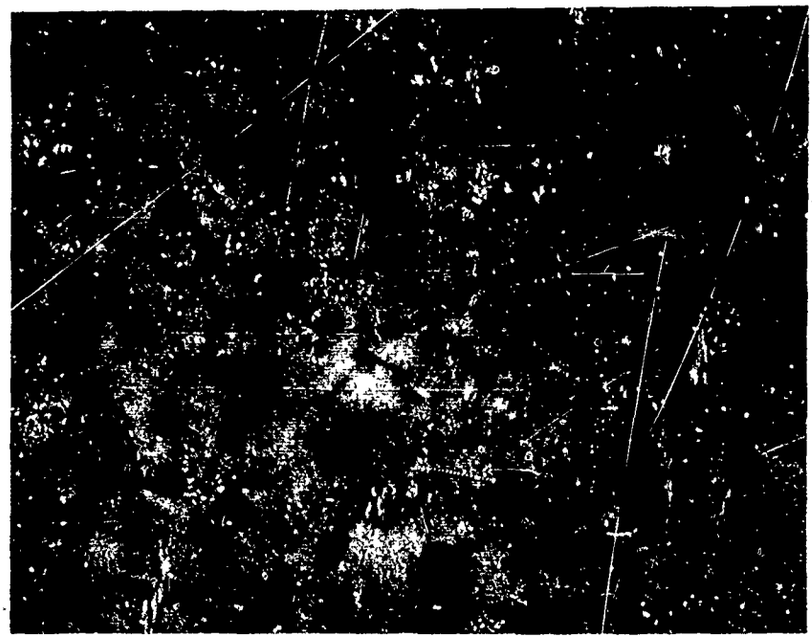

Cold Zone

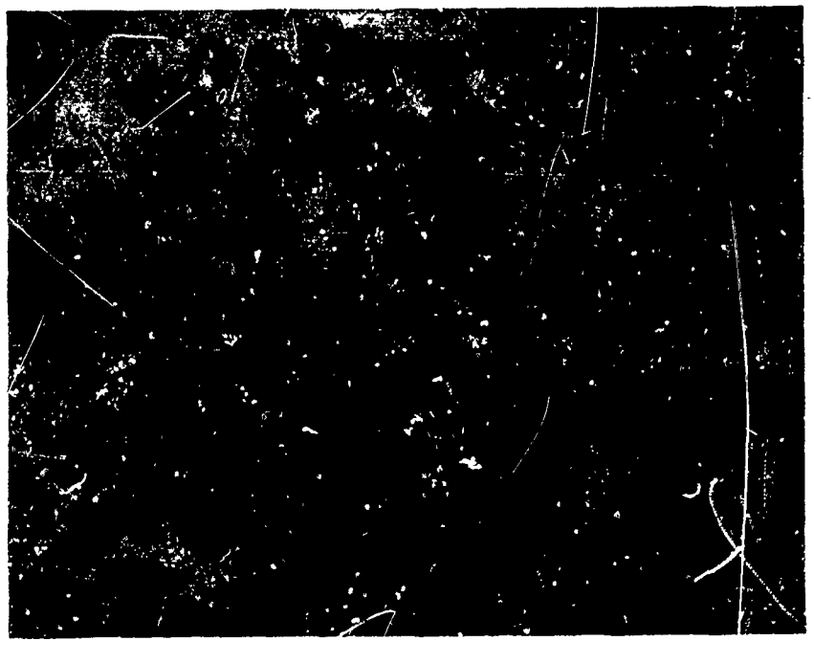

Hot Zone
(after heating
to 2060°C)

Figure 32. Photomicrographs of Cross Sections of Calcia-Stabilized Zirconia Sample (300 X Magnification)

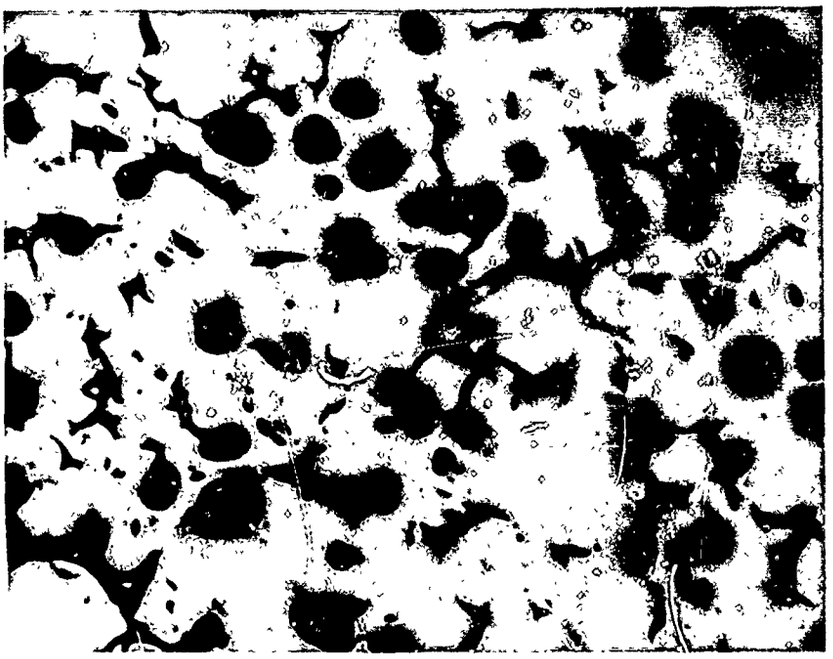

Cold Zone

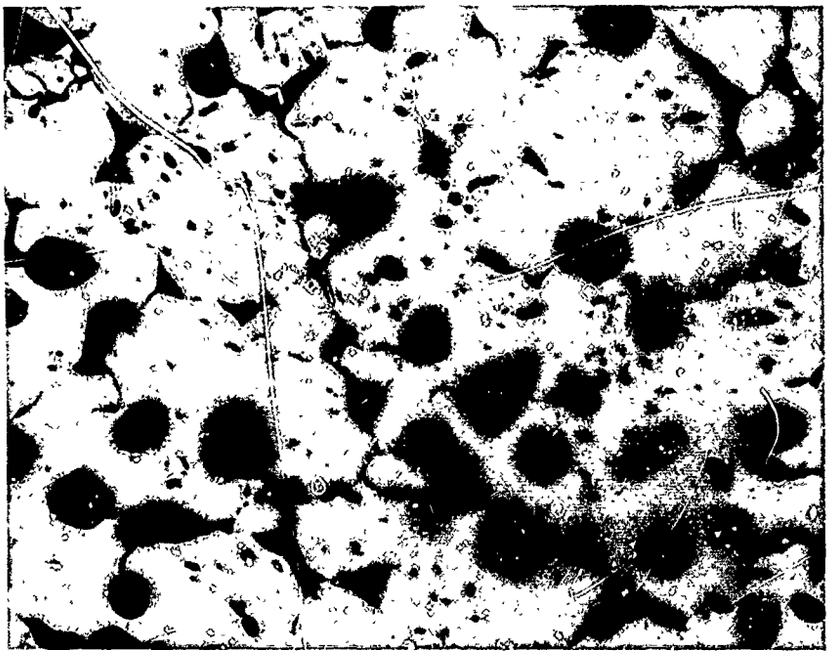

Hot Zone
(after heating
to 1640°C)

Figure 33. Photomicrographs of Cross Sections of Calcia-Stabilized Hafnia Sample (300 X Magnification)

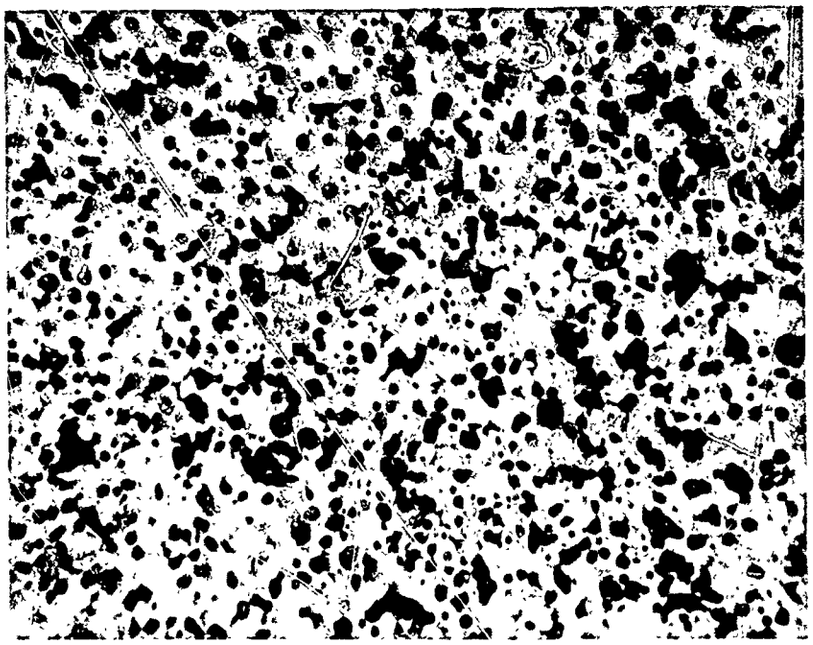

Cold Zone

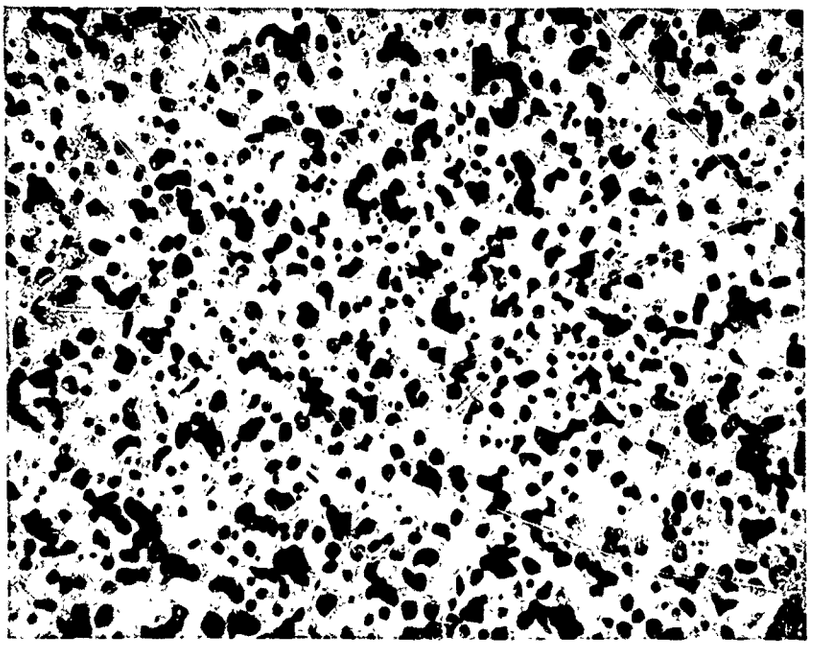

Hot Zone
(after heating
to 1930°C)

Figure 34. Photomicrographs of Cross Sections of Thoria Sample (300 X Magnification)

Figure 35. Electron Image

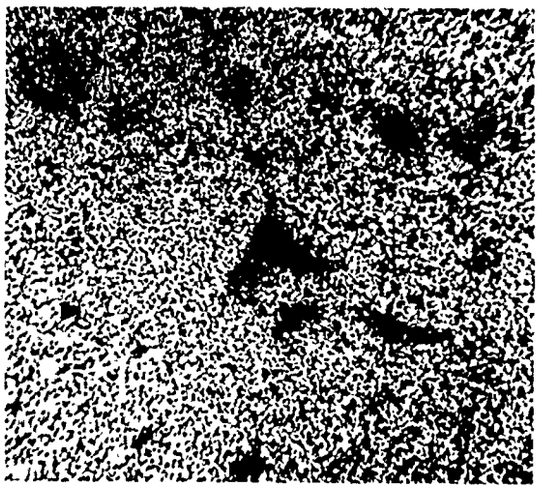

Figure 36. Zr Distribution

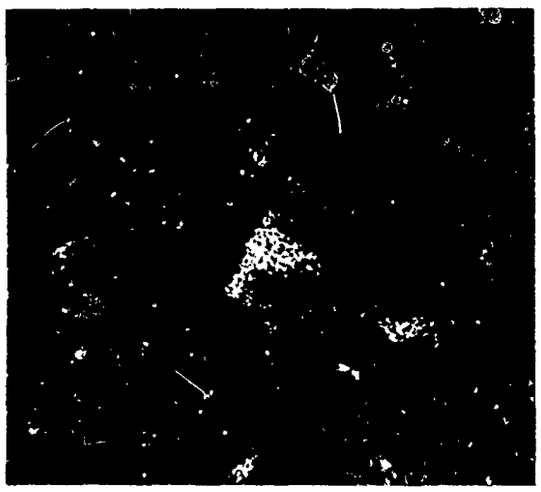

Figure 37. Ca Distribution

Calcia-Stabilized Zirconia, Cold End (700 X Magnification)

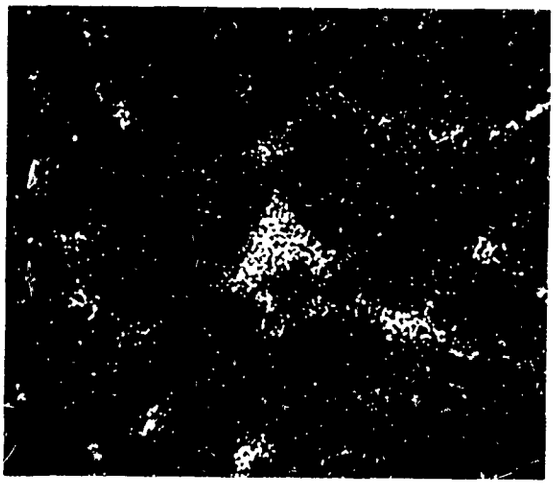

Figure 38. Si Distribution

Figure 39. Fe Distribution

Figure 40. Al Distribution

Calcia-Stabilized ZrO_2, Cold End (700 X Magnification)

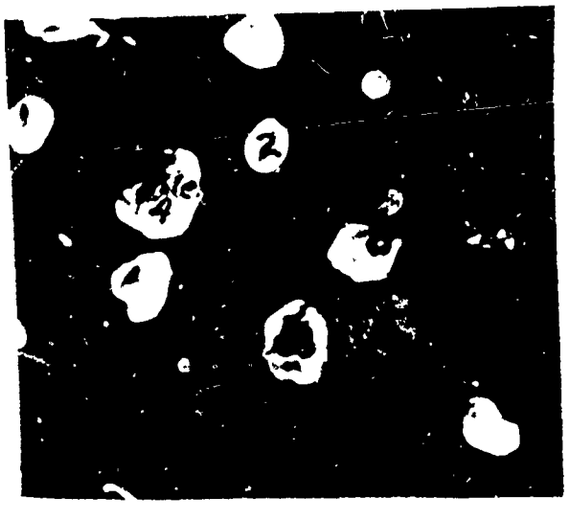

Figure 41. Electron Image

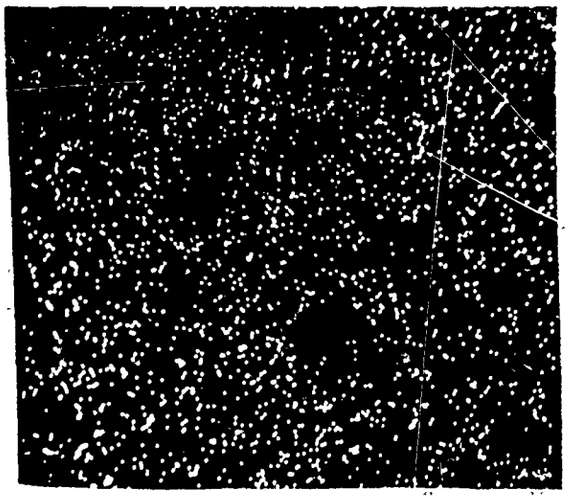

Figure 42. Ca Distribution

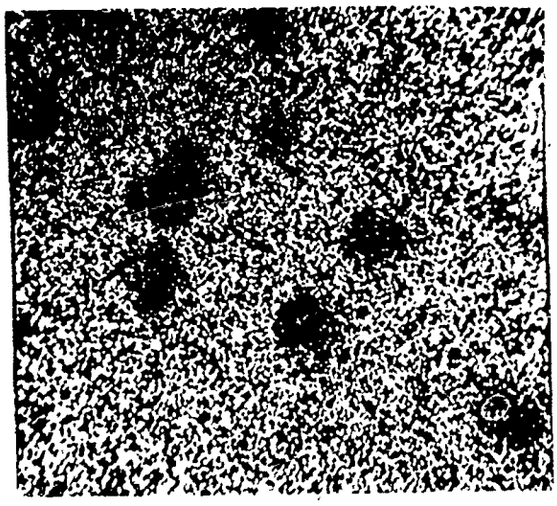

Figure 43. Zr Distribution

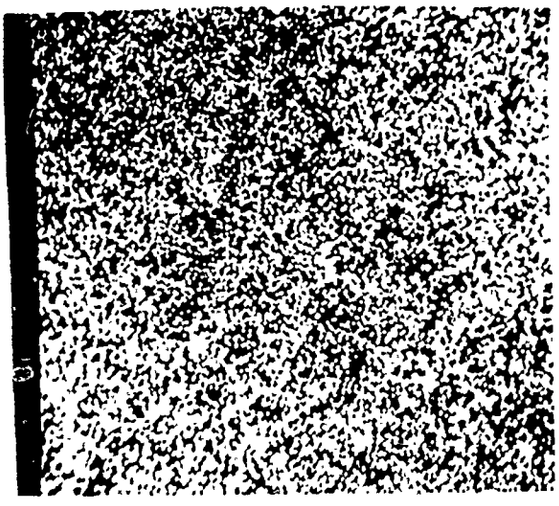

Figure 44. Hf Distribution

Calcia-Stabilized ZrO_2, Hot End (700 X Magnification)

Figure 45. Electron Image

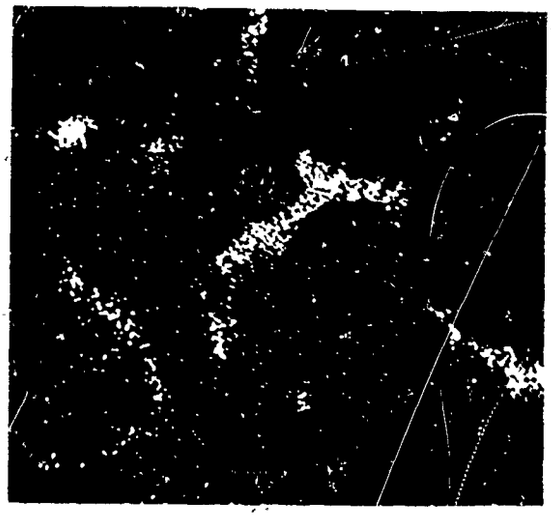

Figure 46. Si Distribution

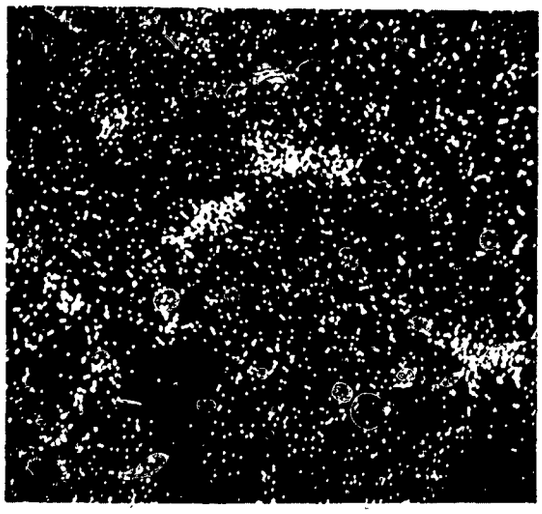

Figure 47. Ca Distribution

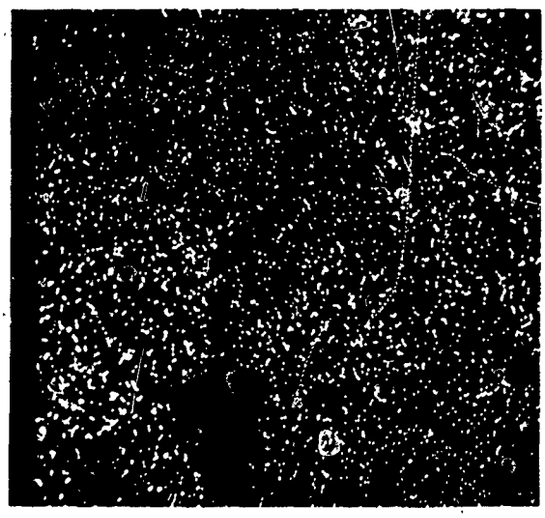

Figure 48. Zr Distribution

Calcia-Stabilized HfO_2, Cold End (700 X Magnification)

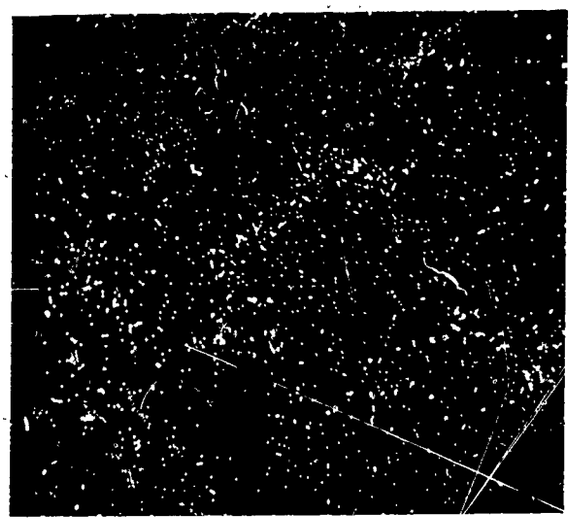

Figure 49. Ti Distribution

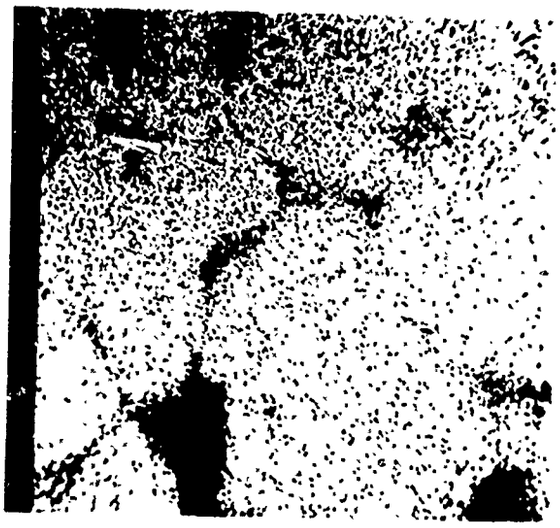

Figure 50. Hf Distribution

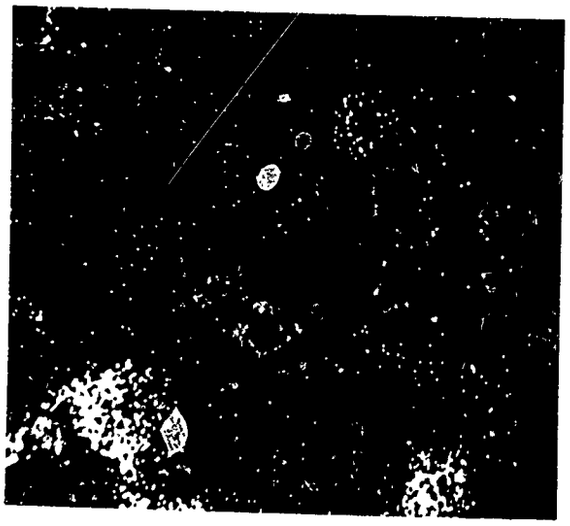

Figure 51. Al Distribution

Figure 52. Fe Distribution

Calcia-Stabilized HfO_2, Cold End (700 X Magnification)

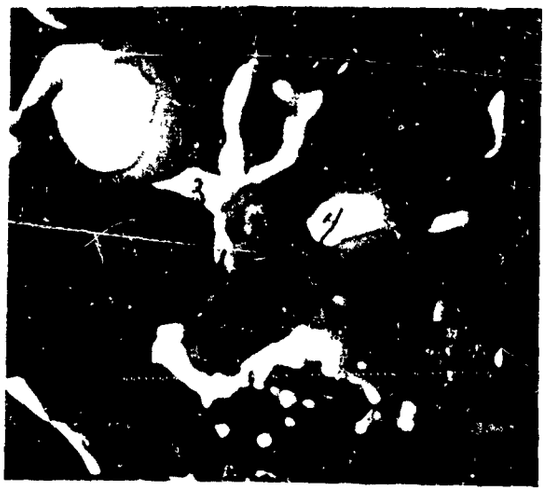

Figure 53. Electron Image

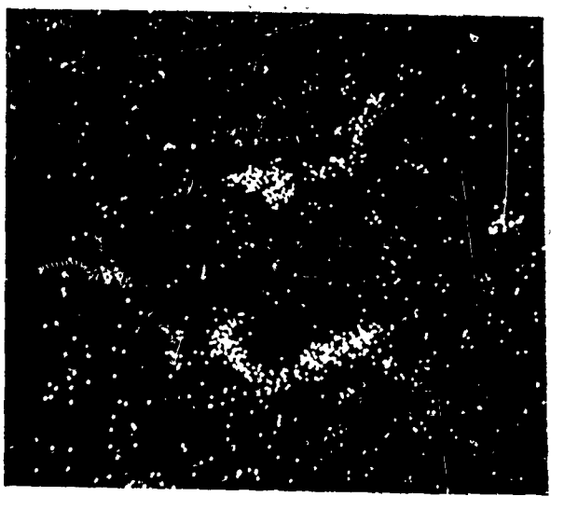

Figure 54. Si Distribution

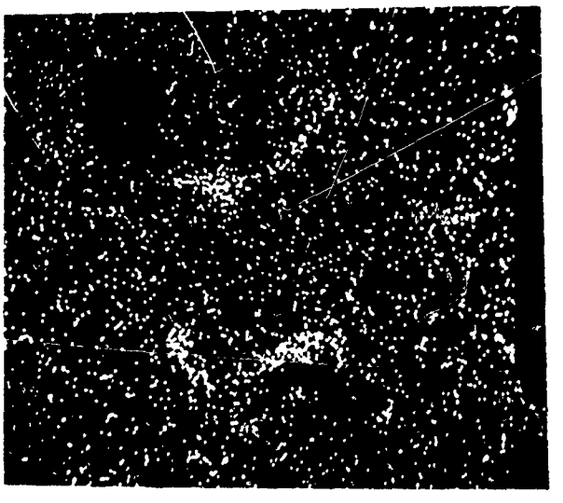

Figure 55. Ca Distribution

Calcia-Stabilized HfO_2, Hot End (700 X Magnification)

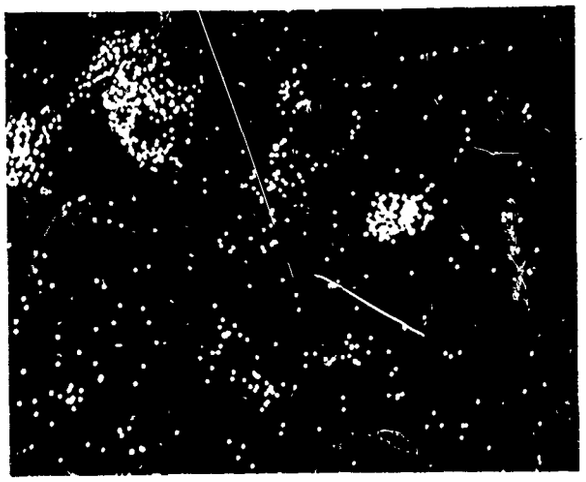

Figure 56. Al Distribution

Figure 57. Zr Distribution

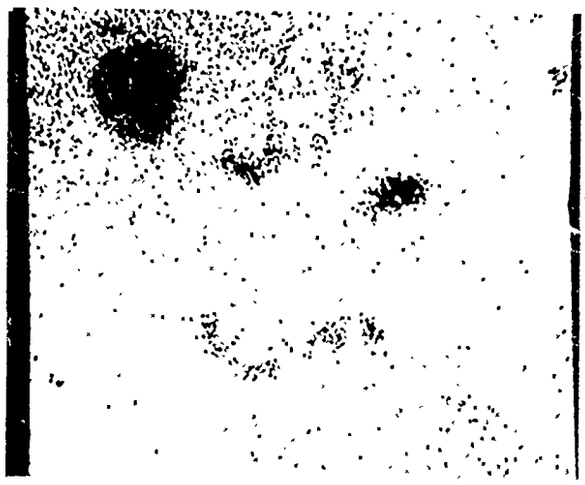

Figure 58. Hf Distribution

Calcia-Stabilized HfO_2, Hot End (700 X Magnification)

TABLE 12

ELECTRON MICROPROBE ANALYSIS OF OXIDE TUBES

Sample	Location	Area Scanned	Pulses per Second (B. G. corrected) Al	Ca	Si	Fe	Ti	Hf	Zr	Th
ZrO_2	Cold End	Light	14	1070	222	132	22	--	165	--
ZrO_2	Cold End	Matrix	0.4	98	0.7	36	5	--	990*	--
ZrO_2	Hot End	1 (gray)	38	22	1	5	0	76	566	--
ZrO_2	Hot End	2 (light)	90	35	1	0	0	77	39	--
ZrO_2	Hot End	3 (matrix)	0	82	1	6	0	78	606*	--
ZrO_2	Hot End	4 (hole)	594	0	0	0	0	0	0	--
HfO_2	Cold End	1 (gray)	22	28	59	17	5	2880	18	--
HfO_2	Cold End	2 (light)	8	612	150	72	42	1920	6	--
HfO_2	Cold End	3 (matrix)	0	70	1	18	9	3260	18	--
HfO_2	Cold End	4 (hole)	650	0	0	0	0	0	0	--
HfO_2	Hot End	1 (gray	24	0	0	0	0	2830	16	--
HfO_2	Hot End	2 (light)	141	743	162	14	10	640	1	--
HfO_2	Hot End	3 (matrix)	0	71	1	9	22	3230	20	--

* In comparing the hot and cold ends of the ZrO_2 sample, it will be noted that the intensity for zirconium in the matrix has dropped from 990 pulses per second to about 600 pulses per second. This resulted from a partial failure of the preamplifier during the hot end measurements and the intensities for other elements in the ZrO_2 hot end must also be considered to be relatively lower.

Figures 35, 41, 45, and 53 are electron scanning images and show the surfaces with contrast depending on the average atomic number of the constituents; that is, the matrices are the darkest, with the pores and the intergranular constituents (secondary phase) containing the lighter elements discernible as the light colored area. The other Figures are also scanning images, but instead of using the specimen current to modulate the brightness, the $K\alpha$ or $L\alpha$ radiation output was used. The lighter element magnesium could not be counted because the sensitivity limit for magnesium is about two per cent.

The aluminum contents for most of the light areas in the electron images are extraordinarily high as a result of the entrapment of aluminum oxide abrasive in cracks and holes.

This analysis shows that the cold end of the calcia-stabilized zirconia has a major zirconia phase which contains approximately three per cent calcia and a minor phase (network) which consists of calcium-silicate containing 12 per cent dissolved ZrO_2, 3 per cent Fe_2O_3, 7 per cent Al_2O_3, and 3 per cent TiO_2. The hot end of the calcia-stabilized zirconia is quite homogeneous and contains about 4 per cent CaO, about 2 per cent HfO_2, and traces of iron and silicon in solution.

Both the hot and cold ends of the hafnia are heterogeneous with the network enriched in lime, alumina, silica, iron oxide, and titania to about the same extent as the previous network in the cold end of the zirconia refractory. The matrix appears to have about 2.5 per cent lime, about 3 per cent zirconia, and traces of iron oxide, silica, and titania in solution. No niobium was detected in the matrix or network.

Electron microprobe analysis on the thoria sample showed that the hot and cold zones were almost identical in composition and showed only traces of silica and iron oxide. No zirconium was detected in the sample.

3. Density Measurements on Previously Studied Materials

According to the manufacturer (Zirconium Corporation of America), the previously studied materials (thoria, calcia-stabilized zirconia, and calcia-stabilized hafnia) should have a (closed pore) porosity of approximately 5 per cent. Photomicrographs of these materials, however, indicated that the porosity (particularly of thoria) was somewhat higher. Attempts to determine both pore structure and total pore volume in a mercury porosimeter were unsuccessful due to packing problems and due to the fact that the apparent pore volume appeared to change on grinding the samples.

Simple density determinations were, therefore, carried out by determining the buoyancy of the samples immersed in water. Water did not penetrate the pores to any significant extent, since the buoyancy did not change with time. The results are presented in Table 13, together with the typical density values given by the manufacturer.

TABLE 13

DENSITY OF VARIOUS OXIDE TUBES

Material	H_2O - Density g cm^{-3}	Manufacturer's Density g cm^{-3}
$Zr_{0.92}Ca_{0.08}O_{1.92}$	5.39	5.4
$Hf_{0.86}Ca_{0.14}O_{1.86}$	7.86	9.51
ThO_2	8.83	9.12

The densities of zirconia and hafnia cannot be translated into porosity values, since the theoretical (single crystal) densities of these materials are a function of the calcia content and are not known. The theoretical density of thoria, as computed from X-ray measurements[12, 13], is 10.01 g cm^{-3}. Using this value, the calculated porosity of thoria is 12 per cent, in reasonable agreement with the structure observed in the photomicrographs.

VI. MECHANICAL COMPATIBILITY OF IRIDIUM WITH GRAPHITE

TASK B1-2

Iridium Coatings on Graphite

In the Summary Report,[2] various methods of coating graphite with iridium (i.e. foil cladding, slurry dipping and sintering, electroplating, and vapor plating) have been described and the advantages and disadvantages of each method have been discussed. To recapitulate briefly, foil clad coatings provide excellent protection but are limited to small sizes and simple geometrical shapes. Slurry dipped and sintered coatings show good thermal shock resistance and coating-to-graphite adherence, but, since they contain pores and occasional pinholes, they are not completely impervious to oxygen. Electroplated iridium coatings are very dense and protective but cannot be applied directly on graphite because of a salt-penetration problem. Finally, dense and protective coatings can be obtained by vapor plating using iridium carbonyl ($Ir_4(CO_{12})$) or iridium chlorocarbonyl ($Ir(CO)_2Cl_2$). Vapor plating, however, is a very slow method due to the low volatility and low thermal decomposition temperature of the iridium carbonyl compounds.

During the present report period, iridium coatings were produced by a combination of the last three methods listed above. This procedure retains the advantages of each method and minimizes the disadvantages. Two cylindrical specimens, ½ inch diameter by 4 inches long, were coated over a length of approximately 3 inches. In order to obtain maximum coating adherence, a base coat of iridium was first applied by slurry dipping and sintering to 2130°C. Each specimen was dipped and sintered three times, and the average thickness of the sintered iridium layer was 1.5 mils. The pores and pinholes in the sintered material were then filled or bridged by a thin layer (0.4 mil) of vapor-plated iridium. The apparatus has been described in the Summary Report.[2] Iridium carbonyl was volatilized at 160°C at a carbon monoxide pressure of approximately 1 mm Hg. The substrate temperature was kept at 500°C. Seventy-two hours were required to obtain a 0.4 mil thick iridium deposit. The coatings were then checked for pinholes by immersing in a molten NaCN-KCN bath; after rinsing with water and drying at 110°C, there was no weight-gain and visual observation under a microscope revealed no salt residues on the surface, indicating that the coatings were dense. The appearance of the vapor-plated specimen is shown in Figure 59. One specimen was then given a final electroplated iridium coating of 0.3 mil thickness. During electroplating, the molten cyanides crept up and penetrated the uncoated end of the graphite specimen. An unsuccessful attempt was made to remove the salt by leaching in boiling water in a Soxhlett apparatus. Even after one week of leaching, traces of cyanide could still be detected in the water. The last traces of cyanide were finally removed by very slow heating in vacuo to 1400°C.

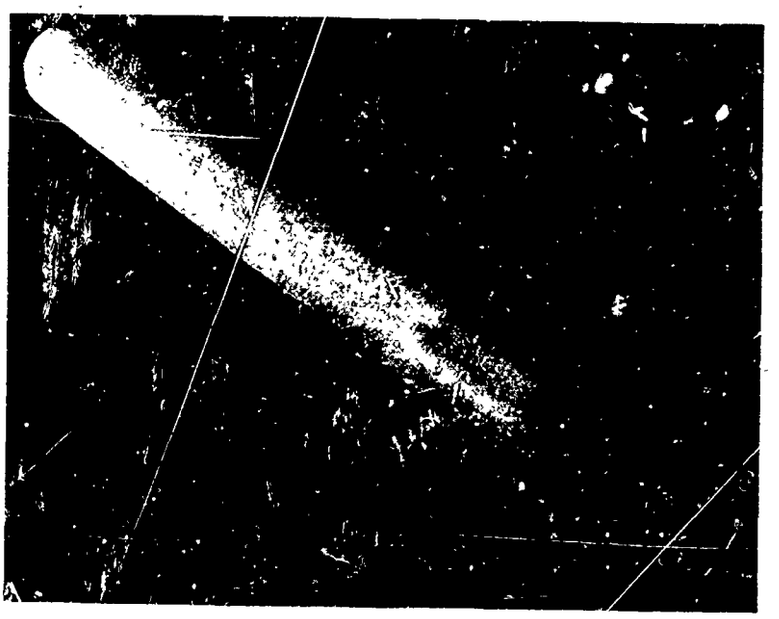

Figure 59. Vapor-Plated Iridium Coating

The protectiveness of the coating was then tested by heating the tip of the specimen in an oxygen rich O_2-CH_4 flame to 2000°C for ten minutes. The total weight loss was 0.0365 gm, but since the hot-zone area was not clearly defined, the weight loss on a per unit area basis is not known.

The specimen was then sectioned in the test area, polished, and electroetched. Figure 60 shows the carbon-iridium interface, and Figure 61 shows the iridium coatings. The much denser vapor-plated and electroplated iridium layers on top of the sintered coating are clearly discernible.

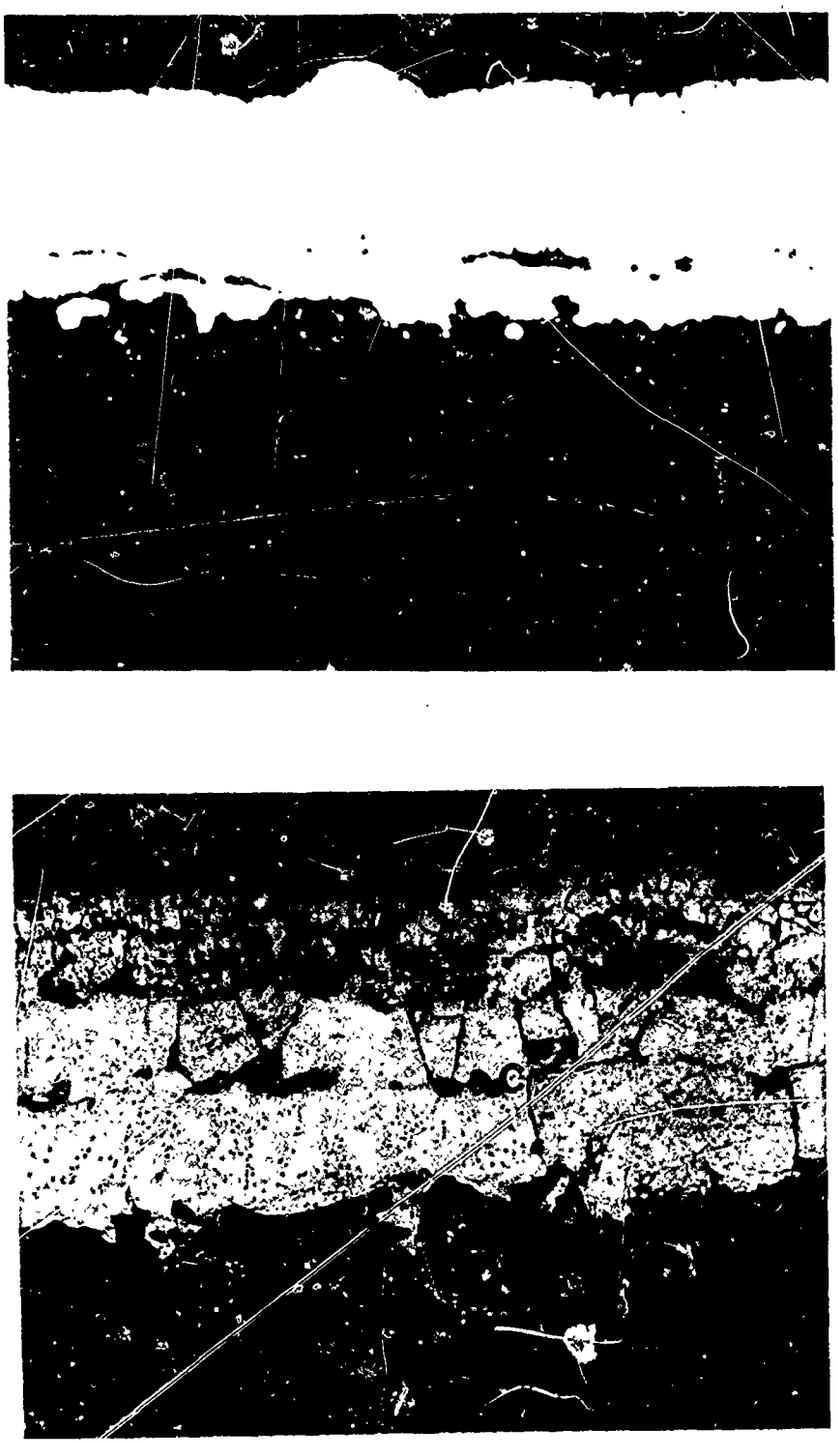

Figure 61. Electroplated (A), Vapor-Plated (B), and Sintered (C) Iridium Coating

The substrate for the above experiments consisted of a very isotropic graphite which has a particularly high thermal expansion of 6.2×10^{-6} cm/cm/°C at room temperature. This material, graphite "D", was prepared at the Parma Research Center from an experimental batch of coke obtained from our Advanced Materials Laboratory at Lawrenceburg, Tennessee. Figure 62 shows a photomicrograph of the structure of graphite "D".

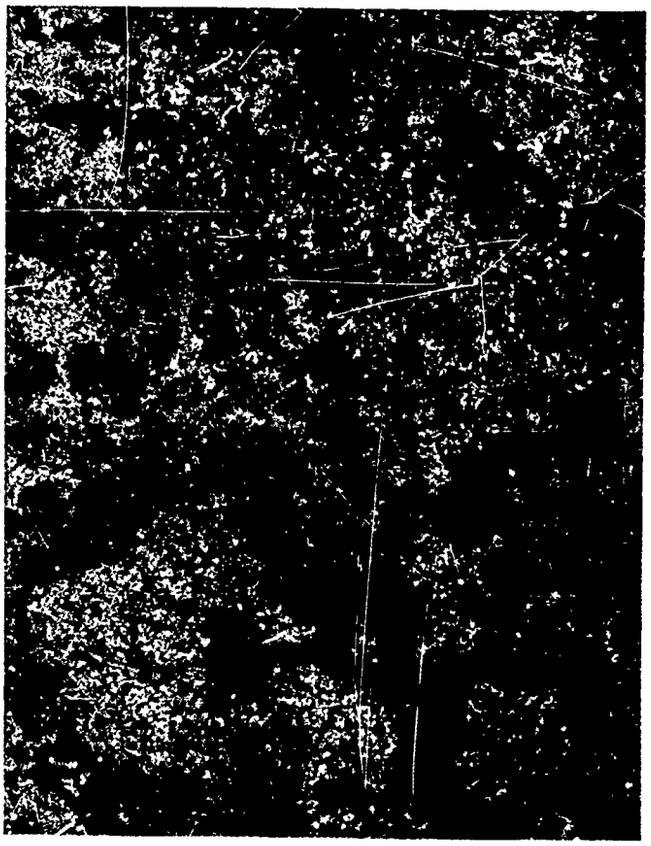

Figure 62. Graphite "D" (250 X Magnification)

Iridium Coatings on Union Carbide Grade PT-0114 Graphite

A specimen ($^1/_2$ inch diameter by 4 inches long) of Union Carbide grade PT-0114 graphite was coated with iridium by the slurry-dip technique. Due to the extreme porosity of the PT graphite, the initial coat tended to be too thick. After some experimenting, a good first coat was obtained by thinning the slurry with 30 per cent by weight of xylene. Subsequent coats could be applied by dipping in a slurry of normal concentration. Altogether,

the specimen was coated seven times over a length of 3.6 inches. Each coating was sintered to 2130°C in argon for $^1/_2$ hour. The total weight of iridium was 5.73 grams, corresponding to a coating thickness of 2.6 mils. The iridium coating adhered very well. The thermal shock resistance was tested by heating the specimen in vacuo to 2000°C in thirty seconds, holding at 2000°C for one minute, and cooling to approximately 400°C in approximately three minutes. This procedure was repeated ten times. Visual inspection under a microscope revealed no cracks or other damage.

An oxidation test was then carried out by heating the upper one-inch of the specimen for one hour to 2050 ± 50°C in air in an induction furnace. The unprotected lower end was cooled by immersion in water. The weight loss during the oxidation test was 0.1954 gram, corresponding to less than 0.3 mil. Subsequent sectioning and metallographic examination showed that the coating was much denser than any sintered coating heretofore obtained on regular graphite grades. A few pores were still evident, but the pores were apparently not interconnected, and the graphite substrate had been very well protected.

One may speculate that the formation of continuous pores during the sintering process is due to gas evolution from the graphite. On regular, dense graphite grades, the gases have no way of escape but through the coating. The very porous PT graphite, however, may permit the gases to escape through the bulk graphite.

Mechanical Compatibility

In repeating this work on coating of PT-0114 graphite, difficulties were encountered. The slurry-dipped coatings could only be built up to a thickness of approximately 1.5 mils thicker coatings tended to crack due to the severe mismatch in thermal expansion of iridium and PT-0114 graphite. The PT-0114 used in the second investigation come from a more recent batch and had much higher strength and higher density than the previously used material. Differences in the substrate structure thus may be responsible for the observed differences in coating behavior.

Fused Iridium Coatings

In an effort to find a simple method of obtaining dense and continuous iridium coatings on flat graphite surfaces, pieces of iridium foil were sandwiched between graphite samples and heated to a temperature above the melting point of iridium. This method is essentially the one used originally for the determination of the carbon-iridium bond. Very short heating times were to be used in order to minimize the amount of carbon dissolved by iridium.

One-half-inch-square pieces of 10-mil iridium foil were used. The graphite specimens, made from high CTE material, consisted of short cylinders $^3/_4$ inch in diameter, the ends of which had been machined flat and polished. In order to apply some pressure, the upper rod was weighted with a larger piece of graphite to a total weight of 48 to 108 grams respectively. Heating was carried out inductively in vacuo to 2500°C for five,

thirty, or sixty seconds, respectively. One graphite section was then machined off to expose the iridium layer. The results were disappointing: in all six experiments, the iridium layer was found to be discontinuous showing large, bubble-like pores.

Two similar experiments were then carried out in a graphite tube furnace in an argon atmosphere, with hold-times of ten minutes at 2500°C. In these cases, the iridium layers appeared to be continuous; X-ray investigation, however, showed the presence of numerous pinholes.

Modifications in Iridium Vapor-Plating Procedure

The vapor plating method described in the Summary Report[2] suffered from the fact that a large fraction (up to 60 per cent) of the iridium carbonyl or iridium chlorocarbonyl charge decomposed thermally in the tube furnace and was lost for plating purposes. To shorten the vapor path, the sintered quartz disk holding the charge was moved upwards closer to the substrate as shown in Figure 63.

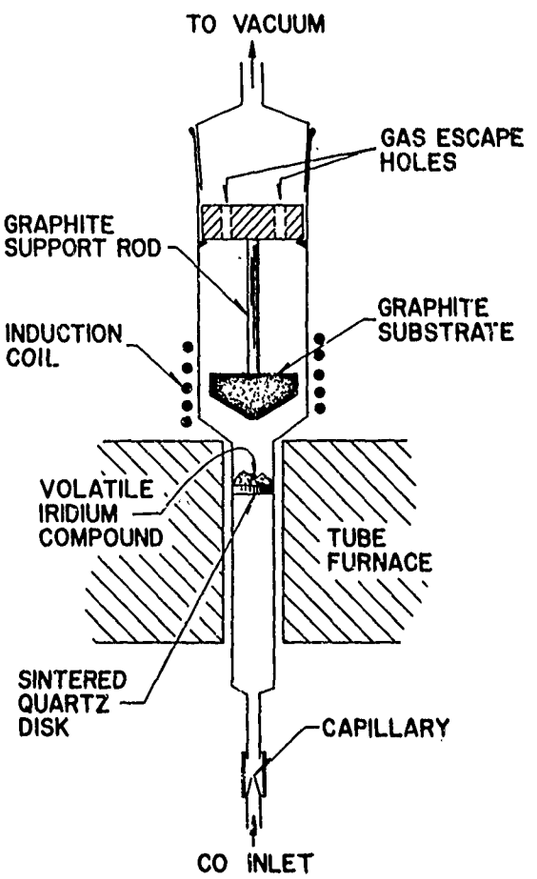

Figure 63. Modified Apparatus for Iridium Vapor Plating

Another large fraction of the carbonyl charge was lost by condensation on the walls of the quartz-tube above the furnace, where it eventually decomposed because of heat radiation from the hot substrate. Furthermore, the vapor deposit was much thicker on the bottom of the rod-shaped substrates than on the sides. Subsequent vapor plating experiments were therefore carried out with cone-shaped substrates, (see Figure 63) and iridium losses due to condensation on the quartz-walls were reduced. Coating uniformity has also been improved, although the coating thickness in the center of the cone-shaped region is still greater than on the edges. Very little iridium is deposited on the cylindrically shaped portion of the specimen and none at all is deposited on the back-side. Figure 64 shows an iridium vapor deposit on a graphite specimen of 4 cm diameter, which had been coated by the slurry dip and sintering technique prior to vapor plating.

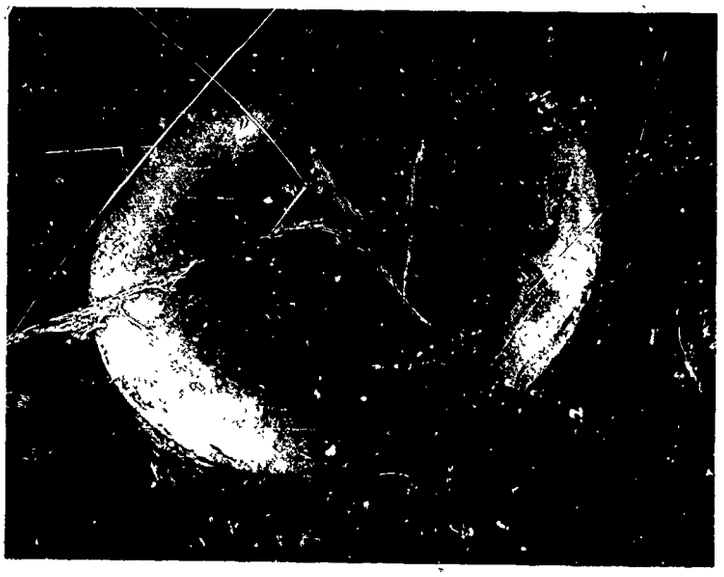

Figure 64. Vapor-Plated Iridium Coating

Tensile Strength of Electrodeposited Iridium

On pages 76 and 77 of the Summary Report[2], a method of electroplating graphite with iridium is discussed. Due to the columnar nature of the iridium deposit, as shown in Figure 65, it was felt that it might have a peculiar tensile strength. To resolve this point, a small graphite plate ($^1/_4$ inch x $1^1/_4$ inches) was electroplated with iridium. The plate was cut

from the graphite, and the remaining graphite was oxidized in a Bunsen flame. A similar sized sample of iridium foil was heated in a Bunsen flame, and then both the plate sample and the foil were submitted for tensile strength tests. Table 14 shows the results of the tests.

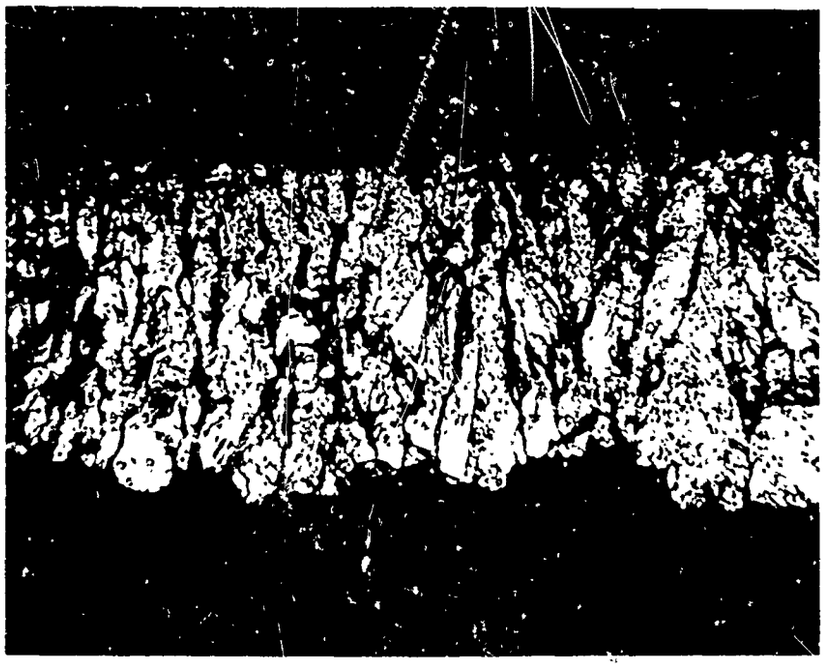

Figure 65. 4 Mil Iridium Plate, (500 X Magnification) Electroetched in 0.2 N HCl for Three Hours

TABLE 14

TENSILE STRENGTH OF IRIDIUM

Sample	Thickness (Inches)	Width (Inches)	Strength (lb/in^2)
Wrought Foil	0.0025	0.195	2.67×10^4
Electrodeposited Plate	0.0068	0.1660	2.46×10^4

It is obvious that there is little difference in the tensile strength of the two samples.

High Temperature X-ray Investigation for Possible Iridium Carbide Formation

Knowledge of the presence or absence of a carbide in the iridium-carbon system is useful in understanding the bonding of an iridium coating on a carbon article. There was enough doubt about the existence of such a carbide to warrant an investigation of the system. The most direct technique of determining the presence of a phase is by X-ray diffraction and since a high temperature X-ray camera was available, this approach was taken.

Two general types of samples were prepared to study the system in both carbon-rich and carbon-poor compositions. The first type consisted of pieces of 0.010 inch iridium wire coated with a slurry of graphite and the second consisted of 0.025 inch graphite rods coated with a slurry of iridium powder.

The samples were loaded in a high temperature X-ray camera, and a series of Debye patterns was made at room and elevated temperatures. The heating was accomplished by use of a carbon heater. In most cases, the sample failed from partial melting before the maximum temperature available with this apparatus, 3000°C, was attained. Patterns at elevated temperatures were obtained from samples in the temperature range of 800° to 2200°C at 100° intervals. Several samples were rapidly cooled from temperatures above 2000°C, removed from the high temperature camera, ground into powders, and room temperature patterns made in Norelco powder cameras for comparison purposes.

In all cases, the Debye patterns contained lines from only two phases: iridium and graphite. This result was true of both carbon-rich and iridium-rich samples. In light of this information, we conclude that there is no carbide of iridium stable in the temperature range from room temperature to 2200°C.

Investigation of Grain Growth of Iridium

Samples of iridium metal were annealed at temperatures of 1475°, 1650°, 1830°, and 1950°C for one hour in an argon atmosphere to demonstrate crystallite growth with increasing temperature. Figures 66 through 70 show an iridium sheet as-received and after the annealings. The photographs were taken at 150X magnification of samples which had been polished and then a.c. electroetched in dilute HCl to bring out the structure. Figure 66 shows the small, coarse, elongated grains of the as-received iridium sample indicative of the distortion generally exhibited by rolled, unannealed sheet stock.

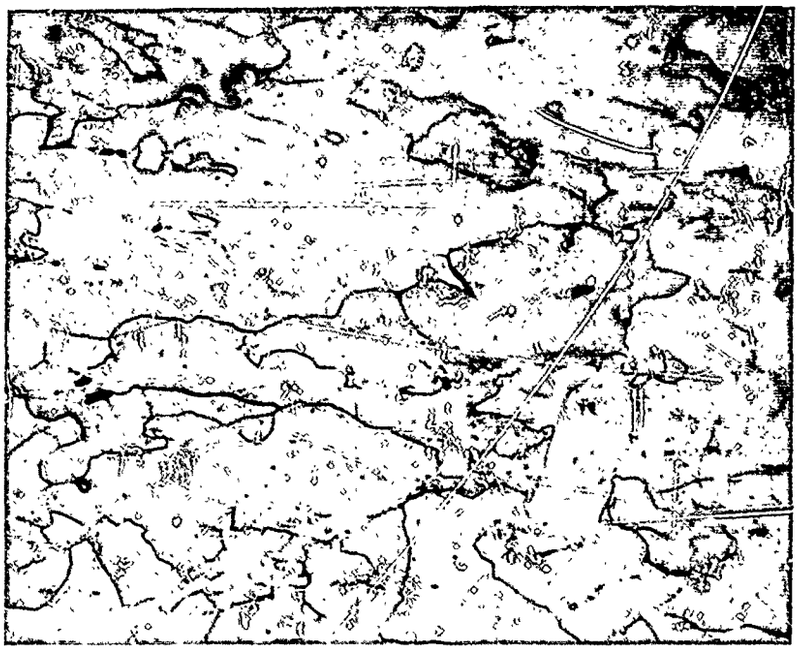

Figure 66. Iridium Metal As-Received, (150X Magnification)

Figures 67 through 70 represent photomicrographs of iridium sheet annealed at 1475°, 1650°, 1830°, and 1950°C, respectively. The large, equiaxed grains of the annealed samples denote complete recrystallization.

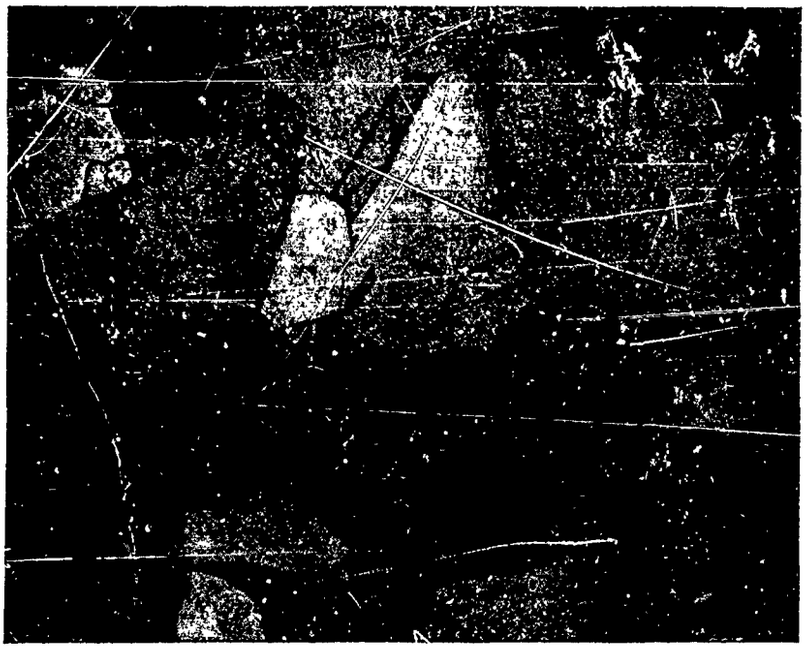

Figure 67. Iridium Sheet Annealed at 1475°C, (150X Magnification)

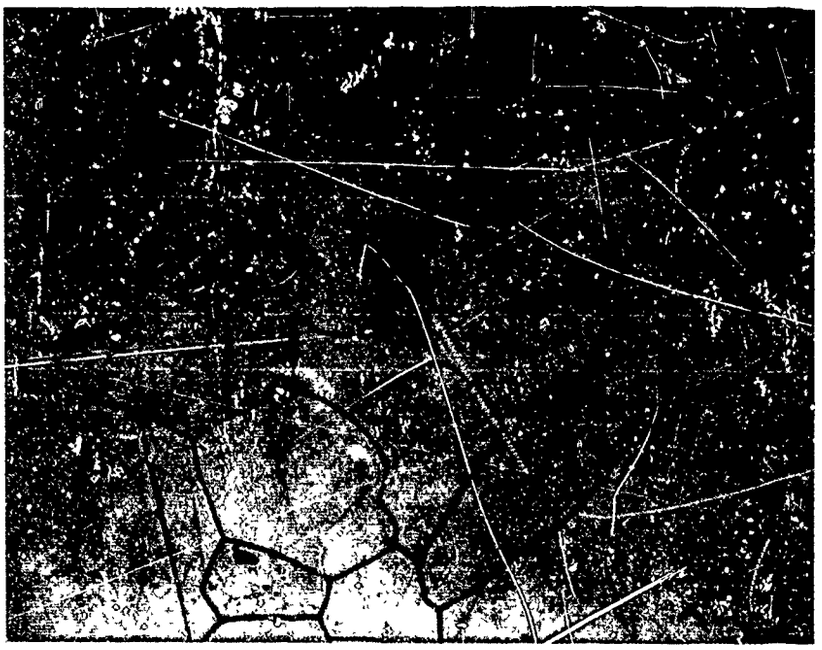

Figure 68. Iridium Sheet Annealed at 1650°C, (150X Magnification)

Figure 69. Iridium Sheet Annealed at 1830°C, (150X Magnification)

Figure 70. Iridium Sheet Annealed at 1950°C, (150X Magnification)

VII. MECHANICAL COMPATABILITY OF MULTILAYER COATINGS WITH GRAPHITE

TASK C2-2

Introduction

The adherence of a protective coating on graphite will depend strongly on the extent to which the coating and substrate are mechanically compatible. Differential expansion matching is an important consideration for a well-adherent coating.

In this phase of the program, the oxides ThO_2, HfO_2, and ZrO_2 and the diborides of hafnium and zirconium are being considered for components of multilayer coatings on graphite. The oxides will function as a barrier to oxygen and the diborides will function as a barrier to carbon.

The thermal expansion of the oxides has been adequately investigated and a review of this information is included here. On the other hand, the thermal expansion of the diborides was derived largely from lattice parameter measurements and thus pertain to single crystals. Polycrystalline materials of less than theoretical density might have considerably lower thermal expansion coefficients (CTE) due to possible internal expansion into void space. Bulk thermal expansion measurements are, therefore, needed and will be carried out in this phase of the program.

The use of a diboride as an intermediate layer between the oxide and substrate suggests another consideration in that the oxide formed by eventual oxidation of this diboride layer would undergo a phase inversion upon being subjected to thermal cycling. For example, eventual interaction of ZrB_2 and HfB_2 with oxygen diffusing through the oxide would result in the formation of ZrO_2 and HfO_2. The presence of these oxides which are known to undergo phase inversion, may cause cracking and spalling of the protective coating. Since the phase stabilization of ZrO_2 and HfO_2 can be accomplished by the presence of alkaline and rare-earth oxides, addition of the borides of calcium, lanthanum, cerium, or yttrium to ZrB_2 and HfB_2 may provide a more stable intermediate layer than the undoped diborides.

In addition to the thermal expansion measurements on pure ZrB_2 and HfB_2, the CTE of HfB_2 and ZrB_2 doped with appropriate amounts of an alkaline earth or rare-earth boride is also being carried out. The possible use of these additives requires some knowledge of their chemical compatibility with other constituents in the coating system.

This section of the report deals with the review of previous work on the thermal expansion behavior of the oxides and diborides. Our initial work on the compatibility of CaB_6 and LaB_6 with graphite, HfO_2, ZrO_2, ZrB_2, and HfB_2 is also presented.

Previous Work on the Thermal Expansion of the Oxides and Diborides

As an initial part of these mechanical compatability studies, a review of the most recent publications concerning the thermal expansion of prospective coating materials (ThO_2, HfO_2, ZrO_2, ZrB_2, and HfB_2) has been carried out.

The thermal expansion of hafnium diboride in the range 25° to 2040°C has been recently investigated by Keihn[14] using X-ray diffraction methods. Houska and Keplin[15] by the same techniques measured the lattice parameters for ZrB_2 in the range 25° to 2040°C. Using the data reported by these investigators, the average CTE of completely dense polycrystalline species was calculated. This information is presented in Table 15. Ohnysty and Rose[16]

TABLE 15

CTE OF HfB_2 and ZrB_2 CALCULATED FROM LATTICE PARAMETER DETERMINATIONS

Temperature °C	CTE of HfB_2[14] in/in/°C	CTE of ZrB_2[15] in/in/°C
25- 750	6.4	6.7
750-1015	8.0	8.3
1015-1260	7.8	8.3
1260-1515	8.3	7.9
1515-1770	7.2	8.7
1770-2040	8.4	6.7

recently reported their determination of the thermal expansion of thoria and hafnia. In their experiments, differential measurements were made relative to the elongation of a tungsten standard with a Gaertner filar cathetometer. This information is summarized in Table 16. Budik and Hoskins[17] investigated the stabilized zirconia systems listed in Table 17. In determining the thermal expansion of these materials from 25° to 1400°C, Budik and Hoskins found that only ZrO_2 containing 15.5 m/o CaO and 22.5 m/o CeO_2 exhibit reproducible thermal expansions. The average CTE for the former composition was 11.47×10^{-6} in/in/°C, and the CTE for the latter composition was 11.91×10^{-6} in/in/°C.

TABLE 16

CTE OF REFRACTORY OXIDES

Temperature °C	ThO_2 in/in/°C x 10^6	HfO_2 in/in/°C x 10^6	HfO_2 + 10 w/o Y_2O_3 in/in/°C x 10^6	HfO_2 + 15 w/o Y_2O_3 in/in/°C x 10^6
24- 540	8.96	6.13	9.7	9.3
540-1090	9.91	6.88	10.3	10.2
1090-1650	11.08	inversion	12.1	11.7
1650-2200	12.34	inversion	12.7	12.9
2200-2480	13.32	inversion	12.8	13.3

TABLE 17

STABILIZED ZIRCONIA COMPOSITIONS

ZrO_2 + 15.5 m/o MgO
ZrO_2 + 10.0 m/o Al_2O_3
ZrO_2 + 15.0 m/o Al_2O_3
ZrO_2 + 15.5 m/o CeO_2
ZrO_2 + 22.5 m/o CeO_2
ZrO_2 + 15.5 m/o CaO
ZrO_2 + 5.0 m/o Ti
ZrO_2 + 15.0 m/o Ti
ZrO_2 + 6.0 m/o Zr
ZrO_2 + 15.0 m/o Zr

Schaffer[18] showed that ZrO_2 could also be stabilized as the cubic form by the presence of ZrB_2; however, he also found that ZrO_2 stabilized with ZrB_2 underwent violent thermal shock failure.

Compatability of CaB_6 and LaB_6
with Graphite, Oxides, and Diborides

The chemical compatability of CaB_6 and LaB_6 with graphite, HfO_2, ZrO_2, HfB_2, and ZrB_2 was examined within temperatures ranging from 1800° to 2200°C.

Experimental

The materials employed in these experiments were fine-powder oxides, diborides, and graphite. The oxides were purchased from the Zirconium Corporation of America; the analyses is given in Table 18.

TABLE 18

ANALYSIS OF OXIDE POWDERS

Calculated for HfO_2		Hf 84.7 O 15.3
Found		Hf 83.53 O 15.0
		Fe 0.60 Si 0.03
Spectroscopic	Major:	Hf
	Minor:	Zr, Al, Fe, Ti, Si, Cu, Mg
	Trace:	Ni, Mn, Cr
Calculated for ZrO_2		Zr 74.0 O 26.0
Found		Zr 74.5 O 25.3

The diborides were purchased from the Atomergic Chemetals Company. The results of the chemical analyses are given in Table 19. Their X-ray diffraction patterns revealed a minor amount of unidentifiable impurities in the ZrB_2 and minor amounts of HfC in the HfB_2.

TABLE 19

CHEMICAL ANALYSIS OF THE DIBORIDES

	HfB_2		ZrB_2	
	Theo.	Found*	Theo.	Found*
Hf	89.2	88.86		
Zr			93.7	93.66
C		0.36		
B	10.8	10.24	6.3	6.04
O		0.66		0.53
H		0.07		0.09
total		100.19		100.32

* Average of three analyses

The CaB_6 was Fisher Scientific Catalog No. C-54 "Pure" calcium boride. No wet chemical analyses were run; however, an X-ray diffraction pattern of the powder showed no indication of impurities.

The lanthanum hexaboride was purchased from the Gallard-Schlesinger Chemical Manufacturing Corporation, and again a diffraction pattern showed no indication of impurities.

The graphite used was Union Carbide spectroscopic grade SP-2.

Procedure

In a typical experiment, a 2-gram sample of equimolar amounts of the powdered test materials were heated to temperature and held for one hour under vacuum (< 1 mm He pressure). Weights and X-ray diffraction patterns were taken before and after each experiment. The container materials for the graphite experiments were graphite, for the ZrO_2 and ZrB_2 zirconium diboride crucibles were used, and in work with HfO_2 and HfB_2 hafnium diboride was the container.

Results and Discussion

Calcium and lanthanum borides did not yield a new product phase when heated in the presence of either HfB_2 or ZrB_2 at temperatures of about 2000°C. The starting materials were essentially unchanged as determined by X-ray diffraction.

Weight losses and X-ray diffraction patterns also indicated the loss of CaB_6 and LaB_6 by volatilization. For example, when a sample of equimolar amounts of CaB_6 and HfB_2 (or ZrB_2) was held in vacuum at 1960°C for one hour, both X-ray diffraction and weight loss demonstrated that most of the CaB_6 (> 90 per cent) had volatilized; at 2190°C weight loss and X-ray diffraction indicated that all of the CaB_6 had volatilized. In similar experiments with LaB_6 and the diborides at 1900° and 1960°C weight changes indicated losses of < 1 per cent and ~2.5 per cent, respectively, which shows that LaB_6 is considerably less volatile than CaB_6. Also in these experiments, zirconium carbide impurities originally present in the ZrB_2 were not detected in the X-ray diffraction pattern of the product indicating a reaction between LaB_6 and ZrC.

Calcium hexaboride and LaB_6 each react with the oxides of hafnium and zirconium at temperatures substantially less than 2000°C, and the reactions are accompanied by considerable weight loss. For example, when CaB_6 was treated with ZrO_2 at 1980° and 2180° the weight losses were 48 and 52 per cent respectively; treatment with HfO_2 at identical temperatures resulted in weight losses of 31 and 43 per cent. The weight loss was most likely the result of the formation of volatile boron oxides plus some loss of CaB_6. Diffraction patterns of the products showed no oxide in either of the high temperature runs indicating complete interaction with the hexaboride to form the transition metal boride and volatiles. In the lower temperature reaction, small amounts of unreacted oxide remained.

The treatment of LaB_6 with ZrO_2 at 1820° and 1925°C resulted in weight losses of 19 and 22 per cent. X-ray diffraction patterns of the products gave no evidence of ZrO_2, but showed ZrB_2, La_2O_3, and unidentifiable products;

the ZrB_2 pattern was strongest at the high temperature while La_2O_3 was weaker (this is probably due to increase in vapor pressure of La_2O_3 though it is only ~ 10^{-3} torr at 1925°C).[19] Treatment of LaB_6 with HfO_2 at 1815° and 2015°C resulted in weight losses of 15 and 22 per cent respectively. Diffraction patterns of the products gave evidence of the formation of some unidentifiable product and HfB_2 in each experimental; however, in both cases unreacted HfO_2 was detected unlike the experiments with ZrO_2.

Heating CaB_6 with Union Carbide grade SP-1 graphite powder in an open crucible at 2060° and 2200°C resulted in weight losses of about 46 and 47 per cent, respectively. The products of each were B_4C and an unidentifiable phase o phases. An additional observation was that the product hydrolized and emitted the odor typical for the hydrolysis of calcium carbide.

On the other hand, LaB_6 appeared stable in the presence of graphite at 2000°C. The resulting weight loss was 2 per cent of the original. A comparison of the X-ray diffraction patterns of both the initial and final reaction mixture showed that no phase change had occurred. Further evidence of the stability of lanthanum hexaborides with carbides is given by Samsanov, et. al., [20] in the preparation of LaB_6 from La_2O_3 and B_4C.

Summary and Conclusions

It has been demonstrated that LaB_6 is more stable in the presence of HFO_2, ZrO_2, and C and also less volatile than CaB_6. This may indicate that the group IIIB hexaborides will offer better performance in mixed boride coatings than the alkaline-earth hexaborides. Composites will be prepared using mixtures of HfB_2 or ZrB_2 with the hexaborides of Ca, Y, Ce, and La. Both thermal expansion and possibly oxidation tests will be run on the resulting specimens.

VIII. CHEMICAL REACTIONS OF OXIDES WITH DIBORIDES

TASK C2-1

Introduction

The diborides of hafnium and zirconium, because of their high temperature stability with respect to carbon, are being considered for intermediate layers separating the refractory oxides from the graphite substrate. This task is primarily concerned with the high temperature chemical interactions of HfB_2 and ZrB_2 with hafnia, zirconia, and thoria.

Experimental

The diborides were supplied by the Atomergic Chemetals Company in powder form. The results of chemical analyses are given in Table 20. The X-ray diffraction patterns obtained from the analytical service group for these materials revealed a minor unidentifiable impurity in the zirconium diboride and minor amounts of hafnium carbide in the hafnium diboride.

TABLE 20

CHEMICAL ANALYSES OF THE DIBORIDES
(-325 Mesh Powders)

Element	ZrB_2		HfB_2	
	Theoretical Wt. %	Found Wt. %	Theoretical Wt. %	Found Wt. %
Zr	80.9	79.21		
Hf			89.2	88.86
C		1.04		0.36
B	19.1	18.22	10.8	10.24
N		0.21		
O		1.16		0.66
H		0.10		0.07
Total		99.94		100.19

The oxide pellets and powders (-325 mesh) were supplied by the Zirconium Corporation of America. The results of chemical analyses are given in Tables 21 and 22.

TABLE 21

ANALYSES OF THE OXIDE POWDERS

Element	HfO_2 Wt. %		ThO_2 Wt. %		ZrO_2 Wt. %	
	Theor.	Found	Theor.	Found	Theor.	Found
Hf	84.7	83.53				
Th			87.9	87.37		
Zr					74.0	74.5
O	15.3	15.0	12.1	12.8	26.0	25.5
Fe		0.6				
Total		99.13		100.17		100.0

TABLE 22

ANALYSES OF THE OXIDE PELLETS

Element	Density		HfO_2*	ThO_2	ZrO_2*
	{	Literature	9.68	9.69	
	{	Determined	9.676	9.76	5.403
Hf			80.0		
Th				87.9	
Zr					65.6
Y			6.4		10.0
O			12.6	13.65	30.5
Total			99.0	101.55	106.1

* Yttria stabilized

The induction heating assembly used for conducting this investigation is shown in Figure 43 of ML-TDR-64-173, Part II, Ocotober 1964.

Pellet Oxide—— Powdered Diboride Experiments

The experiments with oxide pellets and powdered diboride were preliminary in nature and were designed to identify the systems which merit an extensive examination.

In a typical experiment, a ThO_2 pellet (~ 1/4 inch diameter x 1/4 inch long) weighing 2.396 grams was embedded in 7.096 grams of powdered hafnium diboride and contained in a slip cast hafnium diboride crucible (~ 3/4 inch O.D. x 3/4 inch deep, with a wall thickness varying from 1/32 to 1/16 inch) weighing 10.69 grams. It, in turn, was contained in a graphite susceptor 1 inch I.D. x 1 1/2 inches deep and insulated with graphite felt.

The assembly was held in a quartz envelope, evacuated to <1 mm of Hg, then heated by electrical induction to 2210°C and held at temperature for one hour. The power supply was turned off and an atmosphere of helium was admitted for rapid cooling. The reaction container, pellet, and powder were reweighed and examined. The reactant powder adjacent to the pellet and half of the pellet were submitted for X-ray analysis; the other half was mounted, polished, and examined in the metallograph. The conditions and results of the experiments are summarized in Table 23.

TABLE 23

TREATMENT OF THE OXIDES WITH BORIDES

Reactants Pellet**	Reactants Powder	Container Material	Temp. °C	Pellet Weight (gms)	Weight Change (gms)	Analysis by X-ray Diffraction Pellet	Analysis by X-ray Diffraction Powder
None	ZrB_2	ZrB_2	2340	Standard for Powder			ZrB_2
ZrO_2	ZrB_2	ZrB_2	2220	1.618		ZrO_2* (poss. ZrB_2)	ZrB_2, ZrC_2 (poss. Zr)
ThO_2	ZrB_2	ZrB_2	2220	2.437	-0.014	ThO_2	ZrB_2
HfO_2	ZrB_2	ZrB_2	2220	2.007	-0.043	HfO_2 (poss. Hf)	ZrB_2
None	HfB_2	HfB_2	2190	Standard for Powder			HfB_2, weak HfC (poss. HfO_2)
ThO_2	HfB_2	HfB_2	2200	2.396	+0.009	ThO_2	"
HfO_2	HfB_2	HfB_2	2200	2.013	+0.010	HfO_2 (poss. HfB_2)	"
ZrO_2	HfB_2	HfB_2	2200	1.635	+0.007	ZrO_2 (poss. HfB_2)	"

* Some of the boride powder sintered to pellet.
** Hafnia and zirconia pellets are stabilized with yttria and have a cubic structure.

Reactants as Powders

In a typical experiment with powdered reactants, 2-gram samples consisting of equimolar mixtures of oxide and diboride were heated in a container which was fabricated from the diboride corresponding to the powdered diboride involved in the experiment. For example, experiments involving hafnium diboride powder were carried out in a hafnium diboride crucible. When zirconium diboride powder was used as a reactant, the container material was zirconium diboride. The slip cast crucibles, $^3/_4$ inch O.D. x $^3/_4$ inch deep with a wall thickness of approximately $^1/_{16}$ inch,

containing the reactants were heated in a graphite susceptor by electrical induction. The assembly, insulated with graphite felt, was enclosed in a quartz envelope.

The conditions and results of the experiments are summarized in Table 24. Some experiments were of one hour duration; others were run for three hours.

Results and Discussion

In all of the experiments the white oxide pellets turned black; this effect was anticipated since we had observed that these oxides will turn black when heated to temperatures of 2000°C in vacuum. None of the oxides (HfO_2, ZrO_2, ThO_2) showed any evidence of melting when heated with HfB_2 or ZrB_2, and in only one sample (the ZrO_2 in ZrB_2) did the boride sinter to the oxide. In that case, the coating was easily removed with a spatula.

X-ray diffraction patterns of the starting materials and products did not reveal any interaction of the oxides with zirconium diboride or hafnium diboride at 2200°C. The only unusual X-ray findings concern the treatment of stabilized zirconia with ZrB_2. In that experiment, the diboride adjacent to the pellet contained monoclinic zirconia and possibly Zr metal, neither of which was present in the zirconium boride starting material.

Metallographic examination did show a change in the microstructure of the oxide pellets that were heated with the diboride powders. Precipitation of a metallic phase within the grains and at the grain boundaries of the oxide occurs when hafnia, zirconia, and thoria are heated in zirconium diboride at 2200°C. In addition, these oxides show a definite grain growth and densification when heated in contact with zirconium diboride. When heated in the presence of hafnium diboride, the oxides show only a dispersed metallic phase throughout the matrix, a phenomenon which is observed when the oxides are heated alone in vacuo.

Photomicrographs, 500 X magnification of a pellet of yttria-stabilized hafnia and similar samples which have been heated to 2200°C in HfB_2 and ZrB_2, are shown in Figure 71. The hafnia as received (Figure 71 a) appears as a dense well-stabilized, single phase. Hafnia, which was heated in HfB_2 (Figure 71 b) displays a second metallic phase; the glomerate of metal around the large void near the center of the photo is not characteristic of the entire sample but was included to show this unusual occurrence. The white spots are likely free metal rather than borides, since they polish quite readily and are not in low relief as the borides would be. Aside from the free metal content (~ one per cent), which is characteristic of samples merely heated in vacuum and not necessarily heated with HfB_2, there was no other change. A photomicrograph of hafnia which was heated in ZrB_2 is shown in Figure 71 c. The free metal content for this sample is estimated at about 5 per cent and a decrease in void area is evident.

TABLE 24

CONDITIONS AND RESULTS OF OXIDE AND BORIDE HEATS

Reactants 325 mesh	Time (hours)	Temperature °C	Identification of Product via X-ray Diffraction	
$ThO_2 + HfB_2$	1	1800	N.R. *	$ThO_2 + HfB_2$
$ThO_2 + HfB_2$	3	1800	N.R.	$ThO_2 + HfB_2$
$ThO_2 + HfB_2$	1	1955	N.R.	$ThO_2 + HfB_2$
$ThO_2 + HfB_2$	1	2200	N.R.	$ThO_2 + HfB_2$
$ThO_2 + HfB_2$	3	2190	N.R.	$ThO_2 + HfB_2$
$ThO_2 + ZrB_2$	3	1800	N.R.	$ThO_2 + ZrB_2$
$ThO_2 + ZrB_2$	1	1800	N.R.	$ThO_2 + ZrB_2$
$ThO_2 + ZrB_2$	1	1960	N.R.	$ThO_2 + ZrB_2$
$ThO_2 + ZrB_2$	1	2200	N.R.	$ThO_2 + ZrB_2$
$ThO_2 + ZrB_2$	3	2200	N.R.	$ThO_2 + ZrB_2$
$HfO_2 + HfB_2$	1	1635	N.R.	$HfO_2 + HfB_2$
$HfO_2 + HfB_2$	1	1810	N.R.	$HfO_2 + HfB_2$
$HfO_2 + HfB_2$	1	2110	N.R.	$HfO_2 + HfB_2$
$HfO_2 + HfB_2$	1	2200	N.R.	$HfO_2 + HfB_2$
$ZrO_2 + ZrB_2$	1	1635	N.R.	$ZrO_2 + ZrB_2$
$ZrO_2 + ZrB_2$	1	1770	N.R.	$ZrO_2 + ZrB_2$
$ZrO_2 + ZrB_2$	1	2200	N.R.	$ZrO_2 + ZrB_2$
$HfO_2 + ZrB_2$	1	2040	Some HfB_2	$HfO_2 + ZrB_2$
$HfO_2 + ZrB_2$	1	2110	Some HfB_2	$HfO_2 + ZrB_2$
$HfO_2 + ZrB_2$	1	2200	$ZrO_2 + HfB_2$	
$HfO_2 + ZrB_2$	1	2200	$ZrO_2 + HfB_2$	
$ZrO_2 + HfB_2$	1	2000	Some ZrB_2	$ZrO_2 + HfB_2$
$ZrO_2 + HfB_2$	3	2000	Some ZrB_2	$ZrO_2 + HfB_2$
$ZrO_2 + HfB_2$	1	2050	Some ZrB_2	$ZrO_2 + HfB_2$
$ZrO_2 + HfB_2$	1	2200	N.R.	$ZrO_2 + HfB_2$
$ZrO_2 + HfB_2$	3	2200	N.R.	$ZrO_2 + HfB_2$ (Some ZrC formed possibly from insulation)

* N.R. = no reaction as identified by X-ray

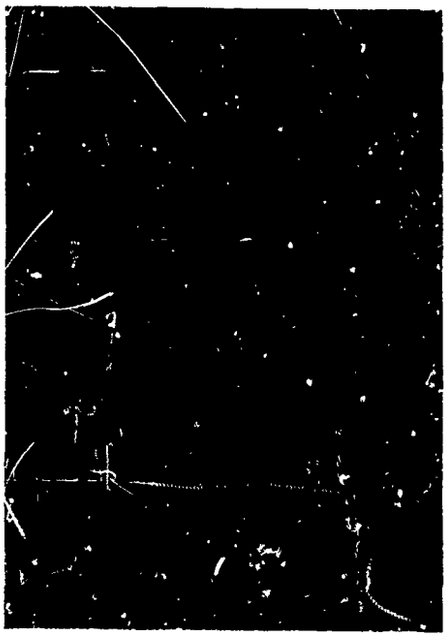

Figure 71 a. Hafnia As-Received, (500 X Magnification)

Figure 71 b. Hafnia Heated to 2200°C in HfB_2, (500 X Magnification)

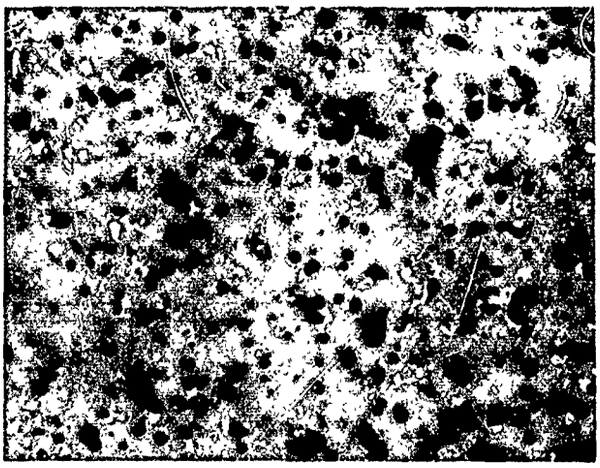

Figure 71 c. Hafnia Heated to 2200°C in ZrB_2, (500 X Magnification)

Figure 72 shows a pellet of thoria and similar pellets which have been heated to 2200°C in HfB_2 and ZrB_2. The thoria sample as received, Figure 72 a, contains a small amount of a second phase evidenced at the grain boundaries and appears more dense than the other oxides. Figure 72 b shows a sample which has been heated with HfB_2; in addition to the impurity phase, a metallic phase is present. Figure 72 c depicts a sample which has been heated with ZrB_2; it shows significant grain growth compared with the two others and contains about twice the free metal as the sample shown in Figure 72 b.

Figure 72 a. Thoria As-Received, (500 X Magnification)

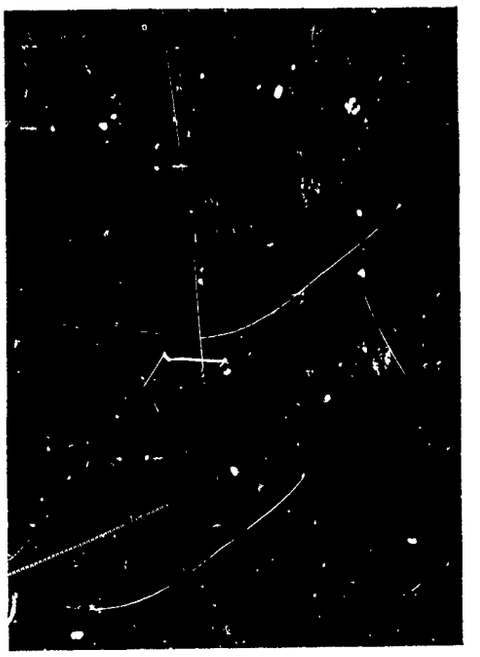

Figure 72 b. Thoria Heated to 2200°C in HfB_2, (500 X Magnification)

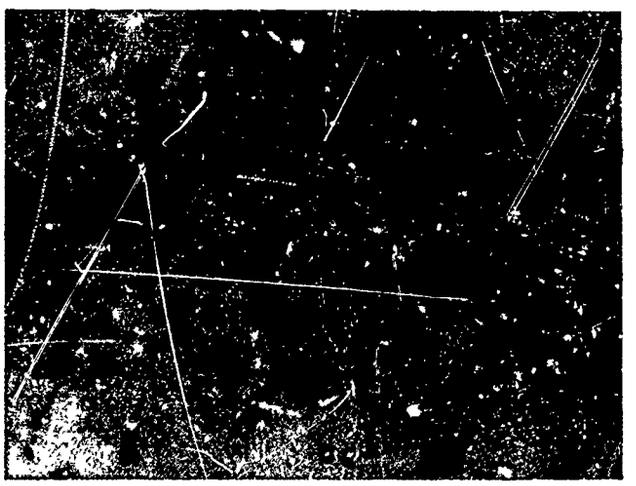

Figure 72 c. Thoria Heated to 2200°C, in ZrB_2, (500 X Magnification)

Figure 73 shows a pellet of yttria-stabilized zirconia and similar pellets which have been heated to 2200°C in HfB_2 and ZrB_2. The photograph in Figure 73 represents an as-received pellet of zirconia and shows the properly stabilized, single phase, dense oxide. Figure 73b shows a sample which has been heated in HfB_2; the photomicrograph gives evidence of about one per cent free metal included in the oxide. Figure 73c, showing a sample heated with ZrB_2 demonstrates that considerable free metal has been precipitated, possibly 5 per cent, in the grain boundaries of the sample. Also densification and crystal development is evident.

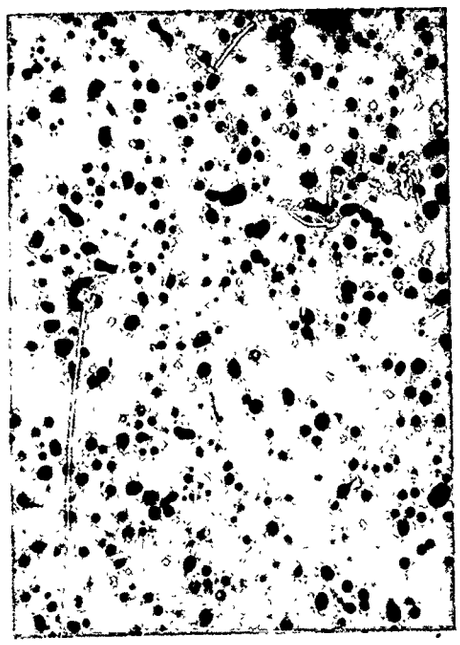

Figure 73a. Zirconia As-Received, (500 X Magnification)

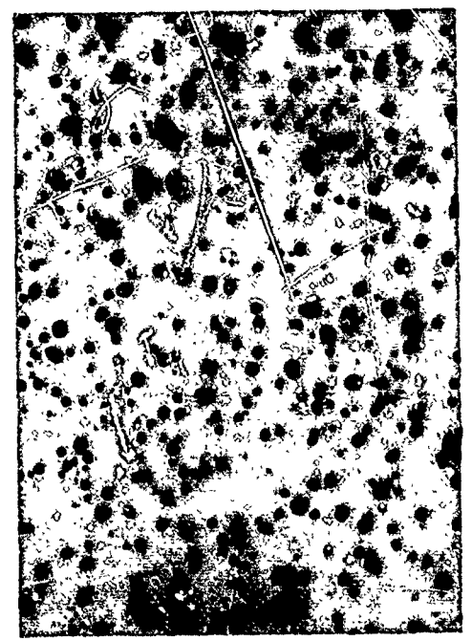

Figure 73b. Zirconia Heated to 2500°C in HfB_2, (500 X Magnification)

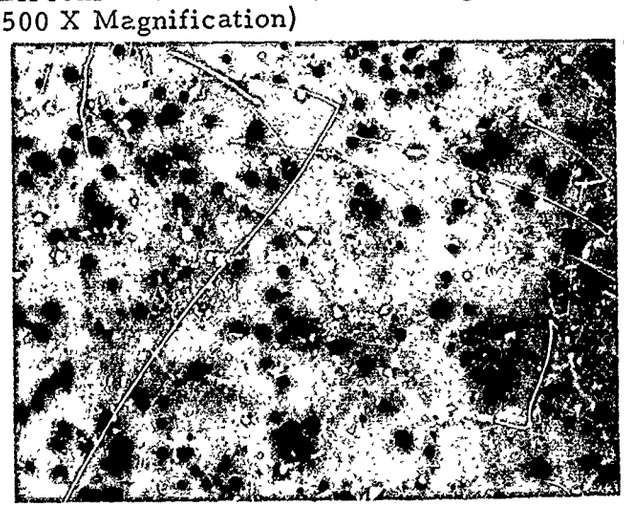

Figure 73c. Zirconia Heated to 2500°C in ZrB_2, (500 X Magnification)

Powder-Powder Experiments

In view of the lack of any gross interactions between the dense oxide pellets and the diborides, experiments involving intimately mixed fine powder reactants were investigated.

The thoria-hafnium diboride and thoria-zirconium diboride systems were investigated in the temperature range 1800° to 2200°C; the hafnia-hafnium diboride and zirconia-zirconium diboride systems were investigated in the 1635° to 2200°C range. None of these systems showed any reactions as evidenced by X-ray diffraction patterns of the mixtures before and after each experiment. No gases evolved during the experiments, nor were there visible changes in the powders.

An investigation of the hafnia-zirconium diboride system revealed the reaction

$$HfO_2 + ZrB_2 \rightarrow HfB_2 + ZrO_2.$$

For this investigation, the reactants were held at 2040°, 2110°, and 2200°C, respectively, in vacuo for one hour. X-ray diffraction patterns taken after heating to 2040° showed only traces of HfB_2 along with the reactants HfO_2 and ZrB_2. At 2110°C, the quantity of HfB_2 in the reaction product had increased, but the reaction was still incomplete. After heating to 2200°C, the reaction was complete. X-ray diffraction showed only the presence of zirconium dioxide and hafnium diboride.

A study of the ZrO_2-HfB_2 system showed that the mixture reacted to form ZrB_2 and HfO_2 at 2000°and at 2050°C, but that no reaction occurred at 2200°C. These findings are again based on X-ray diffraction patterns taken after heating the mixture in vacuo for one hour. Therefore, the following equilibrium exists in the ZrO_2, HfO_2, ZrB_2, and HfB_2 system.

$$HfO_2 + ZrB_2 \underset{< 2100°C}{\overset{> 2100°C}{\rightleftharpoons}} HfB_2 + ZrO_2.$$

A calculation of the free energy change ΔF at 2200°C indicates that the equilibrium should only proceed from the right-hand to the left-hand side. Depending on which thermodynamic data[21,22,23,24] are used, the reverse reaction should be unfavorable by 4 to 10 kcal/mole. The experimental evidence presented here shows that the available thermodynamic data (which are based on extrapolation) are inaccurate.

Oxide Pellets - Diboride Plates

In addition to the chemical compatibility of the various refractory oxide powders with diboride powders, experiments were carried out with the reactants in the compacted state; i.e., dense oxide pellets on diboride plates. Yttria-stabilized hafnia pellets were heated in vacuo on hafnium and zirconium diboride plates for one hour at 2190°C. The oxide pellets did not adhere to the diborides; however, some evidence of interaction at the oxide-diboride interface had occurred in each case. Figure 74 is a photomicrograph (500 X magnification) of the hafnia pellet showing the edge of that pellet which was adjacent to the zirconium diboride surface. There appears to be a diffusion zone approximately 4 to 5 μ thick. The hafnia has retained its pore structure at the interface, suggesting that the diffusion zone migrated into the hafnia.

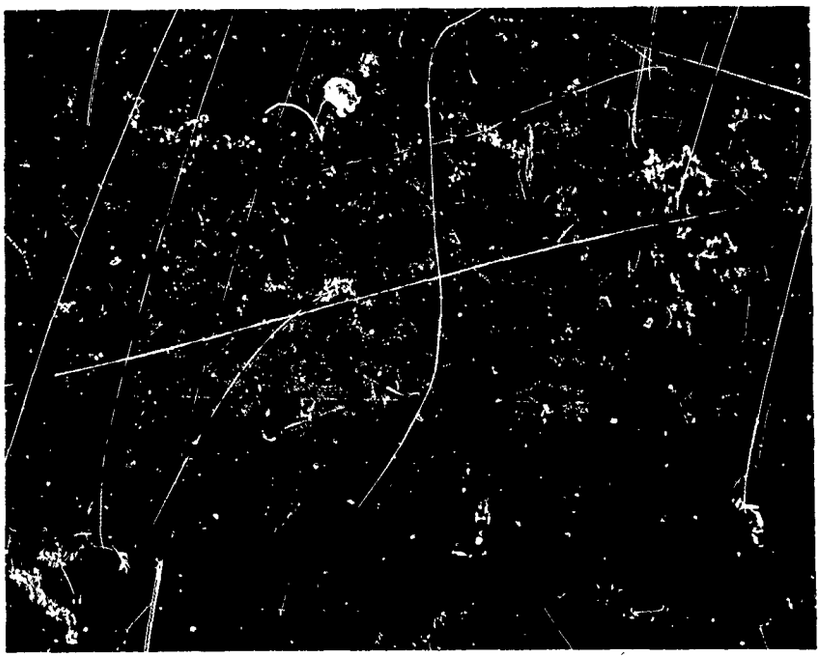

Figure 74. Stabilized Hafnia Heated in Contact with a ZrB_2 Plate, (500 X Magnification)

Figure 75 represents a photomicrograph of the hafnia pellet (500 X Magnification), showing the edge of the oxide surface which was adjacent to the hafnium diboride. There is some densification of the oxide extending to about 10 μ from the interface. It is also noted that the grain growth with a metallic deposit in the grain boundaries appears in the densified zone. Since the HfO_2 powder system showed no reaction with the HfB_2 powders, it may be that the yttria-stabilizer in the oxide pellet is reacting with the diboride.

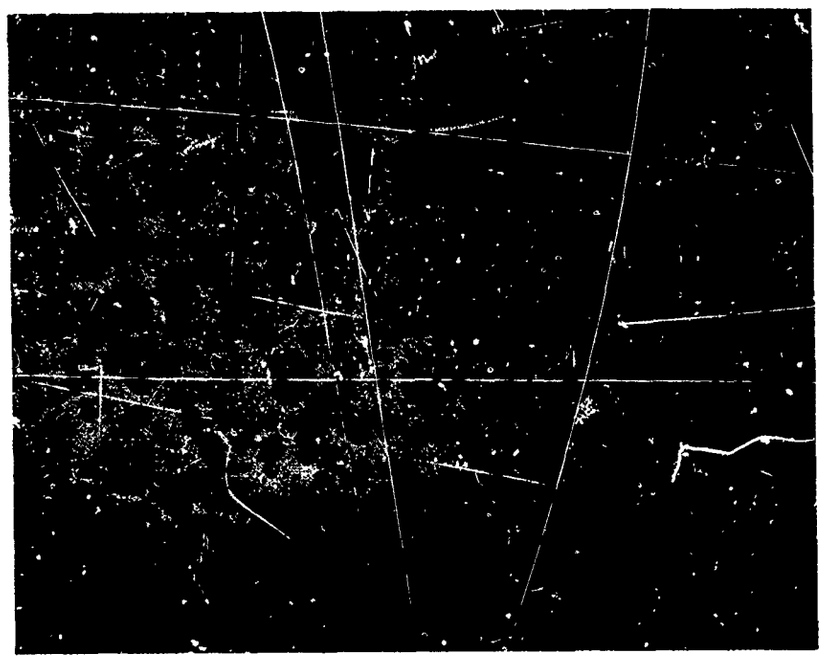

Figure 75. Stabilized Hafnia Heated in Contact with a HfB_2 Plate, (500 X Magnification)

Conclusion

The refractory oxides, ZrO_2, HfO_2, and ThO_2 are, in general, chemically stable with respect to ZrB_2 and HfB_2 at temperatures up to 2200°C. Only the system ZrO_2 - HfB_2 reacted at a temperature of less than 2100°C, and the system HfO_2 - ZrB_2 reacted at a temperature of greater than 2100°C.

IX. CARBOTHERMIC REDUCTION OF OXIDES

TASK B2-1

Introduction

On the basis of existing thermochemical and physical data[1], the single oxides, ThO_2, HfO_2, and ZrO_2 along with the compound oxides $ThZrO_4$ and $HfSiO_4$, have been selected as promising materials for further study at high temperature oxidation barriers. Considering these compounds as coatings directly on a graphite substrate requires information concerning the chemical reaction kinetics which describe interactions of graphite with the oxygen barriers. Even though the oxides are thermodynamically unstable with respect to carbon at 2200°C, the reaction rates may be low enough to justify an investigation of the factors controlling these rates.

Recently, there have been several limited kinetic investigations published on these systems, each with rather disquieting factors[25, 26, 27]. In all cases, the reactants were a mixture of the two species in a finely divided state; thus, the surface effects (such as diffusion and effective area) which are pertinent to a kinetic study of solid-solid system interpretation were based on assumptions of spherical particle size and closest approach approximations and the data corrected accordingly. Other factors included the narrow temperature ranges investigated and data collected for only the first few per cent of the reaction; thus, these results are not subject to any valid extrapolation. It was found in our own initial powder experiments[2] that carbon monoxide evolution was so rapid that each system appeared to obey a linear rate law. However, it is to be noted that such systems do not simulate those in connection with a high temperature protective coating for graphite; and therefore, it is apparent that compacted reactants be used in the further investigation of the kinetics of oxidation of graphite by these refractory oxides.

This final phase of the carbothermic reduction studies on the refractory oxides was concerned with determining the reaction kinetics of graphite-refractory oxide systems using compacted reactants. The oxides studied were ThO_2, ZrO_2, HfO_2, $ThZrO_4$, and $HfSiO_4$.

This section presents the results of these investigations and a discussion of the kinetic effects observed.

Experimental

High purity materials, specified by the manufacturer to be nuclear grade, were used as the reactants in this investigation. No further purification of these materials was carried out.

The oxide pellets of hafnium, thorium, and zirconium, 0.68 cm in diameter by 0.66 cm high, were obtained from the Zirconium Corporation of America, Solon, Ohio. The mixed oxides, thorium zirconate and hafnium silicate, were obtained as -325 mesh powders from the same source. Union Carbide Corporation, Carbon Products Division, grades ATJ and ZTA graphites were used as the carbon source. These materials were examined for purity by chemical and spectrographic analyses:

Calculated for ZrO_2 + 10 per cent Y_2O_3:		Zr, 66.6; O, 25.4; Y, 8.00
Found:		Zr, 65.7; O, 30.5; Y, 10.0
Spectroscopic:	Major:	Zr, Y
	Minor:	Ca, Si, Fe
	Trace:	None
Density		5.403 gms/cc

Calculated for HfO_2 + 10 per cent Y_2O_3:		Hf, 76.3; O, 15.7; Y, 8.00
Found:		Hf, 80.0; O, 12.6; Y, 6.7
Spectroscopic:	Major:	Hf, Y
	Minor:	Ti, Al, Si, Fe
	Trace:	Mn
Density		9.67 gms/cc

Calculated for ThO_2:		Th, 87.9; O, 12.1
Found:		Th, 87.3; O, 13.6
Spectroscopic:	Major:	Th
	Minor:	Fe, Al, Mg, Si
	Trace:	Mn
Density		9.76 gms/cc

All of the reactions were conducted in the furnace assembly shown in Figure 76. This furnace assembly was attached to an all-glass vacuum system similar to the one illustrated in Figure 77. All graphite crucibles were degassed at 2200°C in vacuo prior to making a kinetic run. In a typical experiment, the graphite crucible and oxide pellet were weighed, placed in the susceptor and furnace assembly, connected to the vacuum line, and the entire system evacuated to a pressure of 10^{-6} torr. The induction coil was then energized, and the reaction temperature attained within one to five minutes. The product gas (carbon monoxide) was compressed into a known volume by means of an automatic Toepler pump, while continuous pressure readings on a mercury manometer were made with a Gaertner cathetometer. No meniscus corrections were applied to these direct pressure readings.

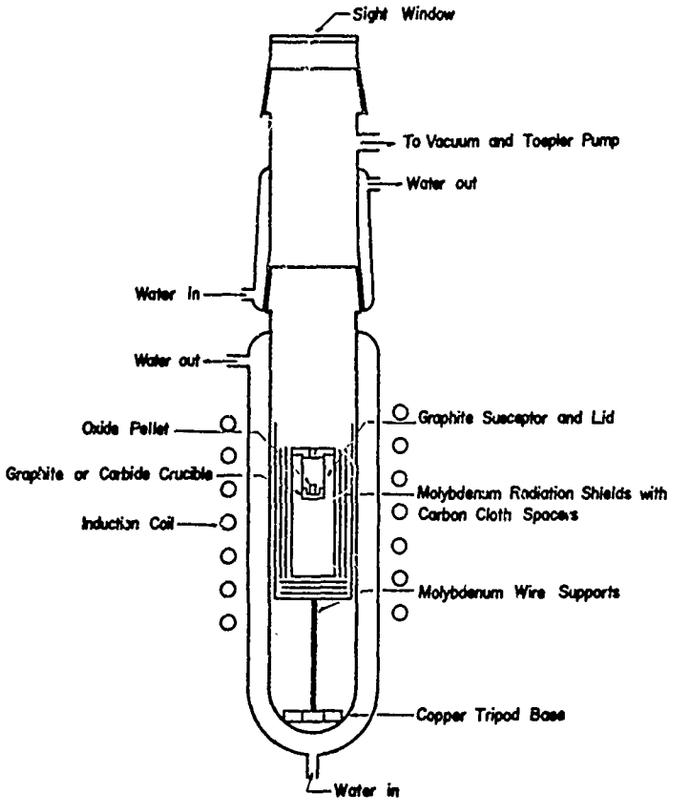

Figure 76. Reaction Furnace Assembly

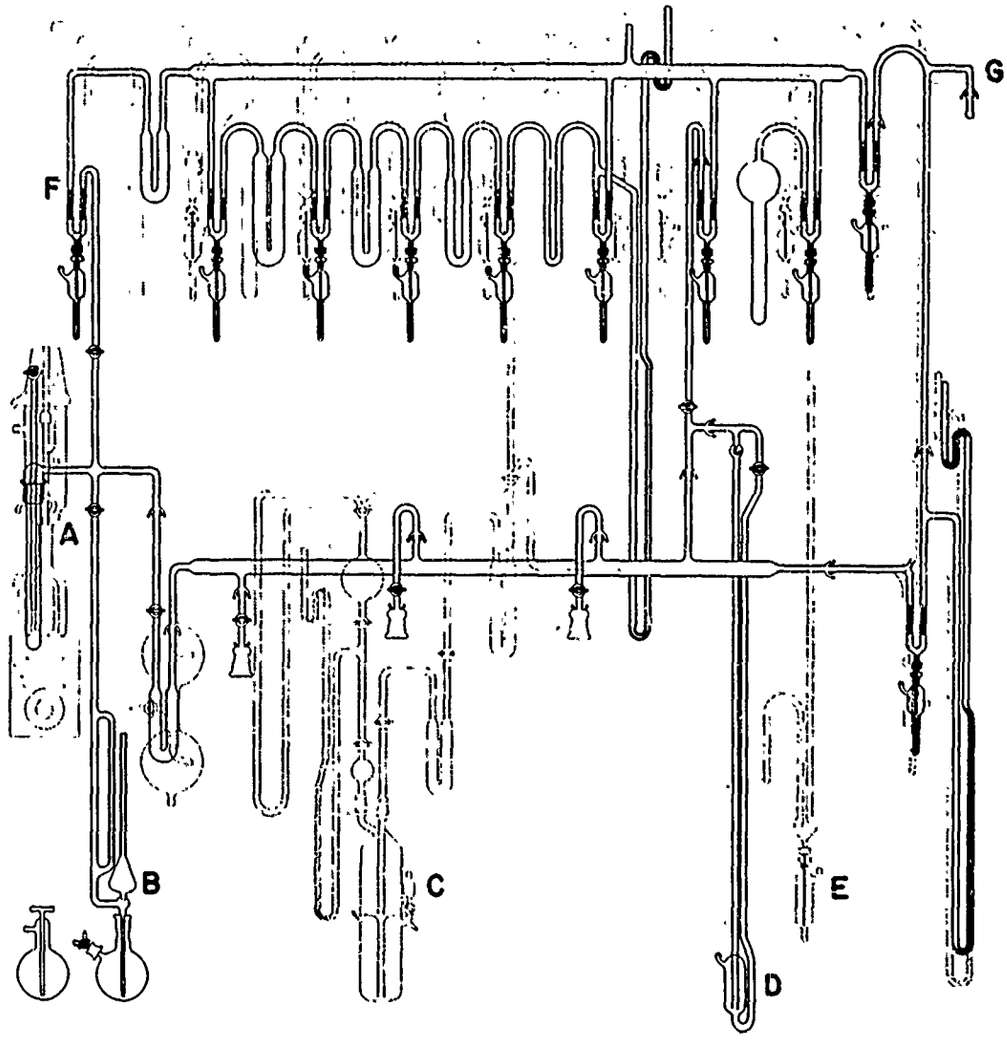

Figure 77. Glass Vacuum System

A. Diffusion Pump
B. McLeod Gauge
C. Automatic Toepler Pump
D. Mercury Manometer
E. Vapor Tensiometer
F. Mercury Float Value
G. Reaction Chamber Attached Here

The purity of the carbon monoxide gas evolved from these reactions was continually monitored by means of a Perkin-Elmer Model 154 vapor fractometer modified to fit integrally into the vacuum system. The column was a Perkin-Elmer silica gel "A", 12 feet in length. This column is used primarily for separation of hydrogen, nitrogen, carbon monoxide, and carbon dioxide. At no time was there observed any gas but carbon monoxide, indicating it to be the sole gaseous reaction product.

The following steps were used in the fabrication of the mixed oxide pellets. To -325 mesh powders of $ThZrO_4$ and $HfSiO_4$ were added 4 weight per cent Carbowax 4000 and water to make a thin slurry. The slurry was stirred in a high-speed Waring blender for fifteen minutes to assure good coating to the oxide particles and then it was poured into a Pyrex baking dish and heated to 120°C until all of the water had been removed. The resulting oxide powder, crushed to -100 mesh was pressed into pellets of 0.375-inch diameter in a steel die at 3000 lb/in^2. The Carbowax binder was removed by heating 300°C/hour to 1000°C and held for two hours at that temperature. Upon cooling, the pellets were placed in the sintering apparatus shown in Figure 78, and a program of 200°C/hour with holds at 1000°, 1500°, and 1950°C for two hours was achieved. Upon completion of slow cooling from 1950° to 800°C at a rate of 200°C/hour, the pellets were grey in appearance most probably due to oxygen deficiency; they were subsequently heated to 1000°C for two hours in an oxygen atmosphre and upon removal, they had turned white in color.

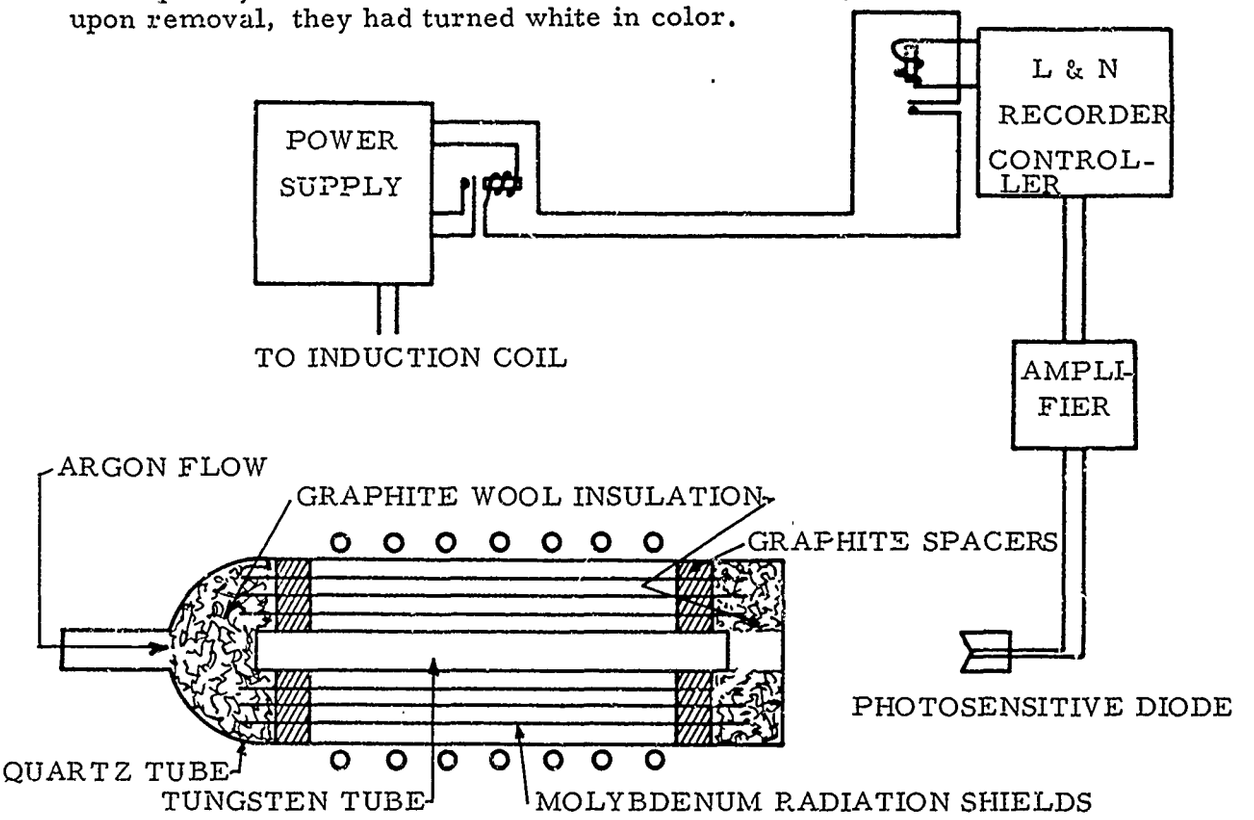

Figure 78. Sintering Apparatus for Mixed Oxide Pellets

Figure 79 and 80 are photomicrographs of the sintered pellets. The black areas are voids and these did not seem to be interconnected to any large extent.

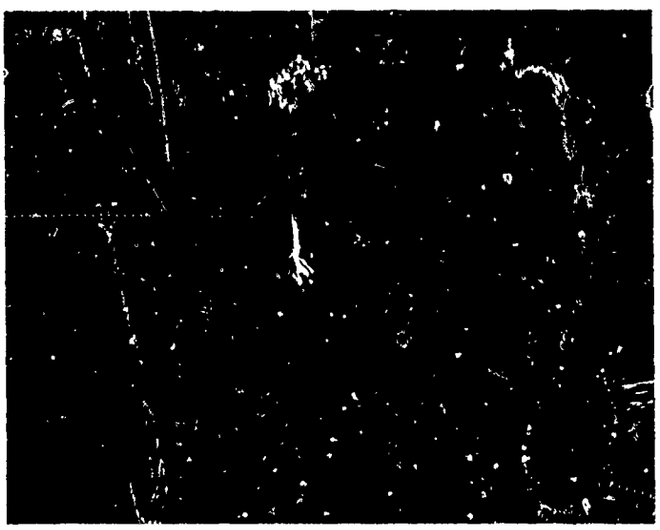

Figure 79. Photomicrograph of $HfSiO_4$ Pellet, (400 X Magnification)

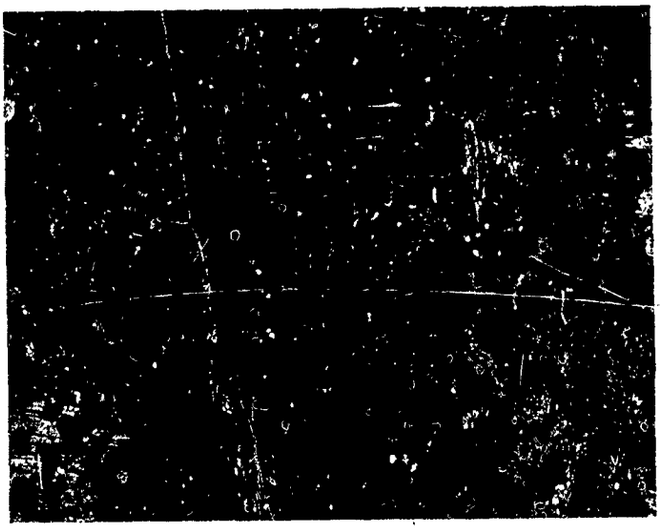

Figure 80. Photomicrograph of $ThZrO_4$ Pellet, (400 X Magnification)

Results and Discussion

The general equation which describes the kinetic behavior of this system is:

$$(CO)^n = kt \qquad (1)$$

where (CO) = the number of mmoles of carbon monoxide evolved per cm^2 of contact area,

k = the reaction rate constant
t = the time in minutes
and n = a positive integer

Taking the logarithm of both sides yields

$$n \log (CO) = \log t + \log k. \qquad (2)$$

Therefore, a plot of log (CO) versus log t yields a straight line whose slope is equivalent to n.

Differentiation of Equation (1) with respect to time yields

$$n (CO)^{n-1} d(CO) = kdt. \qquad (3)$$

In the cases where n = 1, Equation (3) reduces to

$$\frac{d(CO)}{dt} = k, \qquad (4)$$

and where n = 2.0

$$\frac{d(CO)}{dt} = \frac{k^{1/2}}{2t^{1/2}} \qquad (5)$$

Remembering that

$$k = Ae^{-E/RT}, \qquad (6)$$

the overall rate expression for the formation of carbon monoxide with time is

$\frac{d(CO)}{dt} = Ae^{-E/RT}$ mmoles CO/cm^2 minute for a linear rate process

and $\frac{d(CO)}{dt} = \frac{\sqrt{Ae^{-E/RT}}}{2} t^{-1/2}$ mmoles CO/cm^2 - minute$^{1/2}$ for a parabolic rate process. All of the kinetic data obtained in this investigation were found to fit either of these two rate expressions.

With the exception of thorium dioxide, all of the other graphite-oxide reactions were found to obey a parabolic rate law. In these cases, a plot of the square of the carbon monoxide concentration versus the time gave a straight line whose slope was equal to the reaction rate constant. A series of these lines were obtained at various temperatures and plots of log rate constant versus the reciprocal of temperature yielded straight lines indicating they followed Arrhenius-type reaction paths. The slopes of these lines gave the apparent activation energy for the reaction.

The data in Table 25 and the lines in Figure 81 represent the observed rate constants for the zirconium dioxide graphite system. The Arrhenius plot in Figure 82 gave an activation energy of 127.0 kcal/mole. The overall rate expression was found to be

$$\frac{d(CO)}{dt} = 4.28 \times 10^5 \exp^{-127,000/2RT} t^{-1/2} \text{ mmoles CO/cm}^2\text{-minute}^{1/2}.$$

TABLE 25

VARIATION OF REACTION RATE CONSTANT WITH TEMPERATURE FOR THE ZrO_2-C SYSTEM

Temperature °C	Rate Constant (mmoles CO)^2/cm^4 minute
1885	0.0647
1920	0.184
1970	0.276
2050	0.708
2125	1.93

Activation Energy = 127 kcal/mole

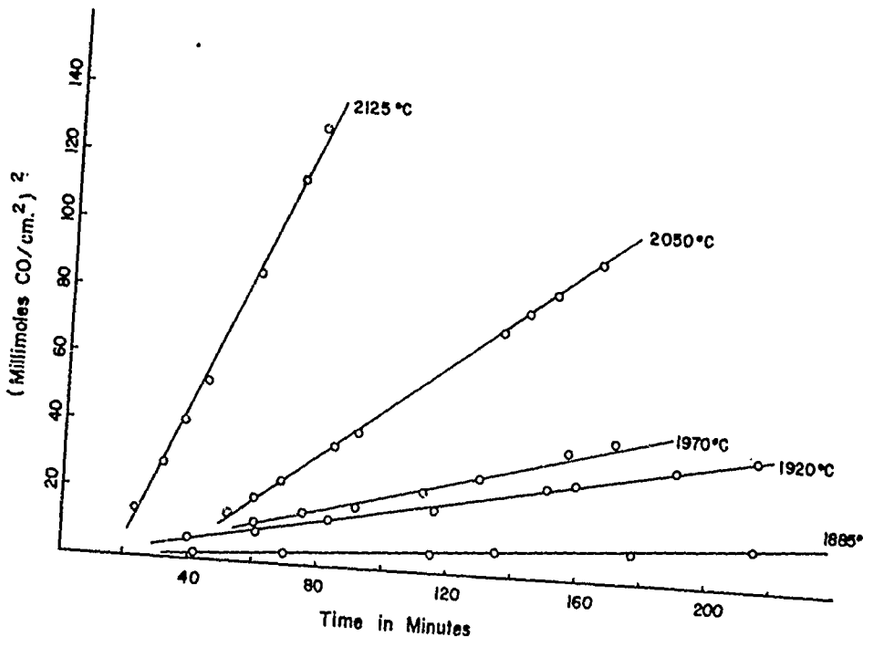

Figure 81. Variation of Rate Constant with Temperature for ZrO_2-C

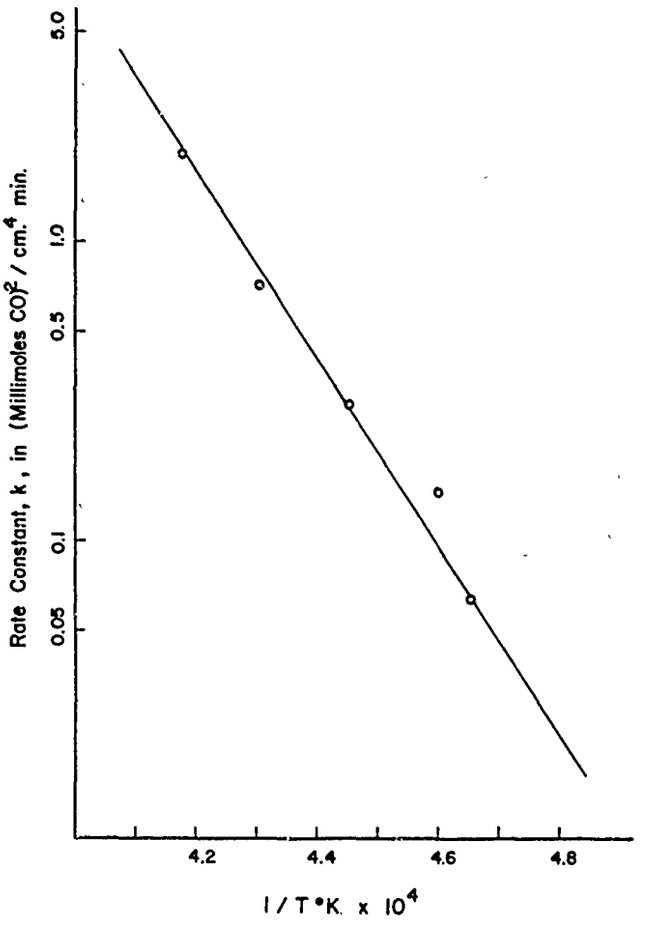

Figure 82. Arrhenius Plot for ZrO_2-C

The chemical reaction observed between zirconium dioxide and graphite was:

$$ZrO_2 + 3C \rightarrow 2CO\uparrow + ZrC.$$

The zirconium carbide formed during the course of reaction is found as a layer between the original carbon-oxide interface, and this layer increases in thickness with time. This carbide layer is shown in Figure 83 and is well bonded to the carbon, while there was no bonding between the carbide and the oxide pellet.

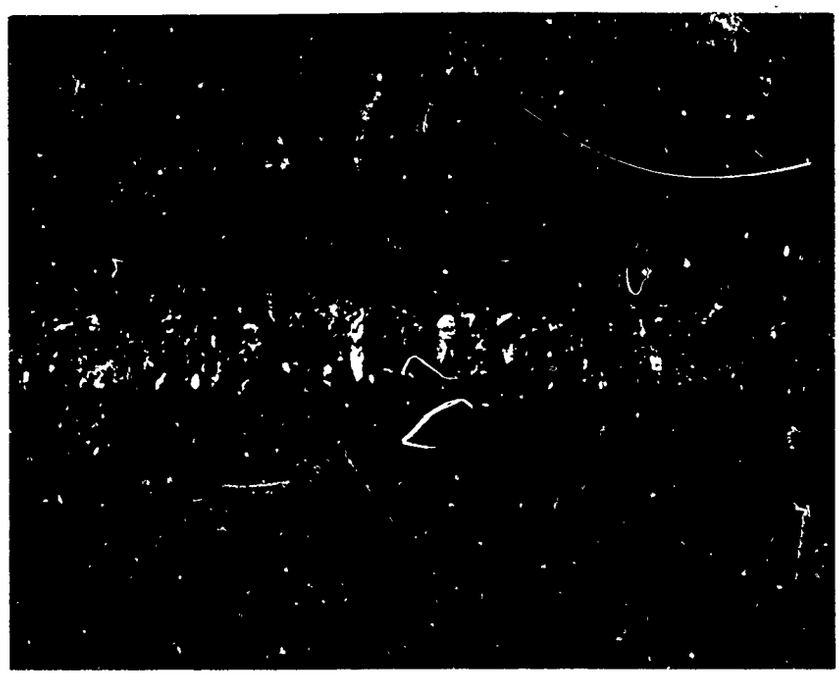

Figure 83. Photomicrograph of ZrC Layer on ZT Graphite Crucible, (500 X Magnification)

Due to the parabolic rate expression which this reaction follows and the build-up of a zirconium carbide layer, the rate-determining step in the reaction sequence to a first approximation probably involves a diffusion process through the carbide layer. The exact nature and chemical composition of the diffusing moiety and the carbide layer is open to speculation. The diagrammatic equations below illustrate two possibilities.

$$C \mid ZrO_2 \rightarrow C \mid ZrC \overset{\nearrow CO}{\mid} ZrO_2 \quad \text{or} \quad C \overset{\nearrow CO}{\mid} ZrC \mid ZrO_2 \qquad (7)$$

$$C \mid ZrO_2 \rightarrow C \mid ZrC \mid ZrC_{1-x} \overset{\nearrow CO}{\mid} ZrO_2 \qquad (8)$$

Equation (7) illustrates the diffusion of carbon through the carbide layer to the oxide surface and reaction to evolve carbon monoxide or diffusion of oxygen to the carbon surface and reaction to evolve carbon monoxide. Which process actually would occur, depends on the relative rates of diffusion of the two species through zirconium carbide.

Equation (7) implies that the reaction between zirconium carbide and zirconium dioxide does not occur at a measurable rate. However, in a

later section of this Summary Report, we find the rates of carbon monoxide evolution from carbide-oxide reactions to be comparable in magnitude to carbon-oxide rates; therefore, the mechanistic path shown in Equation (7) cannot be the correct one. Equation (8) illustrates the carbide layer as having a carbon concentration gradient from one end to the other. The rate-determining step now becomes the meeting of diffusing carbon from one end and the diffusing oxygen from the other end at some point within the growing diffusion layer. The thickness of the layers is found to be approximately 0.001 to 0.003 inch and X-ray analysis gives only zirconium-carbide lines which implies that carbon is diffusing faster than oxygen. Otherwise, zirconium metal would be detectable; and therefore, carbon monoxide evolution must be determined by the rate of carbon arrival at the oxide surface.

The hafnium dioxide-graphite reaction can be written as follows:

$$HfO_2 + 3C \rightarrow 2CO\uparrow + HfC.$$

As was expected, due to the similarity in chemical and physical properties of hafnium and zirconium, a similar rate law was observed for both of these reactions. The data for hafnium dioxide are given in Table 26 and Figures 84 and 85. The activation energy was calculated to be 120.0 kcal/mole. The overall expression for the formation of carbon monoxide is

$$\frac{d(CO)}{dt} = 1.26 \times 10^5 \exp^{-120,000/2RT} t^{-1/2} \text{ mmoles CO/cm}^2\text{-minute}^{1/2}.$$

TABLE 26

VARIATION OF REACTION RATE CONSTANT WITH TEMPERATURE FOR THE HfO_2-C SYSTEM

Temperature °C	Rate Constant (mmoles CO)^2/cm^4 min
1785	0.0111
1915	0.0498
1985	0.143
2025	0.266
2100	0.512

Activation Energy = 120 kcal/mole

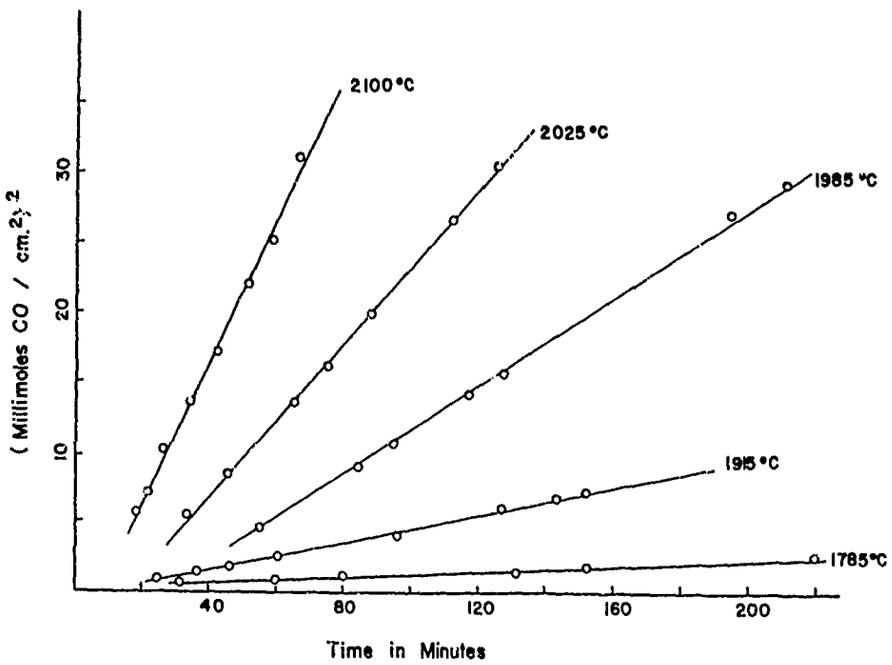

Figure 84. Variation of Rate Constant with Temperature for HfO_2-C Reaction System

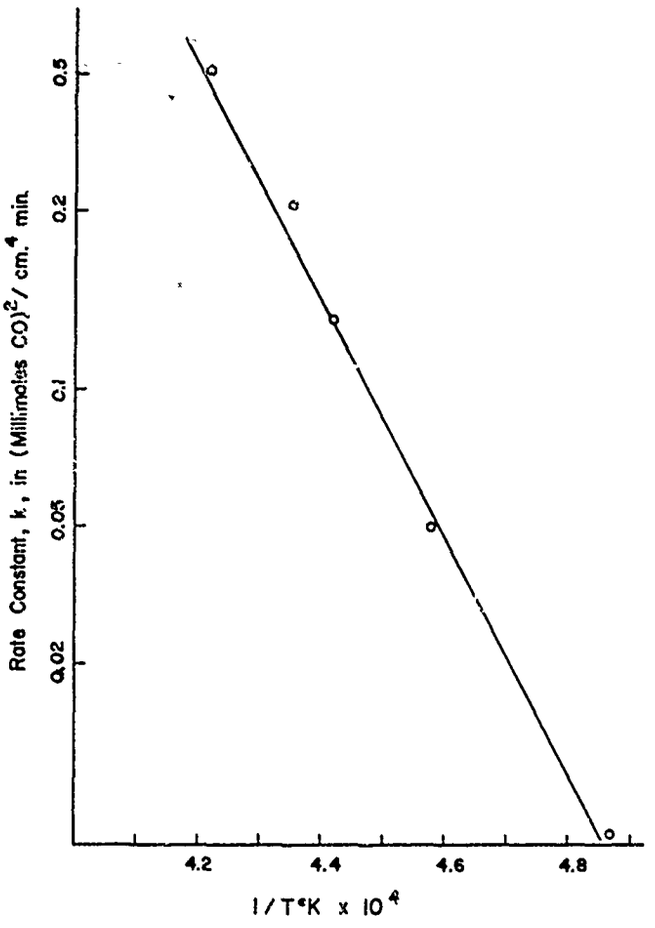

Figure 85. Arrhenius Plot for HfO_2-C System

The reaction product, hafnium carbide, is found as a layer between the original carbon-oxide interface, and the same rate-determining mechanism as described for the zirconium dioxide-carbon reaction may be invoked to explain the parabolic nature of the reaction path. It is interesting to note that the rate of CO evolution in the case of hafnium is less than that of zirconium, in agreement with the thermodynamic stabilities of the two oxides.

In the case of thorium dioxide, an entirely different phenomenon is observed. The kinetics for the thorium dioxide-carbon reaction follow a linear rate law for over 70 per cent completion and the entire temperature range studied. Table 27 gives the rate constants at various temperatures and from the Arrhenius plot, an activation energy of 126 kcal/mole is found (see Figure 86 and 87).

TABLE 27

VARIATION OF REACTION RATE CONSTANT WITH TEMPERATURE FOR THE ThO_2-C SYSTEM

Temperature °C	Rate Constant (mmoles CO)^2/cm^2- minute
1770	0.00356
1820	0.00902
1900	0.0230
1960	0.0446
2040	0.110
2080	0.255
2200	0.469

Activation Energy = 126 kcal/mole

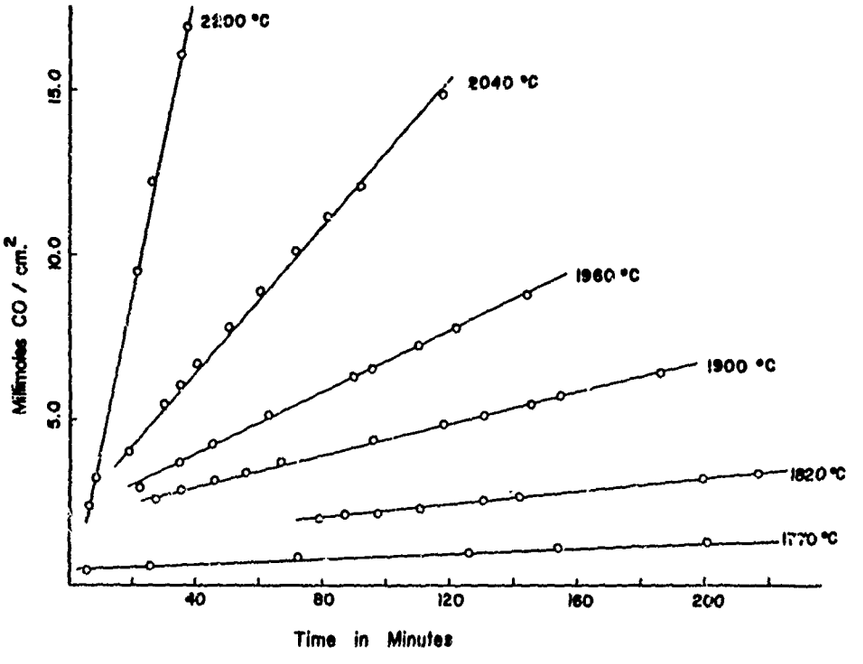

Figure 86. Variation of Rate Constant with Temperature for ThO_2-C System

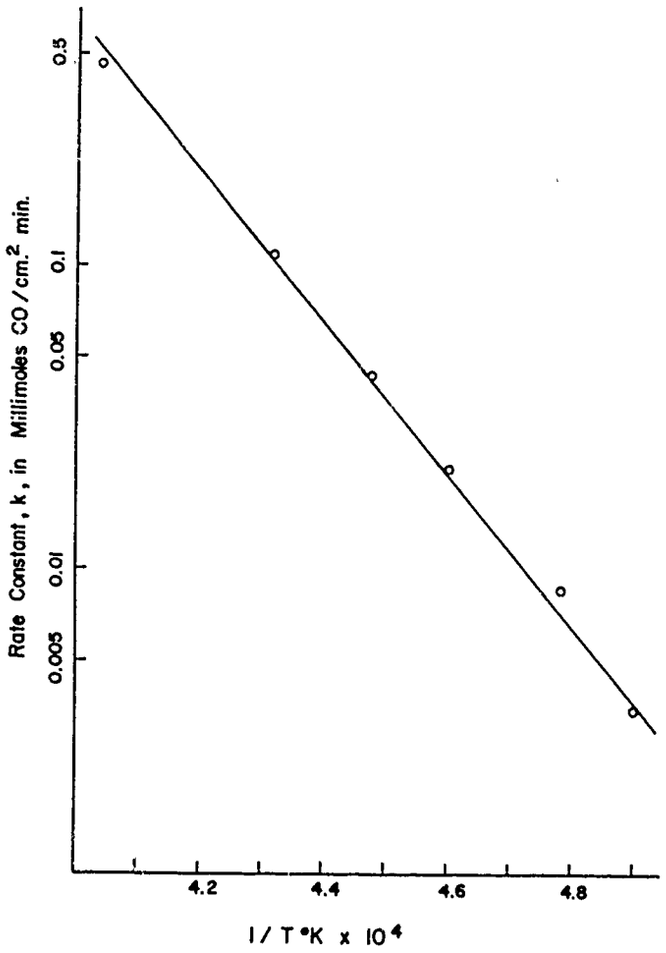

Figure 87. Arrhenius Plot for ThO_2-C System

Thorium dicarbide, ThC_2, is a product of the reaction as described by the following equation:

$$ThO_2 + 4C \rightarrow ThC_2 + 2CO.$$

Contrary to the carbides formed in the zirconium and hafnium dioxide-carbon systems, the thorium carbide was well bonded to both the adjacent carbon and oxide surfaces.

The rate expression for the carbothermic reduction of thoria is

$$\frac{d(CO)}{dt} = 1.05 \times 10^{11} \exp^{-126,000/RT} \text{ mmoles CO/cm}^2 \text{ minute.}$$

Due to the observance of a linear rate, diffusion is most probably ruled out as the rate-determining step in the reaction sequence, although a diffusion process is certainly occurring during the course of the reaction; but rather it is highly suggestive of a gas phase reaction occurring at the oxide-carbide interface as the rate-determining step in the overall reaction sequence. One such possibility would be the breaking of the carbon-carbon bonds in thorium dicarbide after oxygen from the thorium dioxide is adsorbed on the dicarbide surface. Blyholder and Eyring have postulated this desorption step in the oxidation of graphite[28]. They observed a linear rate with an activation energy of 85 kcal/mole. Our observed value for the activation energy is 125 kcal/mole or 40 kcal/mole higher than that observed by Eyring. In our system, however, the carbon is bound as the $C_2^{=}$ moiety and is not purely covalent in character as in the case of graphite. One would, on this basis, predict a higher activation energy for the breaking of the ionic carbon-carbon bond in the $C_2^{=}$ moiety than in graphite itself. Whether or not this difference is 40 kcal/mole would necessitate careful investigation with mass spectrometric techniques. Also, in separate experiments where thorium dicarbide was the primary reactant with thorium dioxide, the rates of carbon monoxide evolution were found to obey a linear rate and the magnitude of the rate constants compared favorably with those of the thorium dioxide-carbon system. All of this experimental evidence seems to point to the formation of carbon monoxide at the thorium carbide surface via the rupture of the $C_2^{=}$ moiety and its subsequent desorption from this surface.

Both of the mixed oxide systems investigated (thorium zirconate and hafnium silicate) were found to evolve carbon monoxide at rates several orders of magnitude larger than any of the single oxides and both obeyed parabolic rate laws. The data for the $ThZrO_4$-C systems are given in Table 28 and Figures 88 and 89. The overall rate expression for carbon monoxide evolution from thorium zirconate is

$$\frac{d(CO)}{dt} = 3.38 \times 10^5 \exp^{-118,100/2RT} t^{-1/2} \text{ mmoles CO/cm}^2\text{-minute}^{1/2}.$$

TABLE 28

VARIATION OF REACTION RATE CONSTANT WITH TEMPERATURE FOR $ThZrO_4$-C SYSTEM

Temperature, °C	Rate Constant $(\text{mmoles CO})^2/\text{cm}^4$ min
1515	0.000423
1650	0.0459
1725	0.121
1895	0.691
2050	1.33

Activation Energy = 118 kcal/mole

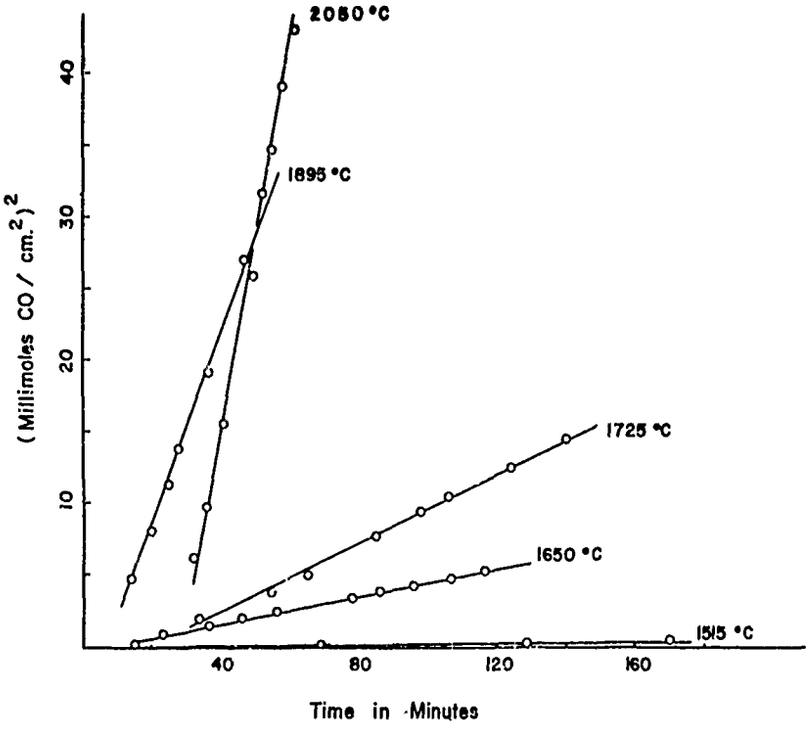

Figure 88. Variation of Rate Constant with Temperature for $ThZrO_4$-C System

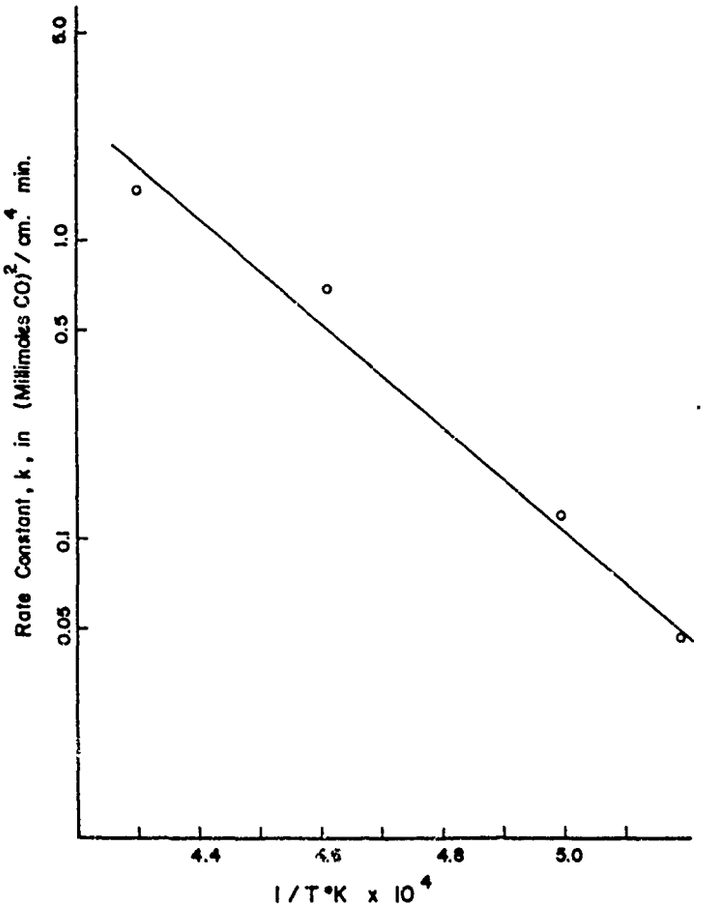

Figure 89. Arrhenius Plot for $ThZrO_4$

For comparison, at 1890°C the rate of carbon monoxide evolution from $ThZrO_4$ is 4.61; from ZrO_2 the rate is 0.0647; and from ThO_2 the rate is 0.023 mmole CO/cm^2 minute. It is evident that this mixed oxide is chemically less stable with respect to carbon than either of the single oxide components individually. The reaction may be written as follows:

$$ThZrO_4 + 7C \rightarrow 4CO + ThC_2 + ZrC.$$

The two carbides formed are found at the original carbon-oxide interface. Figure 90 illustrates the nature of this carbide layer. The graphite substrate is in the extreme left corner. The portion of the barrier which is out of focus is partially hydrolyzed thorium dicarbide, and the particles in focus are zirconium carbide. Random dispersement of the two carbides in the barrier is found with no preferred orientation. The bond between these carbides and the substrate is not well formed, and the layer is not dense, which may account for the faster observed reaction rate constants.

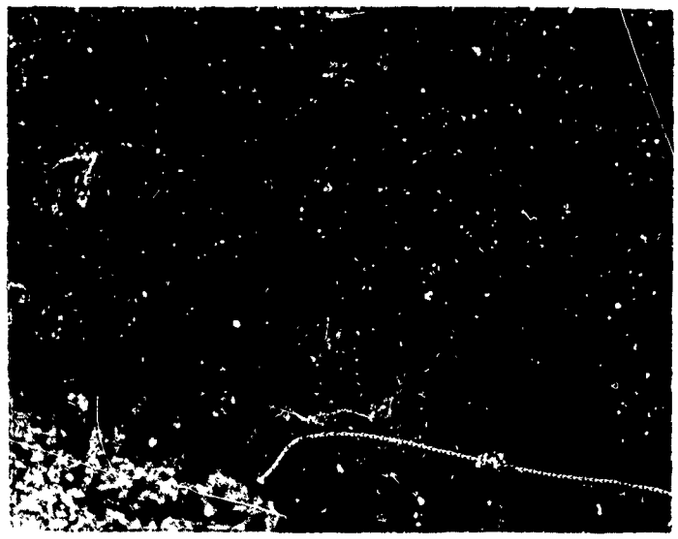

Figure 90. Photomicrograph of ThC_2-ZrC Layer on ATJ Graphite Crucible, (400 X Magnification)

In the case of hafnium silicate, the rate of reaction is so rapid, that above 1675°C the carbon monoxide evolution is immeasurable. Table 29 gives the rate constants while Figures 91 and 92 are the graphs of rate constants and the Arrhenius plot. The observed activation energy is 132.2 kcal/mole. The rate expression is

$$\frac{d(CO)}{dt} = 2.82 \times 10^7 \exp^{-132,200/2RT} t^{-1/2} \text{ mmoles CO/cm}^2 \text{ minute.}$$

TABLE 29

VARIATION OF REACTION RATE CONSTANT WITH TEMPERATURE FOR $HfSiO_4$-C SYSTEM

Temperature, °C	Rate Constant (mmoles CO)^2/cm^4 minute
1505	0.116
1550	0.487
1585	0.994
1625	1.59
1675	3.58

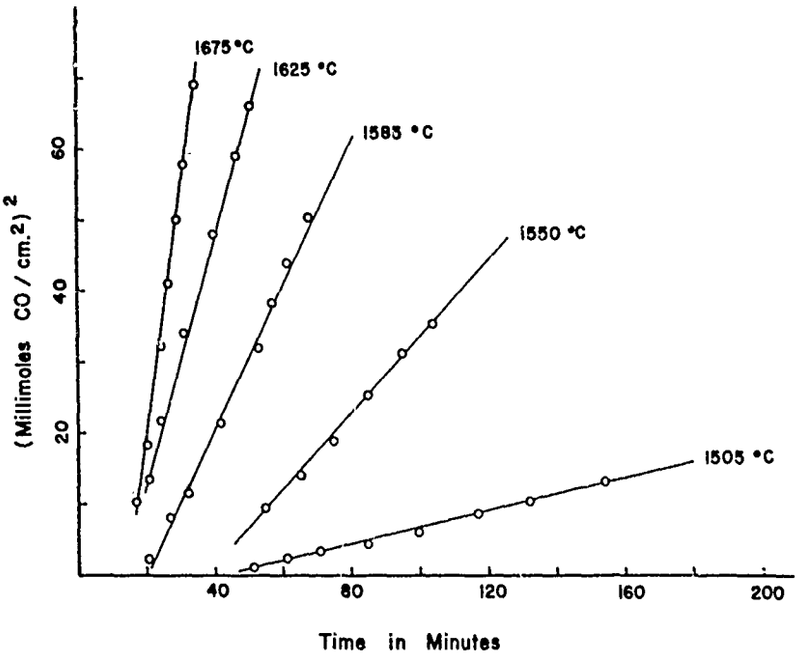

Figure 91. Variation of Rate Constant with Temperature for $HfSiO_4$-C Reaction System

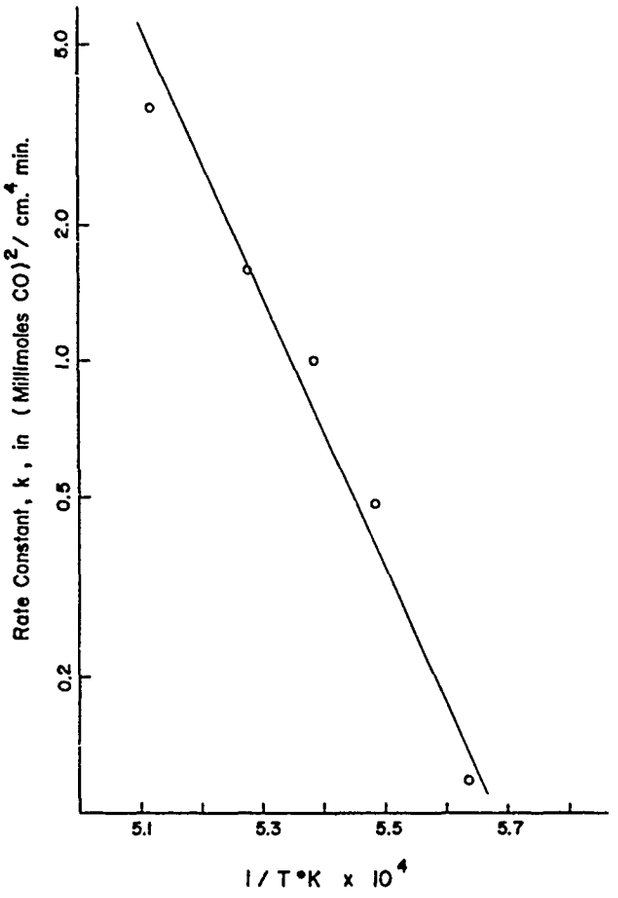

Figure 92. Arrhenius Plot for $HfSiO_4$-C System

There were observed large differences in the weight of carbon monoxide collected and actual weight loss of the reactants. This discrepancy can be attributed to a vaporization process in the mixed oxide pellet. All surfaces of the crucible, susceptor walls, and lid were coated with beta silicon carbide. Figure 93 is a photomicrograph of the bottom of an ATJ graphite crucible after reaction with hafnium silicate. The silicon carbide layer can be seen along the side and the bottom. This coating becomes increasingly thinner as it proceeds toward the center of the crucible.

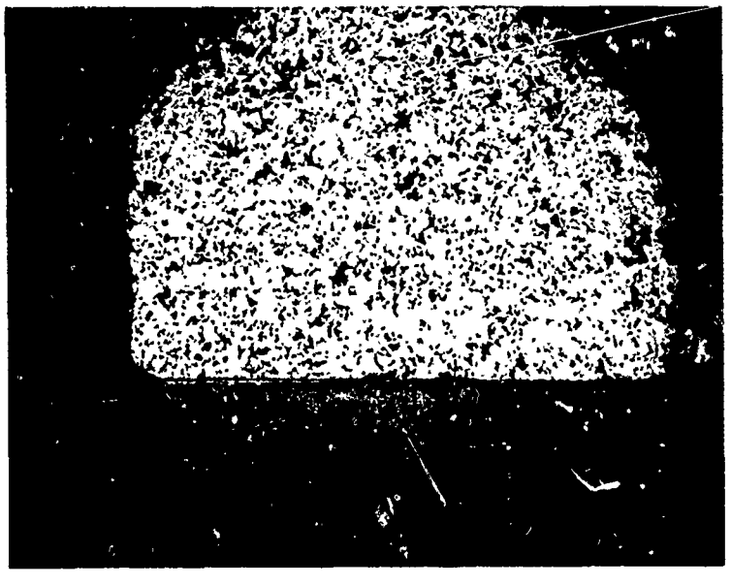

Figure 93. Bottom of ATJ Graphite Crucible After Reaction Between $HfSiO_4$ and Graphite, (25 X Magnification)

The species most likely responsible for the transport of silicon is silicon monoxide (SiO). A brown, pyrophoric substance was found on the lid of the susceptor; and, after this substance ignited, upon contact with the atmosphere, silicon carbide and silicon dioxide were the products. This high volatility of the silicon monoxide is observed in our diffusion studies of zircon $ZrSiO_4$. It was observed upon heating impervious zircon tubes using a graphite susceptor that the rate of diffusion of oxygen (indicated by the amount of carbon monoxide present) was independent of the partial-pressure of oxygen. When the graphite susceptor was removed and an iridium susceptor used, a pressure dependence was found. Thus, there was gross transport of an oxygen-containing species, probably silicon monoxide. One would suspect that the same phenomenon would occur with hafnium silicate. The layer between the oxide pellet and the graphite is a random mixture of hafnium carbide and silicon carbide.

Upon completion of these reaction studies there remained one effect to be determined, whether or not different grades of graphite would significantly alter the kinetics of reduction of an oxide. Therefore, a re-investigation of the zirconium dioxide-graphite reaction was done substituting Union Carbide ZT Grade ($d=2.0\ gm/cm^3$) for ATJ ($d=1.7\ g/cm^3$) graphite. The resulting rate law was found to be parabolic as was the case with ATJ graphite. Figure 94 illustrates the carbon monoxide evolution with time while Figure 95 is the Arrhenius plot.

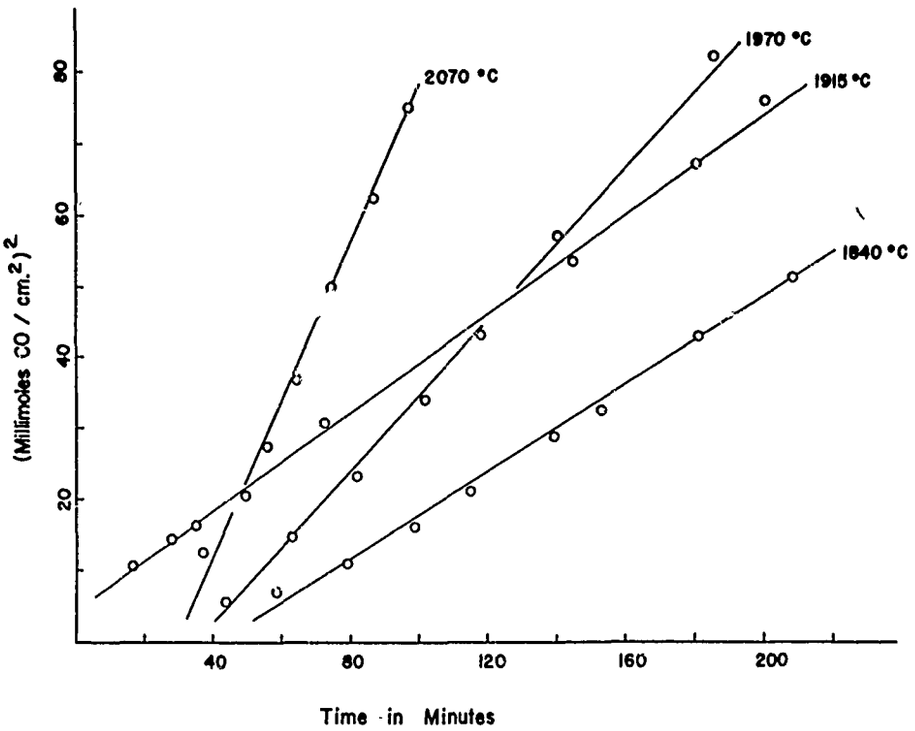

Figure 94. Carbon Monoxide Evolution with Time for the Carbothermic Reduction of ZrO_2 with ZT Grade Graphite

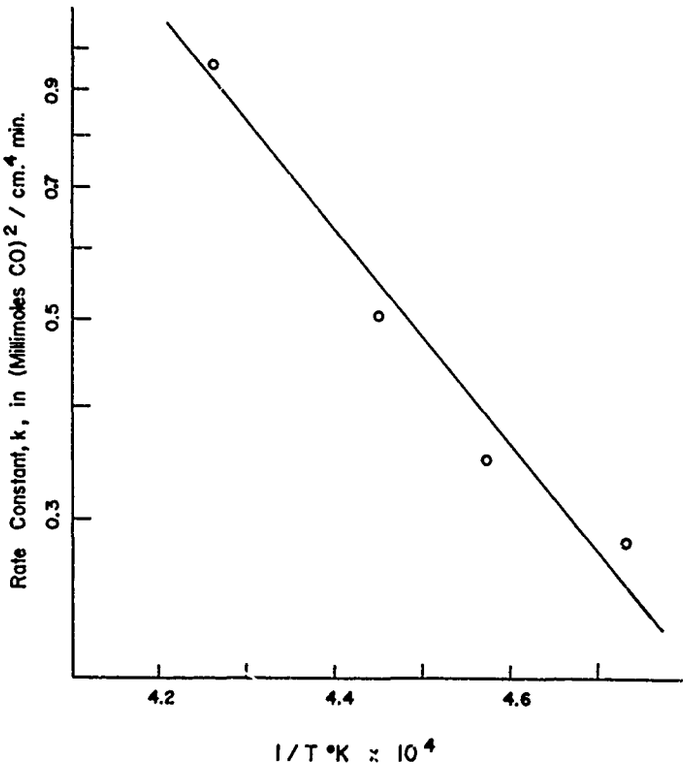

Figure 95. Arrhenius Plot for the Carbothermic Reduction of ZrO_2 with Grade ZT Graphite

Table 30 gives the observed rate constants for both ZT and ATJ studies.

TABLE 30

VARIATION OF RATE CONSTANT, K, WITH TEMPERATURE FOR ZrO_2 + ATJ AND ZrO_2 + ZT GRAPHITE

Temperature	K - ZrO_2 + ATJ (mmoles CO/cm^2)^2 min	K - ZrO_2 + ZT (mmoles CO/cm^2)^2 min
1840°C	--	.287
1915	.184	.350
1970	.276	.503
2070	.810	.980

The activation energy was found to be 52.3 kcal/mole. The overall rate expression is,

$$\frac{d(CO)}{dt} = 1.31 \times 10^2 \, e^{-52,300.2RT} \, t^{-1/2} .$$

As was observed with ATJ graphite, a zirconium carbide layer was formed between the original oxide-graphite interface. A summary of the rate constants for the reaction of the two grades of graphite with zirconia in the 1840 to 2070°C range appears in Table 30. It is seen that increasing the density of the graphite does not sufficiently inhibit the reaction to warrant further consideration of ZrO_2 as a coating directly on graphite.

X. CHEMICAL REACTIONS OF OXIDES WITH CARBIDES

TASK C2-1

Introduction

The results of the oxide-graphite kinetic studies indicated that a single layer coating of an oxide on graphite would not serve as a suitable protective barrier due to their mutual chemical instability. However, the reactions of hafnia with graphite and zirconia with graphite were inhibited by the formation of an intermediate carbide layer; thus, the carbides of hafnium and zirconium may well serve as an intermediate layer between the graphite substrate and the oxide coating. Thorium dicarbide, ThC_2, did not inhibit the interaction of thoria with graphite. On this basis, no kinetic studies were made using thorium dicarbide. This section covers the chemical kinetics of the reactions between hafnium and zirconium carbide with thorium dioxide, hafnium dioxide, and zirconium dioxide.

Experimental

Materials

Hafnium carbide, HfC, and zirconium carbide, ZrC, were purchased from the Atomergic Metals Company, Garden City, New York, as nuclear grade - 325 mesh powders. Chemical analyses were made and the results are:

HfC:	Theoretical:	C 6.28	Hf 93.72
	Found:	C 6.04	Hf 93.66
ZrC:	Theoretical:	C 11.6	Zr 88.4
	Found:	C 11.3	Zr 86.6

An analysis and discussion of the oxide pellets appear in Section IX.

Preparation of Carbide Crucibles

The carbide powders were placed in graphite die assemblies and hot-pressed to yield high density carbide crucibles. The best high density, i.e., 94 to 97 per cent of theoretical, crucibles were made with the following steps:

In a typical experiment, approximately 6.5 grams of the zirconium carbide powder were placed in the ATJ graphite die shown in Figure 96. The loaded die was positioned in the center of a 4-inch diameter resistance-heated graphite tube furnace, 96 inches in length, by means of the L-117 carbon pushrods (see Figure 97).

Argon was used as a flush gas and adjusted to a flow of 5 cubic feet per hour. The furnace was heated at a rate of 1500°C/hour to 2150°C and allowed to equilibrate for thirty minutes. A pressure of 7500 lbs/in^2 was applied by a hydraulic ram on the die and held for ninety minutes. The power was then turned off, the pressure released, and the furnace components allowed to cool to room temperature. The resulting crucible was 0.500 inch in diameter, 0.25-inch deep recess of 0.375 inch in diameter.

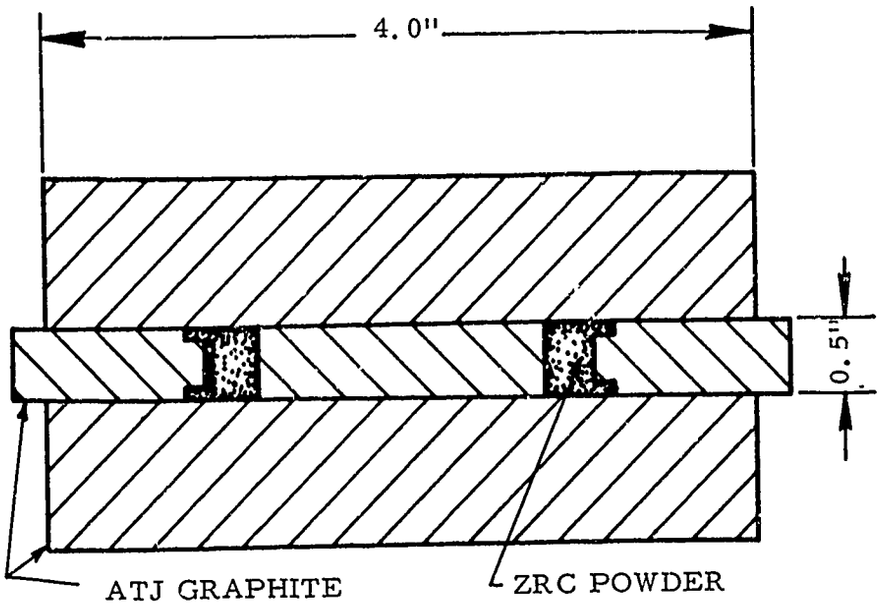

Figure 96. Die Assembly

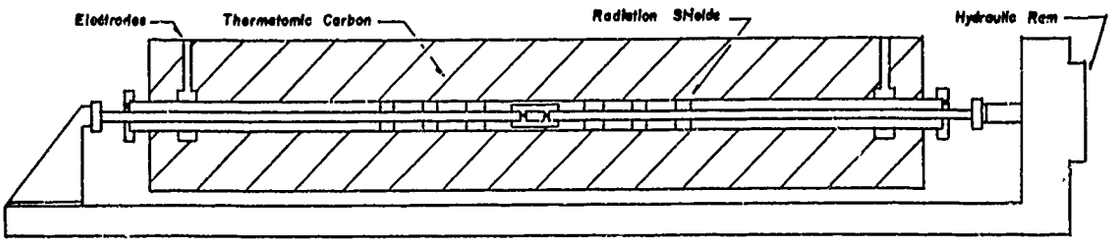

Figure 97. Hot-Pressed Furnace

Procedure

The procedure for obtaining the rate data is the same as that used for the oxide-carbon reactions (Section IX).

Studies on the equilibrium pressure of the zirconium oxide-zirconium carbide system were made on the apparatus shown in Figure 7. The zirconium carbide crucible with the oxide pellet inside was placed on a tungsten support rod and centered in the electromagnetic flux concentrator shown in Figure 6. This concentrator was insulated from the induction coil by means of a Pyrex glass mantle which also served as a vacuum bell jar. The system was evacuated by means of an oil diffusion and mechanical forepump to a pressure of 10^{-6} mm Hg. A shut-off valve was closed, and the leak rate of the system measured by means of thermocouple gauges.

The power source was a 25 KW thermonic Electronic Generator with a saturable core reactor for continuously monitoring the output. Temperature readings were made through a prism and window located on top of the Pyrex mantle. A disappearing filament Pyro-Micro-Optical pyrometer was used for temperature measurement. The carbide crucible and oxide pellet were allowed to react forming carbon monoxide which was exhausted until the temperature had stabilized. The shut-off valve was then closed and pressure readings observed.

Results and Discussion

The kinetic study of the reaction between thorium dioxide and hafnium carbide revealed that the system obeyed a linear rate law over the temperature range of 1695°C to 2070°C. Table 31 gives the variation of rate constants with temperature while Figures 98 and 99 illustrate the data and show the Arrhenius plot. The overall rate expression is:

$$\frac{d[CO]}{dt} = 6.52 \times 10^5 \exp^{-71,500/RT} \text{ mmoles CO/cm}^2 \text{ minute.}$$

TABLE 31

RATE CONSTANT FOR CARBON MONOXIDE EVOLUTION FROM ThO_2-HfC SYSTEM

Temperature, °C	Rate Constant (mmoles CO/cm^2 min)
1695	0.0063
1775	0.0096
1830	0.0428
1960	0.0626
2070	0.1086

Activation Energy = 71.5 kcal/mole

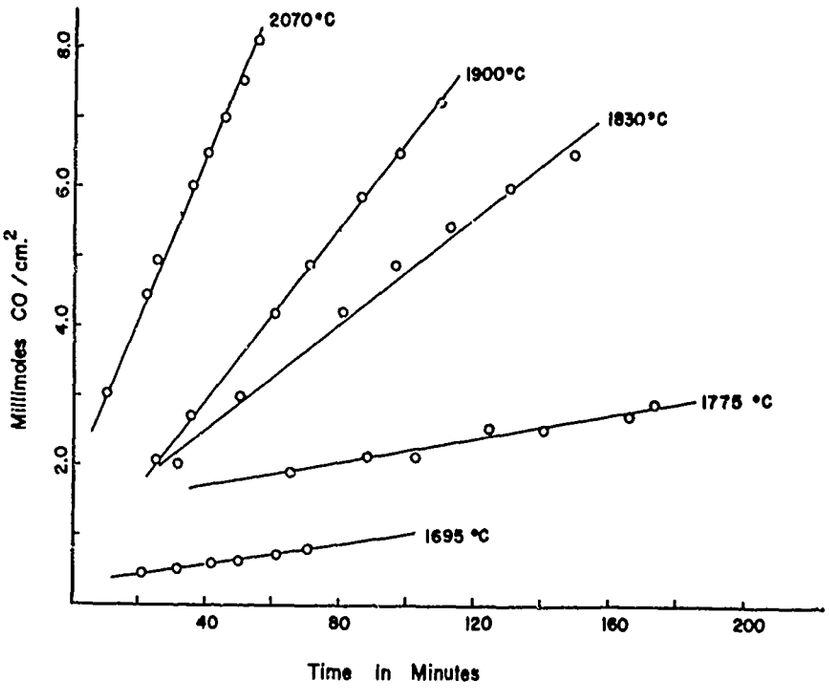

Figure 98. Carbon Monoxide Evolution Vs. Time for ThO_2-HfC Reaction

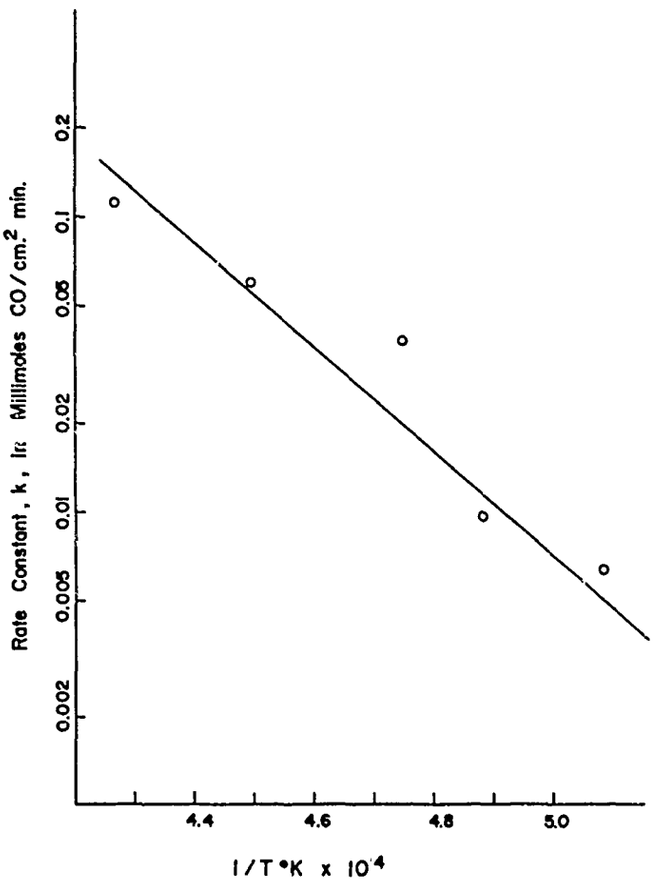

Figure 99. Arrhenius Plot for ThO_2-HfC Reaction

The observation of linearity again implies an interfacial reaction as rate-determining rather than a diffusion process. This interfacial rate-determining step may be envisioned as the desorption of carbon monoxide from the carbide surface as in the case of the thorium dioxide-graphite reaction. The observed activation energy of 71.9 kcal/mole as compared to 126 kcal/mole for the thorium dioxide-graphite reaction is of the correct order of magnitude since the carbon in hafnium carbide is more covalent while in thorium dicarbide it is found as the ionic moiety, $C_2^=$. Also, the value of 80-85 kcal/mole for the oxidation studies on graphite by Eyring, et al.[28] is higher than the 71.9 kcal/mole for hafnium carbide, which in effect, says that the carbon-carbon bonds in graphite are stronger than the carbon-carbon bonds in hafnium carbide and is probably correct due to the interstial nature of the carbon atoms in hafnium carbide. The overall picture then, is a constant carbon activity of unity at the thorium dioxide interface which is maintained by diffusion through the carbide, and the formation and desorption of carbon monoxide at this interface is the rate-determining step.

A temperature dependence on the value of n was observed in the kinetic studies on the thorium dioxide-zirconium carbide reaction. This temperature dependence is illustrated in Figure 100 and in Table 32.

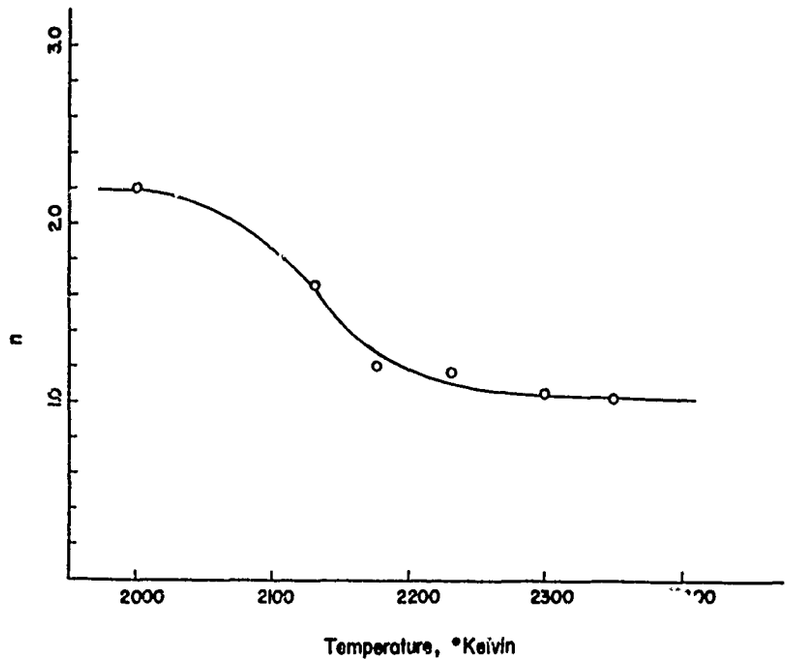

Figure 100. Value of n Vs. Temperature for ThO_2-ZrC Reaction

TABLE 32

VARIATION OF REACTION ORDER WITH TEMPERATURE

Temperature, °C	n
1730	2.22
1860	1.66
1905	1.20
1960	1.19
2020	1.07
2070	1.03

The physical significance which can be attached to this change in n is that the transition from a parabolic rate law to a linear rate law is continuous; no sudden discontinuities or change in slope, which are normally observed and associated with changes in mechanism, were found.

This gradual transition from a parabolic to a linear rate law can be explained, in part, by recalling that the other products of the reaction are thorium and zirconium metals. These metals form a continuous series of solid solutions with a minimum melting temperature of 1350°C at 50 % Zr.[29] Since the atomic ratio of Zr/Th is 2/1 for the interaction of ThO_2 with ZrC, one could expect to obtain a solution of the two metals which would melt at some temperature between 1350°C and 1820°C, the latter being the melting point of pure zirconium. The liquefaction of the diffusion barrier could alter the reaction mechanism from a diffusion controlled process to one which is surface reaction controlled.

Evidence of the formation of zirconium metal was found upon examination of the zirconium carbide crucible after reaction with thoria at 2070°C. Figure 101 is a cross section of the zirconium carbide immediately below the surface, which was in contact with the thoria pellet.

Figure 101. Zirconium Carbide Crucible After Reaction with Thoria at 2070°C, Showing Zirconium Metal at the Grain Boundaries, Etched with 20 Per Cent Ferric Chloride in Methanol--(500 X Magnification)

A second phase is found in the grain boundaries of the zirconium carbide; from the rounded shape of the grain boundaries it is evident that this phase was liquid at one time. The dark areas at the grain boundaries shown in the photomicrograph were brought out by etching the surface with a solution of 20 per cent ferric chloride in methanol. This etchant is specific for zirconium metal. Specific etchants for thorium metal failed to reveal the presence of this metal in the grain boundaries. However, thorium dicarbide was found in large quantities over the entire graphite susceptor and lid when the reaction temperature exceeded 1850°C, indicating the vaporization of thorium from the reaction mixture.

The observed kinetic data on the reactions between hafnium and zirconium dioxide with zirconium carbide fit parabolic expressions and are given in Tables33 and 34 and are shown in Figures 102 to 105.

TABLE 33

RATE CONSTANT FOR CARBON MONOXIDE EVOLUTION FROM HfO_2-ZrC SYSTEM

Temperature, °C	Rate Constant (mmoles CO)^2/cm^4 minute)
1535	0.00299
1665	0.0405
1765	0.1635
1930	0.299
2050	1.310

Activation Energy = 90.9 kcal/mole

TABLE 34

RATE CONSTANT FOR CARBON MONOXIDE EVOLUTION FROM ZrO_2-ZrC SYSTEM

Temperature, °C	Rate Constant (mmoles CO)^2/cm^4 minute
1660	.00924
1730	0.0376
1830	0.246
1950	0.584
2055	1.26

Activation Energy = 109.6 kcal/mole

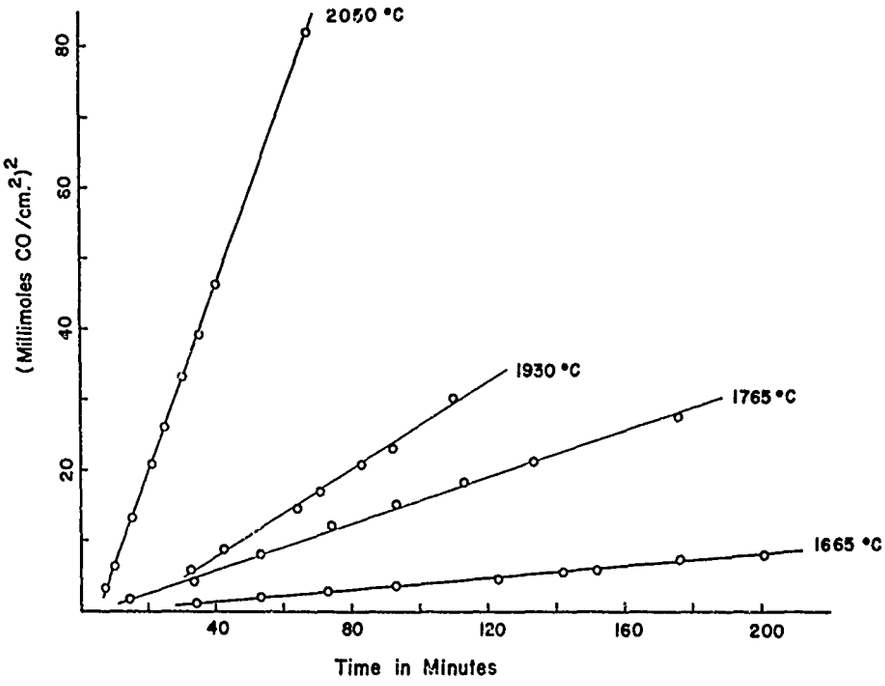

Figure 102. Carbon Monoxide Evolution Vs. Time for HfO_2-ZrC Reaction

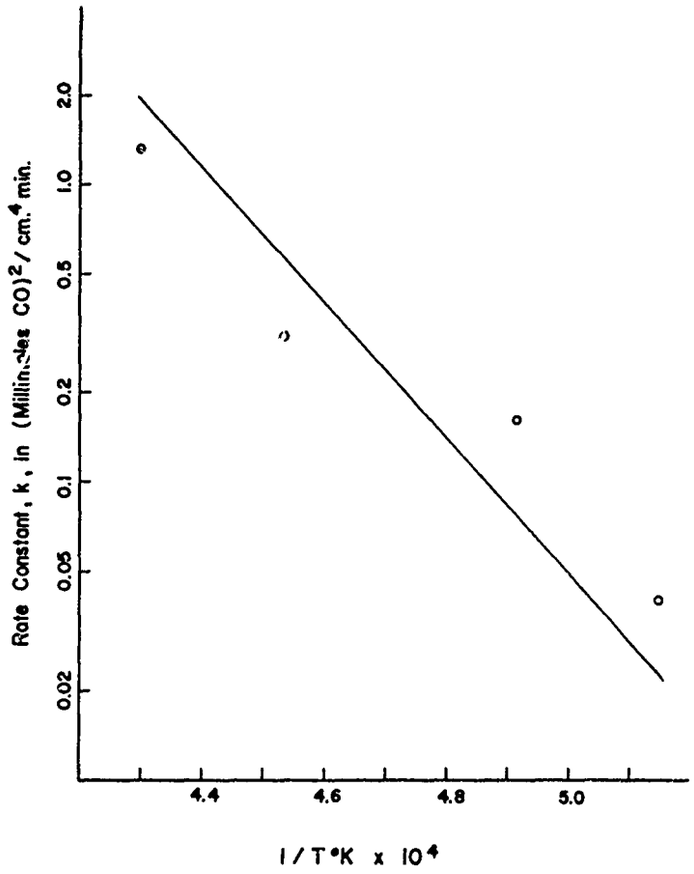

Figure 103. Arrhenius Plot for HfO_2-ZrC Reaction

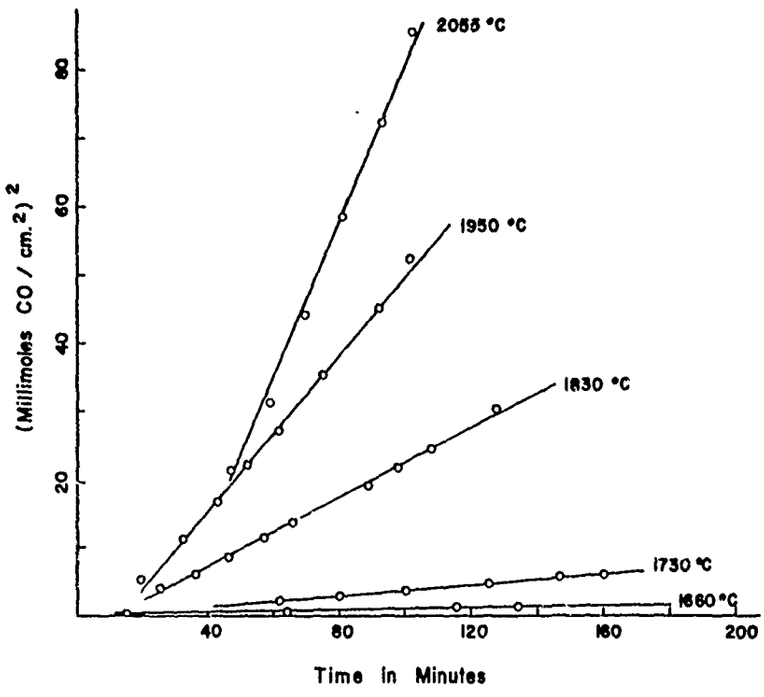

Figure 104. Carbon Monoxide Evolution Vs. Time for ZrO_2-ZrC Reaction

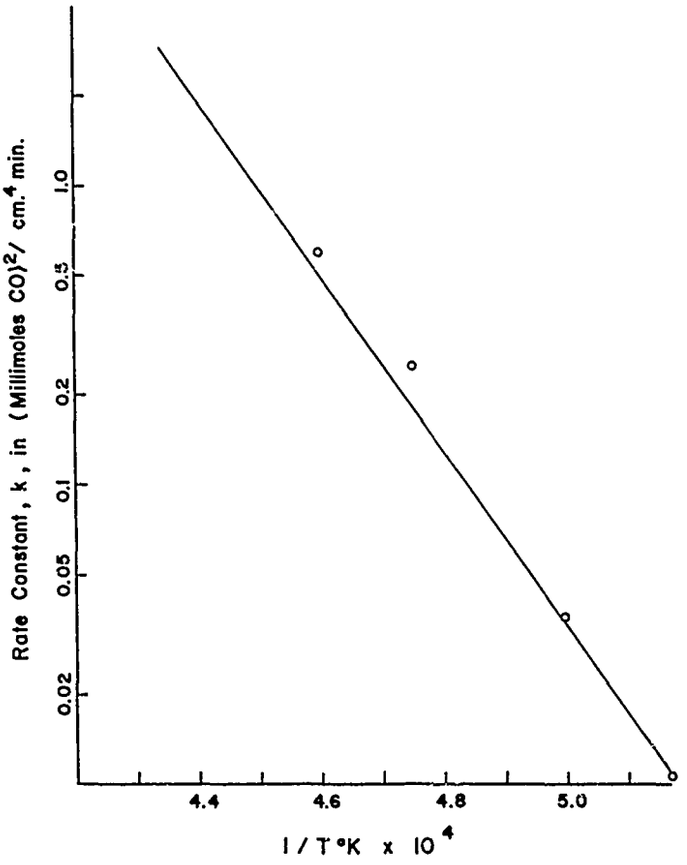

Figure 105. Arrhenius Plot for ZrO_2-Zrc Reaction

Both of these reaction systems obeyed a parabolic rate law over the entire temperature range investigated. The overall rate expressions are:

$$\text{for } ZrO_2\text{-}ZrC \quad \frac{d(CO)}{dt} = 8.95 \times 10^4 \exp^{-109,600/2RT} t^{-1/2} \text{ and,}$$

$$\text{for } HfO_2\text{-}ZrC \quad \frac{d(CO)}{dt} = 1.14 \times 10^4 \exp^{-90,900/2RT} t^{-1/2} .$$

The reaction between zirconium dioxide and zirconium carbide was found to proceed at a rate almost 30 per cent faster than the corresponding zirconium oxide-carbon reaction and, to a first approximation, these results seem anomalous and contradictory to the observed carbide layer formed in the oxide-carbon reaction. The chemical equations describing these two systems are:

$$ZrO_2 + 3C \rightarrow 2CO + ZrC \text{ and}$$

$$ZrO_2 + 2ZrC \rightarrow 2CO + 3Zr.$$

However, zirconium carbide was found as a coating over the entire inner walls and lid of the susceptor when zirconium dioxide was treated with zirconium carbide. This phenomenon was not observed in the zirconium oxide-carbon system. Since the amount of free carbon available to convert the metal to the carbide is at a minimum in the oxide-carbide system, the zirconium metal formed as one of the products vaporizes and upon recondensation on the hot graphite walls of the susceptor assembly is converted to zirconium carbide. Free carbon in the oxide-carbon system is at a maximum; therefore, conversion to zirconium carbide occurs within the reaction mixture. The vaporization process, in effect, serves to keep the metal layer between the oxide and carbide surface growing at a much slower rate than the carbide layer in the oxide-carbon system. Thus, the diffusion process, which is rate controlling in the zirconium oxide-carbon system, is most likely the diffusion of carbon through the zirconium carbide; while in the zirconium oxide-zirconium carbide reaction, the diffusion process which is rate-determining is that of oxygen through the metal layer.

To check this line of reasoning, samples of graphite coated with zirconium carbide, obtained from High Temperature Materials, Incorporated, were subjected to oxidation with pellets of zirconium oxide. Rates of carbon monoxide evolution were found to equal the measured rates of our own zirconium dioxide-graphite reactions. Thus, (1) when carbon is present in excess over zirconium carbide, the rate-determining step is carbon diffusion and (2) zirconium carbide affords no oxidation protection as an intermediate layer between a graphite substrate and the outer refractory oxide coating from a kinetic standpoint.

When the oxides of hafnium and zirconium were treated with hafnium carbide, parabolic rate laws were observed in both cases. The data for these two systems are given in Table 35 and 36 and are illustrated in Figures 106 to 109. The overall rate expressions are:

$$\text{for } ZrO_2\text{-HfC } \frac{d(CO)}{dt} = 2.47 \times 10^5 \exp^{-117,500/2RT} t^{-1/2},$$

$$\text{and for } HfO_2\text{-HfC } \frac{d(CO)}{dt} = 1.38 \times 10^4 \exp^{-98,200/2RT} t^{-1/2}.$$

TABLE 35

RATE CONSTANT FOR CARBON MONOXIDE EVOLUTION FROM ZrO_2-HfC SYSTEM

Temperature, °C	Rate Constant (mmoles CO)^2/cm^4 minute
1630	0.0067
1710	0.0355
1830	0.0908
1940	0.397
1995	1.69

Activation Energy = 117.5 kcal/mole

TABLE 36

RATE CONSTANT FOR CARBON MONOXIDE EVOLUTION FROM HfO_2-HfC SYSTEM

Temperature, °C	Rate Constant (mmoles CO)^2/cm^4 minute
1575	0.00190
1695	0.00825
1800	0.0228
1960	0.213
2175	1.204

Activation Energy = 98.3 kcal/mole

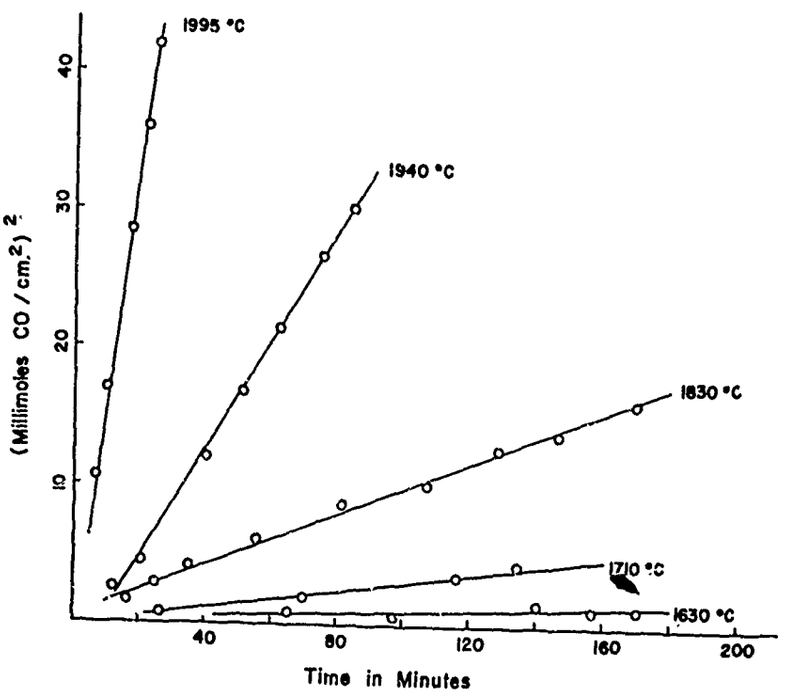

Figure 106. Carbon Monoxide Evolution Vs. Time for ZrO_2-HfC Reaction

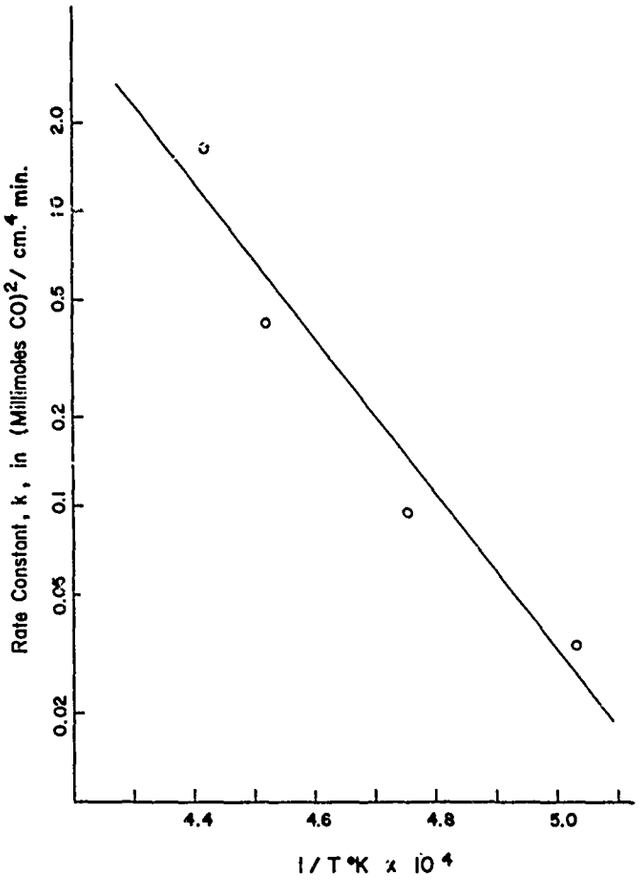

Figure 107. Arrhenius Plot for ZrO_2-HfC Reaction

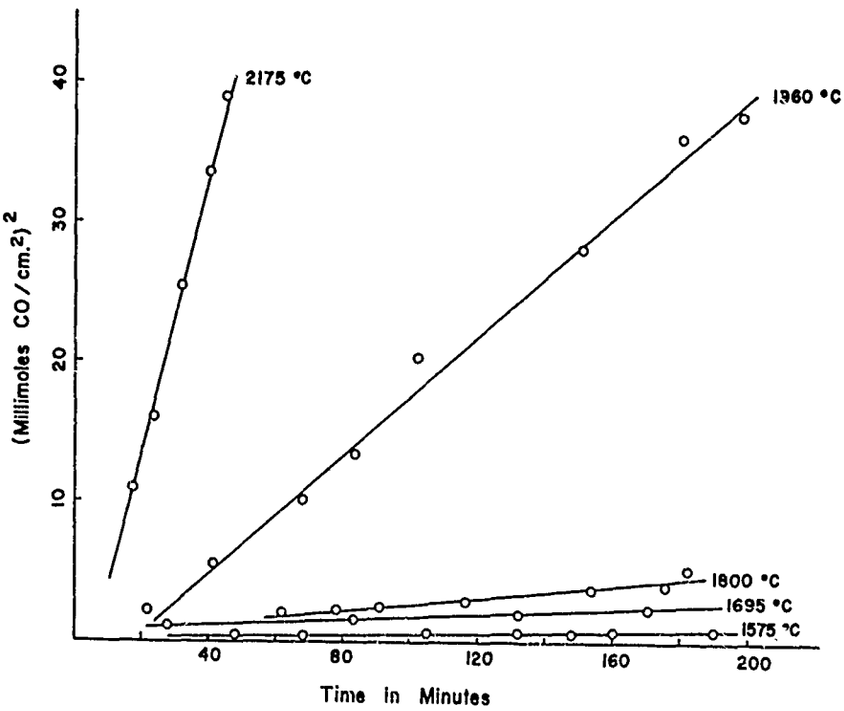

Figure 108. Carbon Monoxide Evolution Vs. Time for HfO_2-HfC Reaction

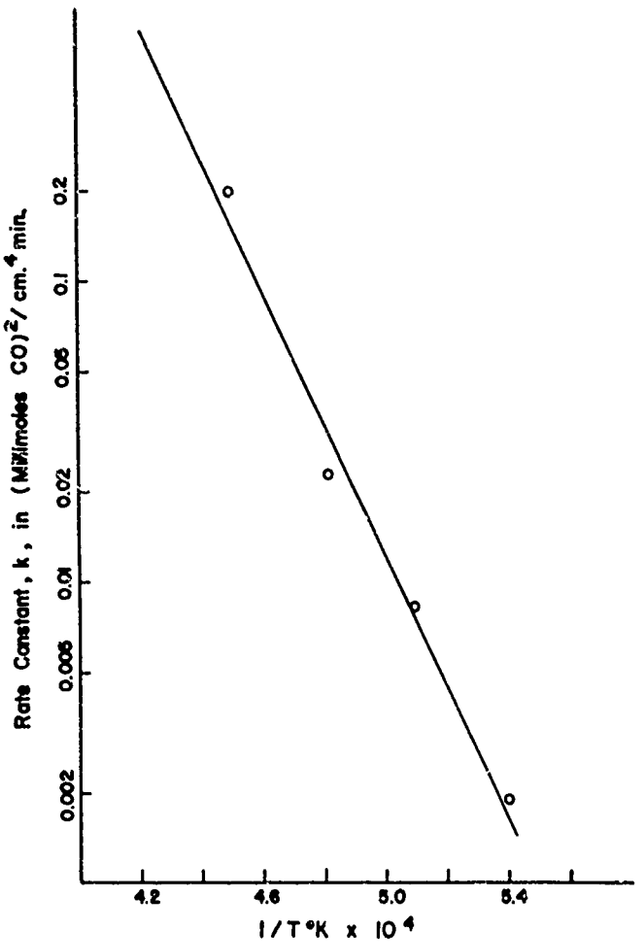

Figure 109. Arrhenius Plot for HfO_2-HfC Reaction

The rates of reaction again parallel the thermodynamic stabilities of the two oxides, i.e., hafnium dioxide is more stable than zirconium dioxide with respect to hafnium carbide.

In the HfO_2-HfC system, there was no hafnium carbide found on the susceptor walls or lid due to metal vaporization as in the zirconium carbide-zirconium dioxide system. Thus, the rate-determining step here can be envisioned as a process dependent on the carbon concentration gradient across the carbide, as was the case with the graphite-oxide studies, and the rate of carbon monoxide evolution is thus determined by the diffusion of carbon to the oxide interface and of oxygen diffusion to the carbide surface.

The above discussions on the chemical reactions between oxides and carbides have presented strong arguments for exclusion of carbides as intermediate barrier materials. However, these conclusions have been drawn from studies of the kinetic effect. No discussion on a chemical

reaction is complete without some consideration of the thermodynamic effects. As an example, the ΔF° values[21] at 2200°K for zirconium dioxide, zirconium carbide, and carbon monoxide are:

$$\Delta F^\circ_{2200} \text{ for } ZrO_2 = -158.5 \text{ kcal/mole}$$

$$\Delta F^\circ_{2200} \text{ for } ZrC = -41.3$$

$$\Delta F^\circ_{2200} \text{ for } CO = -72.3$$

for the reaction $ZrO_2 + 3C \rightarrow ZrC + 2CO$,

$$\Delta F^\circ_{\text{reaction}} = -27.4 \text{ kcal/mole.}$$

Setting $\Delta F^\circ = -RT \ln K_p$ we find $K_p = 525$ atms; but $K_p = P^2_{CO}$ and,

therefore, the equilibrium pressure of carbon monoxide would be 22 atmospheres. Thus, the equilibrium lies far to the right of the reaction as written above. However, using the same values for the equation:

$$2\,ZrC + ZrO_2 \rightarrow 3Zr + 2\,CO$$

$$\Delta F^\circ_{\text{reaction}} = +96.5 \text{ kcal/mole}$$

Setting $\Delta F^\circ = -RT \ln K_p$ we find $K_p = 2 \times 10^{-10}$ atms, or $P^2_{CO} = K_p$ and

the equilibrium pressure of carbon monoxide would then be 1×10^{-2} mm Hg. To test the validity of the thermodynamic functions and the equation for the reaction as written above, we allowed zirconium dioxide and zirconium carbide to react at 1925°C in a static vacuum of 10^{-6} mm Hg. The carbon monoxide pressure built up rapidly to a pressure of 10^{-2} to 10^{-1} mm Hg as read on a thermocouple gauge, after which the pressure increase slowed down to the leak rate of the system. Repeated evacuation to 10^{-6} mm Hg and isolation of the reactants in the system gave the same results several times.

XI. TRANSPORT OF OXIDES IN WATER VAPOR (SINGLE OXIDES)

TASK A2-1

Introduction

The influence of water vapor on the volatility of a coating material is being determined because of its pertinence to possible application areas. Recent information indicates it may be desirable to aspirate water from leading edges of re-entry vehicles to act as a coolant and to dispel the ion sheath which interferes with communication.

Of the single refractory oxides under consideration for coating materials, only the transport of BeO has been studied.[30, 31, 4]

Grossweiner and Seifert[30] demonstrated that the volatility of BeO at high temperatures is greatly increased by the presence of water vapor. Measurements of the effect of temperature and partial pressure of water on the volatilization of BeO indicate that the increased volatility results from the reaction

$$BeO_{(s)} + H_2O_{(g)} \rightarrow Be(OH)_{2(g)} \text{ for which}$$

$$\log_{10} K_p = 1.63 - 9060/T.$$

The experiments were run under equilibrium conditions in the range of 1200° to 1600°C; if an extrapolation of their data to 2200°C is valid, the vapor pressure of the $Be(OH)_2$ is about 9.2 torr as opposed to the vapor pressure of BeO of about 10^{-2} torr.[32]

Stuart and Price[4] found that weight losses of BeO are solely a function of temperature and water throughout as described by the equation

$$\log N_{BeO} = 1.62 - 8.8 \times 10^3/T°K + \log N_{H_2O}$$

where N_{BeO} = number of moles of BeO and

N_{H_2O} = number of moles of H_2O.

McKisson[33] investigated the BeO-H_2O reaction as it would apply in an open cycle, air-cooled, beryllia-moderated, power reactor. Assuming that the rate-controlling step in the process is the diffusion of the gaseous beryllium hydroxide product through a laminar boundary layer at the BeO surface, McKisson has derived the expression

$$r = 3.19 \times 10^7 \frac{D}{T_f t} (Kp_w - p_b) \text{ mm/years}$$

where r = the corrosion rate,
D = the diffusion coefficient of $Be(OH)_2$ through air, cm^2/sec,
T_f = the average temperature of the boundary layer, °K,
t = the boundary layer thickness, cm,
K = the equilibrium constant,
p_w = the partial pressure of water vapor, atm.,
p_b = the partial pressure of $Be(OH)_{2(g)}$ product in the bulk gas stream, atm.

At 1430°C, an air flow rate of 58 ℓ/min, a humidity of 0.026 g H_2O/g air, and a corrosion rate of 15.1 mm/y (595 mils/y) was observed. The interactions of water vapor with the other single oxides selected for study in this program have not been investigated previously. Therefore, this phase of the coatings program is concerned with an investigation of the transport of HfO_2, ZrO_2, and ThO_2 by water vapor at high temperatures.

Experimental

Materials

The chemical analyses and density determinations for ZrO_2, HfO_2, and ThO_2 used in this study are reported in Section IX, page 105.

Apparatus

The furnace unit used in this research has been shown previously in Section IV, Task A1-1, Figure 2. Minor modifications of the apparatus involved the addition of a boiler to saturate the inlet gas with water and a heated gas inlet line to prevent subsequent condensation of the water vapor.

Procedure

In a typical experiment, a right circular cylinder of the oxide ($^1/_4$ inch diameter x $^1/_4$ inch long) was supported by an iridium wire in the center of the furnace hot zone. The furnace was flushed with argon, turned on, and permitted to attain an equilibrium temperature. The argon flush was diverted through a water reservoir maintained at constant temperature and saturated prior to entering the furnace where a linear gas flow rate of approximately 240 cm/minute was maintained. The sample temperature was determined optically at the beginning and at the termination of the 19.5-hour experiment. The sample was cooled slowly to room temperature in argon and was reweighed. It was then crushed and submitted for spectrographic analysis.

Results and Discussion

The conditions and results of the experiments are summarized in Table 37. It was found that ZrO_2, HfO_2, and ThO_2 are relatively stable and are not transported in the presence of high concentrations of water vapor at 1800° and 1900°C. The weight changes in all cases are very small and show up

randomly as weight gains or losses. The specimens did not undergo any major color, dimension, texture, or chemical changes as a result of the treatment. A spectrographic analysis of each specimen after treatment was compared with standards obtained on similar untreated pellets; no major elemental changes were evident. The slight variations noted may be attributed to the starting materials and to the preparation of the samples for analysis. In particular, there was no increase in the alumina content of any of the oxide specimens, indicating that alumina was not transported from the furnace liner to the test sample.

TABLE 37

WEIGHT CHANGE DATA ON OXIDE SAMPLES TREATED WITH WATER VAPOR*

Oxide	Temperature °C**	Hours of Treatment***	Initial Weight (gms)	Weight Change (gms)
ThO_2	1795	19.0	2.5041	-0.0011
ThO_2	1810	19.5	2.5030	+0.0006
ThO_2	1900	17.5	2.3980	no change
HfO_2 (yttria	1780	64.0	2.0332	+0.0002
HfO_2 stabilized)	1910	18.5	2.0178	+0.0011
ZrO_2 (yttria	1810	18.5	1.6104	-0.0003
ZrO_2 stabilized)	1900	66.0	1.5834	+0.0061

* An argon stream was saturated with water vapor at 88°C (approximately two-thirds atmosphere).

** Determined optically.

*** Normal run overnight, long runs over weekend.

Diamond and Dragoo[33] concluded from experiments at 2000° and 2300°C that water vapor does not enhance the vaporization of alumina; however, its vapor pressure at these temperatures might have presented problems.

Added evidence on the stability of zirconia and yttria with respect to water vapor was supplied by Alexander and Ogden[34], their work included holding suitable powder samples of these oxides in a flow stream containing low concentrations of water vapor (1 to 4 x 10^{-4} atmospheres) for as long as fourteen days at 2050°K without measurable weight change.

None of the oxide samples appeared to react chemically with the iridium support wire, and the 10-mil iridium support wire in the immediate vicinity of each sample remained in good condition and in no case lost more than about 4 per cent of its initial weight.

XII. TRANSPORT OF OXIDES IN WATER VAPOR (MIXED OXIDES)

TASK A3-2

Introduction

In addition to the single oxides mentioned previously, the water vapor transport of the mixed oxides $CaZrO_3$, $BaZrO_3$, $SrZrO_3$, $ThZrO_4$, and $HfSiO_4$ has been investigated. This section describes the experiments and results of the volatility of these oxides in the presence of water vapor.

Experimental

Materials

The mixed oxides used for this investigation were obtained from the Zirconium Corporation of America. They were in the form of 0.4 inch O.D. x 0.2 inch I.D. x .2-inch rings cut from high purity, high density slip cast and sintered tubes.

The manufacturer's analyses of the mixed oxides are given in Table 38.

TABLE 38

MANUFACTURER'S ANALYSES OF THE MIXED OXIDES

	$CaO \cdot ZrO_2$	$BaO \cdot ZrO_2$	$SrO \cdot ZrO_2$	$ThO_2 \cdot ZrO_2$	$HfO_2 \cdot SiO_2$
Density (gm/cm^3)	4.4	5.8	5.1	8.0	6.6
Porosity %	8	8	7	8	5
CaO	31.1 w/o	< 250 ppm	250 ppm	trace	100 ppm
MgO	80 ppm	60 ppm	< 50 ppm	trace	trace
Al_2O_3	120 ppm	120 ppm	120 ppm	< 100 ppm	500 ppm
SiO_2	150 ppm	150 ppm	150 ppm	< 200 ppm	22.5 w/o
ZrO_2	68.6 w/o	44.5 w/o	54.2 w/o	31.8 w/o	1.7 w/o
BaO	---	55.2 w/o	---	---	---
SrO	---	---	45.6 w/o	---	---
ThO_2	---	---	---	68.15 w/o	---
HfO_2	20 ppm	20 ppm	20 ppm	< 20 ppm	75.5 w/o

X-ray diffraction methods of analysis were used at this laboratory to further identify the mixed oxides. X-ray diffraction patterns of the oxide ($BaZrO_3$, $CaZrO_3$, $SrZrO_3$, $ThZrO_4$, and $HfSiO_4$) samples demonstrated that the $BaZrO_3$ contains no major impurity phase, the $HfSiO_4$ contained some unidentifiable impurity(s), the $SrZrO_3$ and $CaZrO_3$ each contained some free ZrO_2; and that the $ThZrO_4$ was simply a mixture of ThO_2 and ZrO_2.

The furnace unit used in this task has been described previously in Section IV. Task A1-1, Figure 2. Minor modifications of the apparatus involved the addition of a boiler to saturate the inlet gas with water vapor and a heated gas inlet line to prevent subsequent condensation of the water vapor.

Procedure

The weighed oxide rings were supported in the center of the furnace hot zone with iridium wire. The furnace was flushed with argon, brought to temperature, and then water vapor was added to the gas stream. The temperature was determined optically and controlled by manually varying the power input to the load coil. The sample was cooled in argon to room temperature and reweighed. Each material was run at two temperatures in dry argon to establish a baseline and at three temperatures (1600° to 1900°C) in argon containing two-thirds of an atmosphere of water vapor at a linear flow rate of ~ 350 cm/minute. In addition, barium zirconate was run under varied conditions of flow and partial pressure of H_2O.

Results and Discussion

Alkaline-Earth Zirconates

Table 39 shows the average transpiration rate of the alkaline-earth zirconates during an eighteen-hour exposure to a 350 cm/minute linear flow of a mixture of 0.34 atmosphere of argon and 0.66 atmosphere of water vapor in the temperature range of ~ 1600° to 1900°C. The water vapor transport of the alkaline-earth zirconates follows in the order $BaZrO_3 > SrZrO_3 > CaZrO_3$. This phenomenon parallels the observations of other investigators[34] for the water vapor transport of alkaline-earth oxides, namely, that the order of transport is BaO> SrO> CaO.

TABLE 39

TRANSPIRATION RATE OF ALKALINE-EARTH ZIRCONATES IN A LOW VELOCITY ARGON STREAM CONTAINING 0.66 ATMOSPHERE OF WATER VAPOR

Material	Temperature, °C	Rate* in mg/cm^2 hour
$BaZrO_3$	1600	0.12
	1750	0.35
	1900	1.48
$CaZrO_3$	1625	0.03
	1760	0.20
	1890	0.36
$SrZrO_3$	1600	0.01
	1740	0.08
	1870	0.15

* Average of eighteen-hour exposures

A least-squares solution of the data resulted in the expression,

$$\log K_r = -17,800/T + 7.90$$

for the reaction, $CaZrO_3 + H_2O_{(g)}$,

$$\log K_r = -17,300/T + 7.35$$

for the reaction, $SrZrO_3 + H_2O_{(g)}$,

and $$\log K_r = -14,900/T + 6.95$$

for the reaction, $BaZrO_3 + H_2O_{(g)}$

In these equations, K_r represents the apparent overall rate constant for the reaction.

These equations represent a best immediate value from a limited experimental effort. They are, of course, a summation of both the reaction with water vapor and vaporization. Transpiration experiments with dry argon at 1600 and 1750°C for each zirconate demonstrate that 10 to 30 per cent of the weight loss is through vaporization.

The water vapor transport of $BaZrO_3$ was determined as a function of the partial-pressure of water vapor and the duration of experiment. Table 40 lists the results of the transport of $BaZrO_3$ in water vapor at 1880°C in various partial-pressures of water vapor.

TABLE 40

TRANSPORT OF $BaZrO_3$ IN WATER VAPOR AT 1880°C IN VARIOUS PARTIAL-PRESSURES OF WATER

Partial-Pressure of H_2O Vapor* in Atmospheres	Average Rate of Weight Loss mgs/cm^2 hours
60 torr	0.4
120 torr	0.6
280 torr	0.9
500 torr	1.4

* Plus argon to one atmosphere

There is a linear increase from 0.4 mg/cm^2 hr at a water vapor pressure of 60 torr to 1.4 mg/cm^2 hr at 500 torr.

Increasing the total gas flow rate also increases the rate of transport of $BaZrO_3$ by water vapor. Table 41 summarizes the results obtained in a water vapor partial-pressure of 280 torr at 1870°C.

TABLE 41

TRANSPORT OF $BaZrO_3$ IN VARIOUS FLOW RATES OF WATER VAPOR IN A PARTIAL-PRESSURE OF 280 TORR AND A TEMPERATURE OF 1870°C

Total Flow Rate CFH at STP*	Average Weight Loss mgs/cm^2 hours
3.1	0.8
9.5	1.0
15.7	1.6

* Through a one-inch diameter tube

Here the transport rate increases from 0.8 mg/cm^2 hr to 1.6 mg/cm^2 hr, when the gas flow rate increases from 3.1 to 15.7 CFH. That the transport of $BaZrO_3$ is not congruent is illustrated by the data in Table 42.

TABLE 42

TRANSPORT OF BARIUM ZIRCONATE BY WATER VAPOR

Treatment Number*	Average Rate of Weight Loss**
1	6
2	2
3	1
4	1
5	1
6	1

* Six successive eighteen-hour treatments were given to the sample. T = 1900°C

** Rate in arbitrary units. Linear flow rate = 350 cm/min P_{H_2O} = 500 torr, P_t = 750 torr.

In six successive experiments each of eighteen hours duration at 1900°C, it was seen that the transport rate decreased from the first to the third experiment and then leveled off for the remainder of the experiments.

Further evidence to the fact that vaporization is not congruent was obtained by positioning a condenser axially to the reaction tube and collecting the transported material. Spectrographic analysis of the condensate showed barium and small amounts of irrelevant impurities. X-ray diffraction patterns on $BaZrO_3$ samples before and after treatment with water vapor verify that ZrO_2 remains in the sample inasmuch as the pattern of the starting material exhibits only $BaZrO_3$ while the residue contains a substantial amount of ZrO_2.

A metallographic examination of a $BaZrO_3$ specimen was carried out before and after 108 hours in water vapor at 1900°C to demonstrate that a layer of ZrO_2 remained on the surface of $BaZrO_3$. The photomicrographs, 67 X magnification, are shown in Figures 110 and 111.

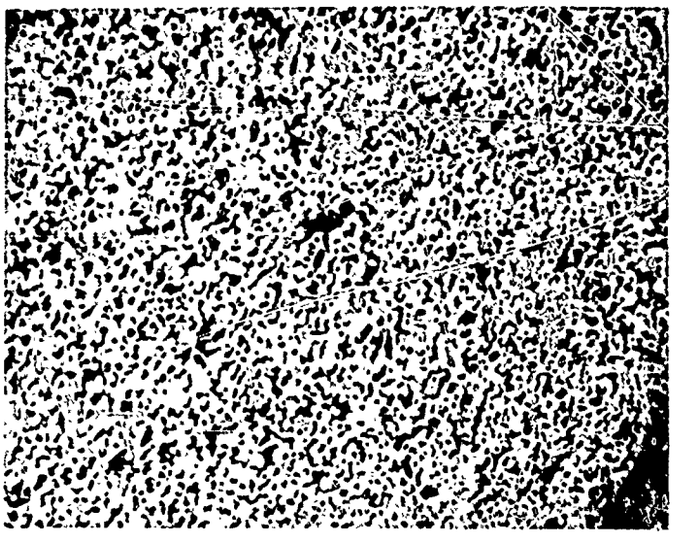

Figure 110. Barium Zirconate Starting Material, (67 X Magnification)

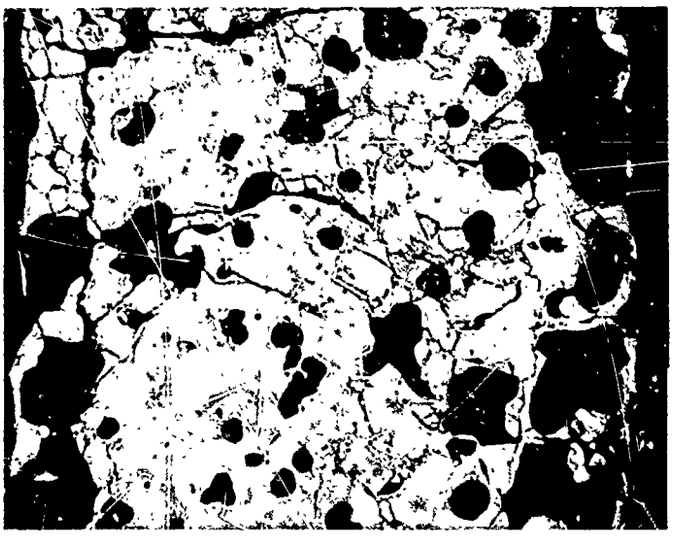

Figure 111. Barium Zirconate After 108 Hours in Water Vapor at 1900°C, (67 X Magnification)

The former represents the $BaZrO_3$ before exposure to water vapor at high temperature and the latter represents the $BaZrO_3$ after exposure to water vapor at high temperature. Each photograph shows a cross section of the wall of the oxide ring. The inner edge is at the right side of the photograph and the outer edge at the left. Before being subjected to water vapor transport, the $BaZrO_3$ (Figure 110) is seen to be essentially a single phase material with small pores and with minor amounts of a liquid phase at the grain boundaries. After being subjected to water vapor transport, the $BaZrO_3$ (Figure 111) exhibited large voids and a multiphase material. The latter consisted of: (1) $BaZrO_3$ shown as a light grey color in the center of the photograph; (2) a dark grey one-time liquid phase which appears at the grain boundaries; (3) a white phase in the grey which appears to have precipitated from the melt, and (4) an almost white phase (probably ZrO_2) at the inner and outer edges and surrounding the large voids near the edges.

The experiments on the alkaline-earth zirconate-water vapor interactions show an appreciable transport of the alkaline-earth constituent. The mechanism probably involves the formation of an alkaline-earth hydroxide of the type $M(OH)_2$ which has a sufficiently high vapor pressure to be transported at high temperatures. The ZrO_2 remains as a porous residue on the surface of the mixed oxide (zirconate).

Thorium zirconate, $ThZrO_4$, and hafnium silicate, $HfSiO_4$, were also subjected to water vapor streams at high temperatures. $ThZrO_4$ was not transported nor did it interact with water vapor in the 1600° to 1850°C range investigated. The volatility of $HfSiO_4$ was not enhanced in the presence of water vapor. For example, in experiments at 1870°C for 18 hours weight losses were similar with argon or in argon containing atmosphere of water vapor. The losses were erratic, when compared with the zirconates, and ranged between three and six per cent at 1870°C. It was also noted that at a temperature between 1750°C and 1870°C hafnium silicate undergoes plastic deformation in both water vapor and dry argon.

Miscellaneous

A few interesting secondary facts have been uncovered in this phase of the program and they are reported here merely for the exchange of information.

In preliminary experiments, it was noted that if the sample touched the alumina furnace liner at high temperatures, eutectic melting occurred. This prompted a cursory examination of the melting points of the mixed oxides with alumina (shown in Table 43) and lead to a slightly modified sample support to insure against touching the furnace wall.

TABLE 43

MELTING POINT OF EQUIMOLAR MIXTURES OF THE MIXED OXIDES AND ALUMINA*

Mixture	Melting Point**
$BaZrO_3 + Al_2O_3$	1570°C
$CaZrO_3 + Al_2O_3$	1650°C
$SrZrO_3 + Al_2O_3$	1650°C
$HfSiO_4 + Al_2O_3$	~1750°C

* Samples consisted of cold-pressed pellets $\frac{1}{8}$-inch diameter x $\frac{1}{4}$-inch long

** Determined optically

The 10-mil diameter iridium support wire which held the zirconate samples was in some cases used as long as sixty hours at 1900°C in two-thirds of an atmosphere of water vapor—in no case was a sample lost due to wire failure.

XIII. CARBON DIFFUSION THROUGH THE MONOCARBIDES AND DIBORIDES OF Hf AND Zr

TASK D-1

The experimental methods for the measurement of the diffusion coefficient of carbon in the monocarbides and diborides of hafnium and zirconium have been roughly outlined. As presently envisioned, it is planned to prepare specimens in the form of short circular cylinders with parallel and planar end faces which have been carefully sectioned and ground. A negligibly thin ($\sim$ 1 to 10 μ) layer of radioactive carbon from the pyrolytic deposition of a mixture of $C^{12}H_4$ and $C^{14}H_4$ will be deposited on one of the planar ends, and the diffusion couple then annealed under vacuum. In order to avoid complication, (in the case of the carbides) which may arise from the presence of chemical gradients, the composition will be adjusted by suitable annealing, to be nearly that given by the monocarbide-graphite equilibrium line. Isotopic exchange between the C^{14} in the thin carbon film and the C^{12} in the semi-infinite carbide specimen corresponds to the boundary conditions for the thin-film solution to Fick's laws and the concentration of tracer, $C(x, t)$ at a distance x from the interface after an annealing time, t, will be:

$$C(x, t) = \frac{c\,(o, o)}{(\pi D^* t)^{1/2}} \exp\,(-x^2 / 4D^* t) \qquad (1)$$

where D^* is the tracer diffusion coefficient. Equation (1) is limited, of course, to the case where the diffusion coefficient is independent of position and time (i.e., in the absence of a macroscopic chemical gradient). After diffusion has occurred, the diffusion coefficient can be determined directly from Equation (1) by sectioning, or by measuring the decrease in activity of the original planar surface (autoradiographic techniques can also be used, but are not under consideration at this time). For the boundary conditions described, the activity at the original surface decreases approximately according to the relationship:

$$F = \exp\,(\mu^2 D^* t)\,[\,1 - \mathrm{erf}\,(\mu\sqrt{D^* t})\,] \qquad (2)$$

where F is the fraction of counts after diffusion has taken place and μ is the linear absorption coefficient for the β radiation. While in principle, both Equations (1) and (2) can be used, the absorption technique suffers from a number of experimental disadvantages as well as the necessity of either knowing, a priori, the absorption coefficient, or measuring it. Its only real advantage lies in not requiring sectioning or otherwise determining the concentration profile and that it can be applied to the measurement of quite small diffusion coefficients. Time permitting, it is hoped to study the diffusion coefficient as a function of composition. For this, the experimental technique and analysis will be modified somewhat from that described.

In the case of the diborides, the same experimental technique will be employed, at least initially, but since a macroscopic chemical gradient exists, the analysis of the carbon concentration (activity) - penetration curves will be of the Grube or Matano type and will yield an apparent chemical interdiffusion coefficient.

At this time, it appears that the best technique will be to section the annealed specimen parallel to the original plane interface. Nonetheless, because of the extreme hardness and brittle character of the materials in question, even the sectioning technique presents some problems. It is possible to abrade a known amount parallel to the original surface and expose the grinding paper to the counter, but this method requires the construction of a special precision lapping and abrading unit to insure planarity, prevent the rounding of edges, etc. In spite of being theoretically highly suspect, it is thought that the necessary measurements might be obtained by measuring the activity on the successive end faces produced by grinding. Correction, normally, must be made for the contribution of the layers beneath the surface; and usually, the absorption function is complicated (i.e., absorption of β rays, for example, is not exponential and the radiation is not monochromatic). Therefore, the difference between two successive activities does not necessarily represent the activity of the layer removed by the abrasion. However, in the case of carbon 14, the β radiation is of sufficiently low energy and the matrix of sufficiently high density that the measured activity corresponds quite close to the activity of the surface alone. The contribution of deeper layers plays a small role and the well-known difficulty of accounting for it is minimized. For example, the range, R, in g/cm^2 for β radiation of maximum energy $0.15 < E_{maximum} < 0.8$ MeV is:

$$R = 0.407\, E_{maximum}^{1.38}. \qquad (3)$$

Taking $E_{maximum} = 0.154$ MeV and an absorber density of about 10 g/cm^3, the penetration depth is only of the order of 0.003 cm. Therefore, it appears that surface counts can be used.

All of the time and effort spent on this phase of the program have been devoted to the construction and procurement of equipment and materials. A resistance furnace, to be used for the annealing of the diffusion couples has been built. The unit is designed to operate in the temperature range of 1000°C to 2400°C under vacuums of at least 10^{-6} mm Hg. The control system will maintain temperatures of at least ± 2°C. The construction allows a variety of resistors and radiation shields to be used. The current will be supplied by means of a 45 KVA power source which will step-down the primary 440 voltage to secondary voltages of 7.5, 15 and 30 volts by means of four independent windings and regulated through use of a 50 EVA saturable core reactor.

A gas train for the pyrolytic deposition of C^{14} from radiomethane has been constructed and tested using cold methane. A thin disk of HfB_2 was induction heated to 900°C in vacuum and an atmosphere of 15 mm CH_4 was introduced into the system. Pyrolysis was instantaneous and a layer of pyrolytic carbon (about 0.05 μ thick) was deposited on the exposed face of the disk. Accomplishing the deposition at such a low temperature and in negligible induction time is important in that no exchange between the atmosphere (and deposited layer) and the substrate will occur. Rapid heatup (which will be possible with the furnace presently under construction) to the annealing temperature then insures a meaningful time zero.

A wafering and grinding unit has been purchased and will be used for the preparation of the diffusion couples and their sectioning. Also purchased, is a ww-level, ww background β proportional counting system. The unit is supplied with an ultra thin window which has a transmittance efficiency of up to 35 per cent for C^{14} and a background of less than 0.5 counts per minute. A sample holding device has also been constructed to keep the counting geometry constant.

XIV. ARC PLASMA TEST—METALLOGRAPHIC ANALYSIS OF JTA TEST SPECIMENS

In the yearly Summary Report[2] under Section XII, "Arc Plasma Tests of Iridium Coatings," it was stated that Union Carbide JTA refractory composite samples (nominal composition, 40 w/o ZrB_2, 12 w/o Si, 48 w/o graphite) were subjected to the arc plasma for comparison of its oxidation resistance with that of iridium coated graphite. Because of its zirconium diboride and silicon content, the oxide protective layer on JTA could likely consist of zircon or zirconia, two of the materials being considered for protective coatings for graphite; therefore, a more detailed examination of the protective layer on JTA was warranted. A metallographic examination of the JTA test specimens has been completed, and the results are summarized as follows:

JTA Specimen Tested in Air at Atmospheric Pressure for Twenty Minutes at an Average Temperature of 2050°C

The sample is completely coated with a porous cellular structure consisting of large particles of a zircon-zirconium oxide mixture, a glass-like phase, and a quantity of small globular metallic occlusions dispersed in some areas of the coating.

Photomicrographs of representative areas of the JTA specimen, which was tested in air at one atmosphere, are shown in Figures 112, 113, and 114. Photomicrographs of the JTA specimen, which was tested at an air pressure of 48 torr, are shown in Figures 115 and 116.

Figure 112. JTA Atmospheric Test Specimen Showing an Outer Edge of Coating with Intermixed Agglomerates of Zircon and Zirconium Oxide

Flame Side,

(250 X Magnification)

A - Zirconium oxide

B - Zircon

C - Glass phase (not apparent)

D - Epoxy mounting resin

Figure 113. JTA Atmospheric Specimen Showing the Intermediate Zone Having Aggregate Particles of Zircon and Zirconium Oxide Dispersed in an Amorphous Glass Phase

Flame Side,

(250 X Magnification)

A - Zirconium oxide

B - Zircon

C - Glass Phase

D - Epoxy

Figure 114. JTA Atmospheric Specimen Showing Outer Zone of Side Opposite Flame Point. The Large Light Grey Particles are Zircon Containing Some White Zirconium Oxide

(250 X Magnification)

A - Zirconium oxide

B - Zircon

C - Glass phase (not apparent)

D - Epoxy

The coating appears to have three zones present from the core to the outer surface. The outer surface (Figure 112) consists of zircon-zirconium oxide particles (A-B) interconnected by point contact. Inward from this region (Figure 113) a zone in the form of a more continuous band is present and consists of large and small zircon-zirconium oxide particles (A-B) bonded together by a glass-like phase (C). The zircon-zirconium oxide particles here are made up of finer subgrains than those of the outer zone and are of higher zirconium oxide content. Also, within the intermediate zone can be seen a trace of a fine metallic dispersion. At the interface between the reaction products and the composite, there is a gap or separation. This may be due to a difference in CTE in the JTA material and the oxide coating or it may be material that is lost by dissolution during specimen preparation. The separation between the oxide layer and the unoxidized composite is greater on the side opposite the flame point and imparts a thicker coating appearance although the zircon-zirconium oxide aggregate is actually thinner here (Figure 114) than that of the flame side. On this side opposite the flame, it can be seen that the zircon phase (B) is more pronounced in the form of large, well-shaped crystals containing a minor amount of small zirconium oxide grains.

JTA Specimen Tested in Air at 48 Torr for Twenty Minutes in the Temperature Range 1600° to 1700°C

The specimen is completely covered with a cellular structure consisting of zircon-zirconium oxide particles bonded by a continuous glass-like phase.

On the flame side (Figure 115), coating is thicker and continuous with a glass phase being the bonding agent. No gap or separation is noted between outer surface and interface. At the interface the glass phase appears to coat the graphite aggregate surface continuously (Figure 116).

On the side opposite the flame point, the coating is thinner and more open. The glass bonding phase diminishes, leaving the particles in a more discontinuous form. The particles are smaller and the phases are not as distinguishable as on the flame side. No glass phase is detectable on the graphite aggregate core surface. Because of the sparse detail, photomicrographs are not shown.

The zircon-zirconium oxide particles, small at the interface region, become larger at the outer surface. No large zircon crystals are observed on either side. Zirconium oxide appears to be the major constituent. No metallic impurities are apparent in this specimen.

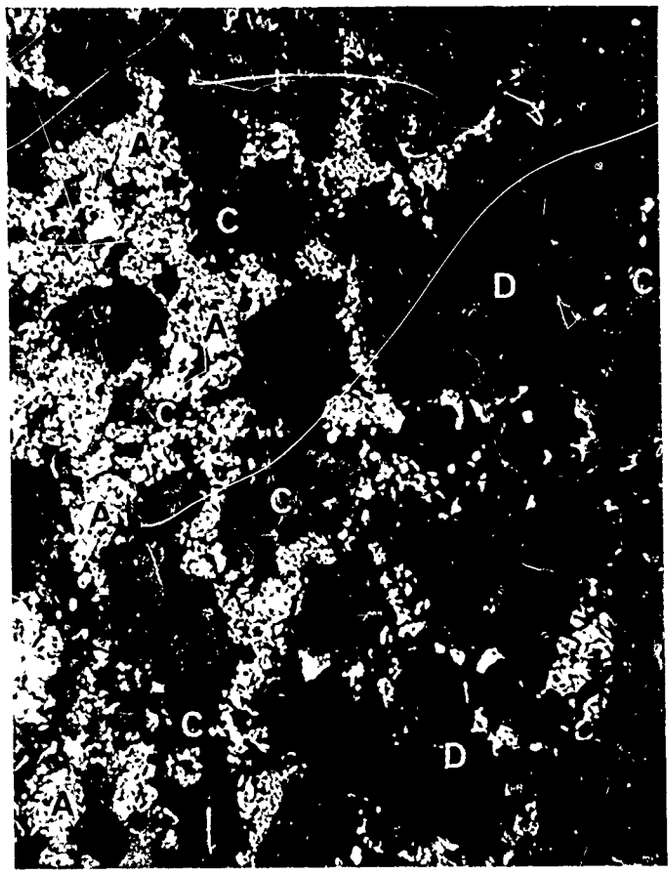

Figure 115. JTA Vacuum Specimen Showing Agglomerated Fine Crystals of Zirconium Oxide Dispersed in Amorphous Glass Phase. Flame Side

(250 X Magnification)

A - Zirconium oxide

B - Zircon (not apparent)

C - Glass phase

D - Epoxy

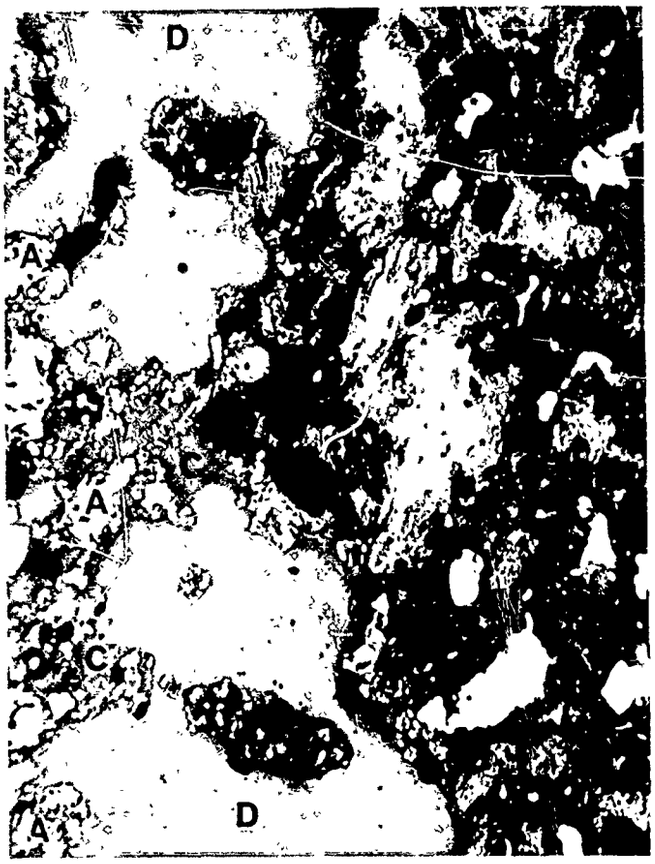

Figure 116. JTA Vacuum Specimen Showing Graphite Interface with a Continuous Covering of Amorphous Glass Phase. Flame Side

(250 X Magnification)

A - Zirconium oxide

B - Zircon (not apparent)

C - Glass phase

D - Epoxy

Evaluation Technique

The determinations were made by observing the specimen cross sections metallographically with the Bausch and Lomb research metallograph. By normal incident illumination the zircon-zirconium oxide, glass, and impurity phases are distinguishable, although some difficulty is experienced in photography due to light scattering caused by the high refractive index of zirconium oxide. When the zircon to zirconium oxide ratio is high, the two phases become more apparent. The glass phase is noted by its low luster and continuous appearance. The metallic impurities are noted by small globular shape and the bright reflectance characteristic of metal.

Initially, the zircon-zirconium oxide particles were thought to be of a singular oxide component having inner structural variation that could have been due to masses of minute transparent crystals; but further observations, both by normal incident and polarized light, indicated that they were duplex in composition. Being concerned with a ZrO_2 and SiO_2 system, it appeared likely to have a zircon constituent present. Small amounts of coating material were probed from the test pieces with the aid of a microscope and submitted for X-ray analyses. The results indicated the presence of zircon and monoclinic zirconia, substantiating the metallographic conclusions.

CORRECTIONS TO TECHNICAL SUMMARY REPORT

No. ML-TDR-64-173, Part II

AF 33(657)-11253

Page 9 Second paragraph, 3rd line:
Change 10^{-17} g cm^{-1} sec^{-1} to read 10^{-7} g cm^{-1} sec^{-1} .

Page 48 The ordinate on Figure 15 should be relabeled to read 10^{-12}, 10^{-11}, and 10^{-10} instead of 10^{-13}, 10^{-12}, and 10^{-11}.

REFERENCES

1. Criscione, J.M., Mercuri, R.A., Schram, E.P., Smith, A.W., and Volk, H.F., "High Temperature Protective Coatings of Graphite" Technical Documentary Report No. ML-TDR-64-173, Part I, June 1964.

2. Criscione, J.M., Mercuri, R.A., Schram, E.P., Smith, A.W., and Volk, H.F., "High Temperature Protective Coatings for Graphite" Technical Documentary Report No. ML-TDR-64-173, Part II (October 1964).

3. Conway, J.B., and Hein, R.A., Nucleonics 22, No. 6, 71 (June 1964).

4. Stuart, W.I., and Price, H.G., "High Temperature Reaction Between Beryllia and Water Vapor," Journal of Nuclear Materials 14 (1964) 417-424.

5. Rexer, J., Prime Contract NOrd 16640, Subcontract No. 232 and Prime Contract NOsp 64110 (FBM), Subcontract No. 0403-09004.

6. Krier, C.A., and Jaffee, R.J., J. Less Common Metals 5, 411 (1963).

7. Rhead, G.E., Acta Met. 13, 223 (1965).

8. Fast, J.D., Phillips Technical Review 6, 365 (1941); 7, 73 (1942).

9. Foster, L.M., Long, G., and Hunter, M.S., J. Am. Cer. Soc. 39, 1, (1956).

10. Oishi, Y., and Kingery, W.D., J. Chem. Phys. 33, 480 (1960).

11. Campbell, I.E., ed., High Temperature Technology, John Wiley and Sons, New York (1956) p. 82.

12. Lang, S.M., and Knudsen, F.P., J. Am. Ceram. Soc. 39, 415 (1956).

13. Burdick, M.D., and Parker, H.S., The Effects of Crystallite Size on the Bulk Density and Strength Properties of Uranium Dioxide Specimens, U.S. AEC Publ. AECU 3189; quoted in Handbook of Thermophysical Properties of Solid Materials, Vol. III: Ceramics H. Goldsmith, Th. E. Waterman, H.J. Hirsckhorn, eds., the MacMillan Company, New York (1961).

14. Keihn, F.G., Research on Physical and Chemical Principles Affecting High Temperature Materials for Rocket Nozzles, Union Carbide Research Institue and Parma Technical Center, Quarterly Progress Report, March 31, 1964, Contract No. DA-30-069-ORD-2728, P. III-54.

15. Houska, C., and Keplin, E., Research on Physical and Chemical Principles Affecting High Temperature Materials for Rocket Nozzles, Union Carbide Research Institue and Parma Technical Center, Quarterly Progress Report, September 30, 1963, Contract No. DA-30-069-ORD-2728, P. III-51.

REFERENCES (Cont'd)

16. Ohnysty, B., and Rose, F.K., Thermal Expansion Measurements on Thoria and Hafnia to 4500°F, Vol. 47, No. 8, Journal of Am. Ceram. Soc., August 1964, Pp. 398-400.

17. Budick, R.B., Hoskins, W.R., Research on the Thermal Properties of Zirconia, Materiadyne ARL 63-170, September 1963.

18. Schaffer, Peter T.B., Summary Report, Development of Ultrahigh Refractory Materials, Carborundum Company Research Contract NOrd-17175, November 1, 1958 to October 31, 1959.

19. Chandrasekharaiah, M.S., "Volatilities of Refractory Inorganic Compounds," BNL-7454 Brookhaven National Laboratory; Upton, New York (September 1963).

20. Samsanov, G.V., Paderno LaB Kreingol'd, S.U., Zhurnal Prikladnoi Khimir Vol. 34, No. 1, 10-15 (January 1961).

21. JANAF Thermochemical Tables, December 31, 1964.

22. Coughlin, J.P., Contributions to the Data on Theoretical Metallurgy, U.S. Bureau of Mines Bull. 542 (1954).

23. Wicks, C.E., and Block, F.E., Thermodynamic Properties of 65 Elements and Their Oxides, Halides, Carbides, and Nitrides, U.S. Bureau of Mines Bull. 605 (1963).

24. Thermodynamic and Kinetic Studies for a Refractory Materials Program, ASD-TDR-62-204, Part III, April 1964.

25. Komarck, K.L., Coucalas, A., and Lkinger, N. J. Electro. Chem. Soc. 110, 783-791 (1963).

26. Hollahan, J.R., and Gregory, N.W., J. Phys. Chem. 68, 2346-2351 (1964).

27. Kutseu, V.S., Ovmont, B.F., and Epelbunm, Doklady Okad. Nauk, SSSR 104, 567 (1956).

28. Blyholder, G., and Eyring, H., J. Phys. Chem 61, 682 (1957).

29. Gibson, E.D., Loomis, B.A., and Carlson, O.N., Trans. ASN 50 1958, preprint 24.

30. Grossweiner, L., and Seifert, R.L., The Reaction of Beryllium Oxide with Water Vapor JACS 74 (1952) 2701-OC1.

31. McKisson, R.L., Journal of Nuclear Materials 2(1959) 196-202.

REFERENCES (Cont'd)

32. Chandrasekharaiah, M. S., Volatilities of Refractory Inorganic Compounds* Brookhaven National Laboratory, Upton, New York, September 1963.

33. Diamond, J. J., Dragoo, A. I., "The Solubility of Water Vapor in Molten Alumina," National Bureau of Standards, Conference of Imaging Techniques, Arthur D. Little, Incorporated, October (1962).

34. Alexander, C. A., and Ogden, J. S., Battelle Memorial Institute, Columbus, Ohio, private communication.

APPENDIX A

KINETICS OF OXIDATION OF IRIDIUM AT HIGH TEMPERATURES*

A. K. Kuriakose and J. L. Margrave
Department of Chemistry
Rice University
Houston, Texas

Although the utilization of the platinum group metals as high temperature materials has been extensive for many years, only recently have there been any substantial quantitative thermochemical and kinetic studies on these metals under various environments at elevated temperatures. Because of its high melting point and other properties, iridium appears especially promising for high temperature applications, but one limitation of iridium is that it is attacked by oxygen at temperatures of ~1000°C with the formation of volatile iridium oxide (or oxides). In spite of this fact, iridium is the only pure metal which can be used unprotected in air for short periods of time at temperatures as high as 2300°C.[1]

Transpiration studies by Alcock and Hooper,[2] Cordfunke and Meyer[3] and Schäfer and Heitland[4] have all indicated that Ir_xO_3, where x is undetermined but probably 1 or 2, is the volatile product of iridium oxidation. Recent mass spectrometric studies on the iridium-oxygen system[5] indicate that the volatile oxides of iridium are IrO(g), IrO_2(g) and IrO_3(g).

Kinetic studies on the oxidation of platinum metals have been scarce and most of them have been done on platinum.[6-10] Only a few include data on oxidation rates of iridium.[1,11-13] Krier and Jaffee[11] reported that weight losses of iridium in air at 1000, 1200 and 1400°C followed a linear reaction rate law and derived an activation energy of 16 kcal/mole for the process, in slowly moving air. The investigation of Phillips,[12] over the temperature range 800-1400°C, showed an activation energy of 9.2 kcal/mole for the same process.

This report presents a detailed account of the oxidation rates of iridium in pure oxygen and oxygen-helium mixtures in the temperature range 1010-2217°C under various flow rates and oxygen partial pressures.

EXPERIMENTAL

Iridium foil of thickness 0.002 inch was used for studies up to 1301°C and iridium wire of diameter 0.01 inch for higher temperatures. The

* Work performed under subcontract with the Carbon Products Division of Union Carbide Corporation, Parma, Ohio, sponsored by the U.S. Air Force.

surfaces of the specimens were cleaned with acetone, and then distilled water and dried in air. Analyzed oxygen gas of purity 99.8± per cent and high purity helium gas were utilized for the experiments.

Foil Experiments

Oxidation studies on the iridium foil were carried out in a vertical, one-inch I.D. Vycor or Mullite combustion tube, about two feet long, heated inside a Kanthal wire-wound furnace. Rectangular pieces of the foil of surface area about 2.5 cm^2 and weight about 0.1 gm were suspended from a sensitive quartz spring balance by means of a quartz fiber into the hot zone of the furnace, down which helium gas was flowing at a desired flow rate. After the specimen had reached temperature equilibrium (about ½ hour), the system was rapidly flushed with pure (99.8 per cent) oxygen and then the oxygen flow rate adjusted slowly to the required flow rates, when the zero reading of the cathetometer was taken. For runs in O_2-He mixtures, either a premixed O_2-He gas mixture (analyzed) was used, or oxygen was injected into the helium stream at zero-time. In the latter case, the mixing of the gases was effected by passing them through a 15-foot length of ¼-inch copper tubing. The changes in extension of the quartz spring were measured with a high-precision cathetometer at suitable time intervals and the reaction was continued until a sufficient number of points (about 10 to 15) was taken to establish the kinetics of the process. The temperature was measured with a calibrated Pt versus Pt-10 per cent Rh thermocouple and was maintained within ±2°C of the reported value. Because of the cost of the iridium foil, some of the oxidized specimens were used again for other experiments. This procedure did not change the surface area of the specimens beyond the experimental error as determined by reproducibility of the runs under identical conditions, i.e., data were reproducible to ±5-10 per cent. The oxidation rate-constants were obtained from plots of the weight losses/cm^2 versus time. It should be mentioned that the zero-times in these runs do not necessarily coincide with the actual onset of the reaction, but this does not affect the linear rate constants.

Wire Experiments

Pieces of iridium wire of length about 1.5-2 inches were mounted vertically on thick copper wires inside a one-inch Pyrex glass tube, (Figure 1a), one foot long, which was provided with a right-angle sidetube about six inches long, with a Pyrex glass window, and closed at the top with a ball and socket joint with a copper electrode-glass seal. An inlet for the gas was also provided below the ground glass joint. The side-arm was constricted in the form of a vertical slit, about 1.5 inches long and 0.25 inch wide (cf. Figure 1b) at the intersection with the main tube in order to maintain as uniform a cross-sectional shape as possible for reducing the eddies and turbulent flow at the intersection. Oxygen or oxygen-helium mixture was swept down the tube at any desired flow rate. The position of the wire was always adjusted a little away from the center of the tube at the observation tube in order to keep it away from the possible eddies at the

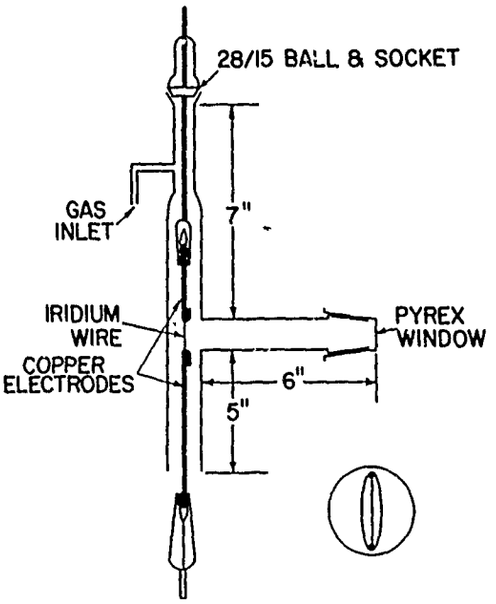

FIGURE Ia (left)
APPARATUS FOR STUDYING THE OXIDATION RATE OF IRIDIUM WIRE

FIGURE Ib (right)
A VIEW OF THE IRIDIUM WIRE THROUGH THE CONSTRUCTION AND GLASS WINDOW

intersection. The gas velocity was calculated from the diameter of the glass tube and the total flow rate. With the gas flowing, a low voltage (12 V., AC, adjusted through a constant voltage transformer and two powerstats in series) was applied between the ends of the wire. The current was gradually increased until the hottest portion of the wire matched the filament on the preset pyrometer. With this particular current adjustment, the power was turned off and the diameter of the wire was measured after it had cooled down to room temperature, at 0.5 mm intervals along the wire with a high precision screw gauge accurate to ±0.001 mm. The smallest value obtained was taken as the diameter of the hottest portion of the wire. The wire (with the copper supports) was then remounted into its proper place and the current turned on again which brought the wire to the experimental temperature in a few seconds. A timer was started and the change of diameter with time was noted at suitable intervals, as before, after turning off the current. It was necessary to observe the temperature of the wire constantly with the pyrometer, since it had a tendency to go up as the wire became thinner. The current was manually adjusted to keep the temperature constant during the heating periods. Thus, for short intervals of time, the temperature fluctuations were of the order of ±10-15° around the reported value. The spectral emissivities of iridium under nearly identical conditions were determined experimentally by two methods described later for correcting the optical pyrometer readings, and the uncertainty in the corrected temperature is believed to be not more than 20° at the highest temperature studied.

Measurements on the diameter change of the iridium wires at temperatures over 1400°C were carried out at oxygen partial pressures of either 15 or 152 torr in helium, except for the investigation of the influence of the oxygen partial pressure on the rate of reaction at 1717°C. Because of the uncertainty in temperature measurements, many of the runs were repeated several times especially when two consecutive values did not agree and most of the rate constants were reproducible to ±5 per cent. In correcting the observed pyrometer readings, it was assumed that the emissivity of iridium did not change drastically with varying flow rates and oxygen partial pressures, as evidenced by the agreement between the observed emissivities of iridium in air and in an O_2-He mixture with P_{O_2} = 15 torr.

Determination of the Emissivity of Iridium

Two types of experiments were conducted which yielded the spectral emissivities of iridium at various temperatures: (a) thermocouple studies and (b) blackbody hole measurements.

(a) Thermocouple Studies:

The junction of a Pt versus Pt 10 per cent Rh thermocouple was spot-welded to a piece of iridium wire and the wire was heated electrically in slowly moving air. The temperature of the junction was determined by measuring the e.m.f. of the thermocouple and by observing the surface through an optical pyrometer. Although the pyrometer showed almost constant temperature, the thermocouple e.m.f. showed fluctuations corresponding to temperature changes of ±5°C. The average temperature obtained from the thermocouple was taken as the true temperature and the emissivity of iridium at various temperatures was evaluated using NBS Monograph 30.[14] The emissivity of iridium was found to decrease with temperature, in air. Table 1 lists emissivities for iridium obtained by this technique at temperatures up to 1605°C.

(b) Blackbody Hole Studies:

On one side of a hollow graphite cylinder, 1.25 inches long and 0.75 inch in diameter, a 0.0625-inch hole was drilled and a piece of iridium wire was attached to the cylinder at the hole so that temperature measurements with an optical pyrometer could be made on the wire and the cavity simultaneously. The assembly was then heated by induction in an atmosphere of pure argon or helium-oxygen mixture with P_{O_2} = 15 torr. The temperature reading of the blackbody hole was accepted as the true temperature and the emissivities were determined as before. The emissivities obtained in pure argon and in a He-O_2 mixture are presented respectively in Tables 2 and 3.

TABLE 1

EMISSIVITY OF IRIDIUM IN AIR FROM THERMOCOUPLE STUDIES

Temperature °C	Emissivity for $\lambda = 0.65\,\mu$
1041	0.58
1165	0.62
1215	0.62
1224	0.56
1265	0.62
1360	0.51
1373	0.54
1445	0.52
1490	0.51
1605	0.50

TABLE 2

EMISSIVITY OF Ir IN ARGON FROM BLACKBODY STUDIES

Temperature °C	Emissivity for $\lambda = 0.65\,\mu$
1180	0.33
1125	0.29
1480	0.27
1490	0.26
1580	0.30
1600	0.30
1640	0.30
1715	0.32
1740	0.32
1760	0.34

TABLE 3

EMISSIVITY OF Ir IN He-O_2 MIXTURE FROM BLACKBODY STUDIES

$P_{O_2} \approx$ 15 torr

Temperature °C	Emissivity for $\lambda = 0.65\mu$
960	0.56
966	0.58
1020	0.58
1025	0.58
1060	0.58
1060	0.60
1091	0.60
1085	0.64
1125	0.60
1122	0.58
1163	0.58
1290	0.58
1375	0.53
1470	0.48
1560	0.51
1630	0.54
1680	0.53
1740	0.48
1815	0.45
1850	0.43

The agreement between the two methods for oxidizing environments is quite satisfactory in the comparable temperature range, although the emissivity of iridium in pure argon is much less in the same temperature range.

An emissivity of 0.42± 0.02 was obtained at the melting point of iridium for oxidized or unoxidized iridium wire as observed by the pyrometer. This indicates that as the melting point is reached, iridium surfaces become equally bright and/or rough due to vaporization of iridium either as oxide or as gaseous element, or both depending on the atmosphere. Between 1900 and 2300°C, an emissivity of 0.43 was assumed, since there is only a small observed change in emissivity from 1850°C to the melting point of iridium. It should be noted that the determinations of the emissivity made with the induction heating technique with the graphite susceptor were not done under exactly identical conditions of the oxidation experiments. Since the graphite was also exposed to the O_2-He mixture during measurement of the emissivities, the iridium must really have been in an atmosphere of O_2, CO, CO_2 and He, although it has been assumed to be in O_2-He mixture.

This is still an oxidizing atmosphere but if there are interactions between carbon and iridium there could be emissivity changes due to compound formation.

RESULTS

The effects of varying the gas flow rate, the oxygen partial pressure and the temperature, and the effect of water vapor, on the oxidation rates of iridium were the main points of the investigation and the results obtained are presented in the following discussion and Tables 4-10.

As expected and in agreement with Krier and Jaffee[11] and Phillips,[12] the oxidation of iridium obeyed a linear rate law under all the experimental conditions studied.

(a) The Effect Of Oxygen Flow Rate

Since the oxidation products of iridium at high temperatures are volatile, the rate of oxidation of iridium depends on the gas flow rate in the system. In the foil experiments, the oxygen flow rate was varied between 4.8 and 2193 ml/min/cm^2 at 1060 and between 7.2 and 928 ml/min/cm^2 at 1162°C. The flow rates and the respective rate constants are presented in Table 4 and the nature of the dependence of the rate constant on the flow rate is illustrated in Figure 2. The value for the rate constant at the highest flow rate at 1060°C has a much greater uncertainty than the others because of vibrations of the spring balance during the experiment due to the high flow rate and hence, this value is not included in Figure 2. It is clear that the oxidation rate of iridium increases with increasing oxygen flow rate, as expected. It should be mentioned that at 1060°C, with the lower flow rates of 4.8 and 48 ml/min/cm^2, the iridium foil surfaces were black due to the incomplete volatilization of the oxide and/or back reflection of the oxide from the walls; but at the higher flow rates at 1060° and at all flow rates at 1162°C, the surfaces were clean showing complete volatilization of the oxide.

The influence of the gas flow rate on the oxidation rate of iridium wire was studied at 1968°C with an oxygen partial pressure of 15 torr. In Table 5 are shown the linear rate constants obtained at the various flow rates and Figure 3 represents the plot of the rate constants against flow rate. As in the case of iridium foil in the lower temperature range, here also the oxidation rate increases with increasing flow rates.

TABLE 4

THE EFFECT OF OXYGEN FLOW RATE ON THE OXIDATION OF IRIDIUM

Oxygen Pressure = 1 atm.

Temperature °C	Flow Rate ml/min/cm^2	Linear Rate Constant mg/cm^2/min
1060	4.8	0.070
1060	48	0.104
1060	210	0.152
1060	210	0.156
1060	928	0.201
1060	2193	0.415*
1162	7.2	0.130
1162	48	0.372
1162	178	0.552
1162	336	0.694
1162	928	0.801

* Value uncertain due to vibrations of spring balance.

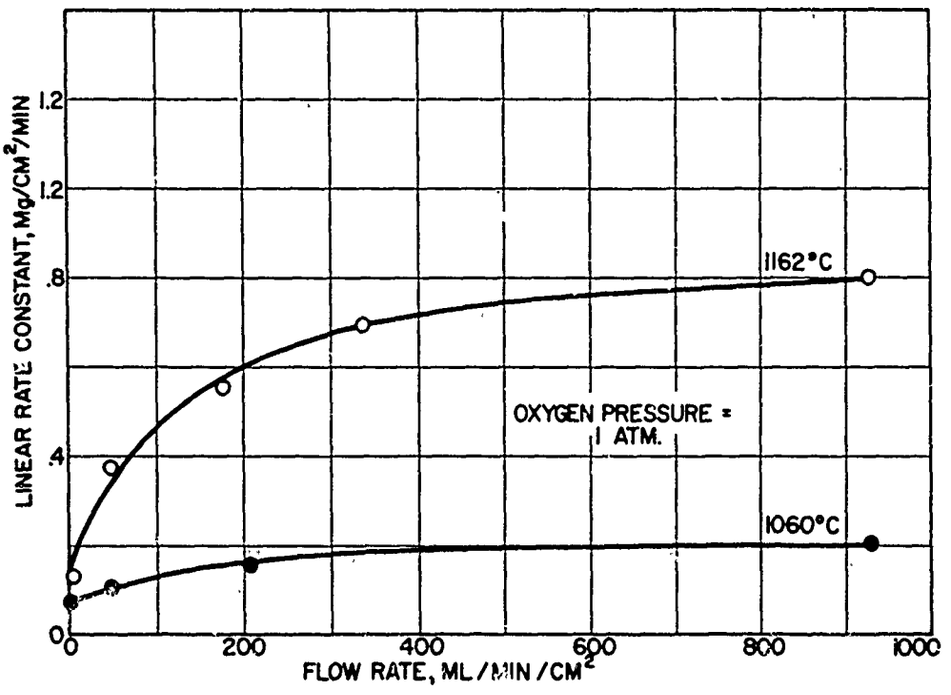

Figure 2. The Effect of Oxygen Flow Rate on the Oxidation Rate of Iridium Foil

TABLE 5

THE EFFECT OF GAS FLOW RATE ON THE OXIDATION RATE OF IRIDIUM WIRE

Temperature = 1968°C; P_{O_2} = 15 torr

Flow Rate ml/min/cm^2	Linear Rate Constant (mm/min) x 10^4
96	1.5
447	2.6
581	3.3
2360	3.8
5234	4.0

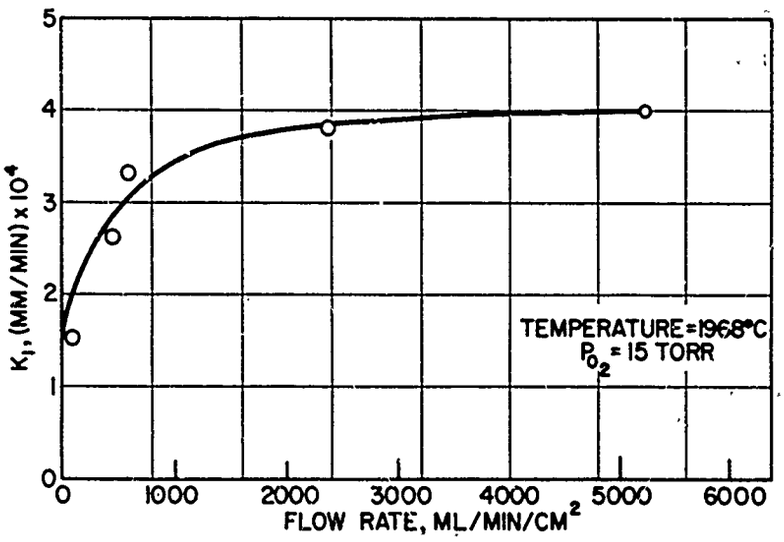

Figure 3. The Effect of Gas Flow Rate on the Oxidation Rate of Iridium Wire

(b) The Effect of Oxygen Partial Pressure

By mixing the oxygen with helium at a constant total flow rate of 48 ml/min/cm^2, various oxygen partial pressures were effected over the iridium foil in the furnace and the rate constants obtained at 1181°C are shown in Table 6.

TABLE 6

THE EFFECT OF OXYGEN PARTIAL PRESSURE AT 1181°C

Total Flow Rate = 48 ml/min/cm^2

P_{O_2} torr	Linear Rate Constant mg/cm^2/min
76	0.028
152	0.048
296	0.115
380	0.146
456	0.236
654	0.272
760	0.320

Figure 4 is a plot of the rate constants against oxygen partial pressure. The approximate linearity of the plot indicates that the rate of oxidation of iridium is directly proportional to the first power (actual value 1.1) of oxygen partial pressure, up to one atmosphere. The expression $k_1 = 4.1 \times 10^{-4} P$ may be derived for the dependence of the iridium oxidation rate on the oxygen partial pressure at 1181°C, where k_1 is the linear rate constant in mg/cm^2/min, of the reaction and P the oxygen partial pressure in torr.

Oxidations of the iridium wire were carried out at 1717°C at a flow rate of 51 ml/min/cm^2 under various oxygen partial pressures ranging from 15 torr to one atmosphere. The average rate constants with the partial pressures are recorded in Table 7. The plot of the rate constants against the oxygen partial pressure (Figure 5) is almost linear as in the case of iridium foil at 1181°C, the actual order for oxygen pressure dependence being 1.2.

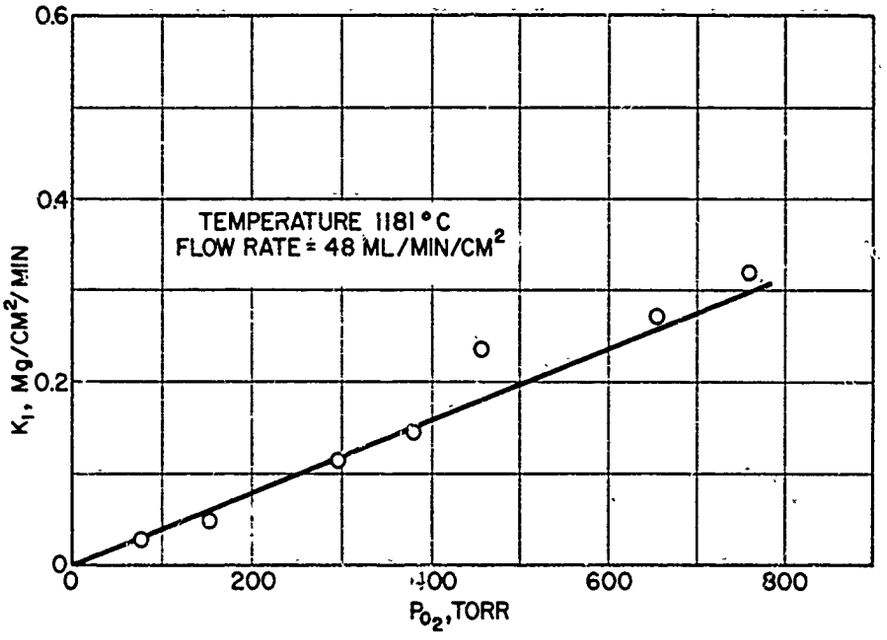

Figure 4. The Effect of Oxygen Partial Pressure on the Oxidation Rate of Iridium

TABLE 7

THE INFLUENCE OF OXYGEN PARTIAL PRESSURE ON THE OXIDATION RATE OF IRIDIUM WIRE AT 1717°C

Gas Flow Velocity = 51 ml/min/cm²

P_{O_2} torr	Linear Rate Constants (mm/min) x 10^4
15.2	0.5
76.0	2.5
152.0	6.2
338.0	19.6
608.0	28.3
760.0	42.3

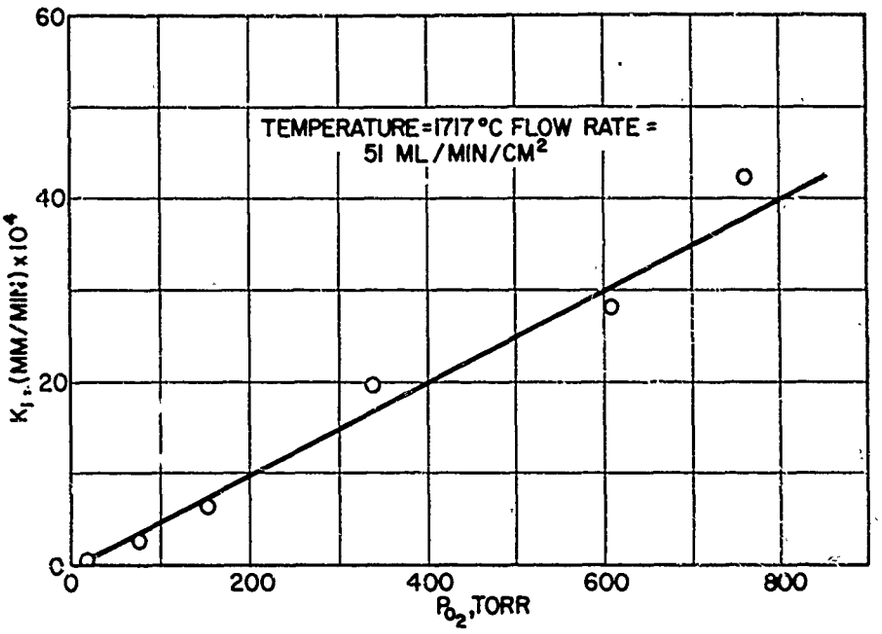

Figure 5. The Influence of Oxygen Partial Pressure on the Oxidation Rate of Iridium Wire

(c) The Influence of Temperature

The effect of temperature on the oxidation rate of iridium foil between 1010 and 1301°C was investigated in pure oxygen at a pressure of one atmosphere, and an oxygen flow rate of 48 ml/min/cm^2, down the combustion tube. The linear rate constants calculated are given in Table 8. An Arrhenius plot of the data (Figure 6) shows a strong temperature dependence of the reaction, characterized by an activation energy of 70 ± 6 kcal/mole up to about 1100°C, and a lower activation energy of only 7.1 ± 1.9 kcal/mole in the 1100-1300°C range.

The dependence of the rate of reaction on the temperature was examined up to 2217°C with iridium wire in oxygen partial pressures of 15 and 152 torr at flow rates respectively of 447 and 3135 ml/min/cm^2, and above 2217°C no reliable data could be obtained since the wire burned up in less than two minutes.

TABLE 8

LINEAR RATE CONSTANTS FOR THE OXIDATION OF IRIDIUM AT VARIOUS TEMPERATURES AT 1 ATM. OXYGEN PRESSURE

Flow Rate = 48 ml/min/cm^2

Temperature °C	Linear Rate Constant mg/min/cm^2
1010	0.034
1050	0.066
1060	0.104
1070	0.108
1100	0.206
1114	0.327
1153	0.379
1156	0.378
1174	0.372
1175	0.364
1181	0.321
1264	0.438
1301	0.451

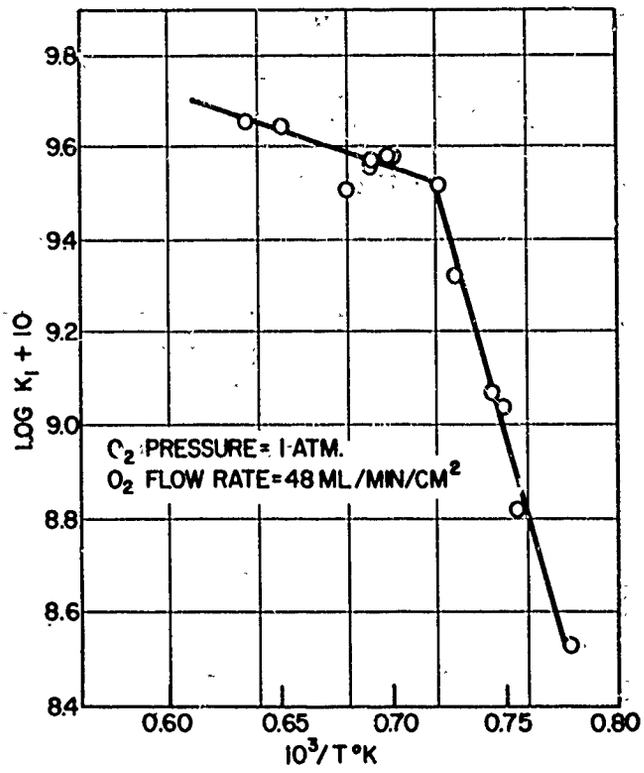

Figure 6. Arrhenius Plot for the Oxidation of Iridium

The rate constants in mm/min at the various temperatures are presented in Tables 9 and 10.

TABLE 9

LINEAR RATE CONSTANTS FOR THE OXIDATION OF IRIDIUM WIRE IN COLD-WALLED REACTION VESSEL

P_{O_2} = 15 torr; Flow Rate = 447 ml/min/cm^2

Temperature °C	Linear Rate Constant (mm/min) x 10^4
1487	0.30; 0.32
1602	0.67; 0.62; 0.58
1717	0.80; 0.75; 0.75
1830	1.67; 1.75
1968	2.42; 2.50; 2.40
2097	3.63; 3.48
2217	5.00; 4.70

TABLE 10

LINEAR RATE CONSTANTS FOR THE OXIDATION OF IRIDIUM WIRE IN COLD-WALLED REACTION VESSEL

P_{O_2} = 152 torr; Flow Rate = 3135 ml/min/cm^2

Temperature °C	Linear Rate Constant (mm/min) x 10^4
1198	3.00; 3.25
1252	4.25; 3.71; 3.90
1359	5.00; 4.25; 4.33; 4.50
1487	6.82; 6.75; 6.83
1602	7.00; 7.50; 8.50; 8.53
1717	14.50; 14.33
1830	21.66; 25.00; 22.33; 22.75
1968	30.00; 28.00; 29.20
2097	46.00; 47.00
2217	57.50; 60.00

Arrhenius plots of the data (Figure 7) yield activation energies respectively of 29.9 ± 1.9 and 32.7 ± 2.3 kcal/mole for P_{O_2} = 152 torr and P_{O_2} = 15 torr in the temperature range 1600-2217°C, but between 1150 and 1600° only 12.5 ± 1 kcal/mole with P_{O_2} = 152 torr. The latter value is comparable

to the value 7.1 ± 1.9 kcal/mole obtained with the foil experiments in pure oxygen in the temperature range 1100-1300°C.

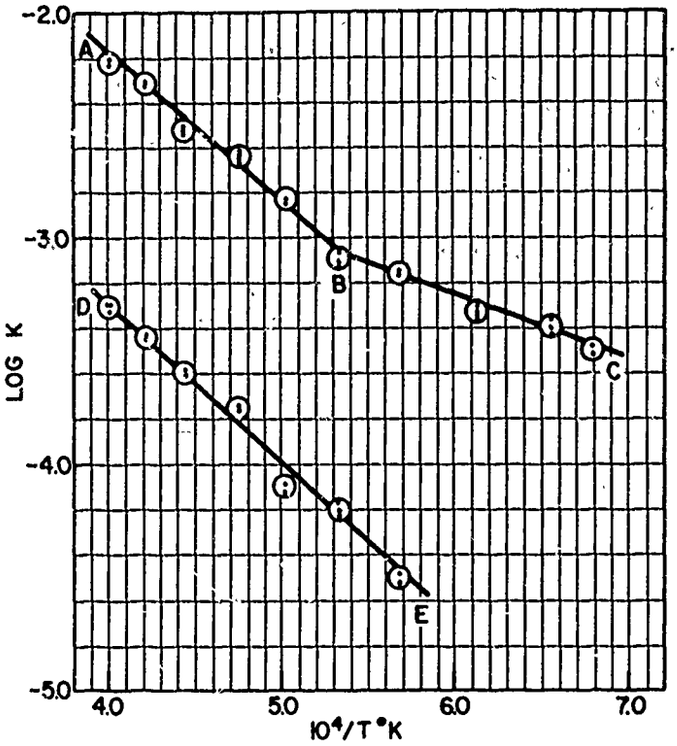

Figure 7. Arrhenius Plot for the Oxidation of Iridium Wire

(d) Presence of Water Vapor in the Oxygen

Reactions at 1156°C with dry oxygen and oxygen bubbled through water at room temperature ($P_{H_2O} \approx 18$ torr) yielded rate constants of 0.38 and 0.33 mg/cm^2/min, respectively, at a flow rate of 48 ml/min/cm^2 which indicates that water vapor in oxygen does not have any pronounced effect on the oxidation rate of iridium at 1156°C, except for causing a slight decrease in the oxygen partial pressure. Also, helium bubbled through water did not cause any measurable reaction at the same temperature.

The reaction of low partial pressure water vapor (about 18 torr; helium bubbled through water at room temperature) with the iridium wire was studied at various temperatures. No measurable reaction was observed up to 2097°C for a period of one hour. At 2217°C, the reaction was quite fast with linear rate constants of 1.0, 1.25, 1.0 and 1.25 x 10^{-4} mm/min, during the course of one hour. Decrease of diameter of the wire due to vaporization of Ir as such was negligible during the time interval used for the reaction as determined by heating the wire in pure helium. No rate measurements could be done at and above about 2350°C, since the wire burned out in less than two minutes.

Hot-Wire Experiments in Pure Oxygen

Runs were carried out at 1150 and 1260°C with the iridium wire in pure oxygen, with the oxygen flow rate the same as used (48 ml/min/cm^2) in the foil experiments in the resistance furnace. The average linear rate constants obtained were 1.14×10^{-3} and 1.4×10^{-3} mm/min at 1150 and 1260°C respectively. These values correspond to 2.55 and 3.14 mg/cm^2/min as compared to 0.36 and 0.44 mg/cm^2/min obtained in the foil experiments at nearly the same temperatures. These results indicate that the rates of oxidation of iridium wire obtained in a cold-walled reaction vessel are faster than those with the foil in a resistance furnace by a factor of 7 in the temperature range examined. This is to be attributed to the pumping action of the cold walls of the oxidation chamber in the wire experiments.

DISCUSSION OF THE RESULTS

The Effect of Flow Rate

No unusual behavior is observed for the influence of the gas-flow rate on the oxidation of iridium at any of the three temperatures (1060, 1162 and 1968°C) investigated. The reaction rate increases rapidly with the flow rate initially and then begins to flatten out at large flow rates. The increase of the rate is approximately proportional to the logarithms of the flow rate. Since no other data are found in literature on the effect of gas flow rate on the oxidation of iridium, a comparative study is not possible.

The Influence of Oxygen Partial Pressure

According to transpiration studies on the Ir-O_2 system,[2-4] the equilibrium oxidation reaction shows a 3/2 order dependence on the oxygen pressure at temperatures below 1400°C, whereas at both 1181 and 1717°C the present investigation shows an approximately linear (1.1 - 1.2 order) pressure dependence. However, at flow rates where equilibrium is not established, as in the present case, this difference cannot be considered serious.

The Influence of Temperature

It is interesting to examine the effect of temperature on the oxidation rate of iridium under various oxygen pressures and flow rates. The high activation energy of 70 kcal/mole below 1100°C obtained with iridium foil in pure oxygen may be only apparent due to the incomplete volatilization of the oxides formed on the iridium surface and/or due to the back reflection of the oxides from the wall on to the sample surface, and hence, not the true activation energy for the oxidation of iridium in the temperature range. Specimens oxidized at 1010, 1050 and 1060°C were black, indicative of the presence of some oxide on the surface. At higher temperatures, however, the surface was shiny and clean. The activation energy of 7.1 in the

temperature range 1100-1300°C with the foil in pure oxygen is comparable with the activation energy of 12.5 kcal/mole between 1200-1500°C with the wire in an O_2-He mixture with P_{O_2} = 152 torr. These values are in the range of the activation energies reported by Krier and Jaffee[11] (16 kcal/mole) and Phillips[12] (9.2 kcal/mole) in slowly moving air, below 1400°C, although the discrepancies are somewhat large.

A direct comparison of the linear rate constants for the oxidation of iridium in our investigation with those in the investigations of Krier and Jaffee[11] and Phillips[12] cannot be made since our experimental conditions were different from theirs. A comparison of the reaction rates found by Krier and Jaffee and Phillips at 1200°C shows that the formers' value is higher by a factor of about 2. Approximate extrapolations of our results indicate that at about the same temperature, our rate constant is even greater than that of Krier and Jaffee[11] by another factor of 2. However, at 1010°C, our value is in excellent agreement with that of Phillips at 1000°C although it is about 50 per cent lower than that of Krier and Jaffee at the same temperature. Discrepancies of this type cannot be considered serious, since for a reaction of the present kind, the rate depends on several factors such as the relative sizes of the specimens and the furnace,[15] the mounting of the sample inside the furnace, the total pressure in the system,[11] the chemical composition of the gas stream,[16-18] the temperature, the oxygen partial pressure, the gas-flow rates and the physical and chemical nature of the substance. If the specimen is mounted perpendicular to the direction of the gas flow in the system, then the rate of reaction at the side opposite to the gas flow will be much less than that at the other side.

Between 1600 and 2217°C, however, for iridium oxidation with both partial pressures of oxygen (15 and 152 torr) the activation energies are nearly equal (32.7 and 29.9 kcal/mole respectively) and are much higher than the value below 1600°C (12.5 kcal/mole for P_{O_2} = 152 torr). This increase in activation energy in the higher temperature range is in contrast to the behavior of several other reactions which produce volatile products.[15,19,20] These reactions normally show a high activation energy at lower temperatures corresponding to a chemisorption-controlled reaction which gives way to a low activation energy as the temperature is raised and a gas diffusion-controlled mechanism becomes predominant. The reason for the unusual behavior of the iridium-oxygen system may be that this reaction never becomes diffusion-controlled under the experimental conditions. The chemisorption-controlled reaction mechanisms may be different and involve the formation of different activated complexes in the two temperature regions below and above 1600°C showing different activation energies. The possible activated complexes in the two regions may be assumed to be $Ir_2O_2(g)$ and $IrO_2(g)$ or $IrO(g)$ respectively below and above the transition points, on the surface of the iridium. These either decompose or react with oxygen on the iridium surface or in the gas phase or at the walls of the reaction vessel giving the known solid product according to the following schemes:

I	Below 1600°C	$Ir_2O_2(g)$	$\xrightarrow{\text{wall}}$ $IrO_2(s) + Ir(s)$
		$\downarrow \frac{1}{2} O_2$	
		$Ir_2O_3(g)$	$\xrightarrow{\text{wall}}$ $IrO_2(s) + Ir(s) + \frac{1}{2} O_2$
IIa	Above 1600°C	$IrO_2(g)$	$\xrightarrow{\text{wall}}$ $IrO_2(s)$
		$\downarrow \frac{1}{2} O_2$	
		$IrO_3(g)$	$\xrightarrow{\text{wall}}$ $IrO_2(s) + \frac{1}{2} O_2$
IIb	Above 1600°C	$IrO(g)$	$\xrightarrow{O_2}$ $IrO_3(g)$ $\xrightarrow{\text{wall}}$ $IrO_2(s) + \frac{1}{2} O_2$

The formation of $IrO_2(g)$ and/or $IrO(g)$ is more endothermic than formation of Ir_2O_2 or IrO_3 and hence must have a greater activation energy. Tentative evidence for mechanism I is provided by a preliminary mass spectrometric investigation of the vapor species in the oxidation of iridium in this laboratory.[21] The only species detected in the 900-1200°C range was $Ir_2O_2^+$, presumably formed either from $Ir_2O_3(g)$ or from $Ir_2O_2(g)$. Mechanisms IIa and/or IIb are reasonable at higher temperatures on the basis of the mass spectrometric studies on the oxides of iridium in the size 1830-2033°K by Norman et al.[5] Two such mechanisms could explain the observed activation energy changes in this system.

Oxidation of Iridium by Water Vapor

Since the dissociation of water vapor into H, O and to some extent OH, becomes appreciable at temperatures over 2000°C, iridium is to be expected to undergo ready oxidation in the presence of water vapor at these high temperatures. The average linear rate constant of 1.125×10^{-4} mm/min obtained at 2217°C in presence of about 18 torr water vapor is higher than one would expect from the partial pressure of oxygen in the system at that temperature. However, oxygen may not be the only active species in such an atmosphere; H, OH and H_2O all could be reacting simultaneously with the iridium giving rise to a larger reaction rate. It will be interesting to investigate further, in detail, the interaction of water vapor with iridium at temperatures in excess of 2000°C before any definite conclusions may be drawn on this system.

Acknowledgment

This work has been supported by funds from the Aeronautical System Division, Air Force Systems Command, U.S. Air Force, through a subcontract with the Carbon Products Division, Union Carbide Corporation, Parma, Ohio, administered by Doctors E. Epremian and J. Criscione.

REFERENCES

Appendix A

1. E. D. Zysk, D. A. Toenshoff and J. Penton, Engelhard Ind. Tech. Bull. 4, 52 (1963).
2. C. B. Alcock and G. W. Hooper, Proc. Roy. Soc. 254A, 557 (1960).
3. E. H. P. Cordfunke and G. Meyer, Rec. Trav. Chim. 81, 495 (1962).
4. H. Schäfer and H. J. Heitland, Z. Anorg. Allgem. Chem. 304, 249 (1960).
5. J. H. Norman, H. G. Staley and W. E. Bell, J. Chem. Phys. 42, 1123 (1965).
6. G. C. Fryburg and H. M. Petrus, J. Electrochem. Soc. 108, 496 (1961).
7. G. K. Burgess and R. G. Waltenburg, Bull. Bur. Standards, 13, No. 280, 365 (1916-17).
8. O. Kubaschewski, Z. Electrochem., 49, 446 (1943).
9. G. C. Fryburg, J. Chem. Phys. 24, 175 (1956).
10. G. C. Fryburg and H. M. Murphy, Trans. AIME 222, 660 (1958).
11. C. A. Krier and R. I. Jaffee, J. Less Common Metals 5, 411 (1963).
12. W. L. Phillips, Jr., Trans. Am. Soc. Metals, 57, 33 (1964).
13. W. Crooks, Chem. News 105, 229 (1912); C. A. 2, 2895 (1912).
14. D. E. Poland, J. W. Green and J. L. Margrave, NBS Monograph 30, April, 1961.
15. E. A. Gulbransen, K. F. Andrew and F. A. Braport, J. Electrochem. Soc. 110, 476 (1963).
16. C. Wagner, J. Appl. Phys., 29(a), 1295 (1958).
17. J. L. Modisette and D. R. Schryer, NASA TND - 222, March 1960.
18. J. T. Waber, "Metals for Supersonic Aircraft and Missiles," Am. Soc. Metals, Cleveland (1958).
19. A. K. Kuriakose and J. L. Margrave, J. Phys. Chem. 68, 2671 (1964).

20. E. A. Gulbransen, A. F. Andrew and F. A. Brassart, J. Electrochem. Soc. 110, 952 (1963).

21. R. A. Kent and J. L. Margrave, Unpublished Work, Rice University, (1965).

APPENDIX B

KINETICS OF OXIDATION OF RHODIUM AT HIGH TEMPERATURES*

A. K. Kuriakose and J. L. Margrave
Department of Chemistry
Rice University
Houston, Texas

Rhodium has been found to be the most resistant of all platinum group metals towards oxidation and there have been several studies[1-5] on its oxidation kinetics at various temperatures ranging from 1000 to 1800°C. All but one of these studies[2] have been carried out in resistance-heated furnaces with hot walls and the use of such furnaces for measuring the rates of reactions which form volatile products generally yields reaction rates which are much lower than the actual values. Fryburg and Murphy[6] have clearly noted this point in the case of the oxidation of platinum and a comparison of the oxidation kinetics of iridium[7] in hot-walled furnaces and in cold-walled reaction vessels has shown that the latter rate is at least seven times faster than the former, other conditions being the same. Holborn and Austin[2] measured weight losses of rhodium strips in a cold-walled bulb by heating them electrically at 1670°C in an atmosphere of air, pure oxygen and nitrogen and their method would have yielded values closer to the true oxidation rate of Rh if the temperature measurement and control techniques had been sufficiently adequate in the early 1900's. In this note are presented results of studies on the oxidation of rhodium wire in a cold-walled reaction chamber in the temperature range of 1337 to 1827°C.

EXPERIMENTAL

The apparatus and experimental procedure were similar to those for the iridium wire oxidation studies reported elsewhere.[7] The emissivity of rhodium in air was determined by methods described earlier[7] and was found to be 0.26-0.30 between 1200°C and the melting point (1966°C) of rhodium.

RESULTS AND DISCUSSION

The Effect of Gas Flow Rate:

With a mixture of 20 per cent oxygen and 80 per cent helium, the gas flow rate was varied between 100 ml and 12.35 liters per minute, at 1827°C.

* Work performed under subcontract with the Carbon Products Division of Union Carbide Corporation, Parma, Ohio, sponsored by the U.S. Air Force.

The rate constants obtained are shown in Table 1.

TABLE 1

THE EFFECT OF GAS FLOW RATE ON THE OXIDATION RATE OF RHODIUM WIRE

Temperature: 1827°C:	P_{O_2} = 152 torr
Flow Rate liters/min	Linear Rate Constant (mm/min) x 10^5
0.10	25.00; 25.00
1.01	27.27; 30.00
3.85	25.00; 25.00
12.35	23.08; 25.00; 27.08

Contrary to expectations, the flow rate has practically no effect on the wire recession rate. The reason for this may be that the reaction rate of rhodium is too small to produce enough of the oxide in the gas phase to saturate the gas stream even at low flow rates.

The Effect of Temperature:

The recession rates of rhodium wire were measured at different temperatures between 1337 and 1827°C in a 20 per cent oxygen-80 per cent helium mixture at a flow rate of 12.35 liters/min., and the rate constants are recorded in Table 2.

TABLE 2

OXIDATION RATES OF RHODIUM WIRE AT VARIOUS TEMPERATURES

P_{O_2} = 152 torr	Flow Rate = 12.35 liters/min
Temperature °C	Linear Rate Constant (mm/min)x 10^5
1337	1.21; 1.41; 1.67
1457	3.75; 4.03
1579	7.50; 6.67; 6.67
1702	15.00; 15.83; 16.25; 15.00
1827	27.10; 25.00; 27.30; 25.00; 30.00

An Arrhenius plot of the data is linear and indicates an activation energy of 39.9 ± 1.4 kcal/mole. Widely differing values are found in the literature for the activation energy of oxidation of rhodium. Phillips[3] obtained an activation energy of only 29.6 kcal/mole between 1000 and 1360°C, while Krier and Jaffee[4] found it to be 51 kcal/mole in the same temperature range in air. Calculation of an activation energy from the data of Hill and Albert[5] gives a value of 45.6 kcal/mole in pure oxygen and 54.2 kcal/mole in air in the temperature range 1400-1800°C. The activation energy obtained in this investigation is also in the same range and it is considered to be in satisfactory agreement with all these workers in view of the variations in the experimental conditions and the already existing discrepancies. However, there is a large difference between the absolute reaction rates measured and those reported by the workers using hot-walled furnaces at all temperatures although the latter agree among themselves fairly well.

Experiments with rhodium foil in a resistance furnace and induction-heated furnace also agreed with the same studies. At about 1800°C, the reaction rate of a rhodium wire in a cold-walled chamber is faster than the reaction rate of rhodium foil in a hot-walled furnaced by a factor of approximately 300, which is too large to be explained in terms of the removal of the oxide gas from around the specimen, since the reaction rate is independent of the gas flow rate in the system. It is interesting that the oxidation rate of rhodium reported by Holborn and Austin[2] at 1670°C is even larger than the rate constant reported here at 1702°C by a factor of about 30, so that it appears certain that the recession rates of rhodium wires reacting in cold-walled reaction vessels are hundreds of times faster than the recession rate of the material in a hot-walled furnace. A combination of the effects of back reflection and/or recapture of the rhodium from the hot walls in the furnace and the very small surface compared to the dimensions of the reaction vessel in the case of the cold-walled experiments tending to exaggerate the pumping action of the cold walls might explain, in part, the tremendous enhancement of the reaction rate in the cold-walled reaction chamber.

The Effect of Oxygen-Partial Pressure:

The dependence of the oxidation rate of rhodium wire on the oxygen-partial pressure was examined at 1702°C and the results are presented in Table 3. As the oxygen-partial pressure is increased, the oxidation rate also increases; the two may be related by the equation:

$$k = 2.5 \times 10^{-6} P^{0.8}$$

where k is the linear recession rate constant in mm/min and P is the oxygen partial pressure in torr, at 1702°C. From studies of the oxidation rates of rhodium in the air and in pure oxygen, Hill and Albert[5] also found a similar dependence on the oxygen partial pressure above 1600°C, although Holborn and Austin[2] observed a direct linear dependence. Hill and Albert[5] pointed out that at temperatures above 1600°C, the volatilization of rhodium metal[8] also becomes significant as found by experiments in argon.

TABLE 3

RECESSION RATES OF RHODIUM WIRE UNDER VARIOUS OXYGEN-PARTIAL PRESSURES

Temperature = 1702°C

Oxygen-Partial Pressure torr	Linear Rate Constant (mm/min)x 10^5
12	1.67; 1.80
56	5.00; 4.67; 4.80
152	15.00; 15.83; 16.26; 15.00
508	35.00; 40.00; 38.00
760	50.00; 50.00; 50.00

In these experiments the recession rates in pure helium were too small to be measured even at 1827°C.

According to the transpiration studies by Alcock and Hooper[9] and the mass spectrometric studies of Bell et al[10], the volatile oxides of rhodium are RhO and RhO_2 from 1200-1500°C and quite likely at higher temperatures.

ACKNOWLEDGMENTS

The authors are pleased to acknowledge the support of this work by the United States Air Force through a subcontract administered by the Union Carbide Corporation. Mr. David Bonnell assisted with the computer processing of the experimental data.

REFERENCES

Appendix B

1. W. Crookes, Proc. Roy. Soc. A86, 461 (1912).
2. L. Holborn and L. W. Austin, Phil. Mag. 7 (6th Series), 388 (1904).
3. W. L. Phillips Jr., Trans. Amer. Soc. Metals 57, 33 (1964).
4. A. J. Krier and R. I. Jaffee, J. Less-Common Metals 5, 411 (1964).
5. J. S. Hill and H. J. Albert, Engelhard Ind. Tech. Bull. 4, 59 (1963).
6. G. C. Fryburg and H. M. Murphy, Trans. AIME 212, 660 (1958).
7. A. K. Kuriakose and J. L. Margrave, to be published, J. Phys. Chem. (1965).
8. (a) L. Dreger and J. Margrave, J. Phys. Chem. 65, 2106 (1961).
   (b) M. Panish and L. Reif, J. Chem. Phys. 34, 1915 (1961).
9. C. B. Alcock and G. W. Hooper, Proc. Roy. Soc. A 254, 551 (1960).
10. J. H. Norman, H. G. Staley and W. E. Bell, J. Phys. Chem. 68, 662 (1964).

Unclassified
Security Classification

DOCUMENT CONTROL DATA - R&D

(Security classification of title, body of abstract and indexing annotation must be entered when the overall report is classified)

1. ORIGINATING ACTIVITY (Corporate author)	2a. REPORT SECURITY CLASSIFICATION
Union Carbide Corporation Carbon Products Division Parma, Ohio 44130	Unclassified
	2b. GROUP

3. REPORT TITLE

High Temperature Protective Coatings for Graphite (Part III)

4. DESCRIPTIVE NOTES (Type of report and inclusive dates)

Annual Technical Report - 1 June 1964 to 31 May 1965

5. AUTHOR(S) (Last name, first name, initial)

Criscione, John M.; Mercuri, Robert A.; Volk, Herbert F.; Rexer, Joseph; Nuss, James W.; Sarian, Suren; Meszaros, Frank W.

6. REPORT DATE	7a. TOTAL NO. OF PAGES	7b. NO. OF REFS
December 1965	199	65

8a. CONTRACT OR GRANT NO.	9a. ORIGINATOR'S REPORT NUMBER(S)
AF 33 (657) - 11253	ML-TDR-64-173
b. PROJECT NO. 7350	Part III
c. TASK 735002	9b. OTHER REPORT NO(S) (Any other numbers that may be assigned this report)
d.	

10. AVAILABILITY/LIMITATION NOTICES "This document is subject to special export controls and each transmittal to foreign governments or foreign nationals may be made only with prior approval of the Metals and Ceramics Division (MAM), Air Force Materials Lab., Wright-Patterson Air Force Base, Ohio

11. SUPPLEMENTARY NOTES	12. SPONSORING MILITARY ACTIVITY
	Metals and Ceramics Division (MAMC) Air Force Materials Laboratory Wright-Patterson Air Force Base, Ohio

13. ABSTRACT

The second year progress is reported in several areas of research on high temperature oxidation protective coatings for graphite.

Work presented includes: the oxidation kinetics of iridium and rhodium; the permeability of $ZrSiO_4$, ZrO_2, ThO_2, Al_2O_3, and BeO to oxygen; an investigation of the iridium-carbon system by means of high temperature X-ray diffraction techniques and the deposition of iridium on graphite; the volatility of HfO_2, ZrO_2, ThO_2, $ThZrO_4$, $SrZrO_3$, $BaZrO_3$, $ZrSiO_4$, and $HfSiO_4$ in the presence of water vapor; the chemical kinetics of the carbothermic reduction of ZrO_2, ThO_2, HfO_2, $ThZrO_4$, and $HfSiO_4$; the chemical kinetics of the reaction of ZrO_2, HfO_2, and ThO_2 with ZrC, HfC, and ThC_2, respectively; the chemical reactions of HfO_2, ZrO_2, and ThO_2 with HfB_2 and ZrB_2; initial work on carbon diffusion through diborides and carbides; and the mechanical compatibility of components of multilayer oxidation protective coatings for graphite.

The experimental results are discussed as to their practical implication to oxidation-protective coatings.

DD FORM 1 JAN 64 1473

Unclassified
Security Classification

14. KEY WORDS	LINK A		LINK B		LINK C	
	ROLE	WT	ROLE	WT	ROLE	WT
Oxidation Protection High Temperature Coatings Graphite Iridium Borides Carbides Oxides Reaction Kinetics Permeability Diffusion Volatility						

INSTRUCTIONS

1. ORIGINATING ACTIVITY: Enter the name and address of the contractor, subcontractor, grantee, Department of Defense activity or other organization *(corporate author)* issuing the report.

2a. REPORT SECURITY CLASSIFICATION: Enter the overall security classification of the report. Indicate whether "Restricted Data" is included. Marking is to be in accordance with appropriate security regulations.

2b. GROUP: Automatic downgrading is specified in DoD Directive 5200.10 and Armed Forces Industrial Manual. Enter the group number. Also, when applicable, show that optional markings have been used for Group 3 and Group 4 as authorized.

3. REPORT TITLE: Enter the complete report title in all capital letters. Titles in all cases should be unclassified. If a meaningful title cannot be selected without classification, show title classification in all capitals in parenthesis immediately following the title.

4. DESCRIPTIVE NOTES: If appropriate, enter the type of report, e.g., interim, progress, summary, annual, or final. Give the inclusive dates when a specific reporting period is covered.

5. AUTHOR(S): Enter the name(s) of author(s) as shown on or in the report. Enter last name, first name, middle initial. If military, show rank and branch of service. The name of the principal author is an absolute minimum requirement.

6. REPORT DATE: Enter the date of the report as day, month, year; or month, year. If more than one date appears on the report, use date of publication.

7a. TOTAL NUMBER OF PAGES: The total page count should follow normal pagination procedures, i.e., enter the number of pages containing information.

7b. NUMBER OF REFERENCES: Enter the total number of references cited in the report.

8a. CONTRACT OR GRANT NUMBER: If appropriate, enter the applicable number of the contract or grant under which the report was written.

8b, 8c, & 8d. PROJECT NUMBER: Enter the appropriate military department identification, such as project number, subproject number, system numbers, task number, etc.

9a. ORIGINATOR'S REPORT NUMBER(S): Enter the official report number by which the document will be identified and controlled by the originating activity. This number must be unique to this report.

9b. OTHER REPORT NUMBER(S): If the report has been assigned any other report numbers *(either by the originator or by the sponsor)*, also enter this number(s).

10. AVAILABILITY/LIMITATION NOTICES: Enter any limitations on further dissemination of the report, other than those imposed by security classification, using standard statements such as:

(1) "Qualified requesters may obtain copies of this report from DDC."

(2) "Foreign announcement and dissemination of this report by DDC is not authorized."

(3) "U. S. Government agencies may obtain copies of this report directly from DDC. Other qualified DDC users shall request through

_____."

(4) "U. S. military agencies may obtain copies of this report directly from DDC. Other qualified users shall request through

_____."

(5) "All distribution of this report is controlled. Qualified DDC users shall request through

_____."

If the report has been furnished to the Office of Technical Services, Department of Commerce, for sale to the public, indicate this fact and enter the price, if known.

11. SUPPLEMENTARY NOTES: Use for additional explanatory notes.

12. SPONSORING MILITARY ACTIVITY: Enter the name of the departmental project office or laboratory sponsoring *(paying for)* the research and development. Include address.

13. ABSTRACT: Enter an abstract giving a brief and factual summary of the document indicative of the report, even though it may also appear elsewhere in the body of the technical report. If additional space is required, a continuation sheet shall be attached.

It is highly desirable that the abstract of classified reports be unclassified. Each paragraph of the abstract shall end with an indication of the military security classification of the information in the paragraph, represented as *(TS), (S), (C), or (U)*.

There is no limitation on the length of the abstract. However, the suggested length is from 150 to 225 words.

14. KEY WORDS: Key words are technically meaningful terms or short phrases that characterize a report and may be used as index entries for cataloging the report. Key words must be selected so that no security classification is required. Identifiers, such as equipment model designation, trade name, military project code name, geographic location, may be used as key words but will be followed by an indication of technical context. The assignment of links, rules, and weights is optional.